

Alma Mater Studiorum – Università di Bologna

DOTTORATO DI RICERCA IN

Scienze Biotecnologiche, Biocomputazionali, Farmaceutiche e
Farmacologiche

Ciclo XXXIII

Settore Concorsuale: 03/D1

Settore Scientifico Disciplinare: CHIM/08

*Design and Synthesis of Novel Kinase Inhibitors for the
Treatment of Chronic Respiratory Diseases*

Presentata da: Roberta Mazzucato

Coordinatore Dottorato
Prof. Maria Laura Bolognesi

Supervisore
Prof. Marinella Roberti

Co-Supervisore
Dr. Fabio Rancati

Esame finale anno 2021

A mia nonna Edda.

Contents

Abstract	7
Abbreviations	8
Preface.....	13
Where Does a Lead Come From?.....	14
Part I: From an HTS Hit to a Potent and Selective PI3Kδ Inhibitor for the Treatment of Asthma and COPD.....	21
1. Introduction	22
1.1 An overview of Asthma and COPD	22
1.2 Class PI3K δ as Therapeutic Target in COPD and Severe Asthma.....	25
1.3 Phosphoinositide 3-Kinases Family	28
1.4 Class I PI3Ks Signalling Inputs, Outputs and Distribution	31
1.5 Structural Determinants of the PI3K Catalytic Subunit	33
1.6 Class I PI3K Inhibitors.....	39
2. Aim of the Project	46
2.1 Design and Synthesis of New, Potent and Selective PI3K δ Inhibitors.....	46
3. Results and discussion	47
3.1 Hit Evaluation.....	47
3.2 First SAR Exploration.....	50
3.3 2D Library Design and Synthesis.....	53
3.4 Biological Assay Results and SAR Analysis.....	57

3.5	Second SAR Exploration.....	66
3.6	Synthesis and Biological Evaluation of the Second SAR Exploration.....	69
4.	Conclusions	76
5.	Material and Methods.....	77
5.1	General Chemistry Method	77
5.2	General Procedure for Urea Derivatives	78
5.3	General Procedure for 2,9-disubstituted-8-oxopurine-6-carboxamide (A _x B _y).....	86
6.	Biological Assays	105
6.1	PI3K δ , - γ , - β , - α ADP-Glo Assay.....	105
6.2	THP-1 Cellular Assay	105
6.3	Solubility Measurements.....	106
6.4	Caco-2 Cell Permeability Assay.....	106
6.5	Determination of the hPI3K δ Crystal Structure.....	109
Part II: Exploring Macrocycles as New Rho-associated protein kinase (ROCK) Inhibitors		110
1.	Introduction	111
1.1	Rho-Associated Protein Kinases (ROCK).....	111
1.2	ROCKs as Mediator of Vasoconstriction	113
1.3	ROCKs as Drug Target for Pulmonary Arterial Hypertension (PAH)	115
1.4	Structural Biology of ROCK	117
1.5	ROCK Inhibitors: State of Art	121

2. Aim of the Project	123
2.1 Design and Synthesis of New Macrocyclic Rho-associated protein kinase (ROCK) inhibitors.....	123
3. Result and Discussion	124
3.1 Reference Compound Selection	124
3.2 The Rational Design of Macrocyclic Scaffolds	127
3.3 Acyclic Derivatives Series.....	154
4. Biological Evaluation and SAR Considerations	162
5. Conclusion and Perspectives.....	167
6. Material and Methods.....	168
6.1 General Chemistry Methods.....	168
6.2 Scheme 6-Route B.....	170
6.3 Scheme 9-Route A/A2.....	178
6.4 Scheme 10.....	195
6.5 Scheme 11.....	201
6.6 Scheme 12.....	207
6.7 Scheme 13.....	210
7. Biological Assays	213
7.1 In vitro Inhibitory Activity Assay	213
7.2 Cell-based Assay	214
8. Computational Methodologies	215

8.1	Prime Macrocycle Conformational Sampling (Prime-MCS).....	215
8.2	General Procedure for Docking Simulations	215
9.	Crystal Structure Determination	216
	Acknowledgements	218
	References	219

Declaration

The research work described in this PhD thesis was carried out in the Chemistry Research and Drug Design (CRDD) Department, at Chiesi Farmaceutici SpA, Parma, under the supervision of Prof. Marinella Roberti, Alma Mater Studiorum Università di Bologna, and Dr. Fabio Rancati, CRDD Department, Chiesi Farmaceutici SpA.

For sake of clarity, my PhD thesis has been focused on the design, synthesis and characterization of new small molecules. Computational Chemistry Unit, CRDD Department, has carried out all the computational studies described in this thesis. Biological evaluation of new molecular entities, Phys-chem measurements, ADME assays and crystal structures determination have been carried out by other Chiesi Farmaceutici SpA Pre-Clinical Departments or by Contract Research Organizations that supports Chiesi Farmaceutici SpA in Pre-Clinical Research.

Abstract

In 2017, Chronic Respiratory Diseases accounted for almost four million deaths worldwide. Unfortunately, current treatments are not definitive for such diseases. This *unmet medical need* forces the scientific community to increase efforts in the identification of new therapeutic solutions.

PI3K delta plays a key role in mechanisms that promote airway chronic inflammation underlying Asthma and COPD. The first part of this project was dedicated to the identification of novel PI3K delta inhibitors.

A first SAR expansion of a Hit, previously identified by a HTS campaign, was carried out. A library of 43 analogues was synthesised taking advantage of an efficient synthetic approach.

This allowed the identification of an improved Hit of nanomolar enzymatic potency and moderate selectivity for PI3K delta over other PI3K isoforms. However, this compound exhibited low potency in cell-based assays. Low cellular potency was related to sub optimal phys-chem and ADME properties. The analysis of the X-ray crystal structure of this compound in human PI3K delta guided a second tailored SAR expansion that led to improved cellular potency and solubility.

The second part of the thesis was focused on the rational design and synthesis of new macrocyclic Rho-associated protein kinases (ROCKs) inhibitors. Inhibition of these kinases has been associated with vasodilating effects. Therefore, ROCKs could represent attractive targets for the treatment of pulmonary arterial hypertension (PAH). Known ROCK inhibitors suffer from low selectivity across the kinome. The design of macrocyclic inhibitors was considered a promising strategy to obtain improved selectivity. Known inhibitors from literature were evaluated for opportunities of macrocyclization using a knowledge-based approach supported by Computer Aided Drug Design (CADD). The identification of a macrocyclic ROCK inhibitor with enzymatic activity in the low micro molar range against ROCK II represented a promising result that validated this innovative approach in the design of new ROCKs inhibitors.

Abbreviations

A	ACN	Acetonitrile
	ADME	Absorption, Distribution, Metabolism, and Excretion
	ADP	Adenosine diphosphate
	AHR	Airway Hyper-Responsiveness
	ALK	Anaplastic Lymphoma Kinase
	AMU	Atomic Mass Unit
	ATP	Adenosine triphosphate
B	Boc	Tert-Butyloxycarbonyl protecting group
C	CCG	Chemical Computing Group
	CD4	Cluster of Differentiation 4
	CD8	Cluster of Differentiation 8
	CDI	Carbonyldiimidazole
	CRC	Concentration Response Curve
	CV	Column Volume
D	Da	Dalton
	DCM	Dichloromethane
	DDT	DL-Dithiothreitol
	DECL	DNA Encoded Chemical Library
	DIPEA	<i>N,N</i> -Diisopropylethylamine
	DMA	Dimethylacetamide
	DMAP	4-Dimethylaminopyridine
	DMF	Dimethylformamide
	DMSO	Dimethylsulfoxide

	DPPA	Diphenyl phosphoryl azide
E	EGF	Epidermal Growth Factor
	EGTA	Ethylene Glycol-bis(β -aminoethyl ether)-N,N,N',N'-Tetraacetic Acid
	eNOS	Endothelial nitric oxide synthase
	EtOAc	Ethyl Acetate
	EtOH	Ethanol
	Et ₂ O	Diethyl Ether
F	FDA	Food and Drug Administration
	Fmoc	Fluorenylmethoxycarbonyl protecting group
G	GPCRs	G protein-coupled receptors
	GTP	Guanosine-5'-triphosphate
H	HATU	1-[Bis(dimethylamino)methylene]-1H-1,2,3-triazolo[4,5-b]pyridinium 3-oxide hexafluorophosphate
	HCV	Hepatitis C virus
	hERG	Human Ether-a-go-go-Related Gene
	HIV	Human Immunodeficiency Virus
	HPLC	High Performance Liquid Chromatography
	hr	Hour
	HRMS	High Resolution Mass Spectrometry
	HSQC	Heteronuclear Single Quantum Correlation
	Hz	Herz
I	Ig	Immunoglobulin
	IL	Interleukin
	<i>i</i> -PrOH	2-Propanol
L	LC-MS	Liquid Chromatography-Mass Spectrometry

	LPA	Lysophosphatidic acid
	LPS	Lipopolysaccharide
M	MD	Molecular Dynamic
	MeOH	Methanol
	mmHg	millimetre of mercury
	MW	Microwave
N	NS3	Non-structural protein 3
	NS5B	Non-structural protein 5B
	NO	Nitric oxide
O	on	Over night
P	PASLI	p110 delta activating mutation causing senescent T cells, lymphadenopathy, and immunodeficiency
	PBS	Phosphate Buffer Solution
	PDB	Protein Data Bank
	PDGF	Platet-derived growth factor
	PKA	Protein Kinase A
	PtdIns	Phosphatidylinositol
	PtdIns4P	Phosphatidylinositol 4-phosphate
	PtdIns(4,5)P ₂	Phosphatidylinositol 4,5-bisphosphate
	PyBrop	Bromotripyrrolidinophosphonium hexafluorophosphate
R	RMSD	Root-Mean-Square Deviation
	ROESY	Rotating frame Overhause Effect Spectroscopy
	Rt	Room Temperature
	RTKs	Receptor tyrosine kinases
S	SAR	Structure Activity Relationship

	SCX	Strong Cation Exchange
	S _N Ar	Nucleophilic aromatic substitution
T	TEA	Triethylamine
	Th	T-helper
	THF	Tetrahydrofuran
	TLC	Thin-Layer Chromatography
	TNF	Tumour Necrosis Factor
	TPSA	Total Polar Surface Area
	t _R	Retention Time
	Tris	Tris(hydroxymethyl)aminomethane chloride
U	UPLC	Ultra-Performance Liquid Chromatography
V	VEGF	Vascular Endothelial Growth Factor

Amino acids Abbreviations

Three letter code	Name	One letter code
Ala	Alanine	A
Arg	Argine	R
Asn	Asparagine	N
Asp	Aspartic Acid	D
Cys	Cysteine	C
Glu	Glutamic Acid	E
Gln	Glutamine	Q
Gly	Glycine	G
His	Histidine	H
Ile	Isoleucine	I
Leu	Leucine	L
Lys	Lysine	K
Met	Methionine	M
Phe	Phenylalanine	F
Pro	Proline	P
Ser	Serine	S
Thr	Threonine	T
Trp	Tryptophan	W
Tyr	Tyrosine	Y
Val	Valine	V

Preface

In 2019, the US Food and Drug Administration (FDA) approved 48 new drugs (38 New Chemical Entities and 10 Biologics) (**Figure 1**). Even if this number is lower than that registered in 2018 (59 divided between 42 New Chemical Entities and 17 Biologics), it confirms a positive trend that started in 2017 when 46 new drugs were approved¹. Although 2019 was a successful year in terms of approved drugs, it is important to point out that it has been estimated that only one out of 5,000 compounds that Pharma and Biotech companies discover and put through preclinical testing becomes an approved drug². Consequently, the high attrition rate of candidate drugs has highlighted the importance of delivering high-quality leads during the pre-clinical development showing the value of finding an efficient and rapid lead generation strategy to identify good chemical starting points.

The following introduction will give a brief description of the different lead generation strategies frequently employed in identifying new candidate drugs. This description will help to introduce the two different lead strategies, employed in this research thesis, aimed at identifying new kinases inhibitors for the treatment of respiratory diseases.

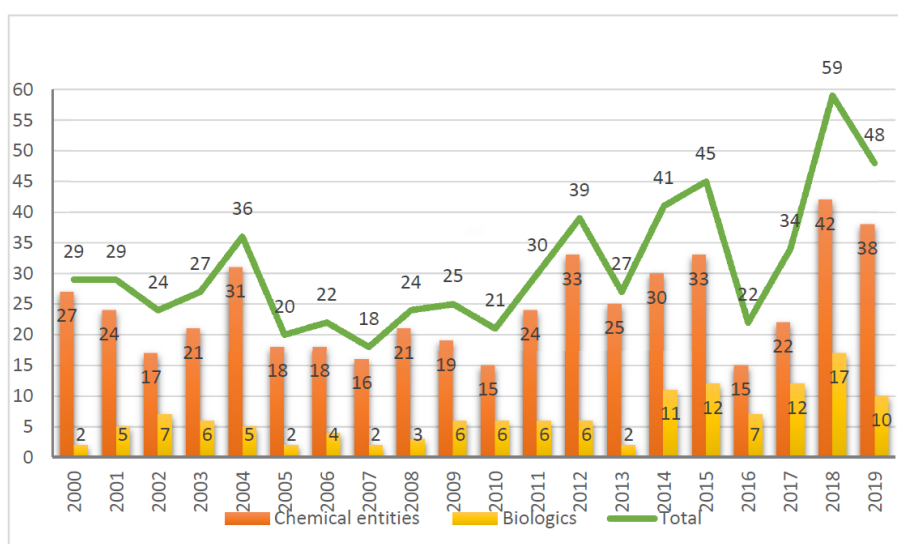


Figure 1: New chemical entities and biologics approved by FDA in the last two decades.¹

Where Does a Lead Come From?

Brown *et al.* recently reported³ an analysis conducted on 66 published clinical candidates from *Journal of Medicinal Chemistry* between 2016 and 2017. Overall, this study showed as the most widely used lead generation approach was based on use of a previously known compound as starting point (Known, 43%), (**Figure 2**). This was followed by screening methods subdivided into random screening (29%), focused screening (8%), FBLG Fragment-Based Lead Generation (5%), and DNA-encoded library screening (1%)³, while Structure Based Drug Design (SBDD) was used in the 14% of the examined cases. Hereafter, an overview of these strategies is reported. It is important to underline that, in many cases, the identification of a clinical candidate is determined using a combination of these lead generation approaches.

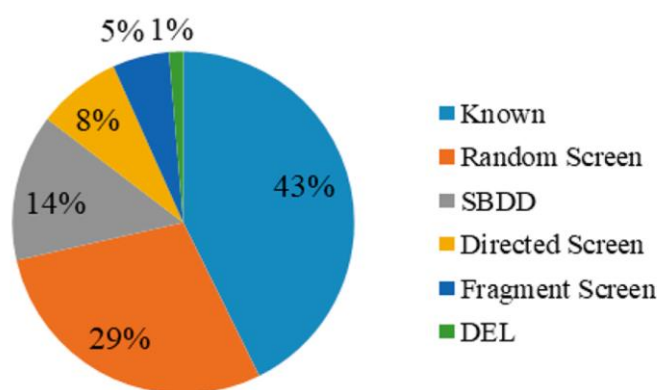


Figure 2: Distributions of six sources of lead generations strategies.³

- **Lead Identification Based on Known Compounds**

This is the strategy most frequently used to develop new drugs. A new pharmaceutical program can be based on a previous disclosure of an active compound or on a prior developed program. Fast follower, Me too and repurposing approaches can be included in this category. The major advantage of this kind of approaches is that usually the biological target has already been validated in the clinic and this usually accelerates the development process⁴. However, this strategy is not without risks since it is essential to guarantee the novelty of the new generated intellectual property. Moreover, the new compound must be at least non-inferior to the original drug. In this type of approach,

minimal chemical changes are introduced with the aim of providing differentiation and opportunities of claim invention and novelty³.

- **Screening Methods for Lead Generation**

Progress in screening technology made these methods fundamental in drug discovery process. Among them, *High-Throughput Screening*, commonly known as HTS, has become a standard procedure in early stages of Hit identification. An analysis conducted on 58 drugs, that were approved from 1991 and 2008, reported that the origin of 19 of them was associated to HTS⁵.

The main objective of HTS is to deliver different chemical series from which the most suitable for the drug development process will be identified⁴. It is basically a process of screening and assaying a large number of biological modulators and effectors against selected and specific targets.

However, screening of 1 million of compounds can take 1-3 months, can be highly expensive and not always accessible to smaller biotech companies or academic laboratories. Therefore, new techniques have recently emerged as alternative strategies to HTS of large collections of small molecules.

The screening of focused sets of compounds or focused library is among them. In *Focused HTS*, subsets of compounds can be created within corporate collections according to some chemoinformatic criteria or target biased libraries. This approach has different advantages: first, it is an integration of drug-discovery knowledge and expectations about the structure essential for a particular target (the so-called protein family targeted library); secondly it is cost and timesaving since smaller sets of compounds can be screened faster. Moreover, the synthesis of target focused library allows to cover a precise chemical space which is often incompletely covered in random collections compounds⁶, providing a preliminary SAR analysis.

Recently, another emerging technique, DNA-encoded chemical libraries, has attracted the interest of pharmaceutical company. The DNA-encoded chemical libraries represent a new tool for the fast and efficient identification of ligands for a certain protein target. Basically, these libraries are large collections of organic molecules coupled to DNA tag, functioning as amplifiable identification barcodes⁷. DNA-encoding permits the easy identification of ligand bound to supported protein at sub-picomolar concentration, in similar fashion to what happens with other methodologies like antibody phage display⁸. This technique allows to prepare combinatorial libraries of thousands to

millions of small molecules. Moreover, it is less costly compared to HTS. Overall, the cost of screening HTS library of 1 million compounds would cost between 400 million and 2 billion of dollars while screening a DECL library of 800 million compounds would cost on the order of \$150,000⁹. Additionally, the advantage is related to possibility of being applied to target, for whom specific assay are not available and therefore HTS cannot be applied. At the moment, one successful clinical candidate derived from this technology is GSK2982772, first-in-class Receptor Interacting Protein 1 (RIP1) for the treatment of inflammatory diseases¹⁰.

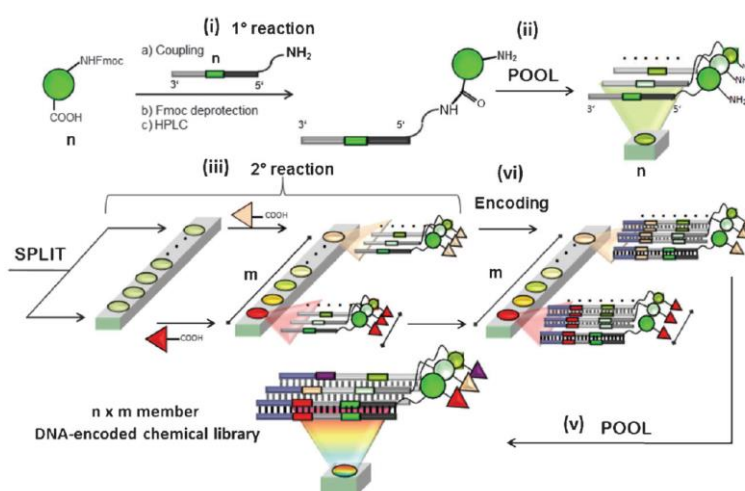


Figure 3: Synthetic scheme of a single pharmacophore DNA encoded chemical library.⁸

However, even if DECL technology has reached a good level of maturity, it still shows some drawbacks: such as the limitations in types of Building Blocks and reactions that can be used since not all chemical reactions can guarantee the preservation of DNA integrity⁷. Moreover, not all proteins (e.g., integral membrane proteins) are compatible with all the standard selection procedures, as they are difficult to be kept in solution and to be immobilized on solid supports¹¹.

Another screening methodology, firmly established in the drug discovery process, is the Fragment-based drug discovery (FBDD) which involves the construction of small-molecule ligands linking together low-molecular mass fragment molecules of ≤ 300 Da¹² which showed even a weak interaction with the target. Fragment-based methodology has two primary advantages compared to HTS: firstly, a significant larger proportion of chemical space can be sampled with a fragment library (usually $\sim 10^3$ fragments) as compared with the $\sim 10^5$ – 10^6 larger molecules typical for an HTS campaign; secondly even if fragment hits are weakly binding, they must make high-quality

interactions with the target to bind with enough affinity for detection. Ultimately, a high variety of screening assay can be used in FBDD: biochemical screens, terminal shifts, ligand observed NMR and X-ray crystallography³.

However, FBDD has its own drawbacks too and it is not “one size fits all” solution for the drug discovery problems. Some targets seem to be less amenable to FBDD methodology and moreover low potency fragments are not suitable for whole cell screening and for kinetic assays because they might need for higher concentration of the fragment leading to false positive. Nonetheless, 5% of 66 published clinical candidates reviewed by Brown et al³. were discovered through this methodology. Additionally, Johnson and colleagues reported 26 recent examples of successful fragment-to-lead published case studies in 2018 and highlighted the broadening of target class coverage by FBDD methodology¹³.

- **Structure Based Drug Design**

Structure Based Drug Design (SBDD) is a methodology that relies on possessing the knowledge of 3D structures of biological targets.

SBDD is typically an iterative process that begins with the identification and the validation of the target structure¹⁴. The outstanding progress made in structural and molecular biology along with improvements biomolecular spectroscopic structure determination methods have provided the determination of 3D structures of more than 100,000 proteins¹⁵. These improvements have made SBDD the most powerful and efficient process in the drug-discovery. However, target structure is not always available, thus in these cases, *in silico* methods must be used to model the protein's 3D structure. Homology modelling or comparative modelling are examples of these methods which allow to build 3D structures for unresolved proteins based on known homologous protein.

Once the target structure is identified, it is fundamental to recognize the binding site or the active residues in the target structure¹⁴. When targets and binding sites are well defined, the next step is the Hit identification. Hit discovery can be carried out essentially using two strategies: virtual high-throughput screening (vHTS) and *de novo* design.

vHTS envisages the computationally screening of large chemical libraries to discover compounds suitable for the target of interest. Compounds are filtered and ranked based on docking simulations and score.

The *de novo* drug design is a computational method of building new lead compounds from scratch, starting from molecular units. The aim is to develop small chemical structure that fits perfectly in the target space. This can be carried out through two different approaches: target-based design and ligand-based design; the first one more prevalent than the second. Basically in the target-based design hits are created by putting small fragments in key sites of the protein¹⁴, building the chemical connections that maintain the required geometry of the ligand's moieties.

In the field of *de novo* design, a new interesting area has been recently attracting medicinal chemistry interest: the macrocyclization¹⁶.

Natural product macrocycles and their synthetic analogues along with peptidic macrocycles are well-known in medicinal chemistry. However, the attention now is focused on a wider use of macrocycles scaffolds and a rising number of synthetic macrocycles are being reported in the rational identification of new therapeutic agents¹⁶.

One of the main reason of the growing interest in macrocyclization is due to identification of new biochemical pathways based on protein-protein interactions¹⁷. This new class of target seems to be less druggable since the region of interaction is larger and lacks of well-defined binding regions making harder the inhibition by classical small molecules¹⁸. Therefore, molecules have to be larger and consequently become less “drug like” than classical small molecules¹⁷. Thus, macrocyclization represents a new strategy to overcome these new druggability problems. In this regard, cell permeability, a frequent problem in large molecules, can be positively influenced by macrocyclization since it can mask amide NH groups from solvation and favour intramolecular hydrogen bonding. Therefore, by shielding polar groups from solvent, it offsets the free energy of desolvation and facilitates diffusion across the membrane¹⁹.

Additionally, macrocyclization can improve potency^{20,21,22} and selectivity^{23,24} over targets. Since their lower conformational freedom, compared to their acyclic counterparts, macrocycles can show improved binding affinity due to reduced entropic loss during the binding²⁵. Moreover, they have higher selectivity due to the difficulty to assume conformations required to bind other targets¹⁶.

Macrocycle design is mainly guided by SBDD; 3D structure information on ligand- protein complexes are fundamental to design and direct macrocyclization into the right direction. Some ligands, bound to their target, present conformational pre-disposition, such as U-shaped or C-shaped¹⁷, consistent for macrocyclization. Once these opportunities of macrocyclization are identified, several molecular modelling protocols, provided by eg. CCG, Openeye or Schrodinger²⁶ can be applied to build new macrocyclic analogues.

Lorlatinib, a macrocyclic kinase inhibitor for the treatment of ALK-positive metastatic non- small cell lung cancer²³ and Simeprevir²⁷, the first macrocyclic NS3 inhibitor to be approved by the FDA for HCV therapy are two successful examples of the application of Structure Based Macrocyclic Drug Design to small molecules.

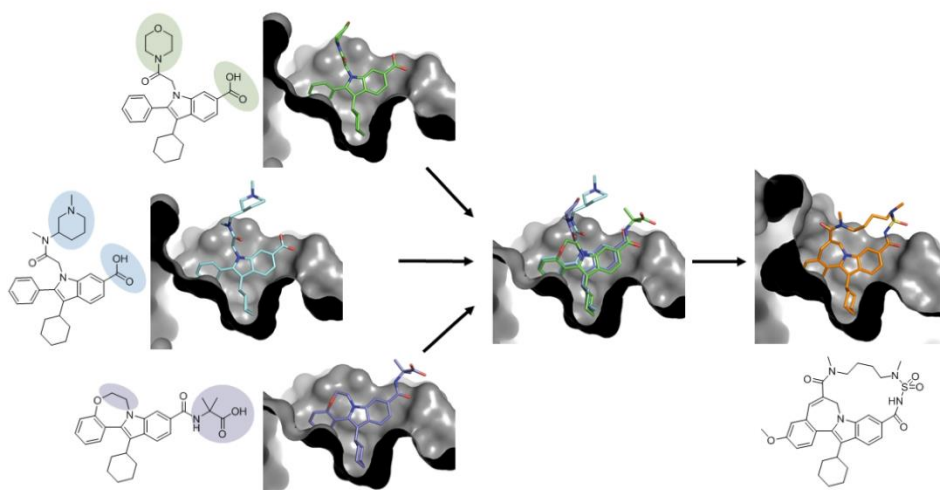


Figure 4: Structure Based Design of a macrocyclic HCV NS5B polymerase.¹⁷

**Part I: From an HTS Hit to a Potent and Selective PI3K δ Inhibitor
for the Treatment of Asthma and COPD**

1. Introduction

1.1 An overview of Asthma and COPD

COPD and Asthma are two chronic respiratory diseases characterized by airways obstruction and chronic inflammation of respiratory tract. It has been estimated that in 2016 more than 339 million people suffered from Asthma globally while COPD caused 3.17 million deaths in 2015, representing the 5% of all deaths globally in that year²⁸.

Asthma is a heterogeneous disease featured by lung inflammation coupled to airway hyper-responsiveness (AHR) caused by direct and/or indirect stimuli such as exercise, exposure to allergens or irritants, weather change, and respiratory infections²⁹. Use of bronchodilators and inhaled corticosteroids represent the main strategy to manage this disease but, despite the availability of these effective therapies, approximately 20% of patients are poorly controlled and 3–5% of patients suffer from a more serious form which is defined as Severe Asthma³⁰.

Severe Asthma is described by European Respiratory Society (ERS) and American Thoracic Society (ATS) guidelines as “asthma which requires treatment with high dose inhaled corticosteroids (ICS) plus a second controller to prevent it from becoming “uncontrolled” or which remains “uncontrolled” despite this therapy”³¹.

Severe asthma phenotypes are mainly composed of the following classification: type 2 (T2) high or T2-low³² (**Figure 5**). Currently, most of the new drug development has been focused on targeting Type 2 (T2) high asthma.

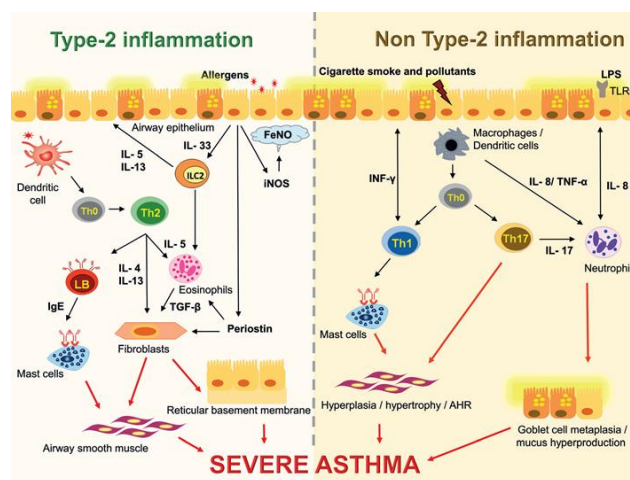


Figure 5: Severe Asthma Phenotypes.³²

Three immune response modifiers approved by the FDA and EMA are available for treating severe TH2-high asthma such as omalizumab (anti-IgE); mepolizumab, reslizumab and benralizumab (anti-IL-5 pathways), and dupilumab (anti-IL-4/IL-13). On the other hand, the TH2-low endotype does not have any readily available point-of-care biomarkers, so TH2-low asthma is often diagnosed based on a lack of TH2-high biomarkers and lacks of specific treatments³³. These patients tend to have greater resistance to steroids. Indeed, treatment options for TH2 low asthma are limited and the development of therapies has lagged behind that for TH2-high asthma³⁴. Overall, Asthma is an extremely complex disease and there is a great need to develop new treatment to ameliorate life of patients and to reduce its global burden.

COPD is a progressive lung disease characterized by chronic obstruction of lung airflow that interferes with normal breathing. In most of COPD patients, chronic inflammation is an amplification of the normal inflammatory response to tobacco smoking or constant exposure to toxic fumes in poorly ventilated environment³⁵. COPD is also characterized by acute exacerbations in many cases caused by an infection in the lungs resulting in increased inflammatory burden leading to worsening respiratory symptoms. This inflammation in lungs is characterised by infiltration and overactivation of macrophages and neutrophils and by increase of lymphocytes ³⁶(Figure 6).

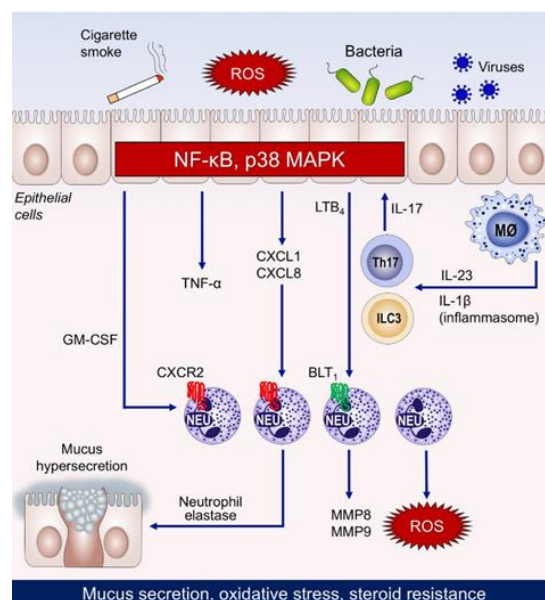


Figure 6: Neutrophilic inflammation in COPD.³⁶

Current treatments for COPD are only able to relieve symptoms but they do not reduce progressive decline in lung function or mortality³⁷ and they have a very little effect on preventing exacerbations.³⁰ Moreover, COPD patients are poorly responsive to corticosteroids treatments. One of the causes for this lack of response is connected to oxidative stress that characterizes the inflamed lung tissue and is often associated with tobacco smoke exposure. The oxidative stress impairs the activity of the glucocorticoid receptor (GR) corepressor histone deacetylase 2 (HDAC-2), which consequently reduces the ability of glucocorticoids to mediate trans repression of proinflammatory genes^{29,35,37,38}. Therefore, there is an extreme need for alternative treatments capable of preventing and reversing the natural progression of this disease.

Overall, the heterogeneity of these two pathologies and the lack of responsiveness to mainstay therapies make their therapeutic management extremely difficult and force the scientific community to focus on new pathways that regulate inflammatory response to find alternative and more effective therapeutic treatments.

1.2 Class PI3K δ as Therapeutic Target in COPD and Severe Asthma

In the last decade, there has been a great interest on the development of kinase inhibitors as inflammatory modulators, especially where traditional anti-inflammatory therapies are less effective³⁰, as in severe Asthma and COPD. Class I PI3Ks are among this group of kinases. PI3Ks are involved in cellular mechanisms that lead to the activation of inflammation, corticosteroid resistance, cellular senesce resulting in accelerated aging, especially under conditions of oxidative stress³⁹ (Figure 7).

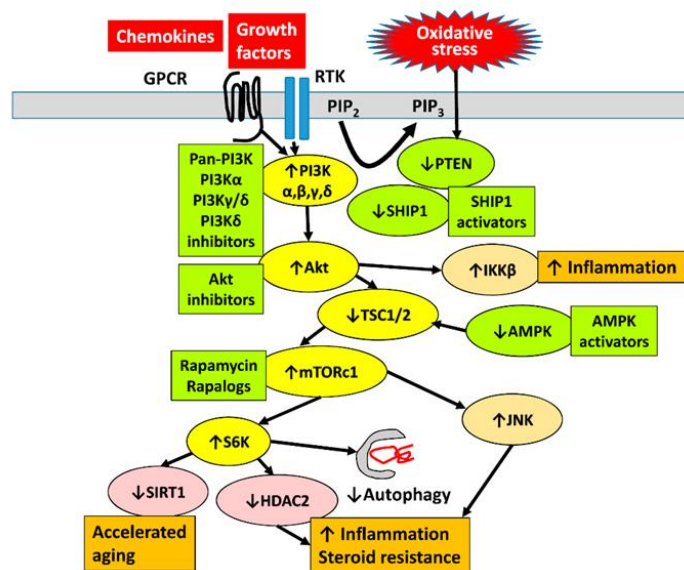


Figure 7: PI3K signalling pathway and its engagement in inflammation.³⁰

Recent studies on murine knockouts have elucidated the structure, the distribution and the functions of PI3Ks and enabled their classification. Based on these studies, the biological role of PI3K δ and γ isoforms in the immune response has clearly emerged.

The key function of PI3K δ in immune response has been demonstrated by numerous studies with mutant mice and PI3K δ selective inhibitors. Additionally, researches conducted in airway inflammation models have highlighted the specific role of this isoform in airway inflammatory condition which characterizes respiratory diseases such as Asthma and COPD.

PI3K δ is implicated in the development, differentiation and in the functioning of T and B cells⁴⁰ and required for cell activation of TCR and BCR. Linked to that, T cells from p110 δ mutant mice showed reduced antigen induced proliferation *in vitro*, while p110 δ -deficient B-cells proliferation in

response to B cell receptor stimulation is inhibited and their function as antigen presenting cells (APC) is impaired⁴⁰.

PI3K δ is also responsible for mast cells homeostasis and plays an important part in the allergic response⁴¹. Its involvement in the allergic response has been confirmed with a study conducted in an acute allergic airway inflammation and hyperresponsiveness murine model. The use of a PI3K δ selective inhibitor, IC87114, led to a reduction of cell infiltrates in the lung, mucus hypersecretion, cytokine and chemokine levels, ICAM-1 (intercellular adhesion molecule 1) and VCAM-1 (vascular cell adhesion molecule 1) expression and airway hyperresponsiveness⁴².

Implications of PI3K δ in promoting neutrophil trafficking into inflamed tissue has also been revealed. PI3K δ participates in neutrophil trafficking by modulating the proadhesive state of these cells in response to tumour necrosis factor α (TNF α)⁴³. Moreover, PI3K δ inhibition with IC87114 led to a reduction of neutrophil accumulation into inflamed tissue in a murine LPS model acute lung injury⁴³.

Another study demonstrated as PI3K δ is overexpressed in lung macrophages of COPD patients and causes the hyperphosphorylation and ubiquitination of histone deacetylase 2 that reduces its activity and, consequently, its glucocorticoid sensitivity⁴⁴. Consequently, the selective inhibition of PI3K δ might restore glucocorticoid responsiveness in patients affected by COPD and Severe Asthma³⁸.

Additionally, a study has revealed as PI3K δ inhibition can induce human airway smooth muscles cells relaxation producing airway dilation comparable to that obtained with β agonists⁴⁵.

In sum, PI3K δ shows considerable promise as a drug target for the treatment of airways chronic inflammation underlying diseases such as Asthma and COPD (**Figure 8**).

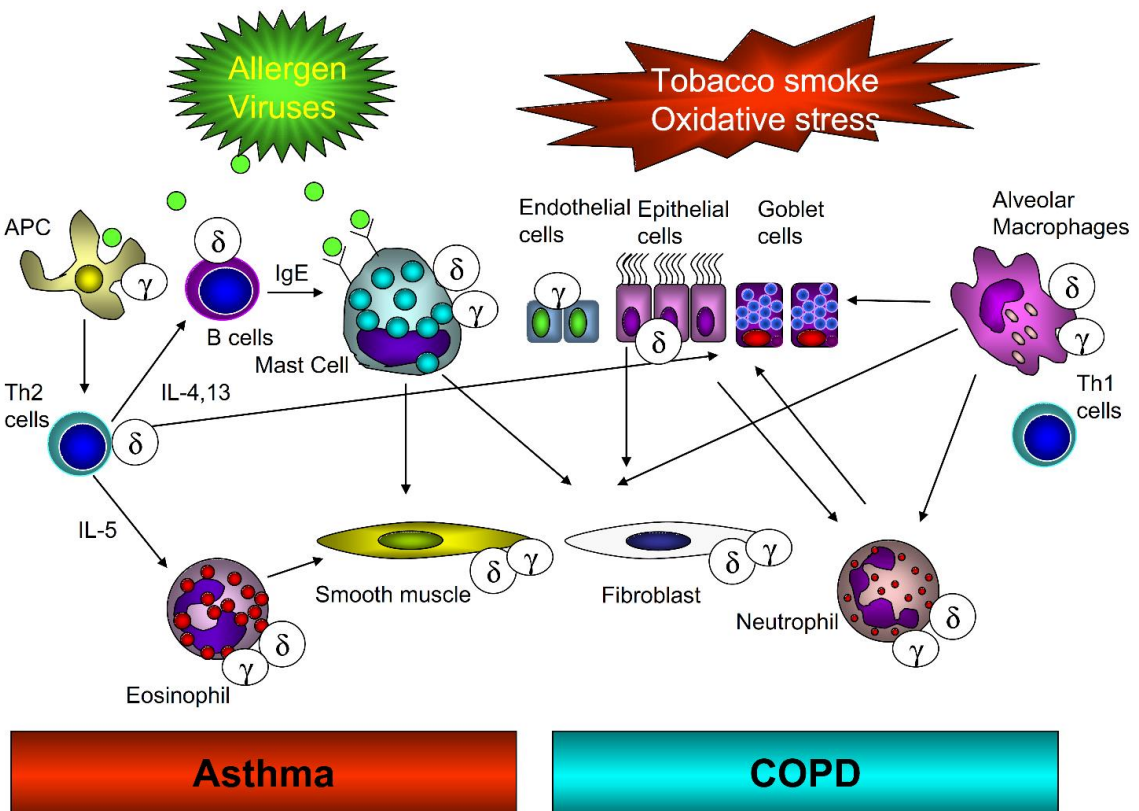


Figure 8: Targets for PI3K δ and γ in airway inflammation in asthma and COPD³⁹.

1.3 Phosphoinositide 3-Kinases Family

The PI3-kinases (PI3Ks) belong to a family of lipid kinases that are able to phosphorylate the 3-hydroxyl group of the inositol ring leading to three different substrates: PtdIns, PtdIns4P, and PtdIns(4,5)P₂⁴⁶. These phosphorylated phosphoinositides act as second messengers and their dephosphorylation is mainly catalysed by two phosphatases: PTEN (Phosphatase and tensin homolog deleted on chromosome 10) and SHIP (SH2 domain-containing inositol 5-phosphatase)⁴⁷. PI3K activities have been reported in all eukaryotic cells and linked to many key cellular activities such as cell growth, proliferation, motility, differentiation, survival and intracellular trafficking⁴⁸. Moreover, the link between PI 3-kinase activity and many human diseases such as allergy, inflammation, heart disease and cancer has made this kinase family an interesting and attractive therapeutic target⁴⁸.

The PI3-kinases can be divided in three functional classes based on their protein domain structure, lipid substrate specificity and associated regulatory subunits: Class I enzymes are receptor-regulated PtdIns(4,5)P₂ kinases; Class II enzymes are PI3K-C2 kinases and Class III is the PtdIns-specific enzyme Vps34. Mammals present eight isoforms of PI3K: four isoforms for Class I, three for Class II and only one for Class III isoform 34, whereas *C. elegans* and *D. melanogaster* present a single representative for each class. Yeast and plants have only a sole Class III PI3K⁴⁹.

Additionally, there is also a class IV group of PI-3-kinase-related protein serine-threonine kinases which have been identified in all eukaryotes. Mammals present four of these kinases: TOR (the target of the rapamycin, ATM (Ataxia telangiectasia mutated), ATR (Ataxia telangiectasia mutated related) and DNA-PK (DNA- dependent protein kinase).

1.3.1 Class I PI3Ks

The Class I PI3Ks family is the most studied among all the three classes due to its association with human pathologies such as cancer, inflammation, cardiovascular and metabolic human diseases.

Class I PI3Ks are heterodimeric enzymes made of a 110-kilodalton catalytic subunits, called p110, and an adaptor-regulatory subunit. Catalytic subunits catalyse the ATP-mediated phosphorylation of membrane localized phosphatidylinositol-4,5-bisphosphonate (PIP₂) to phosphatidylinositol (3,4,5)-triphosphate (PIP₃)⁴⁶.

Class I is further divided in two classes: Class IA and Class IB according to the type of their regulatory subunits and their upstream activators.

Class IA PI3K are heterodimeric proteins constituted of different catalytic subunits, p110 α , p110 β and p110 δ encoded by *PIK3CA*, *PIK3CB*, and *PIK3CD* genes, respectively. Each catalytic subunit shares the same domain composition: an amino-terminal adaptor-binding domain (ABD) or p85-binding domain, a Ras-binding domain (RBD), a C2 (protein-kinase-C homology-2) domain, a helical domain and a carboxyl-terminal kinase domain (**Figure 9**). The kinase domain is responsible for the primary function of the PI3Ks: the phosphorylation of PIP₂ to PIP₃. PIP₃ is then responsible for the activation of several downstream protein kinases, including promoting phosphorylation and activation of AKT⁵⁰.

Class IA catalytic subunits physically interact through the amino terminal domain with a family of Src homology 2 (SH2)-domain-containing regulatory adaptor proteins p85 α , p85 β , p55 α , p55 γ and p50 α . The P85 proteins interacts through two SH2 domains with sequence-specific phosphorylated tyrosine residues on auto phosphorylated RTKs⁴⁸.

Class IB is represented only by p110 γ , expressed by the *PIK3CG* gene, which differs from other Class IA proteins in its extreme N-terminus domain that lacks the adaptor-binding domain (ABD) and in its regulatory partners, p101 or p87 subunits^{50,49}; p101 and p87 lack SH2 domains and do not have homology to other proteins (**Figure 9**). The Class IB protein are mainly activated by GPCR proteins: the activation process seems to predominantly involve interactions with G $\beta\gamma$ subunits and possibly G α subunits⁵¹

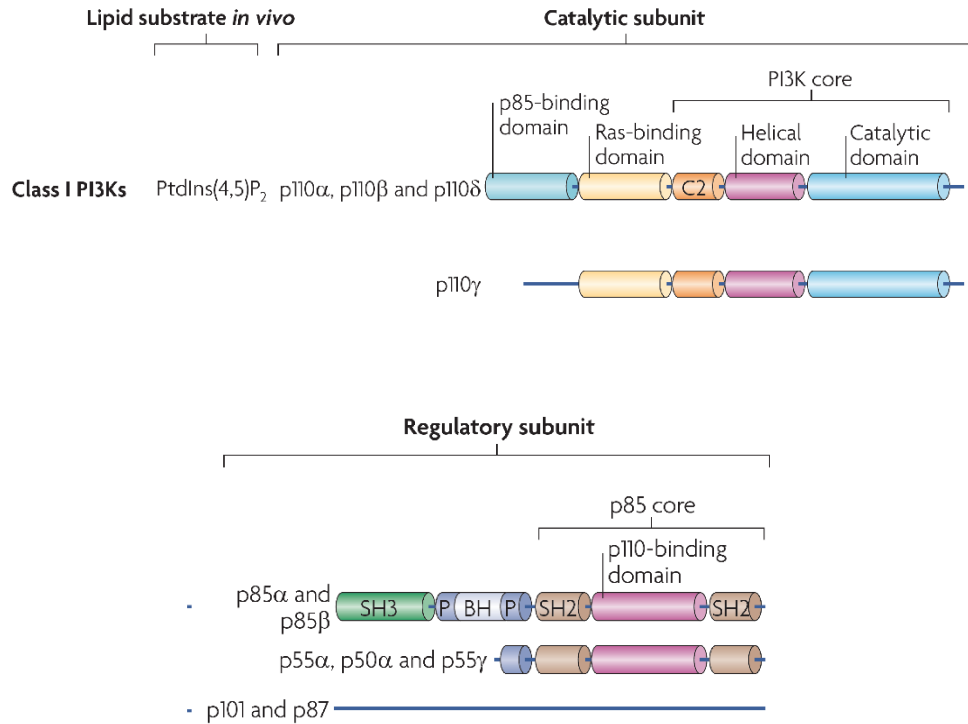


Figure 9: Structure of Class I catalytic domain and regulatory subunits.⁴⁹

1.3.2 Class II PI3K

Human Class II PI3K encompasses PI3K-C2 α , PI3K-C2 β and PI3K-C2 γ . Class II PI3Ks were not isolated in association with a regulatory subunits⁴⁸. They are large (170-200 kDa) monomeric enzymes. They are thought of producing $\text{PtdIns}(3)\text{P}$ or $\text{PtdIns}(3,4)\text{P}_2$. They are not cytosolic, but they are associated with membrane structures, including plasma membrane and intracellular membranes^{48,47}. Their activation can be triggered by extracellular signals, such as integrin engagement, growth factors (e.g. insulin, EGF, SCF and HGF) and chemokines⁴⁷.

1.3.3 Class III PI3K

The vacuolar protein-sorting protein (Vps34p) represents the class III PI3K and it is only able to convert PtdIns to $\text{PtdIns}-3\text{-P}$ and it was first identified in *Saccharomyces cerevisiae*⁴⁸. This protein seems to have an essential role in the trafficking cellular events encompassing autophagy and phagosome formation. Based on its role in autophagy, Class III PI3K has become an attractive target for the treatment of many human diseases such as cancer, pathogen infection and neurodegeneration⁵².

1.4 Class I PI3Ks Signalling Inputs, Outputs and Distribution

Class IA PI3Ks are activated through the interaction with p85 regulatory subunits. These subunits contain Src homology domains which bind phosphorylated tyrosine (pTyr) in a specific sequence. p85 subunits have the important role of stabilizing the inactive catalytic subunits. The engagement of the p85 SH2 domains by the pTyr relieves the p85 mediated inhibition and bring the catalytic subunits in contact with PIP2 in the membrane. In the same way, in ClassIB p101 and p87 acts for p110 γ . However, p101 and p87 are predominantly activated by GPCRs.

GPCR transmit their signals through heterotrimeric G proteins. *In vitro*, G $\beta\gamma$ activates p110 β and p110 γ but not p110 α and p110 δ . However, GPCRs can activate Tyr kinase and Ras and, in this fashion, in turn activate isoforms which are not receptive to G $\beta\gamma$ ⁴⁹.

Ras family has also a documented role in the activation for all Class I PI3K apart from p110 β for whom the role of Ras is less clear. Moreover, the RAS family member TC21 seems to have a role in the upstream signalling of p110 δ ⁵³.

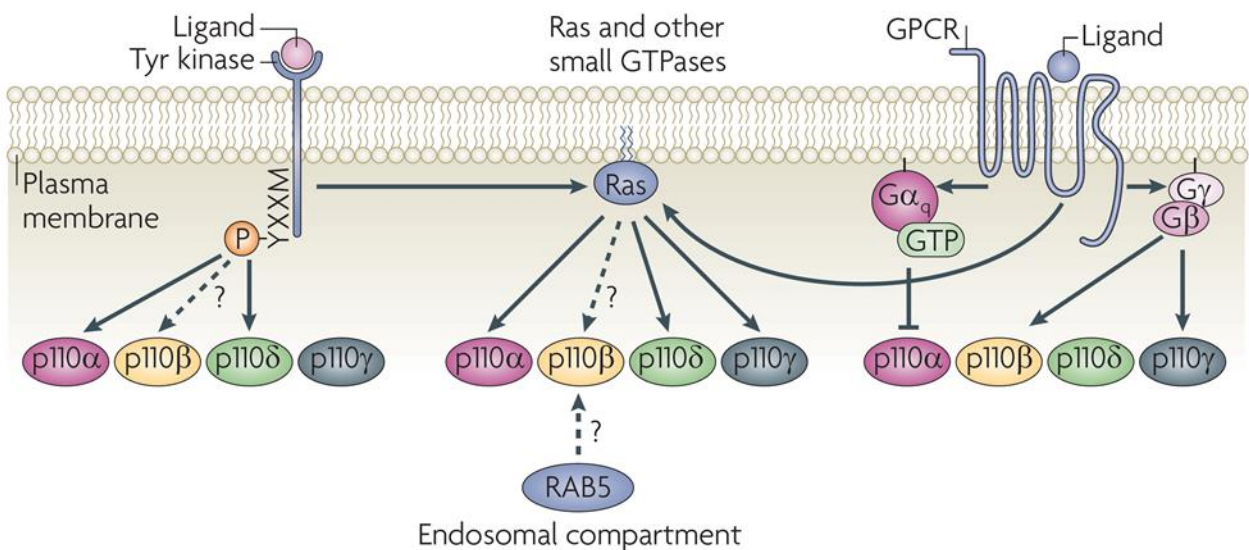


Figure 10: Class I PI3Ks signalling inputs.⁴⁹

The major product of the Class I PI3K activation is PIP3 which can coordinate the function of many proteins that can bind these lipids through a PH domain; Ser/Thr and Tyr protein kinases such as AKT and PDK1, protein tyrosine kinases of Bruton's tyrosine kinases (BTKs) and Tec family, the Cytohesins (GRP1/ARNO), and further more diverse GEFs (Guanine nucleotide Exchange Factors) and GAPs (GTPase Activating Proteins) for GTPases of the Ras superfamily⁵⁴. All these PI3K

downstream effectors are involved in many processes like cell growth, proliferation, survival, cell growth, differentiation, apoptosis, and cytokine production⁴¹.

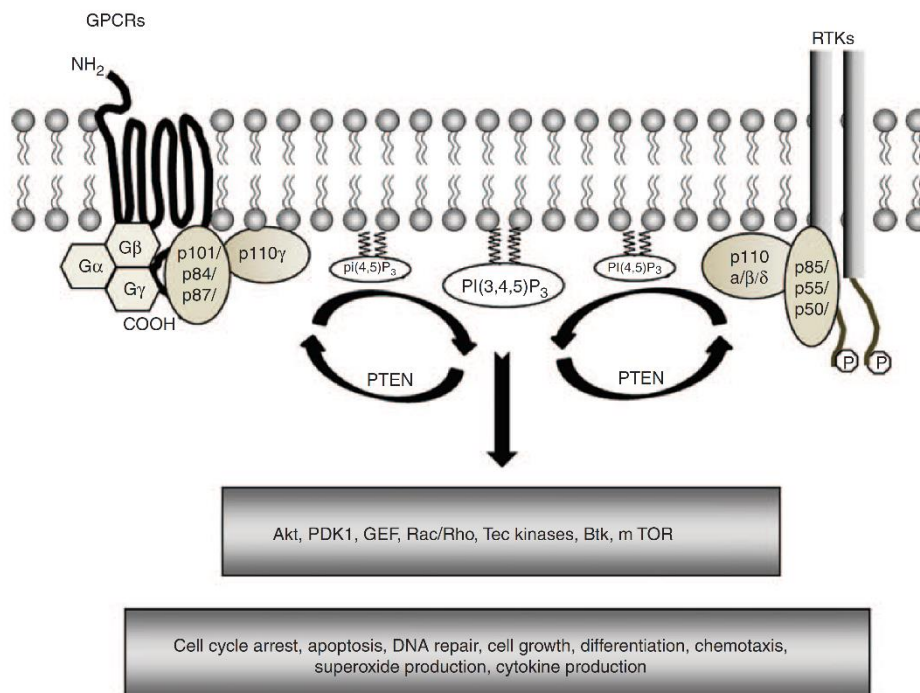


Figure 11: Class I PI3K effectors.⁵⁵

The expression of Class I PI3K can vary among different cells and tissue. Commonly, p110α and p110β are ubiquitous and present in embryonic and adult tissues. It has been reported as p110α plays a critical role in the insulin signalling in two cell types, adipocytes and myotubes⁵⁶ whereas p110β is involved in the platelet aggregation⁵⁷. P110δ is highly enriched in leukocytes⁵³ and present at intermediate levels in neurons⁵⁸. p110γ are mostly expressed in leucocytes but it has also been found at lower levels in other cell types, including cardiomyocytes, endothelial cells, pancreatic islets and smooth muscle cells⁵⁸.

1.5 Structural Determinants of the PI3K Catalytic Subunit

The crystallization of p110 γ in 1999 by Walker et al⁵⁹. revealed fundamental structural features of the catalytic subunits of Class I PI3K kinases.

The catalytic domain exhibits a bilobal organization: a smaller N-terminal lobe (residues γ 726-883) and a larger C-terminal lobe (residues γ 884-1092), (**Figure 12**).

The N-terminal lobe presents a five-stranded anti parallel β -sheet surrounded on one side by a helical hairpin ($k\alpha$ 1- $k\alpha$ 2) and a small two-stranded β -sheet ($k\beta$ 1- $k\beta$ 2) and on the other side by $k\alpha$ 3 helix and the C-terminal lobe⁵⁹. The $k\beta$ 3- $k\beta$ 4 loop corresponds to the protein kinase glycine-rich loop also known as *P-loop*. This loop interacts closely with the phosphates of the bound ATP, but unlike the protein kinases, it contains no glycine.

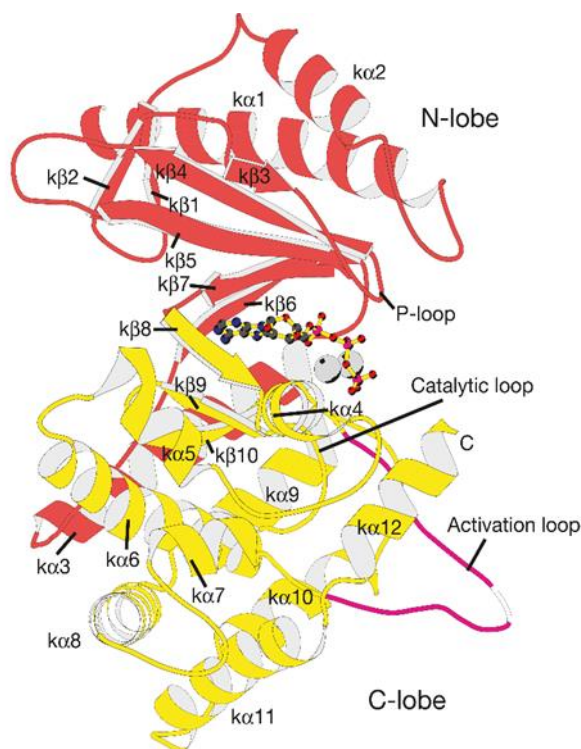


Figure 12: The catalytic subunit of PI3K γ .⁵⁹

The C-terminal domain contains part of the ATP binding site, the binding site for the phospholipid substrates, the catalytic loop and the activation loop. The structure of the catalytic domain is highly conserved among class I PI3Ks^{60,61}, especially for residues around the substrate-binding pocket situated between the N and C-terminal lobes of the kinase domain which identified the ATP binding pocket.

1.5.1 Structural Features of the ATP Binding Site

Further studies on Class I PI3K structures in complex with several inhibitors⁶² have revealed a set of common interactions in the ATP binding pocket which have been extremely useful for the design and the develop of pan or selective PI3K inhibitors.

The PI3K binding pocket can be divided in four different regions: an “adenine” pocket (hinge), a “specificity” pocket, an “affinity” pocket (hydrophobic region I) and the hydrophobic region II located at the mouth of the active site⁶³ (**Figure 13**).

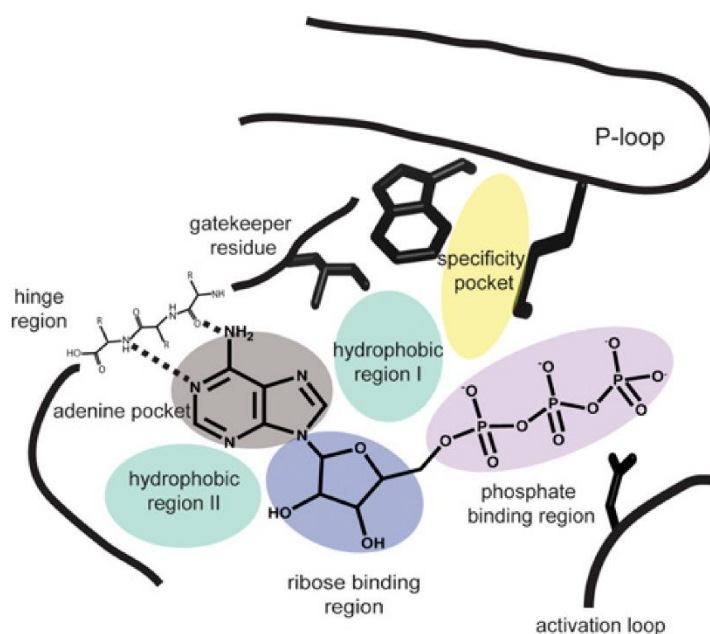


Figure 13: Schematic representation of the PI3K binding pocket.⁶⁴

In Class I PI3K kinases, the adenine region is delimited by three key isoform-conserved residues: a hinge valine, a gatekeeper isoleucine and a tyrosine residue.⁵⁰ The isoleucine is only a formal gatekeeper because due to a change in orientation of the $\kappa\beta 7$ strand it is actually a tyrosine that acts as functional gatekeeper. This structural change compared to other protein kinases allows the accommodation of more sterically encumbering hinge binding motif and this might explain the ease of obtaining selectivity for PI3K family over other protein kinases⁵⁰. In the Hinge Region, there are key amino acids γ Ile881 (Val in α , β and δ) and/or γ Val882 and no conserved residues, such as Glu880 in p110 γ that normally interacts with the adenine ring via hydrogen bonds (**Figure 14**). Therefore, one of the most important features for Class I PI3K inhibitors is the presence of a “hinge binding

motif". This Hinge binder is characterized by a morpholinyl, purinyl or amidic substituents which anchor the inhibitor in the ATP binding site via hydrogen bonds and mimic the interaction that N1 or N6 of adenine ring establishes with the enzyme.^{50,62,65}.

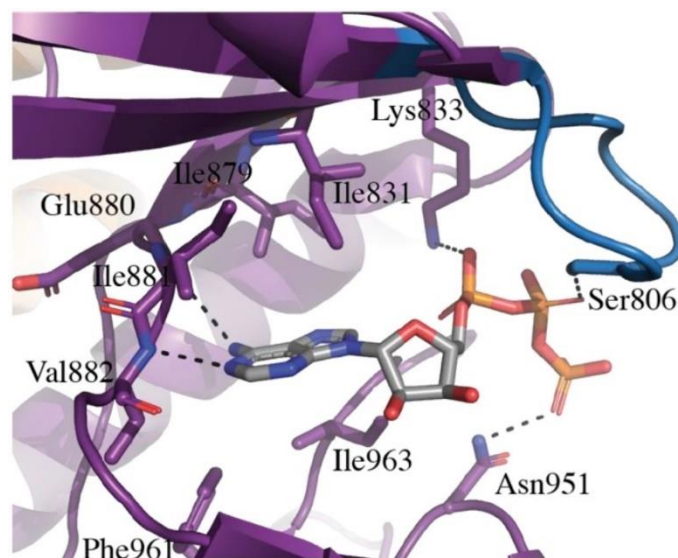


Figure 14: ATP binding site (PDB ID 1E8X), N1 and N6 of adenine ring interacts in the hinge region establishing hydrogen bonds with the backbone of γ Glu880 and γ Val882⁶⁵. The α -phosphate interacts with γ Lys833 and the β -phosphate with γ Ser806 and γ -phosphate with γ Asn951.

The hydrophobic region I also referred as *affinity pocket* in PI3K is not accessed by ATP and it is surrounded by conserved residues. Extension of PI3K inhibitors in this region has shown to have a boost in potency. It has been reported as the establishment of interactions with the *affinity pocket* had also an impact on selectivity towards isoforms⁶³. Difference in selectivity can be influenced by hydrogen bonding networks to non-conserved amino acids surrounding the pocket (**Figure 15**). However, the role of the affinity pocket on selectivity is still not fully understood and difficult to rationalize⁶⁵.

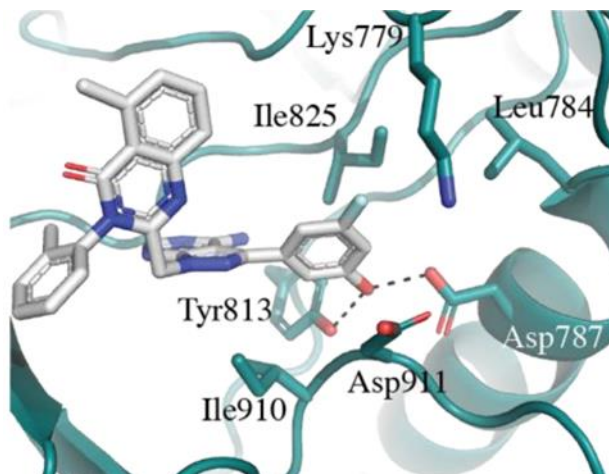


Figure 15: The affinity pocket (PDB ID 2WXG), the hydrogen bond network established by the ligand with δ Tyr813, δ Asp911 and δ Asp787.⁶⁵

The hydrophobic region II also known as ribose binding pocket is a region formed by eight amino acids C-terminal to the Hinge Region and has four positions that are not conserved in the four isoforms. The interaction with this region has been shown to be decisive for the development of selective inhibitors.

The *P-loop* which lines above the hydrophobic region II (**Figure 13**) presents less variability between isoforms but minimal differences in this region can affect the conformational plasticity of the *P-loop* and the accessibility of the specificity pocket which plays the major role in determining selectivity over PI3K isoforms. Its role will be described in detail in the following paragraph.

1.5.2 The Specificity Pocket and its Role in Determining PI3K δ Selectivity

The specificity pocket was first discovered in the PIK39-p110 γ crystal structure⁵⁶. PIK39 is a PI3K δ selective inhibitor exhibiting a 100x selectivity over PI3K β and γ no inhibition of PI3K α up to 100 μ M. Knight et al. demonstrated as this inhibitor was able to induce a movement of a conserved methionine residue on the P-loop. In this complex, γ Met804 shifts from an “up” position, in which it forms the ceiling of the ATP binding pocket, to a “down” position. The main consequence of this movement is to create an induced-fit, hydrophobic pocket at the entrance of the ATP-binding site⁵⁶, named as *specificity pocket*. Mutation of Met752 in p110 δ (M752I and M752V) led to an achieved resistance to PIK-39 activity supporting the critical role of this conserved amino acid in gating the pocket⁵⁶ and its role in obtaining inhibition for p110 δ .

The experimental determination of the complex of the protein with Idelalisib, the first-in-class selective inhibitor of PI3K δ , confirmed that the engagement of the specificity pocket upon kinase binding contributes to the extreme selectivity of this compound⁶⁶(**Figure 16**).

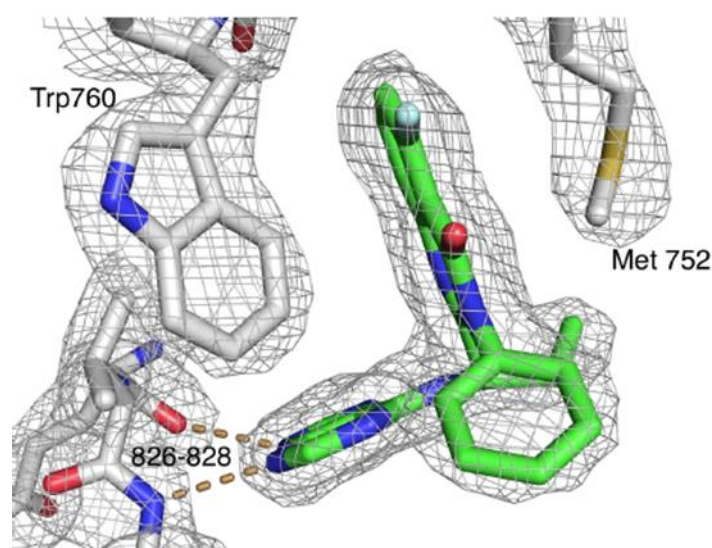


Figure 16: The specificity pocket in the cocrystal structure of the p110 δ isoform in the presence of Idelalisib, PBD ID 4XE0.⁶⁶

Berndt et al. showed as movement in the P-loop (residues 752–758 in p110 δ) is limited to local changes, whereas in p110 γ requires a conformational change that involves much of the N-lobe moving with respect to the C-lobe. Moreover, dynamic simulation showed that the opening of the

specificity pocket is accompanied with a synchronized movement of δ Trp760 and δ Met752(**Figure 17a**). However, in p110 γ Trp812 is involved in a hydrogen bond to γ Glu814 which in turns interacts with γ Thr827. This hydrogen bond network reduces the flexibility of the Trp812 residue disfavoring the opening of the pocket in p110 γ compared to p110 δ ⁵⁰. Same behaviour was observed in p110 α crystal structure⁵⁶ (**Figure 17b**).

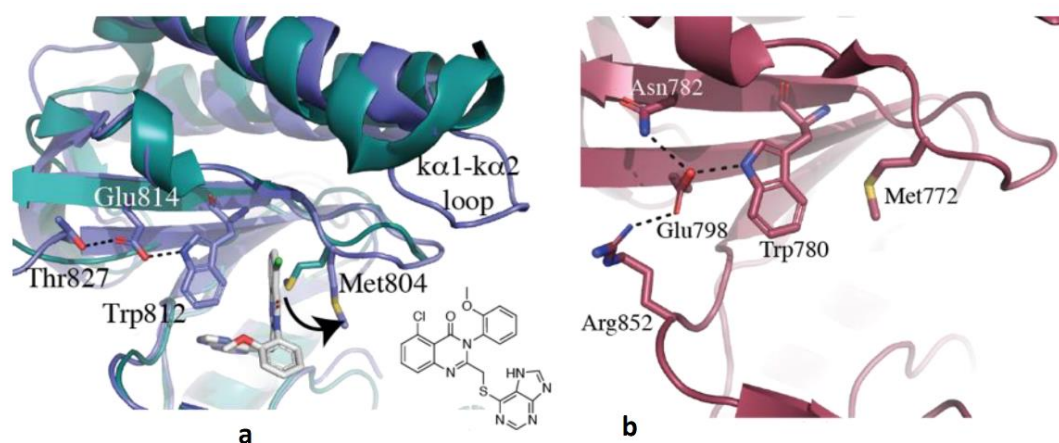


Figure 17: **a)** The specificity pocket in p110 δ and p110 γ and PIK39 shown in the binding site. P110 δ shown in green and p110 γ and in purple. The movement of γ Met804 required for the opening of the specificity pocket. **b)** Stabilizing interactions of α Trp780 in p110 α .⁶⁵

A study of reciprocal mutagenesis on p110 β demonstrated as a non-conserved amino acid β Tyr778 close to the conserved Met residue is responsible for the conformational plasticity of the P-loop. Loss of affinity for p110 β selective inhibitor in the mutated p110 β showed as this residue is important in determining selectivity and potency also for this isoform. In the same position, the residue is aliphatic for p110 α and p110 γ (Ileu and Val, respectively) while in p110 δ , like in p110 β , is aromatic (Phe). This could suggest a potential similar behaviour for p110 δ and p110 β in the interaction with their inhibitors⁶⁷.

All these findings demonstrated as, although the specificity pocket is induced by the movement of two conserved residues, the accessibility of this pocket is mainly influenced by the non-conserved amino acids surrounding this area and moreover by the energy required to open the pocket explaining why this region is more accessible in the p110 δ .

1.6 Class I PI3K Inhibitors

The validation of the role of PI3K as a therapeutic target in many diseases has led to an increasing of research outputs from pharmaceutical industry and academic groups. This is proved by the huge amount of medicinal chemistry-based patent disclosures, with a total of 418 chemical patents and 192 medicinal publications being published since 2012⁶⁸ (**Figure 18**).

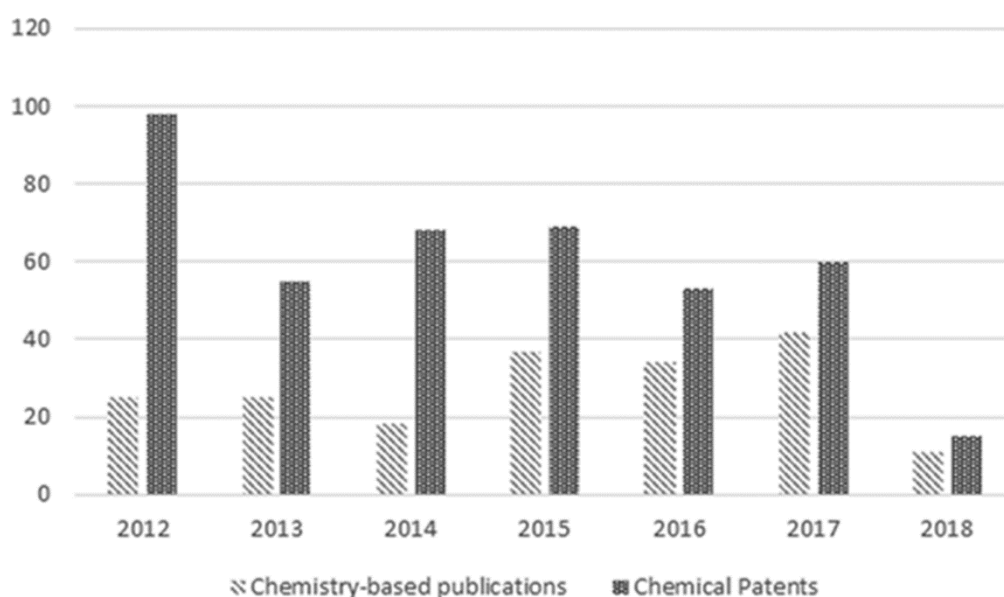


Figure 18: PI3K medicinal chemistry based publications and PI3K chemical patents from 2012 to 2018.⁶⁸

Recently, evidences supporting the role for inhibition of PI3K α in diabetes, PI3K β in thrombosis therapy and PI3K δ and γ in inflammatory and autoimmune diseases led to an increasing effort in developing selective rather than pan PI3K inhibitors. One the main advantages in fact of selective inhibition is the high reduction of side effects.

This growing interest in selective inhibition is particularly true for PI3K δ and PI3K γ inhibitors where there has been a great deal progress in chemistry and biology proved by the high number of released patents and by the entering of 19 compounds in clinical trials⁶⁹. The approval of Idelalisib, for the treatment of lymphoma is for sure the most successful result of investment in this field. Now, 13 PI3K δ , 5 PI3K δ/γ and 1 PI3K γ inhibitors are under clinical evaluation⁶⁸. These numbers prove as

interest of pharmaceutical companies is still more focused on PI3K δ , or dual (PI3K δ and PI3K γ) inhibition, rather than PI3K γ .

The majority of the reported PI3K δ inhibitors belongs to Type I ATP group but there is also one covalent PI3K δ inhibitor described⁷⁰. Following paragraphs present an overview of some selective PI3K δ inhibitors of public domain, their binding mode to the enzyme and their therapeutic applications.

1.6.1 Propeller Shaped PI3K δ -Selective Inhibitors

First propeller-shaped PI3K δ selective inhibitors were described by Berndt et al⁶³. They described compounds that were able, in complex with the protein to adopt a propeller shape binding mode with “three blades” at an angle of approximately 120° to each other. Generally, these three blades are represented by a central core heterocycle, typically a bicyclic aromatic system, a hinge binding moiety linked to the core by one or two atoms that allows it to adopt an orthogonal arrangement, and a third blade which is typically but not always an aromatic ring⁶⁹. By assuming this particular conformation, these inhibitors are able to open the specificity pocket, that has been previously described in paragraph 1.5.2, gaining potency and selectivity for the isoform of interest, PI3K δ (**Figure 19**).

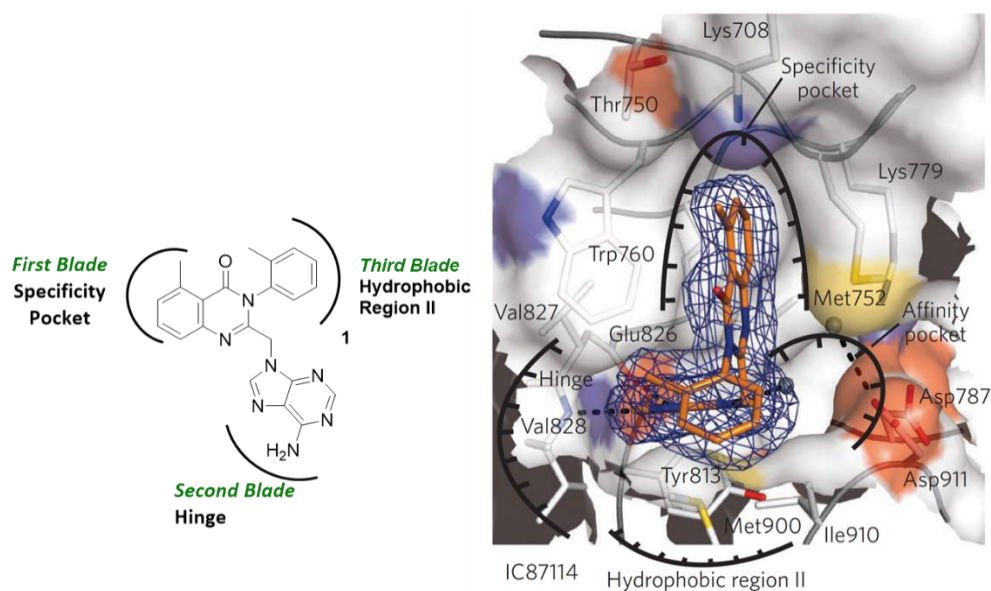


Figure 19: The propeller-shaped p110 δ -selective inhibitor **IC87114** and its main interactions in the p110 δ ATP binding site. Image adapted from Berndt et al.⁶³

The purine group resides within the adenine pocket and establishes hydrogen bonds to the hinge residues Glu826 and Val828. The quinazolinone moiety is sandwiched into the induced hydrophobic specificity pocket and the phenyl ring protrudes into the hydrophobic region II.

1.6.1.1 Propeller Shaped Inhibitors: 6,6 and 5,6 fused systems

One of the most successful propeller-shaped PI3K δ inhibitor is Idelalisib, **2 (Figure 20)**. This compound was discovered by Calistoga and then further developed by Gilead and approved by the FDA in 2014 for the treatment of chronic lymphocytic leukemia (CLL), follicular lymphoma (FL), and small lymphocytic lymphoma (SLL). Idelalisib is characterized by a 6,6-fused ring systems, a quinazolinone core connected to a purine moiety that acts as hinge binder while the phenyl ring interacts with Asp832, Thr833, and Asn836^{66,69,68}. The binding mode of this compound is very similar to that of **IC87114**, compound **1, (Figure 19)**.

The use of 6,6-fused rings demonstrated to be a winning idea that was followed by other research groups for the design of their selective inhibitors. In this regard, Umbralisib, **3 (Figure 20)** a PI3K δ selective inhibitor developed by Rhizen Pharmaceutical, shows a chromenone as central core. At the moment, Umbralisib has entered phase III for the treatment of CLL⁶⁸. Here, the 4-amino-pyrazolo pyrimidine serves as the hinge binder and the chromone binds in the specificity pocket while the additional decorated phenyl ring interacts with the affinity pocket⁶⁵.

Another central core suitable for the design of PI3K δ selective inhibitors is quinoline which was used by Amagen for its clinical candidate AMG319, **4 (Figure 20)**. This compound has entered phase 2 for the treatment of Human Papillomavirus (HPV) and negative head and neck squamous cell carcinoma (HNSCC)⁶⁸.

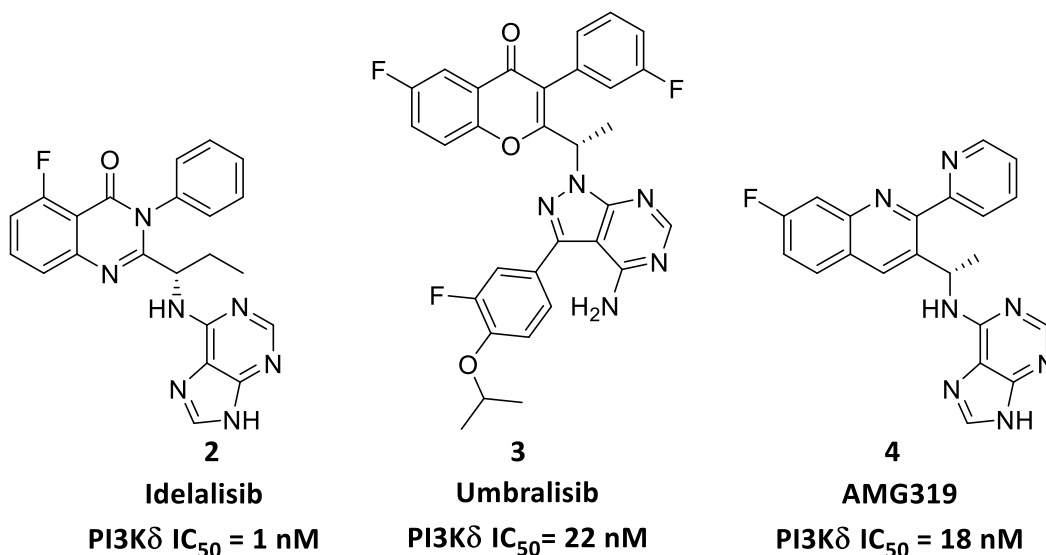


Figure 20: Propeller shaped 6,6-fused systems inhibitors and their enzymatic p110 δ IC₅₀.

5,6 fused systems such as pyrrolo-triazinones, imidazo-pyridazine/pyridines, pyrazolo-pyrimidine/pyridines and thiazolopyridinones were deeply explored as central cores for the design of PI3K δ inhibitors.

LAS195319, (**5**) and LAS191954 (**6**) (**Figure 21**) are the result of the extensive SAR exploration conducted by Ammirall on 5,6 fused systems, specifically on pyrrolo-triazinone scaffold⁷⁰. LAS191954 has entered clinical development for the treatment of pemphigus⁶⁸ while LAS195319 was presented as a future clinical candidate for the treatment of respiratory diseases⁷¹.

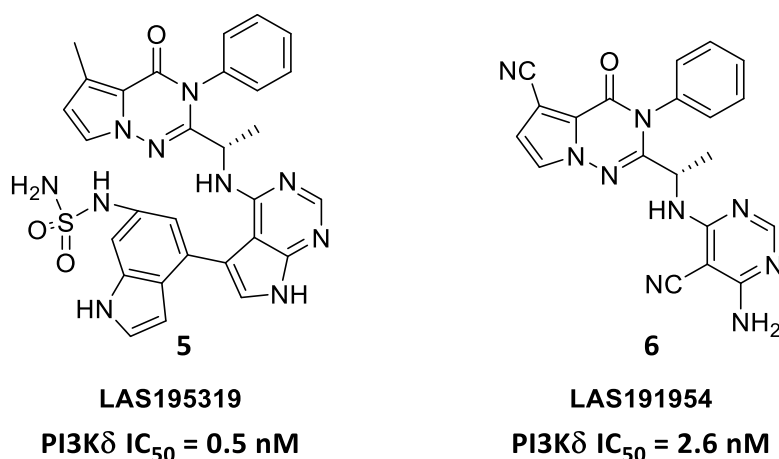


Figure 21: PI3K δ inhibitor 5,6 fused system class designed by Ammirall.

1.6.2 “NonPropeller” Shaped PI3K δ Inhibitors

Adopting the propeller shaped binding mode is not the only way to achieve PI3K δ selectivity. Genentech scientist discovered a series of selective pyrido-pyrimidines which showed high selectivity for PI3K δ isoform. These compounds are characterized by a pyrido-pyrimidine central core, a morpholine group acting as hinge binder, a substituted indole and a substituted basic group which were both considered accountable for PI3K δ selectivity. Indole can interact with the affinity pocket making a peculiar hydrogen bond network with Tyr867 and D964, which is more favourably accommodated in PI3K δ than in other isoforms. The substituted basic group, on the other hand, is able to target a specific area, the so-called “Tryptophan-shelf”^{68,72}, created by the Thr750 which is distinct in PI3K α , β and γ (Arg770, Lys771 and Lys802). This non-conserved residue allows inhibitors to access δ Trp760 which cannot be reached in other isoforms.

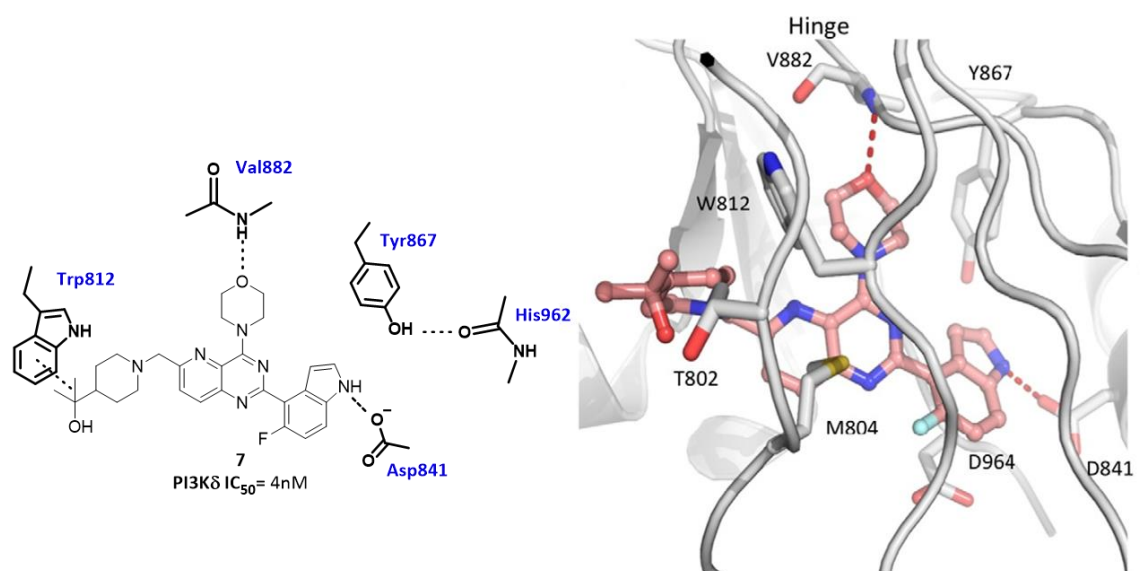


Figure 22: Co-crystal structure of **7** bound to PI3K γ and its key interactions in the ATP binding site.⁷²

The most active compounds of this series, compound **7** (PI3K δ = 3.8 nM) progressed to in vivo studies in mouse and rat and demonstrated PK properties that support its use in animal models of diseases where PI3K δ is involved⁷².

Another non propeller shaped PI3K δ selective inhibitor is CDZ173 (Leniolisib) (**8**), (**Figure 23**). This compound (PI3K δ IC₅₀ = 11 nM) demonstrated to potently inhibit antigen-specific antibody

production and reduced disease symptoms in a rat collagen-induced arthritis model. CDZ173 is currently undergoing phase II/III for primary Sjögren's syndrome and in PASLI, a disease caused by gain-of-function mutations of PI3K δ ⁶⁸⁷³. CDZ173 shows 5,6,7,8-tetrahydropyrido[4,3-d]pyrimidine as a central core, where pyrimidine is the hinge binder, the 2-methoxy-3-(trifluoromethyl)pyridine extends to the affinity pocket while the propionamide group stacks to the side chain of Trp760 showing a binding mode very similar to that described for compound **7**.

The same key interaction with Trp760 was also observed for a series of indazole-based PI3K δ inhibitors developed by GSK for the treatment of respiratory diseases. This series was optimized to two compounds GSK2269557 (**9**), also called Nemiralisib, and GSK2292767 (**10**), (**Figure 23**). The first one is currently in phase 2 for treatment in COPD but was also developed for asthma and activated PI3K δ syndrome⁷⁰. The second one is the clinical back up of Nemiralisib and was selected because of a beneficial kinetic profile and improved selectivity for hERG channel⁷⁰.

The optimization of this series was focused on achieving very high potency (PI3K δ IC₅₀ < 1 nM) which is a requirement for inhaled delivery due to dose limitations⁷⁴. Moreover, the target PK profile was aimed to minimizing systemic exposure. Compounds with moderate to high clearance were developed in order to facilitate removal of the drug from systemic circulation once absorbed through the lung. They were also characterized by low oral bioavailability which is necessary to limit absorption of the swallowed fraction of the inhaled dose⁶⁸.

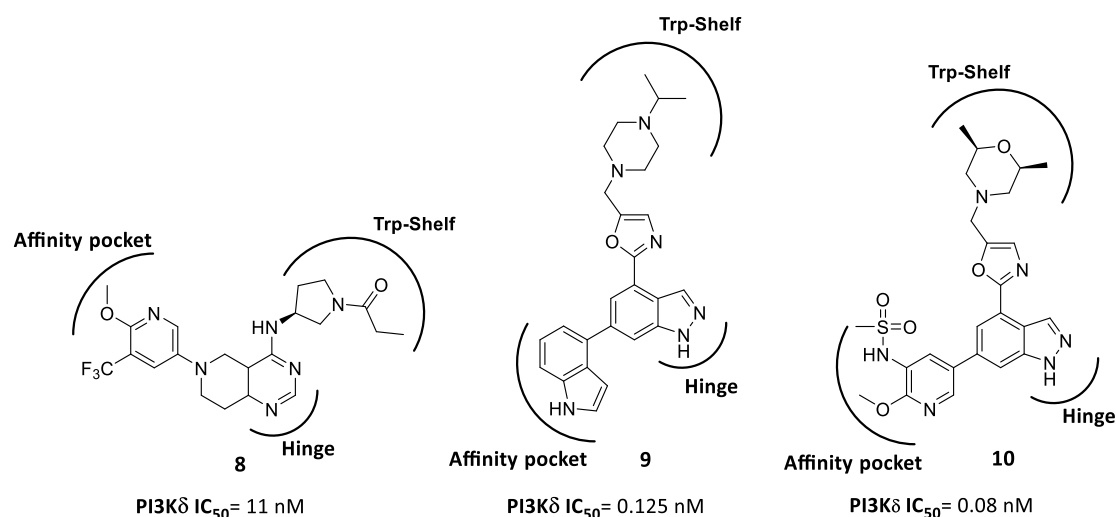


Figure 23: Structures of **8**, **9** and **10**.

2. Aim of the Project

2.1 Design and Synthesis of New, Potent and Selective PI3K δ Inhibitors

The first part of this research project was focused on targeting PI3K δ with the aim of finding a new treatment for two chronic respiratory diseases, COPD and Asthma. COPD and Asthma are both characterized by an overactive inflammatory response. Understanding the complex mechanisms underlying these pathological conditions is certainly challenging and makes finding new targets to modulate very difficult. However, targeting signalling pathway involved in immune system response could be the new route to success for defeating this type of diseases.

Class I PI3K (phosphoinositide 3-kinase) δ is overexpressed in COPD patients³⁸ and it is involved in generating of type 2 cytokine responses and allergic airway inflammation⁷⁵. Therefore, PI3K δ could represent an attractive target for finding a new treatment for those pathological conditions characterized by an over reactive immune response. Moreover, PI3K δ activation attenuates steroid responsiveness⁷⁶, thus PI3K δ inhibitors could limit corticosteroid resistance in severe Asthma and COPD. Therefore, the objective of this work was to design and synthesise a library of PI3K inhibitors with the aim of building a SAR expansion of a HIT, previously identified through an HTS of a focused library.

A simple synthetic strategy entailing only two reaction steps was identified, which allowed the synthesis of a high number of compounds in a relatively short time.

Taking advantage of this synthetic strategy, two waves of SAR expansions were designed and carried out. The first one was focused on improving δ pKi potency and achieving moderate selectivity towards other PI3K isoforms; the following one was focused on improving PI3K δ potency in cellular models and ADME properties.

3. Results and discussion

3.1 Hit Evaluation

In a previous research project focused on identifying novel PI3K inhibitors, around 7000 compounds were selected from LifeChemicals using ligand-based similarity methods and physchem property profiles and tested in PI3K δ and PI3K γ assay at two different concentrations (1 μ M and 10 μ M). 134 compounds showing a residual activity lower than 35% of the control were selected for the CRC determination. Compounds presenting a γ pKi > 6 and δ pKi > 6 were tested again in luminescence PI3K $\alpha,\beta,\gamma,\delta$ assays (ADP-glo) leading to the identification of 44 compounds exhibiting pKi \geq 6 at either PI3K γ or PI3K δ isoforms. This preliminary screening brought to the identification of seven different scaffolds. The evaluation of different parameters such as PI3K inhibitory profile, novelty and structural characteristics highlighted compound **A₁B₁** as the most promising Hit (**Figure 24**). This compound features a 7H-purin-8(9H)-one scaffold as a central core, an F-phenyl and a 4-hydroxyphenyl at position 9 and 2 respectively (**Figure 24**).

In literature, it has been reported as the aforementioned scaffold showed activity on other targets. A receptor–ligand interaction-based virtual screening identified this scaffold as no selective Eg5 inhibitor⁷⁷. Additionally, this scaffold targets other two kinases, the C-Met⁷⁸ and mTor⁷⁹.

Selective inhibition of kinases has always been a tough challenge. Most of the kinase inhibitors are ATP antagonists and their ability to inhibit specifically a selected target is not always a foregone conclusion due to the high structural similarities of their site of action. Our scaffold is not an exception showing promiscuity among different targets. However, pursuing the selectivity towards PI3K isoforms will hopefully lead to a decreased activity on other kinases.

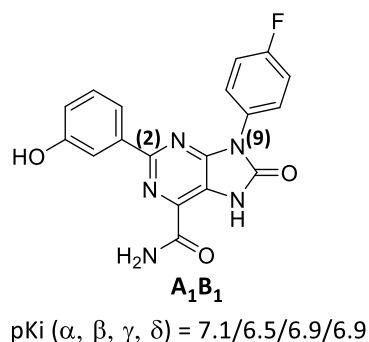


Figure 24: Hit compound from HTS.

Once identified the Hit, close structural analogues of Hit compound were selected and purchased from LifeChemicals databases and tested to perform a preliminary SAR analysis and identify structural moieties essential for the inhibitory activity. Therefore, 469 derivatives were tested in CRC mode as PI3K γ and PI3K δ inhibitors. The biological profile of the most interesting compounds is reported in **Table 1**.

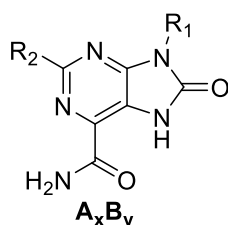
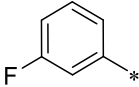
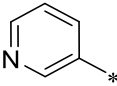
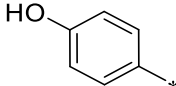
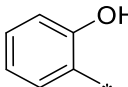
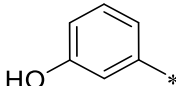
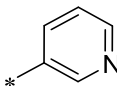
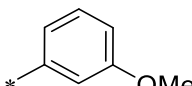
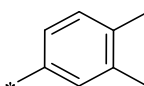
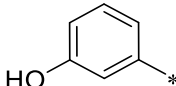
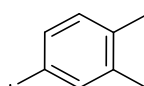


Figure 25: General structure of purchased compounds.

Despite the high number of compounds tested, the chemical diversity of these derivatives was limited. Thus, a further SAR exploration was mandatory to better understand the role of the two different substituents, such as F-phenyl and phenol rings, and their interactions with the ATP binding site in the PI3K δ catalytic subunit.

Table 1: Biological data of most interesting compounds from the preliminary SAR expansion.

Compound	R ¹	R ²	Enzymatic pK _i	
			PI3K δ	PI3K γ
A ₂ B ₃			6.0	5.8
A ₂ B ₄			6.1	5.0
A ₂ B ₅			6.1	5.9

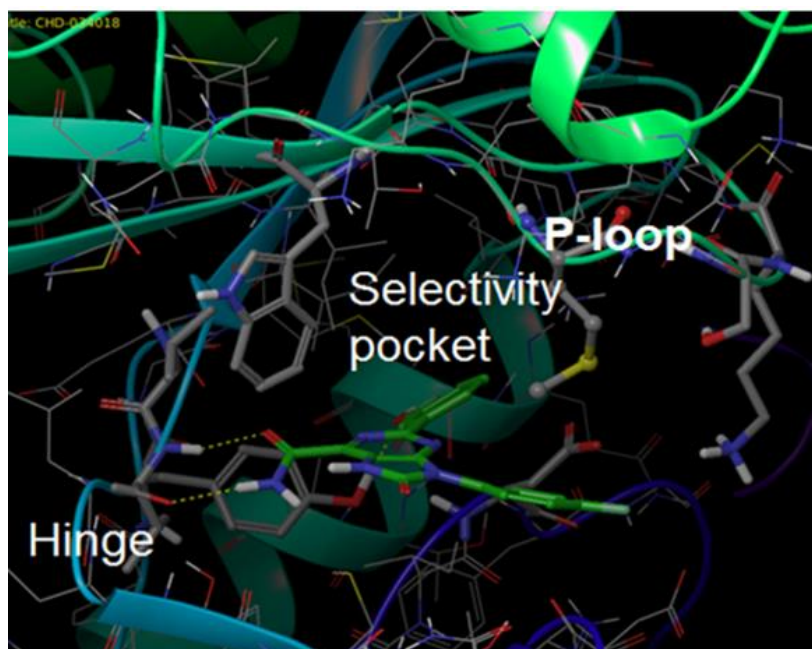
A₂B₆			6.4	6.2
A₂B₇			6.1	6.1
A₂B₈			6.1	6.0
A₂B₉			6.7	6.3
A₂B₁			7.6	7.3
A₃B₁			6.1	6.1
A₄B₁			7.0	7.0
A₅B₁			6.8	6.8
A₆B₁			7.7	7.7

3.2 First SAR Exploration

As emerged from the preliminary test, the Hit compound **A₁B₁** is a pan PI3K inhibitor. A docking study was performed to map key interactions of the Hit in the ATP binding site in murine PI3K δ catalytic domain (PDB ID: 2WXF) and to investigate lack of selectivity and sub-optimal potency for the isoform of interest (δ).

Figure 26 shows how the primary amide interacts with Val828 in the *Hinge Region*, while the phenol extends in the *Affinity Pocket* creating a network of hydrogen bonds with three different amino acids Asp787, Asp911 (DFG-in motif) and Tyr813.

Ultimately, the F-phenyl ring is projected towards the solvent and is close to Lys755 in the *P-loop* (**Figure 26**).



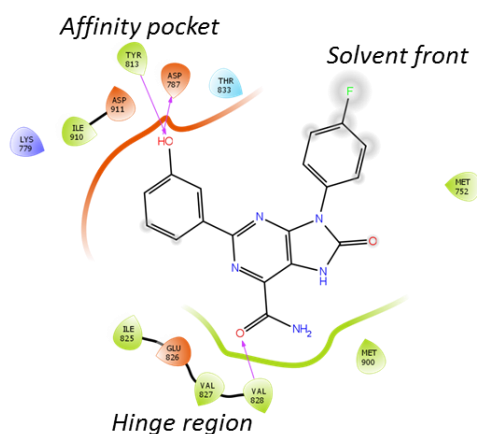


Figure 26: The putative binding mode of compound **A₁B₁** in the p110 δ subunit.

Interaction with highly conserved amino acids in ATP binding domain might be a cause for lack of selectivity and sub-optimal potency of our Hit. Furthermore, the flat binding mode of compound **A₁B₁** prevents its interaction with the *selectivity/ specificity pocket*. This pocket has been described in detail in paragraph 1.5.2. The structural characteristic and the inherently pliability of p110 δ P-loop could be exploited to design flexibility-based inhibitors which will be able to open the pocket and gain potency and selectivity over the isoform of interest.

Therefore, to increase potency and selectivity of compounds belonging to this class, the design of a 2D library exploring both the *affinity* and the *selectivity* pocket was developed. The SAR exploration was focused on mapping the chemical space close to the selectivity pocket introducing a high chemical diversity including mainly hydrophobic and flexible decorations or basic moieties at position 9 (*Head Groups, R¹*). On the contrary, the affinity region was explored in a less extent because the interaction established between the phenol and amino acids of the DFG-motif was considered fundamental to achieve enzymatic inhibition. Nevertheless, it was decided to identify heterocyclic groups that maintained the potential to act as hydrogen bond donors. Thus, 4-indazolyl group was found to be the best replacement for the phenol⁸⁰ (*Affinity Binder, R²*), (**Figure 27**).

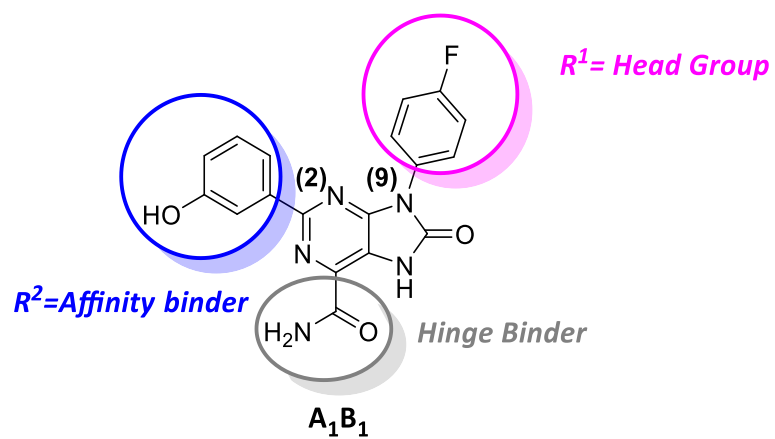
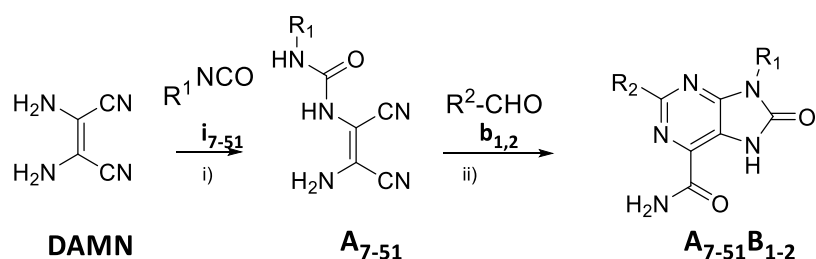


Figure 27: Compound **A₁B₁** with the mapped moieties (**R¹ = Head Group** and **R² = Affinity Group**)

3.3 2D Library Design and Synthesis

To build the two-dimensional library, a parallel synthetic approach was adopted. The synthetic strategy allowed us to synthesise the 7H-purin-8(9H)-one central core in only two steps (**Scheme 1**).



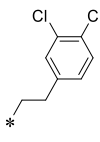
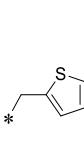
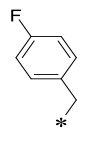
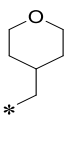
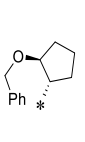
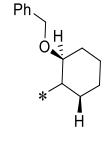
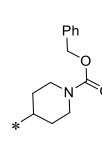
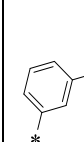
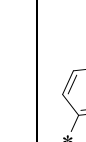
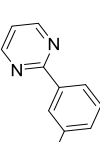
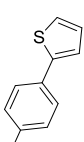
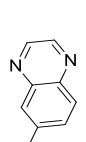
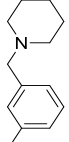
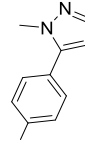
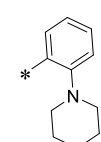
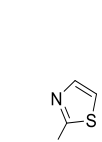
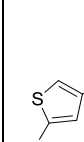
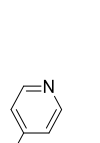
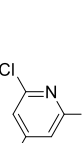
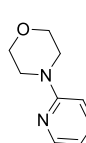
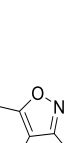
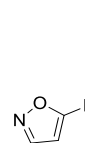
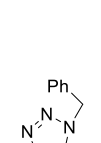
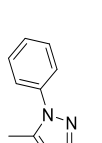
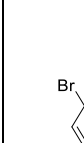
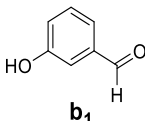
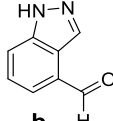
Reaction conditions: i) R^1NCO , ACN, rt, 24-48 hr; ii) R^2CHO , I_2 , TEA, MeOH, rt, 24-48 hr

Scheme 1: Reaction conditions: i) R_1NCO , ACN, rt, 24-48 hr; ii) R_2CHO , I_2 , TEA, MeOH, rt, 24-48 hr⁸¹.

In the first step, 2,3-diaminomaleonitrile (DAMN) reacts with an isocyanate (**i_x**), **Table 2**, affording the synthesis of a urea intermediate (**A_x**) bearing the first substituent, defined as Head group (R^1). The second step envisages the reaction with an aldehyde (**b_y**) in the presence of TEA which allows the formation of the central core and the introduction of the second substituent, named Affinity group (R^2).

Table 2: Isocyanates (**i_x**) bearing Head Groups (R^1) and aldehydes (**b_y**) bearing the Affinity Group (R^2).

Isocyanates (i_x) bearing Head Groups (R^1)								
(* = NCO)								
i₇	i₈	i₉	i₁₀	i₁₁	i₁₂	i₁₃	i₁₄	i₁₅
i₁₆	i₁₇	i₁₈	i₁₉	i₂₀	i₂₁	i₂₂	i₂₃	i₂₄

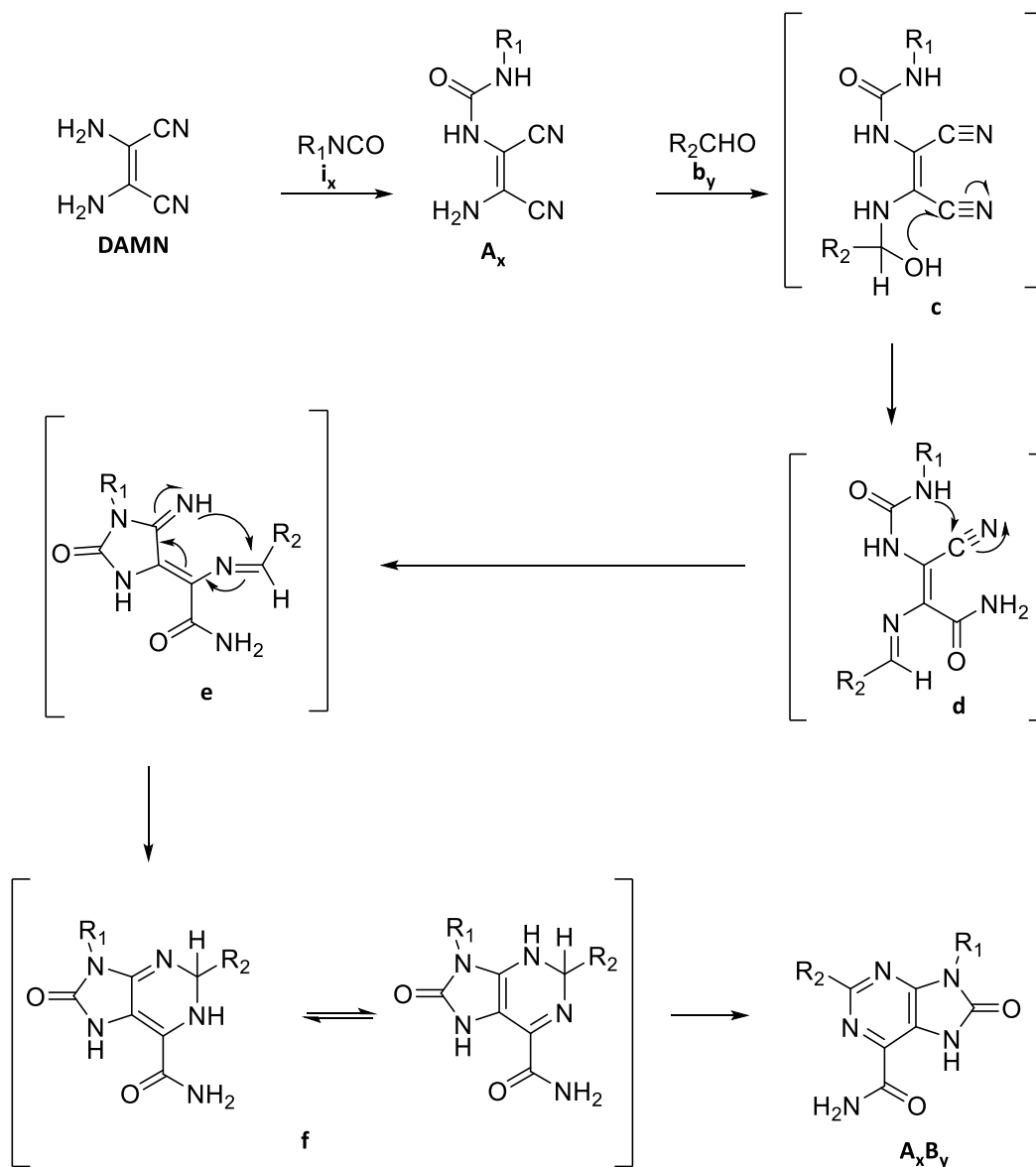
 i ₂₅	 i ₂₆	 i ₂₇	 i ₂₈	 i ₂₉	 i ₃₀	 i ₃₁	 i ₃₂	 i ₃₃
 i ₃₄	 i ₃₅	 i ₃₆	 i ₃₇	 i ₃₈	 i ₃₉	 i ₄₀	 i ₄₁	 i ₄₂
 i ₄₃	 i ₄₄	 i ₄₅	 i ₄₆	 i ₄₇	 i ₄₈	 i ₄₉	 i ₅₀	 i ₅₁
Aldehydes (b_y) bearing Affinity Group (R²)								
 b ₁					 b ₂			

45 commercially available isocyanates (i_x) were selected and purchased (**Table 2**), endorsing chemical diversity and introducing bulky, apolar and flexible decorations. Moreover, since the presence of basic moieties helps pulmonary drug delivery⁷⁴, isocyanates bearing basic groups were also selected for this exploration.

The use of commercially available isocyanates allowed the synthesis of a 43 compounds library. However, the quality of purchased starting materials proved unsatisfactory in several cases. Purchased isocyanates were analysed and in several cases their conversion in the corresponding symmetric urea was observed, limiting the reagents easily available.

Experimental procedures to synthesise the scaffold reported in literature were applied with minor modifications⁸¹. In the second step, the formation of a side product was observed by UPLC-MS analysis. Its mass was 2 AMU higher with respect to our desired compound. Our hypothesis was that the side product could be the corresponding 1,2-dihydro-purine-6-carboxamide (**f**), precursor of the

desired product as illustrated in **Scheme 2**. Hence, to avoid its formation, a catalytic amount of I_2 was added to the reaction mixture. Oxidative conditions led to the disappearance of the side product confirming our hypothesis.



Scheme 2: Mechanism of formation of the 8-oxapurine-6-carboxamides.⁸¹

The second step yielded the desired compound in all cases apart from preparation of compound $A_{23}B_1$ (Table 5, see paragraph 3.4) likely because of the hydrolysis or cleavage of the trifluoroacetamide under basic conditions even if the synthesis of its analogue compound $A_{23}B_2$ was successfully completed.

In most cases, purification was not needed neither for the first intermediate nor for the final compound since derivatives precipitated as pure solid and were isolated by simple filtration.

Overall, the reaction proved to be appropriate for parallel synthesis and to the production of final compounds in adequate quantity (at least 5 mg) and purity (>85% LC-MS).

3.4 Biological Assay Results and SAR Analysis.

All 43 derivatives were evaluated for their biological activity as PI3K inhibitors. Compounds were first submitted to preliminary cell free assays. Inhibition of the PI3K enzymatic activity was determined in human (h) recombinant kinases hPI3K α (p110 α /p85 α), hPI3K β (p110 β /p85 α), hPI3K δ (p110 δ /p85 α) and hPI3K γ (p110 γ) by means of a flash-type luminescence assay, named ADP-Glo. The experiment was carried out at ATP concentration equal to K_m of the tested isoform (PI3K α at 50 μ M, PI3K β at 100 μ M, PI3K δ at 80 μ M, and PI3K γ at 30 μ M). The observed IC_{50} was then converted into the corresponding K_i using the Cheng-Prusoff equation⁸². In following tables, the corresponding pK_i for each isoform is reported.

As mentioned before, position 9 of the 7H-purin-8(9H)-one core was explored more extensively. In following tables, synthesised compounds are grouped according to the different head groups (aliphatics, aromatics and heteroaromatics).

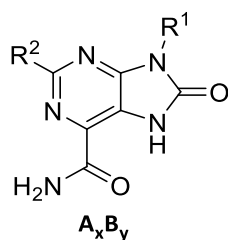
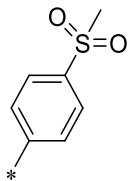
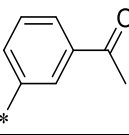
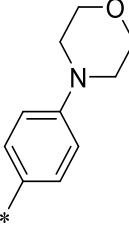
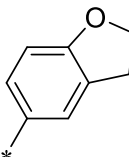
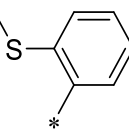
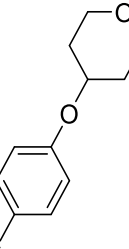
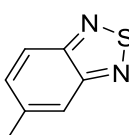
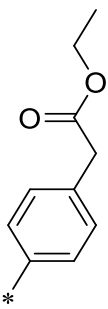


Table 3: 9-Aryl substitutions and 2 position modifications to give compounds.

General Structure	Affinity Group (R^2) ↓									
Head Group (R^1) ↓	Name	δ pK_i	γ pK_i	β pK_i	α pK_i	Name	δ pK_i	γ pK_i	β pK_i	α pK_i
	A_1B_1	6.9	6.9	6.5	7.1	A_1B_2	≤ 5.0	7.3	≤ 5.0	≤ 5.0

	A₇B₁	7.8	7.3	7.0	7.7	A₇B₂	6.9	6.9	≤ 5.0	≤ 5.0
	A₈B₁	7.2	6.6	6.2	7.1	A₈B₂	6.8	7.0	≤ 5.0	≤ 5.0
	A₉B₁	7.3	6.9	6.8	7.4	A₉B₂	≤ 5.0	6.3	≤ 5.0	≤ 5.0
	A₁₀B₁	7.3	7.0	6.3	7.0	A₁₀B₂	7.1	6.7	≤ 5.0	6.6
	A₁₁B₁	7.0	7.2	6.8	6.5	A₁₁B₂	7.6	6.6	6.0	≤ 5.0
	A₁₂B₂	6.9	6.2	6.6	6.8	A₁₂B₂	≤ 5.0	6.1	≤ 5.0	5.8
	A₁₃B₁	6.3	6.7	5.9	6.5	A₁₃B₂	6.4	7.0	≤ 5.0	5.9

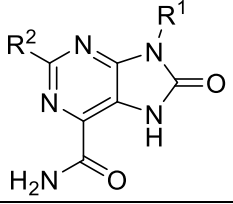
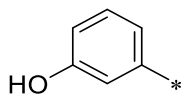
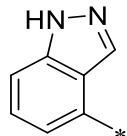
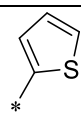
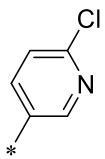
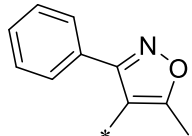
	A₁₄B₁	≤ 5.0	7.0	5.9	6.4	A₁₄B₂	7.0	6.7	≤ 5.0	6.0
---	------------------------------------	-------	-----	-----	-----	------------------------------------	-----	-----	-------	-----

Compounds in **Table 3** bear differently decorated aryl groups at position 9 (R^1) and phenol or indazole as Affinity groups (R^2) at position 2. All compounds displayed PI3K δ $pK_i \leq 8$. Compound **A₇B₁** proved to be 8-fold more potent on δ than Hit, compound **A₁B₁**. However, this compound demonstrated a pan PI3K inhibitory profile. Compound **A₁₁B₂** showed good to moderate selectivity towards α and β isoforms. However, δ pK_i of both compounds was considered too low to progress them to cellular assay.

Compounds bearing heteroaromatic decorations were reported in **Table 4**. The best compound in this group was **A₁₇B₂** which showed a δ pK_i 6-fold higher than **A₁B₁**. The methyl-3-phenyl-4,3-isoxazole head group (R^1) seemed to have a good influence on selectivity. Compounds **A₁₇B₂** and its hydroxy-phenyl analogue, **A₁₇B₁** showed in fact a moderate selectivity against γ and an outstanding selectivity against α ($\cong 250$ folds). Unfortunately, both compounds showed a moderate activity on β isoforms.

The use of Cl-pyridine as Head group (R^1) did not have a good impact in terms of potency and selectivity, but it is important to underline how the use of indazole as affinity binder (R^2) in combination with this Head group had a detrimental effect on potency over all the isoforms compared to the hydroxy-phenyl analogue.

Table 4: heteroaryl modifications at 9 position to give compounds **A₁₅₋₁₇B₁** and **A₁₅₋₁₇B₂**.

General Structure	Affinity Group (R ²) ↓									
										
Head Group (R ¹) ↓	Name	δ pK _i	γ pK _i	β pK _i	α pK _i	Name	δ pK _i	γ pK _i	β pK _i	α pK _i
	A₁₅B₁	7.0	7.2	6.7	6.9	A₁₅B₂	6.8	6.9	≤ 5.0	6.2
	A₁₆B₁	6.7	6.3	6.0	6.8	A₁₆B₂	≤ 5.0	≤ 5.0	≤ 5.0	≤ 5.0
	A₁₇B₁	7.4	5.8	7.1	≤ 5.0	A₁₇B₂	7.7	6.1	6.9	≤ 5.0

To better understand this different behaviour, compounds **A₁₆B₁** and **A₁₆B₂** were docked in hPI3Kδ. In **Figure 28**, both Glide GS score and Glide Emodel show how compound **A₁₆B₁** (Clpyr_1) is clearly more energetically favoured in terms of polar and Van der Waals interactions with the binding site respect to **A₁₆B₂** (Clpyr_2). This analysis could be a reasonable explanation for the lower potency displayed by almost all the compounds bearing indazole as affinity respect to those presenting the phenol.

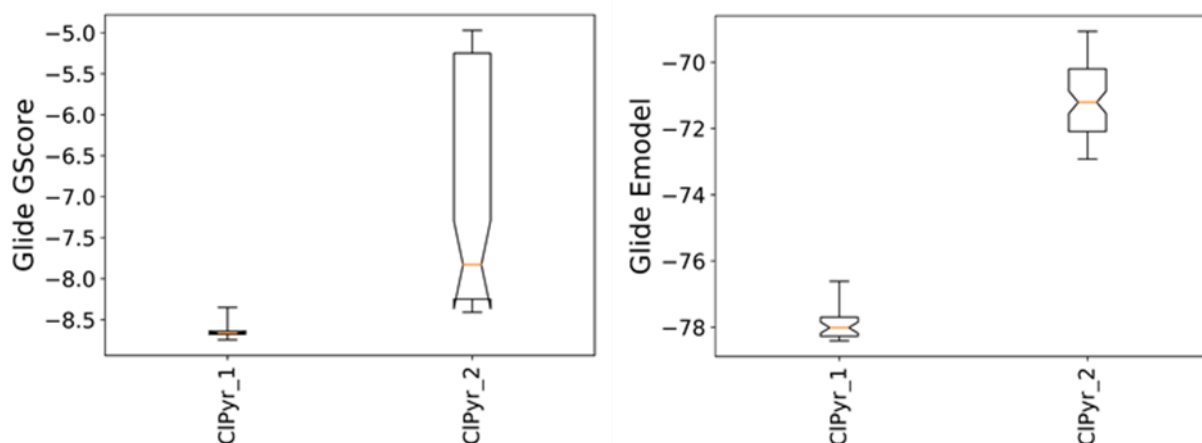
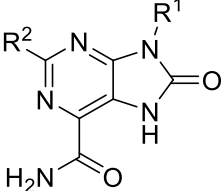
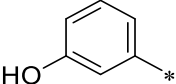
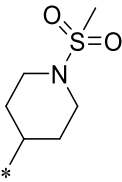
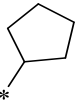
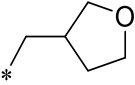
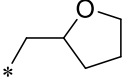
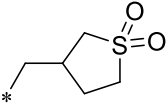
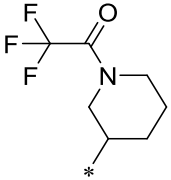


Figure 28: Glide GScore and Glide Emodel for compounds **A₁₆B₁** (CIPyr_1) and **A₁₆B₂** (CIPyr_2).

Saturated five or six membered rings were also selected as Head groups (R^1) (**Table 5**). Most of them carried heteroatoms in the ring except for compounds **A₁₉B₁** and **A₁₉B₂** which bear a cyclopentane. Rings moieties were directly connected to the core (**A₁₈B₁**, **A₁₈B₂**, **A₁₉B₁**, **A₁₉B₂**) or through a methylene linker (**A₂₀B₁**, **A₂₀B₂**, **A₂₁B₁**, **A₂₁B₂**, **A₂₂B₁**, **A₂₂B₂**). The introduction of the linker was supposed to make more flexible these compounds and facilitate establishing key interactions with selectivity pocket. Disappointingly, this did not lead to the expected result. Despite that, compounds **A₁₈B₁**, **A₁₉B₁**, **A₁₉B₂** and **A₂₀B₁** showed an improved PI3K δ potency compared with the Hit compound, **A₁B₁**.

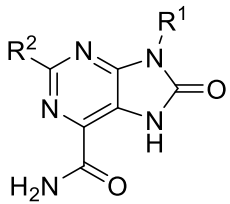
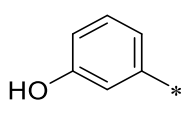
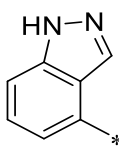
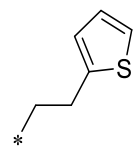
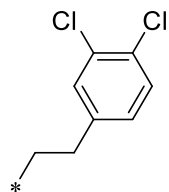
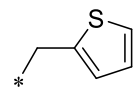
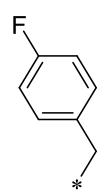
Table 5: six-five saturated membered rings modifications to give compounds **A₁₈₋₂₂B₁** and **A₁₈₋₂₃B₂**.

General Structure	Affinity Group (R ²) ↓									
										
Head Group (R ¹) ↓	Name	δ pK _i	γ pK _i	β pK _i	α pK _i	Name	δ pK _i	γ pK _i	β pK _i	α pK _i
	A₁₈B₁	7.6	7.1	6.9	7.4	A₁₈B₂	6.9	6.9	6.4	7.1
	A₁₉B₁	7.4	7.4	6.7	7.4	A₁₉B₂	7.4	6.2	5.8	6.9
	A₂₀B₁	7.4	6.6	6.5	7.4	A₂₀B₂	7.0	6.6	6.2	6.7
	A₂₁B₁	6.5	6.7	5.8	6.7	A₂₁B₂	≤ 5.0	6.0	≤ 5.0	≤ 5.0
	A₂₂B₁	≤ 5.0	5.9	6.2	7.0	A₂₂B₂	6.6	6.3	5.9	6.3
	A₂₃B₁	NA	NA	NA	NA	A₂₃B₂	6.6	6.3	5.8	6.6

Compounds reported in **Table 6** showed an aryl or heteroaryl decorations connected by a methylene or ethylene linker to the core. The introduction of the ethylene linker resulted in an increased PI3K δ potency. Compound **A₂₄B₁** showed in fact a pK_i δ 25-fold higher than its analogue compound **A₁₅B₁** (**Table 4**) and 12.5-fold higher than compound **A₂₆B₁**. However, this single modification did not result for **A₂₄B₁** in an improved selectivity towards other isoforms.

Compound **A₂₅B₁** proved to be the most PI3K δ selective inhibitor of this first iteration. The insertion of a dichloro-phenylethyl decoration led to a 22-fold selectivity of δ towards α , 44-fold towards β and 35-fold towards γ .

Table 6: Aryl and heteroaryl decorations at position 9 to give compounds **A₂₄₋₂₇B₁** and **A₂₄₋₂₇B₂**.

General Structure	Affinity Group (R ²) ↓									
										
Head Group (R ¹) ↓	Name	δ pK _i	γ pK _i	β pK _i	α pK _i	Name	δ pK _i	γ pK _i	β pK _i	α pK _i
	A₂₄B₁	8.4	7.0	7.4	7.5	A₂₄B₂	7.0	6.4	≤ 5.0	6.5
	A₂₅B₁	8.0	6.5	6.4	6.7	A₂₅B₂	6.9	5.8	≤ 5.0	≤ 5.0
	A₂₆B₁	7.3	7.0	≤ 5.0	6.8	A₂₆B₂	6.8	6.7	≤ 5.0	≤ 5.0
	A₂₇B₁	6.8	≤ 5.0	6.2	≤ 5.0	A₂₇B₂	≤ 5.0	6.3	≤ 5.0	≤ 5.0

On the contrary, compound **A₂₄B₂** and **A₂₅B₂** showed a dramatic decrease in potency compared with their phenol analogues. These data once again confirmed as indazole has a negative impact on potency.

Since compounds **A₂₄B₁** and **A₂₅B₁** showed the highest enzymatic PI3K δ inhibition, their δ inhibitory activity was also determined in cell-based assay in THP-1 monocytes. AKT phosphorylation was

measured through Homogeneous Time Resolved Fluorescence (HTRF) technology after Macrophage Colony-Stimulating Factor (M-CSF) stimulation. These two compounds both showed a high drop in PI3K δ potency in the THP-1 assay (**Table 7**), probably due to a low passive cellular permeability (Papp) (compounds **A₂₄B₁** and **A₂₅B₁**) (**Table 8**).

Passive cellular permeability was determined by using Caco-2 cells, measured in both directions (apical-to-basolateral [A→B] and basolateral-to-apical [B→A]). The test was also run in the presence of a P-glycoprotein-1 (P-gp) inhibitor, GF120918, to investigate whether tested compounds are P-gp substrates. For further details, see experimental section.

Table 7: PI3K δ enzymatic activity (enzymatic pIC₅₀), Cell based activity (cell pIC₅₀), Drop-off values, Selectivity values towards isoforms of compounds **A₂₅B₁** and **A₂₄B₁**.

Compound	PI3K enzymatic Assay δ pIC ₅₀	PI3K Cell based Assay δ pIC ₅₀	Drop-Off cell IC ₅₀ / Enz IC ₅₀	Selectivity (k _i)		
				α/δ	β/δ	γ/δ
A₂₅B₁	7.7	5.8	91	22	44	35
A₂₄B₁	8.1	6.1	100	8	10	25

The high potency over δ and the moderate selectivity towards other isoforms led us to the selection of compound **A₂₅B₁**. This compound was considered the starting point for a further exploration focused on improving cellular PI3K δ inhibition through the improvement of both permeability and solubility.

Table 8: Passive permeability (P_{app}), cLogD calculated with Percepta software by Advanced Chemistry Development (ACD), kinetic solubility and TPSA of compounds **A₂₅B₁** and **A₂₄B₁**.

Compounds	TPSA	P_{app} AB/BA (nm/s) CACO-2 w GF ³	cLogD (Percepta-ACD)	Solubility (μM)
A₂₅B₁	121.4	BQL at A-B and B-A directions	3.5	Low (≤100 μM)
A₂₄B₁	121.4	Low permeability, Possible PGP substrate	2.1	High (≥250 μM)

3.5 Second SAR Exploration

The binding mode of compound **A₂₅B₁** in human PI3K δ was further investigated to design and develop the second iteration. Therefore, co-crystal structure of **A₂₅B₁** in complex with hPI3K δ was obtained (**Figure 29**). Human PI3K δ in complex with **A₂₅B₁** was determined at Proteros Biostructures GmbH.

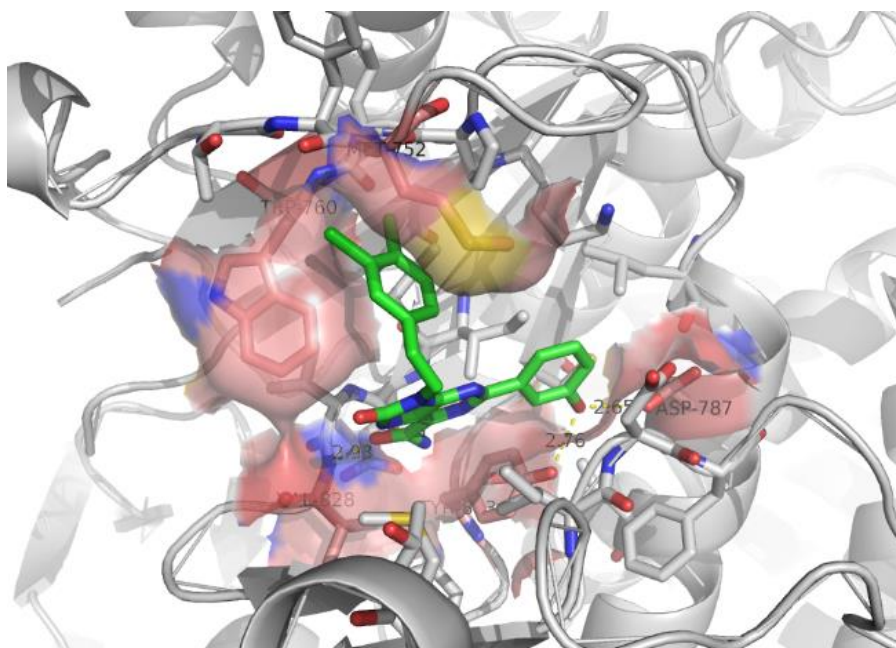


Figure 29: X-ray crystal structure of compound **A₂₅B₁** in human PI3K δ , (ligand in green and protein in grey, resolution at 2.43 Å). View from the solvent exposed region.

The ligand amide group makes a bidentate hydrogen-bond interaction with the backbone oxygen of Glu826 and with the backbone NH of Val828. Interestingly, the orientation of the exocyclic primary amide is promoted by the formation of intramolecular hydrogen-bonds, which lock the hinge-binding group in a well-defined conformation (**Figure 30**).

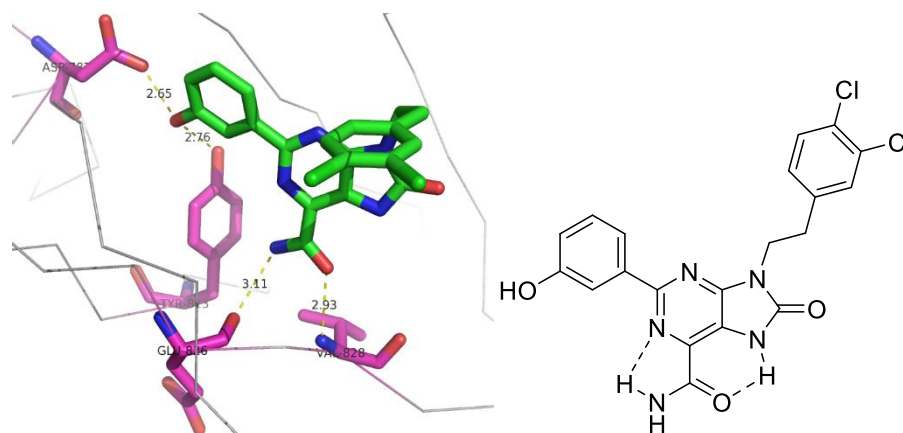


Figure 30: The cooperative effect on the locking of the conformation of the amide.

Notably, this binding mode differs from that observed in the docking simulation of the Hit compound (**Figure 26**) where the amide group was rotated by 180 degrees, establishing a bidentate hydrogen bond with Val828 backbone. The phenol substituent is accommodated in the affinity region and makes two hydrogen bonds with Asp787 and Tyr813.

All the interactions formed by **A₂₅B₁** with the hinge region and the affinity pocket of PI3K δ involve residues that are conserved among all four kinase isoforms and, therefore, cannot rationalize the moderate isoform selectivity observed for this compound. However, the head group of **A₂₅B₁**, which is constituted by a dichloro-phenyl-ethyl moiety, can promote a rearrangement of Met752, opening the so-called *selectivity pocket*. In particular, this structural change allows the dichloro-phenylethyl group to establish π - π stacking interactions with the indole ring of Trp760 and van der Waals interactions with Met752 side chain^{72,63,71}.

In the light of the binding mode of compound **A₂₅B₁**, a second SAR expansion was designed and planned. Firstly, new decorations around the phenyl group (**Figure 31**) were further examined and hydrophobic modifications or Cl isosteres were introduced to enhance interaction with the *selectivity pocket*. Secondly, small heterocycles and cycloalkyl moieties were considered to evaluate their effect on pre-orienting the phenyl group in the pocket. These rings were basically designed also with the aim of increasing the fraction of C sp³ atoms (Fsp³) in the molecule. Increasing the level of saturation could allow access to more isoforms and therefore to establish new interactions improving potency and selectivity. Moreover, an increased fraction of C sp³ atoms could result in a reduced aromatic character of the molecule and this could increase the likelihood of obtaining

higher solubility and permeability⁸³. As result of this considerations, a cycle propyl and pyrrolidine groups were selected as new linkers (**Figure 31**).

With the aim of improving Phys-chem and ADME properties, the synthesis of methylated analogues was also considered. A methyl group was introduced in the linker, generating a stereogenic centre in the molecule and another one was inserted at the *ortho*-position in the *Affinity binder*. These methyl groups could disrupt the molecular planarity and symmetry resulting in an increased solubility^{84,85}. Moreover, the addition of a methyl could induce conformational changes of the molecule leading to improved potency and selectivity⁸⁴.

The use of hydrophilic substituents was not considered in this iteration because it could have decreased LogP and negatively affected the permeability.

Regarding the affinity binder, this portion was explored more extensively than in the previous SAR exploration: new affinity binders inspired by literature evidence⁷² or characterized by basic groups were inserted while the Head group (dichloro-phenylethyl moiety) was kept unvaried.

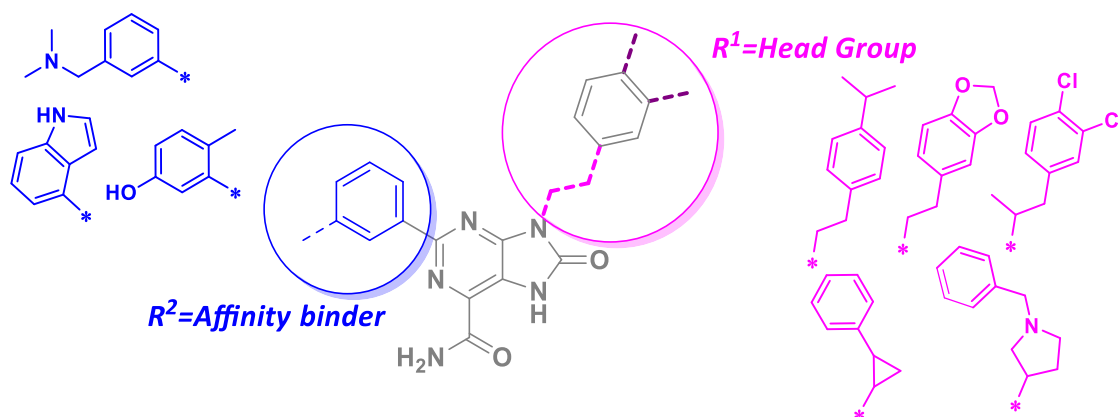


Figure 31: General structure of compound **A₂₅B₁** with explored portions Head group and Affinity binder highlighted in different colours.

This series is characterized by high TPSA values ($\cong 120$) which could implicate low permeability. A high number of N atoms and the presence of a primary amide in the central core could be the main explanation for this feature. However, in this second SAR exploration the central scaffold was not subjected to modifications since the unique orientation of the primary amide was considered a key interaction to achieve enzymatic inhibition.

3.6 Synthesis and Biological Evaluation of the Second SAR Exploration

Compounds synthesised were submitted to enzymatic assays as described in paragraph 1.4.

New analogues characterized by modifications in the affinity portion at position 2 of compound **A₂₅B₁** are reported in **Table 9**. These three analogues were synthesised following the procedure shown in Scheme 1, chapter 1.3.

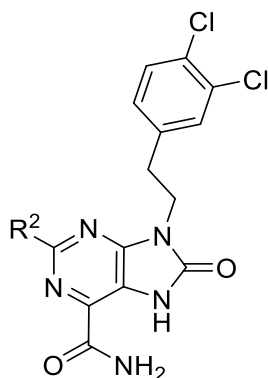


Table 9: Decorations introduced at position 2 (R^2) to give compounds **A₂₅B₁₀₋₁₂**.

Compound	R^2	Enzymatic pKi			
		PI3K δ	PI3K γ	PI3K β	PI3K α
A₂₅B₁₀		7.3	<5	7.4	<5
A₂₅B₁₁		7.7	6.3	7.3	6.5
A₂₅B₁₂		<5	<5	<5	<5

Substitution of the phenolic moiety with an indole (compound **A₂₅B₁₀**), did not lead to a potency gain or an improved selectivity towards other isoforms. On the contrary, **A₂₅B₁₀** showed δpK_i 5-fold lower and βpK_i 10 fold higher than compound **A₂₅B₁**. Same trend was observed for compound **A₂₅B₁₁**

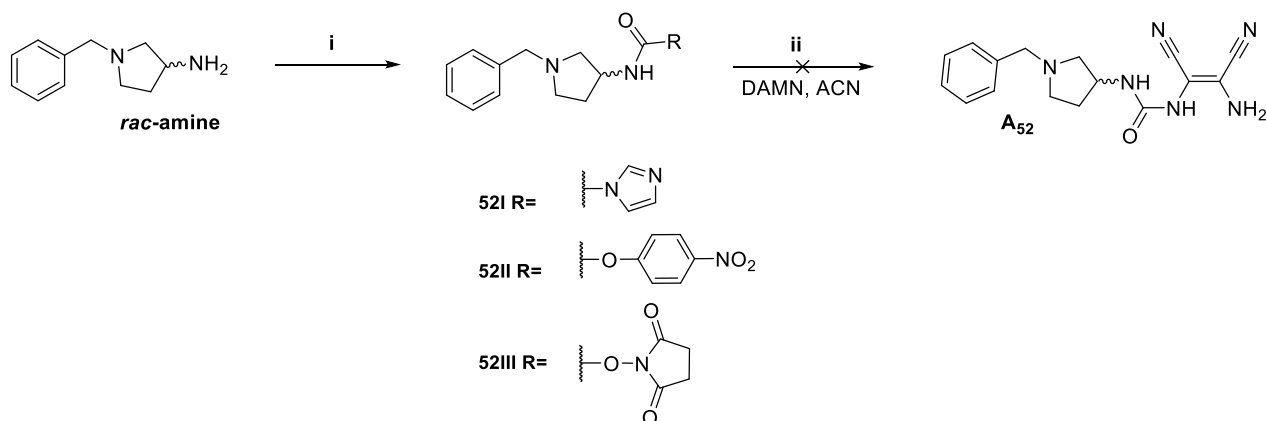
which had a methyl decoration on the phenyl ring. However, compound **A₂₅B₁₁** showed a complete loss of activity on α and γ isoforms.

The introduction of a *N,N* dimethyl methanamine on the aromatic ring was expected to improve the interactions with Asp787 residues in the DFG *motif*. Disappointingly, this led to a dramatic loss of activity over all the isoforms probably due to a higher steric hindrance which caused a clash in the binding site (compound **A₂₅B₁₂**, **Table 9**).

Inserting modifications on the Affinity group did not result in the expected modulation of PI3K δ inhibition or selectivity. Thus, we turned our attention on the exploration of Head group again.

Regarding Head group exploration, all compounds were synthesised following the synthetic procedure reported in chapter 1.3 except for compounds **A₅₂B₁** and **A₅₃B₁**. The required isocyanates were not commercially available thus different synthetic pathways were followed.

Compound **A₅₂B₁** was synthesised starting from the 1-benzylpyrrolidin-3-amine (**Scheme 3**). The first synthetic attempt was to transform the amine in a reactive urea or carbamate. The synthesis of intermediates **52I** and **52II** was completed in a yield of 48% and 17%, respectively, while the preparation of intermediate **52III** failed. Conditions for the synthesis of these intermediates are reported in **Table 10**.



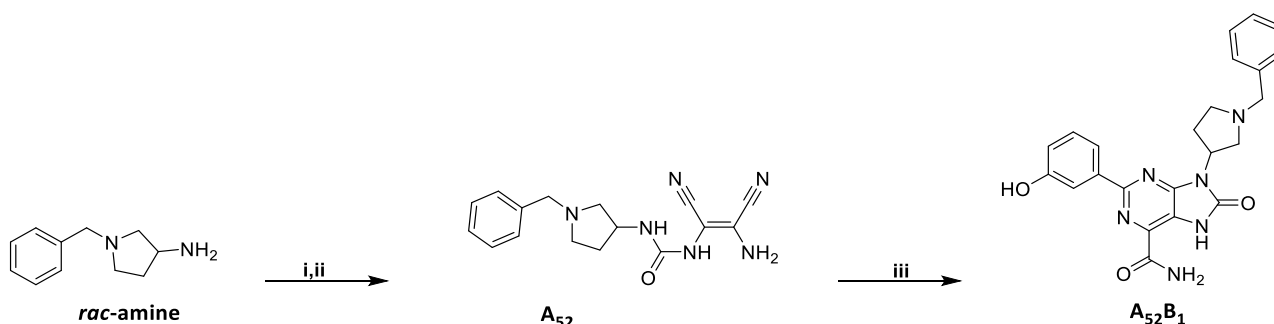
Scheme 3: Synthetic pathway for the synthesis of intermediate **A₅₂**.

Table 10: Conditions used to synthesise intermediates **52I**, **52II** and **52III**.

Step	Intermediate	Reagents and conditions	Temperature	Solvent	Yield
i	52I	1.5 eq. CDI	rt	DCM	48%
i	52II	1 eq. 4-Nitrophenyl chloroformate	rt	DCM	17%
i	52III	2 eq. Succinimide	rt	DCM	No reaction

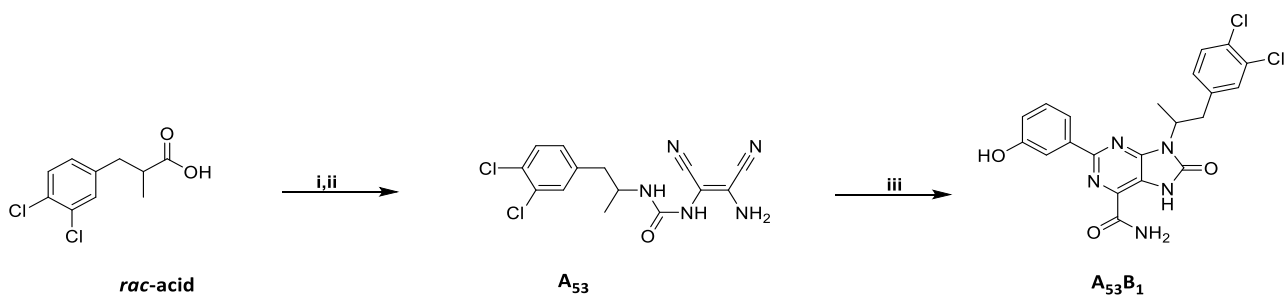
Disappointingly, following reaction with DAMN was unsuccessful for both intermediates (**52I** and **52II**) as reported in **Table 10**. Less electrophilic nature of these two intermediates could be an explanation for the failure of the reaction with a poorly nucleophile like DAMN.

The preparation of the isocyanates required for the synthesis of **A₅₂** and **A₅₃** was in a first instance not considered, as instability of similar analogues was observed during the set-up of the first compounds library. Nevertheless, the synthesis of the corresponding isocyanate started from the commercially available amine (*rac*-amine) which was transformed into the isocyanate using triphosgene and reacted *in situ* with DAMN. This approach led to the formation of **A₅₂** in a 57% yield over two steps. The following addition of 3-hydroxybenzaldehyde (**b₁**) gave the desired final product as racemic mixture in a 23% yield (**Scheme 4**).



Scheme 4: Reagents and conditions: (i) 2 eq. Cl₃COCOOCCl₃, DCM, rt, 2 hr; (ii) 3 eq. DAMN, 2 hr, rt, 57% over two steps; (iii) 2 eq. 3-hydroxybenzaldehyde (**b₁**), 1 eq. TEA, MeOH, rt, 2 hr, 23%.

Compound **A₅₃B₁** was prepared starting from the acid, *rac*-acid. The corresponding isocyanate was synthesised through Curtius rearrangement using DPPA and reacted *in situ* with DAMN which led to the synthesis of intermediate **A₅₃** in a 16% yield. Despite the low yield, the last step was completed successfully (**Scheme 5**).



Scheme 5: Reagents and conditions (i) 2eq. DPPA, Toluene, 80 °C, (ii) 3eq. DAMN 3 eq. TEA, 40 °C, 16%. (iii) 2 eq. 3-hydroxybenzaldehyde, 1 eq. TEA, MeOH, rt, 15%.

The biological results of synthesised compounds are reported in **Table 11**. A marginal increase in PI3K δ potency for compounds **A₅₂B₁** and **A₅₃B₁** was observed. However, this was also associated with an increased β pK_i. The increased activity on β was unexpected but a possible explanation for this loss of selectivity could be found in structural similarities between these two isoforms, especially in the non-conserved residues surrounding the specificity pocket. A mutagenesis study identified a non-conserved residue in PI3K β , β Tyr778, close to the conserved Met that could favour the conformational plasticity of the β P-loop. This residue is aliphatic in p110 α and p110 γ (Ile and Val, respectively), but aromatic in p110 β and p110 δ (Tyr and Phe, respectively)⁶⁷. This common feature may account for the similar profiles of these two inhibitors (**A₅₂B₁** and **A₅₃B₁**).

The increased β inhibition has been also encountered in compounds **A₂₅B₁₀** and **A₂₅B₁₁**. In these compounds, modifications were introduced only on the affinity binder and not on the head group. However, selectivity was affected. Therefore, this result demonstrated that selectivity is not only determined by the interaction with the specificity pocket, but it is the result of a complex set of inhibitor interactions throughout the binding site.

Different substituents on the phenyl ring (compounds **A₅₄B₁** and **A₅₅B₁**) inserted to improve hydrophobic interactions with the Trp760 residue had an influence neither on potency nor on selectivity. The use of a cyclopropane as a linker (compound **A₅₆B₁**) resulted in decreasing pK_i of all isoforms.

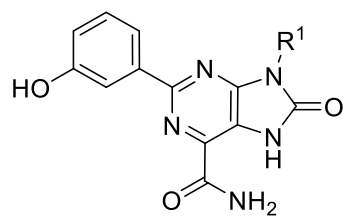
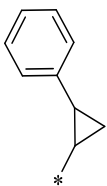


Table 11: Decorations introduced at position 9 to give compounds **A₅₂₋₅₆B₁**.

Compound	R ¹	Enzymatic pK _i			
		PI3K δ	PI3K γ	PI3K β	PI3K α
A₅₂B₁		8.3	6.5	7.7	6.9
A₅₃B₁		8.5	6.4	8.2	6.7
A₅₄B₁		6.7	<5	<5	<5
A₅₅B₁		7.7	6.3	6.7	7.1

A₅₆B₁		7.2	6.8	6.8	6.8
------------------------------------	---	-----	-----	-----	-----

Compounds **A₂₅B₁₁**, **A₅₂B₁** and **A₅₃B₁** that showed the highest affinity for PI3K δ were submitted to cellular assay. Moreover, solubility and permeability were measured to investigate whether these focused modifications had an impact not only on cellular PI3K δ inhibitory activity but also on Phys-chem and ADME properties. Results are reported in **Table 12** and **Table 13**.

Table 12: PI3K Enzymatic activity (pIC₅₀), Cell-based activity (pIC₅₀) and Drop-off values of compounds **A₂₅B₁₁** and **A₅₂B₁** and **A₅₃B₁**.

Compound	PI3K enzymatic Assay δ pIC ₅₀	PI3K Cell based Assay δ pIC ₅₀	Drop-Off cell IC ₅₀ / Enz IC ₅₀
A₂₅B₁₁	7.4	6.2	15
A₅₂B₁	8.0	6.5	31
A₅₃B₁	8.1	7.0	12

Overall, these three compounds displayed a markedly reduced cellular drop-off compared to their parent compound **A₂₅B₁**. Compound **A₅₃B₁** exhibited a good cellular PI3K δ inhibitory activity, 16-fold higher than compound **A₂₅B₁** (**Table 7**).

Regarding Phys-chem properties, as expected, the introduction of a methyl group positively influenced solubility. Compounds **A₂₅B₁₁** and **A₅₃B₁** present an expected increased cLogD and nonetheless their solubility increased (solubility $\geq 400\mu\text{M}$).

The introduction of a basic group (compound **A₅₂B₁**) led to a reduction of the cLogP which led to an improved solubility, albeit to a lesser extent than **A₂₅B₁₁** and **A₅₃B₁**. Likely, the presence of an additional N atom resulted in decreasing solubility, probably due to the formation of other hydrogen-bonds leading to a higher crystal packing energy.

Unpleasantly, permeability was not improved in this SAR exploration. Compound **A₅₃B₁**, despite its higher cellular potency, showed a permeability below the detectable limit. Reasons for this lack of permeability were unclear and still matter of investigation.

Table 13: TPSA, cLogD, permeability and kinetic solubility of compounds **A₂₅B₁₁** and **A₅₂B₁** and **A₅₃B₁**

Compounds	TPSA	P_{app} AB/BA (nm/s) CACO-2 w GF ³	cLogD (Percepta-ACD)	Solubility (μM)
A₂₅B₁₁	121.4	Below limit of detection	3.9	High ($\geq 250 \mu\text{M}$)
A₅₂B₁	124.7	Below limit of detection	1.1	Medium ($100 \mu\text{M} \leq \text{Sol} \leq 250 \mu\text{M}$)
A₅₃B₁	121.4	Below limit of detection	3.8	High ($\geq 250 \mu\text{M}$)

4. Conclusions

The research project here detailed describes a med-chem work, whose primary goal was to build a SAR exploration on a Hit previously identified by a focused screening study to discover new PI3K δ inhibitors.

First, a convenient and parallel synthetic approach was found which allowed to prepare a library of 43 derivatives with two points of diversity. In this fashion, two important regions of the PI3K ATP binding site, the *affinity* and the *selectivity* pocket, had been explored. Among all the synthesised compounds, **A₂₄B₁** and **A₂₅B₁** demonstrated a higher enzymatic PI3K δ potency compared to the Hit. Notably, compound **A₂₅B₁** showed also a moderate selectivity towards other PI3K isoforms.

The crystal structure of compound **A₂₅B₁** in complex with hPI3K δ was also obtained. The complex with the protein highlighted how dichlorophenyl-ethyl decoration was able to open and interact with the *specificity pocket*. However, despite the high enzymatic potency, derivative **A₂₅B₁** demonstrated a low cellular PI3K δ potency associated with sub optimal Phys-Chem and ADME properties. Therefore, in the light of these results, a second SAR expansion tailored on improving cellular potency, Phys-chem and ADME properties of compound **A₂₅B₁** was planned and carried out.

The introduction of subtle and focused modifications, as a methyl group, brought to an improvement of solubility and cellular potency. Compound **A₅₃B₁** in fact showed a cellular PI3K δ potency 16-fold higher than its close analogue compound **A₂₅B₁** and solubility was highly increased too. On the other hand, passive permeability was not improved. Even if **A₅₃B₁** demonstrated an improved cellular PI3K δ inhibitory activity, its passive permeability measured in CACO-2 experiment was still below the limit of detection.

To conclude, the first SAR expansion accomplished the goal of improving enzymatic PI3K δ potency which was observed for the majority of 43 derivatives. Moreover, compound **A₂₅B₁** showed a moderate selectivity towards other PI3K isoforms. The second SAR expansion with focused and tailored modifications allowed to achieve cellular PI3K δ potency and good solubility with compound **A₅₃B₁**.

5. Material and Methods

5.1 General Chemistry Method

Chemicals:

Reagents and solvents were used as supplied from different providers without any further purification. All deuterated and dry solvents were purchased from Merk-Sigma-Aldrich. Anhydrous sodium sulphate (Na_2SO_4) was used as the drying agent for the organic phases.

Chromatography:

When needed purifications were performed on flash chromatography, with a Biotage Isolera instrument, using Biotage Columns (SNAP Cartridges: Silica, Silica-NH and C18).

Thin layer chromatography was performed on Glass TLC plates (5X10 cm), silica gel coated with fluorescent indicator F254.

Analytical Techniques:

Analytical UPLC and Electron Spray Ionization (ESI) condition were performed on a Waters ACQUITY UPLC equipped with a Photo Diode Array (PDA) detector and a Single Quadrupole Mass Detector (QDA) or equipped with a Triple Quadrupole (Waters Xevo -TQS).

UPLC-MS Methods:

- **Method 1:** Acquity UPLC CSH C18 column (50mm x 2.1mm i.d. 1.7 μm particle size). Column Temperature ($^{\circ}\text{C}$) 40.0. Mobile phases: 0.1% v/v solution of HCOOH in water (A); 0.1% v/v solution of in Acetonitrile (B). Flow (ml/min) 1. Stop Time (mins) 2.0.
- **Method 2:** Acquity UPLC CSH C18 column (50mm x 2.1mm i.d. 1.7 μm particle size). Column Temperature ($^{\circ}\text{C}$) 50.0. Mobile phases: HCOONH_4 , 0.025M, pH=3 (A); 0.1% v/v solution of HCOOH in Acetonitrile (B). Flow (ml/min) 0.35 Stop Time (mins) 10.0.

Data were processed using Masslynk software.

$^1\text{H-NMR}$ spectra were recorded at room temperature on a Varian spectrometer operating at 400 MHz or on a Bruker Avance 600 spectrometer. Chemical shifts are reported as δ values in ppm relative to trimethyl silane (TMS) as an internal standard. Coupling constants (J values) are given in hertz (Hz) and multiplicities are reported using the following abbreviations (s= singlet, d=doublet, t=triplet, q=quartet, m=multiplet, br=broad, nd=not determined).

High Resolution Mass Spectrometry (HRMS) analysis for compounds (**A_{25B₁}**, **A_{25B₁₁}**, **A_{52B₁}**, **A_{53B₁}**) was performed with a Q Exactive Hybrid Quadrupole-Orbitrap Mass Spectrometer.

5.2 General Procedure for Urea Derivatives

All the isocyanates were commercially available and purchased from Sigma-Aldrich, Enamine, Fluorochem and Abcr.

In a 20 mL vial, 1 eq. of 2,3-diaminomaleonitrile was dissolved in 15 mL of ACN and the solution was stirred on PLS organic synthesizer at rt for 10 minutes. Afterwards, 1.06 eq. of the corresponding isocyanate was added. After stirring for 24 hr, a precipitate formed and filtered off using Solid Phase Extraction (SPE) tubes equipped with polyethylene frits. The precipitate was washed with ACN and dried under N₂ flow for 12 hr affording the desired urea intermediate.

All synthesised intermediates were reported in **Table 14**.

Where not specified, UPLC-MS Method 1 was generally used to determine purity of final compounds.

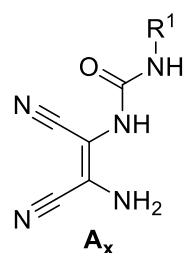
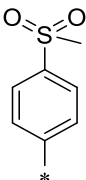
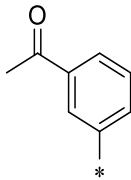
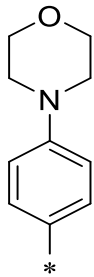
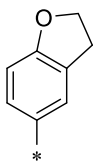
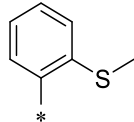
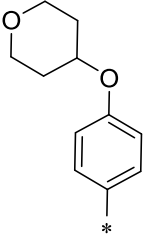
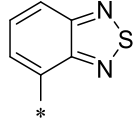
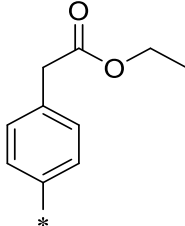
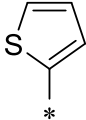
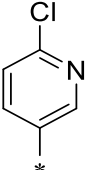
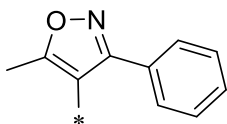
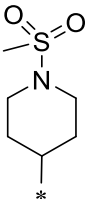


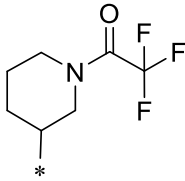
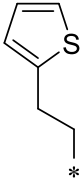
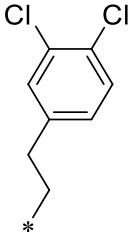
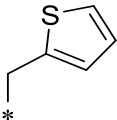
Table 14: Structure of intermediates **A_x**.

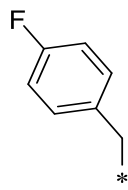
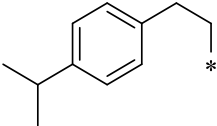
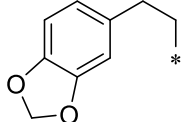
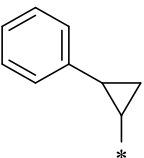
Intermediate	R ¹	¹ H-NMR UPLC-MS Purity Yield (calculated on DAMN mmol)
A₁		¹ H NMR (400 MHz, DMSO-d ₆) δ ppm 7.05 - 7.15 (m, 2 H) 7.21 (s, 2 H) 7.44 (dd, J=8.99, 5.04 Hz, 2 H) 7.56 (br s, 1 H) 8.87 (s, 1 H) UPLC-MS: t _R = 0.66 min; MS (ESI): m/z 245.9 [M + H] ⁺

		<p>UPLC-MS Purity= 90%</p> <p>Yield 89% (6.88mmol)</p>
A₇		<p>¹H NMR (400 MHz, DMSO-d₆) δ ppm 3.15 (s, 3 H) 6.58 - 6.73 (m, 1 H) 6.65 (br s, 1 H) 7.32 (s, 2 H) 7.68 (d, J=8.55 Hz, 2 H) 7.78 - 7.86 (m, 3 H) 7.99 -8.13 (m, 2 H) 9.39 (s, 1 H)</p> <p>UPLC-MS: t_R=0.53 min; MS (ESI): m/z 306.0 [M + H]⁺</p> <p>UPLC Purity= 95%</p> <p>Yield 10% (1.30 mmol)</p>
A₈		<p>¹H NMR (400 MHz, DMSO-d₆) δ ppm 9.07 (s, 1 H), 8.04 (t, J=1.76 Hz, 1 H), 7.56 - 7.77 (m, 3 H), 7.37 - 7.49 (m, 1 H), 7.27 (s, 2 H), 2.55 (s, 3 H)</p> <p>UPLC-MS: t_R=0.65, MS (ESI): m/z 269.9 [M + H]⁺</p> <p>H-NMR Analysis Purity= 90%</p> <p>Yield=56% (4.63 mmol)</p>
A₉		<p>¹H NMR (400 MHz, DMSO-d₆) δ ppm 2.96 - 3.07 (m, 3 H) 3.67 - 3.79 (m, 4 H) 6.87 (d, J=8.99 Hz, 2 H) 7.09 - 7.19 (m, 1 H) 7.29 (d, J=8.11 Hz, 2 H) 7.48(s, 1 H) 8.24 - 8.32 (m, 1 H) 8.58 (s, 1 H)</p> <p>UPLC-MS: t_R= 0.48 min, MS (ESI): m/z 313.0 [M + H]⁺</p> <p>UPLC Purity= 83%</p> <p>Yield 39% (0.46 mmol)</p>
A₁₀		<p>¹H NMR (400 MHz, DMSO-d₆) δ ppm 3.14 (t, J=8.66 Hz, 2 H) 4.47 (t, J=8.66 Hz, 2 H) 6.65 (d, J=8.55 Hz, 1 H) 7.05 (dd, J=8.55, 1.97 Hz, 1 H) 7.10 (s, 2 H) 7.33 (d, J=0.88 Hz, 1 H) 7.58 (br s, 1 H) 8.63 (s, 1 H)</p> <p>UPLC-MS: t_R = 0.63min; MS (ESI): m/z 270 [M + H]⁺</p> <p>UPLC purity= 90%</p>

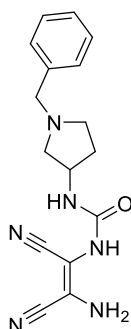
		Yield 76% (5.85 mmol)
A₁₁		<p>¹H NMR (400 MHz, DMSO-d₆) δ ppm 2.41 (s, 3 H) 7.05 (td, J=7.56, 1.32 Hz, 1 H) 7.17 (br s, 2 H) 7.19 - 7.25 (m, 1 H) 7.42 (dd, J=7.89, 1.32 Hz, 1 H) 7.92 (dd, J=8.22, 0.99 Hz, 1 H) 8.20 (s, 1 H) 8.44 (s, 1 H)</p> <p>UPLC-MS: t_R= 0.72 min, MS (ESI): m/z 274, [M + H]⁺</p> <p>UPLC Purity= 72%</p> <p>Yield 41% (1.78 mmol)</p>
A₁₂		<p>¹H NMR (400 MHz, DMSO-d₆) δ ppm 1.48 - 1.60 (m, 2 H) 1.88 - 1.98 (m, 2 H) 3.42 - 3.48 (m, 2 H) 3.83 (dt, J=11.46, 4.47 Hz, 2 H) 4.45 (tt, J=8.52, 4.08 Hz, 1 H) 6.89 (d, J=8.99 Hz, 2 H) 7.14 (s, 2 H) 7.31 (d, J=8.99 Hz, 2 H) 7.49 (s, 1 H) 8.64 (s, 1 H)</p> <p>UPLC-MS: t_R= 0.69 min, MS (ESI): m/z 328.5 [M+H]⁺</p> <p>UPLC Purity= 97%</p> <p>Yield 71 % (2.15 mmol)</p>
A₁₃		<p>¹H NMR (400 MHz, DMSO-d₆) δ ppm 7.19 - 7.37 (m, 2 H) 7.56 - 7.77 (m, 3 H) 8.12 - 8.26 (m, 1 H) 8.50 (s, 1 H) 9.35 (s, 1 H)</p> <p>UPLC-MS: t_R= 0.69 min, MS (ESI): m/z 285. [M + H]⁺</p> <p>UPLC Purity= 80%</p> <p>Yield 91% (2.79 mmol)</p>
A₁₄		<p>¹H NMR (400 MHz, DMSO-d₆) δ ppm 1.15 - 1.20 (m, 3 H) 3.57 (s, 2 H) 4.02 - 4.12 (m, 2 H) 7.12 - 7.23 (m, 4 H) 7.37 (d, J=8.33 Hz, 2 H) 7.52 - 7.60 (m, 1H) 8.81 (s, 1 H)</p> <p>UPLC-MS: t_R= 0.76 min, MS (ESI): m/z 314 [M + H]⁺</p> <p>UPLC Purity= 99%</p> <p>Yield 34% (2.29 mmol)</p>

<p>A₁₅</p>		<p>¹H NMR (400 MHz, DMSO-d₆) 1H NMR (400 MHz, DMSO-d₆) δ ppm 6.56 - 6.61 (m, 1 H) 6.78 - 6.81 (m, 1 H) 6.86 (d, J=5.48 Hz, 1 H) 7.32 (br s, 2 H) 7.68 (s, 1 H) 9.87 (s, 1 H)</p> <p>UPLC-MS: t_R= min, MS (ESI): m/z 234.1 [M + H]⁺</p> <p>UPLC Purity= 86%</p> <p>Yield 25% (3.88 mmol)</p>
<p>A₁₆</p>		<p>UPLC-MS: t_R= 0.63 min, MS (ESI) m/z 263.15 [M+H]⁺</p> <p>UPLC Purity= 83%</p> <p>Yield 59 % (3.05 mmol)</p>
<p>A₁₇</p>		<p>¹H NMR (400 MHz, DMSO-d₆) δ ppm 2.35 (s, 3 H) 6.71 (s, 1 H) 7.24 (br s, 1 H) 7.41 - 7.58 (m, 6 H) 7.84 (br s, 1 H) 8.19 (s, 1 H)</p> <p>UPLC-MS: t_R= 0.69 min, MS (ESI): m/z 309.2 [M + H]⁺</p> <p>UPLC Purity= 94%</p> <p>Yield=70% (4.63 mmol)</p>
<p>A₁₈</p>		<p>¹H NMR (400 MHz, DMSO-d₆) δ ppm 1.38 - 1.50 (m, 2 H) 1.79 - 1.91 (m, 2 H) 2.78 - 2.88 (m, 5 H) 3.42 - 3.53 (m, 2 H) 6.42 - 6.49 (m, 1 H) 6.94 (s, 2 H) 7.34 (s, 1 H)</p> <p>UPLC-MS: t_R= 0.44 min, MS (ESI): m/z 313.1 [M + H]⁺</p> <p>UPLC Purity= 99%</p> <p>Yield=45% (2.12 mmol)</p>
<p>A₁₉</p>		<p>¹H NMR (400 MHz, DMSO-d₆) δ ppm 1.29 - 1.41 (m, 2 H) 1.44 - 1.68 (m, 4 H) 1.74 - 1.85 (m, 2 H) 3.87 (sxt, J=6.80 Hz, 1 H) 6.34 (br d, J=7.02 Hz, 1 H) 6.87 (s, 2 H) 7.23 (s, 1 H)</p> <p>UPLC-MS: t_R= 0.6 min, MS (ESI): m/z 220.3 [M + H]⁺</p> <p>UPLC Purity= 99%</p>

<p>A₂₃</p>		<p>¹H NMR (400 MHz, DMSO-d₆) δ ppm 1.43 - 1.62 (m, 3 H) 1.66 - 1.93 (m, 3 H) 3.52 - 3.69 (m, 2 H) 3.75 (br d, J=13.15 Hz, 1 H) 6.46 - 6.60 (m, 1 H) 6.97 (brd, J=6.36 Hz, 2 H) 7.36 (br d, J=19.07 Hz, 1 H)</p> <p>UPLC-MS: t_R= 0.63 min, MS (ESI): m/z 331.2 [M + H]⁺</p> <p>UPLC Purity= 90%</p> <p>Yield 55% (2.12 mmol)</p>
<p>A₂₄</p>		<p>¹H NMR (400 MHz, DMSO-d₆) δ ppm 2.93 (t, J=7.23 Hz, 2 H) 3.24 - 3.30 (m, 2 H) 6.49 (br t, J=5.59 Hz, 1 H) 6.88 - 7.01 (m, 4 H) 7.34 (dd, J=5.15, 1.21 Hz, 1 H) 7.54 (s, 1 H)</p> <p>UPLC-MS: t_R= 0.67 min MS (ESI): m/z 261.7 [M + H]⁺</p> <p>UPLC Purity= 95%</p> <p>Yield 65% (4.63 mmol)</p>
<p>A₂₅</p>		<p>¹H NMR (400 MHz, DMSO-d₆) δ ppm 2.73 (t, J=7.02 Hz, 2 H) 3.23 - 3.29 (m, 2 H) 5.28 - 5.35 (m, 1 H) 6.42 (t, J=5.59 Hz, 1 H) 6.94 (s, 2 H) 7.22 (dd, J=8.33, 1.97 Hz, 1 H) 7.44 - 7.57 (m, 3 H)</p> <p>UPLC-MS: t_R= 0.93 min, MS (ESI): m/z 324.0 [M + H]⁺</p> <p>UPLC Purity= 95%</p> <p>Yield=52% (4.37 mmol)</p>
<p>A₂₆</p>		<p>¹H NMR (400 MHz, DMSO-d₆) δ ppm 4.39 (d, J=5.92 Hz, 2 H) 6.92 - 7.08 (m, 5 H) 7.35 - 7.43 (m, 1 H) 7.54 (s, 1 H)</p> <p>UPLC-MS: t_R= 0.56 min, MS (ESI): m/z 274 [M + H]⁺</p> <p>UPLC Purity= 99%</p> <p>Yield 47% (3.54 mmol)</p>

<p>A27</p>	 <p>The structure shows a benzene ring with a fluorine atom at the para position and a propyl chain at the other para position. The terminal carbon of the propyl chain is marked with an asterisk (*).</p>	<p>¹H NMR (400 MHz, DMSO-d₆) δ ppm 4.22 (d, J=5.92 Hz, 2 H) 6.95 (br t, J=5.92 Hz, 1 H) 6.91 - 6.99 (m, 1 H) 6.93 - 6.97 (m, 1 H) 7.03 (br s, 1 H) 7.14 (t, J=8.88 Hz, 2 H) 7.32 (dd, J=8.33, 5.70 Hz, 2 H) 7.52 (br s, 1 H)</p> <p>UPLC-MS: t_R= 0.69 min, MS (ESI): m/z 259.9 [M + H]⁺</p> <p>UPLC Purity= 95%</p> <p>Yield 73% (6.88 mmol)</p>
<p>A54</p>	 <p>The structure shows a benzene ring with an isopropyl group at the para position and a propyl chain at the other para position. The terminal carbon of the propyl chain is marked with an asterisk (*).</p>	<p>¹H NMR (400 MHz, DMSO-d₆) δ ppm 1.18 (d, J=7.02 Hz, 6 H) 2.67 (t, J=7.34 Hz, 2 H) 2.84 (dt, J=13.81, 6.91 Hz, 1 H) 3.20 - 3.27 (m, 2 H) 5.30 (br s, 1 H) 6.38 (br t, J=5.48 Hz, 1 H) 6.90 (s, 2 H) 7.09 - 7.19 (m, 4 H) 7.48 (s, 1 H)</p> <p>UPLC-MS: t_R= 1.0 min, MS (ESI): m/z 298.1 [M + H]⁺</p> <p>UPLC Purity = 81%</p> <p>Yield 5% (2.49 mmol)</p>
<p>A55</p>	 <p>The structure shows a benzene ring fused to a five-membered ring containing two oxygen atoms (a benzofuran derivative). A propyl chain is attached to the benzene ring at the 5-position. The terminal carbon of the propyl chain is marked with an asterisk (*).</p>	<p>¹H NMR (400 MHz, DMSO-d₆) δ ppm 2.63 (t, J=7.23 Hz, 2 H) 3.22 (q, J=6.80 Hz, 2 H) 5.96 (s, 2 H) 6.35 (br t, J=5.48 Hz, 1 H) 6.67 (d, J=7.89 Hz, 1 H) 6.78 - 6.85 (m, 2 H) 6.90 (br s, 2 H) 7.47 (s, 1 H)</p> <p>UPLC-MS: t_R= 0.71 min, MS (ESI): m/z 300.0 [M + H]⁺</p> <p>UPLC Purity= 99%</p> <p>Yield 50% (4.93 mmol)</p>
<p>A56</p>	 <p>The structure shows a cyclopropyl ring attached to a benzene ring. The carbon of the cyclopropyl ring that is not bonded to the benzene ring is marked with an asterisk (*).</p>	<p>¹H NMR (400 MHz, DMSO-d₆) δ ppm 1.08 - 1.21 (m, 2 H) 1.93 - 2.02 (m, 1 H) 2.64 - 2.74 (m, 1 H) 6.87 (br d, J=2.19 Hz, 1 H) 7.01 (s, 2 H) 7.07 - 7.19 (m, 3 H) 7.22 - 7.31 (m, 2 H) 7.41 (s, 1 H)</p> <p>UPLC-MS: t_R= 0.78 min, MS (ESI): m/z 268.1 [M + H]⁺</p> <p>UPLC Purity= 100%</p> <p>Yield 41% (1.48 mmol)</p>

5.2.1 Synthesis of 1-(2-amino-1,2-dicyanovinyl)-3-(1-benzylpyrrolidin-3-yl)urea (A₅₂)

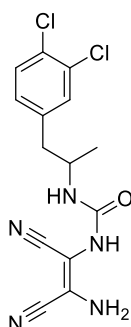


To an ice-cold stirring solution of 1-benzylpyrrolidin-3-amine (100 mg, 0,567 mmol) in 3 mL of DCM was added triphosgene (337 mg, 1.135 mmol). The solution was stirred at rt and added of a solution of 2,3-diaminomaleonitrile (184 mg, 1.702 mmol) in THF. Solution was stirred for 12 hr at rt and then evaporated. Reaction was quenched with HCl 1N (1mL). Solvent was evaporated under vacuum to give (Z)-1-(2-amino-1,2-dicyanovinyl)-3-(1-benzylpyrrolidin-3-yl)urea (100 mg, 0.322 mmol, 56.8 % yield).

UPLC-MS: $t_R = 0.29$ min, MS (ESI): m/z [M + H]⁺ 311.03

UPLC Purity= 85%

5.2.2 Synthesis of 1-(2-amino-1,2-dicyanovinyl)-3-(1-(3,4-dichlorophenyl)propan-2-yl)urea (A₅₃)



3-(3,4-dichlorophenyl)-2-methylpropanoic acid (100 mg, 0.429 mmol) and TRIETHYLAMINE (0.149 ml, 1.287 mmol) were dissolved in Toluene (Volume: 3 ml) then DPPA (0.269 ml, 0.858 mmol) was added at rt. The solution was heated up to 80 °C for 2 hr. Then 2,3-diaminomaleonitrile (139 mg,

1.287 mmol) dissolved in 2 ml of THF was added to the reaction. The solution was cooled down to 50 C° and stirring was continued for another 2 hr. The solution was diluted with DCM (10 mL) and organic phase was washed with NaHCO₃ saturated solution, brine, dried over Na₂SO₄. Organic phase was evaporated to give 23 mg of crude which was used in the next step without any further purification.

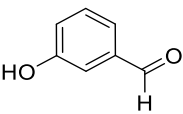
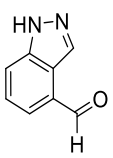
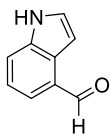
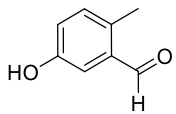
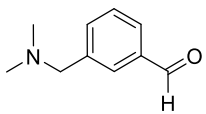
UPLC-MS: $t_R = 0.9$ min, MS (ESI): m/z [M + H]⁺ 338.05

Yield 15%

5.3 General Procedure for 2,9-disubstituted-8-oxopurine-6-carboxamide (A_xB_y)

In an 8 mL vial, 0.120 mmol of the corresponding diaminomaleonitrile urea was dissolved in 5 mL of MeOH. Then the corresponding aldehyde (B1, B2, B10, B11, B12, **Table 15**) (0.030 g, 0.246 mmol) was added to the suspension and kept stirring at rt for 10 minutes. TEA (0.017 mL, 0.120 mmol) was added to the reaction mixture after 10 min. A homogeneous solution was obtained and shortly after a solid started to precipitate out. A catalytic amount of I₂ was added to the mixture. The mixture was stirred for 12 hr at room temperature. In all cases the desired product was filtered, washed with MeOH, Et₂O and dried under vacuum.

Table 15: Structure of Aldehydes.

	B ₁	B ₂	B ₁₀	B ₁₁	B ₁₂
Aldehydes					

All the title compounds are reported in the following table.

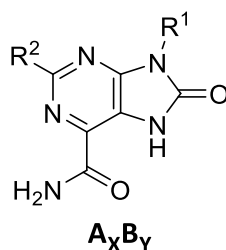
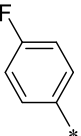
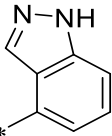
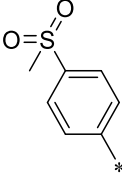
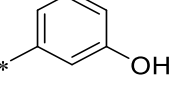
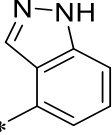
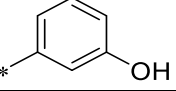
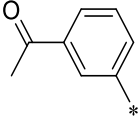
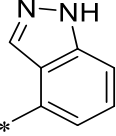
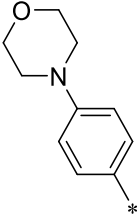
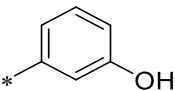
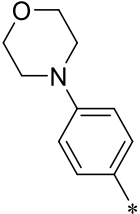
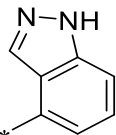
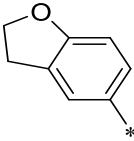
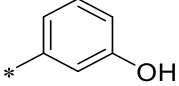
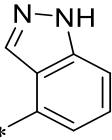
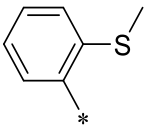
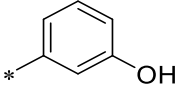
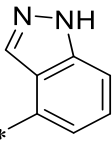
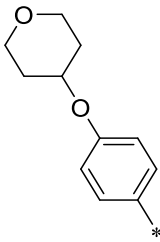
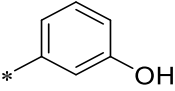
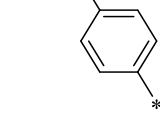
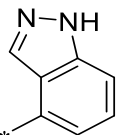
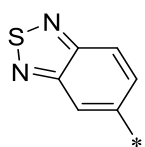
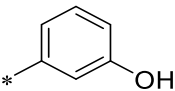


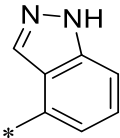
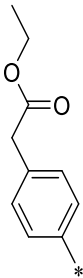
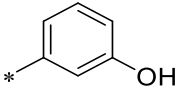
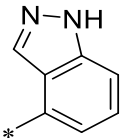
Table 16: Final compounds A_xB_y .

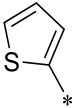
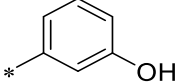
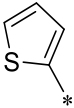
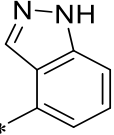
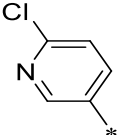
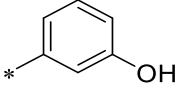
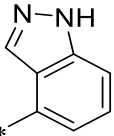
Compound	R ¹	R ²	¹ H-NMR UPLC-MS Purity Yield
A ₁ B ₂			<p>¹H NMR (400 MHz, DMSO-d₆) δ ppm 7.42 - 7.54 (m, 3 H) 7.65 (d, J=8.33 Hz, 1 H) 7.78 - 7.85 (m, 2 H) 8.01 (br s, 1 H) 8.40 (br s, 1 H) 8.44 (d, J=7.23 Hz, 1H) 8.55 (s, 1 H) 11.82 (br s, 1 H) 13.10 - 13.32 (m, 1 H) 13.19 (s, 1 H)</p> <p>UPLC-MS: t_R= 0.83 min, MS (ESI): m/z 390.3 [M+H]⁺</p> <p>UPLC Purity= 95%</p> <p>Yield 77%</p>
A ₇ B ₁			<p>¹H NMR (400 MHz, DMSO-d₆) δ ppm 11.89 (s, 1 H), 9.49 (s, 1 H), 8.41 (br. s., 1 H), 8.07 - 8.21 (m, 4 H), 7.93 - 8.01 (m, 2 H), 7.77 -7.84 (m, 1 H), 7.27 (t, J=7.9 Hz, 1 H), 6.81 - 6.89 (m, 1 H), 3.33 (s, 3 H)</p> <p>UPLC-MS: t_R= 0.71 min, MS (ESI): m/z 242.2 [M+H]⁺</p> <p>UPLC Purity= 95%</p> <p>Yield 32%</p>
A ₇ B ₂			<p>¹H NMR (400 MHz, DMSO-d₆) δ ppm 13.10 (s, 1 H), 11.85 (br. s., 1 H), 8.28 - 8.70 (m, 3 H), 7.90 - 8.18 (m, 3 H), 7.52 - 7.83 (m, 2 H), 7.17 - 7.49 (m, 1 H), 2.66 (s, 3 H)</p> <p>UPLC-MS: t_R= 0.69 min, MS (ESI): m/z 450.2 [M+H]⁺</p> <p>UPLC Purity= 90%</p> <p>Yield 10%</p>
A ₈ B ₁			<p>¹H NMR (400 MHz, DMSO-d₆) δ ppm 2.61 - 2.69 (m, 3 H) 6.85 (dd, J=8.00, 1.86 Hz, 1 H) 7.25 (t, J=8.00 Hz, 1 H)</p>

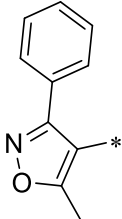
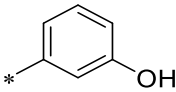
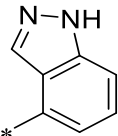
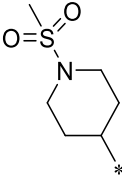
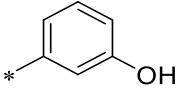
			<p>7.74 - 7.82 (m, 2 H) 7.92 - 8.04 (m, 3 H) 8.08 (d, J=7.89 Hz, 1 H) 8.35 (t, J=1.75 Hz, 1 H) 8.39 (s, 1 H) 9.47 (s, 1 H) 11.82 (s, 1 H)</p> <p>UPLC-MS: t_R= 0.80 min, MS (ESI): m/z 390.1 [M+H]⁺</p> <p>UPLC Purity= 90%</p> <p>Yield 74%</p>
A₈B₂			<p>¹H NMR (400 MHz, DMSO-d₆) δ ppm 13.19 (s, 1 H), 11.93 (s, 1 H), 8.60 (bs, 1 H), 8.34 - 8.44 (m, 1 H), 8.05 - 8.22 (m, 4 H), 8.02 (bs, 1 H), 7.59 - 7.68 (m, 1 H), 7.44 (t, J=7.7 Hz, 1 H), 3.30 (s, 3 H)</p> <p>UPLC-MS: t_R= 0.76 min, MS (ESI): m/z 414.0 [M+H]⁺</p> <p>UPLC Purity= 90%</p> <p>Yield=12%</p>
A₉B₁			<p>¹H NMR (400 MHz, DMSO-d₆) δ ppm 11.66 (bs, 1 H), 9.46 (s, 1 H), 8.37 (bs, 1 H), 7.90 - 7.95 (m, 2 H), 7.76 (s, 1 H), 7.50 (d, J=9.2 Hz, 2 H), 7.24 (t, J=7.9 Hz, 1 H), 7.13 (d, J=9.2 Hz, 2 H), 6.80 - 6.90 (m, 1 H), 3.75 - 3.84 (m, 4 H), 3.18 - 3.26 (m, 4 H)</p> <p>UPLC MS: t_R= 0.79 min, MS (ESI): m/z 433.3 [M+H]⁺</p> <p>UPLC Purity= 91%</p> <p>Yield 15%</p>
A₉B₂			<p>¹H NMR (400 MHz, DMSO-d₆) δ ppm 3.21 - 3.28 (m, 4 H) 3.77 - 3.83 (m, 3 H) 3.77 - 3.84 (m, 1 H) 7.18 (d, J=8.99 Hz, 2 H) 7.41 - 7.49 (m, 1 H) 7.57 (d, J=8.77 Hz, 2 H) 7.64 (d, J=8.33 Hz, 1 H) 8.01 (br s, 1 H) 8.40 (br s, 1 H) 8.44 (d, J=7.23 Hz, 1 H) 8.59 (s, 1 H) 11.74 (s, 1 H) 13.18 (s, 1 H)</p> <p>UPLC-MS: t_R= 0.76 min, MS (ESI): m/z 457 [M+H]⁺</p> <p>UPLC Purity= 85%</p>

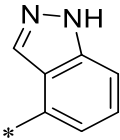
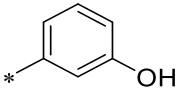
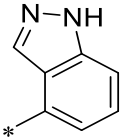
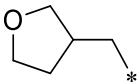
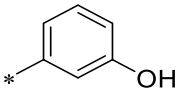
			Yield 52%
A₁₀B₁			<p>¹H-NMR (400 MHz, DMSO-d₆) δ ppm 3.27 - 3.30 (m, 2 H) 4.65 (t, J=8.77 Hz, 2 H) 6.80 - 6.86 (m, 1 H) 6.96 (d, J=8.55 Hz, 1 H) 7.24 (t, J=8.00 Hz, 1 H) 7.34 (dd, J=8.44, 2.08 Hz, 1 H) 7.47 (s, 1 H) 7.71 - 7.80 (m, 1 H) 7.89 - 7.99 (m, 2 H) 8.36 (br s, 1 H) 9.46 (s, 1 H) 11.65 (br s, 1 H)</p> <p>UPLC-MS: t_R= 0.83 min, MS (ESI): m/z 388 [M-H]⁻</p> <p>UPLC Purity= 85%</p> <p>Yield 73%</p>
A₁₀B₂			<p>¹H NMR (400 MHz, DMSO-d₆) δ ppm 3.25 - 3.29 (m, 2 H) 4.61 (t, J=8.77 Hz, 2 H) 6.92 - 6.97 (m, 1 H) 7.34 - 7.42 (m, 2 H) 7.50 (s, 1 H) 7.58 (d, J=8.33 Hz, 1 H) 7.93 (br s, 1 H) 8.20 (s, 1 H) 8.34 (br s, 1 H) 8.39 (d, J=7.23 Hz, 1 H) 8.52 (s, 1 H) 11.67 (br s, 1 H) 13.11 (s, 1 H)</p> <p>UPLC-MS: t_R= 0.79 min, MS (ESI): m/z 414.1 [M+H]⁺</p> <p>UPLC Purity= 80%</p> <p>Yield 40%</p>
A₁₁B₁			<p>¹H-NMR (400 MHz, DMSO-d₆) δ ppm 2.40 (s, 3 H) 6.81 (dd, J=8.00, 2.30 Hz, 1 H) 7.22 (t, J=7.89 Hz, 1 H) 7.35 - 7.45 (m, 1 H) 7.49 - 7.69 (m, 4 H) 7.86 (d, J=7.89 Hz, 1 H) 7.98 (br s, 1 H) 8.38 (br s, 1 H) 9.36 - 9.58 (m, 1 H) 11.78 (br s, 1 H)</p> <p>UPLC-MS: t_R= 0.85 min, MS (ESI): m/z 394.2 [M-H]⁺</p> <p>UPLC Purity= 86%</p> <p>Yield 44%</p>
A₁₁B₂			<p>¹H-NMR (400 MHz, DMSO-d₆) δ ppm 2.41 (s, 3 H) 7.38 - 7.51 (m, 2 H) 7.57 - 7.67 (m, 4 H) 8.03 (br s, 1 H)</p>

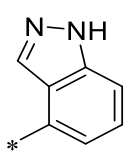
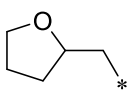
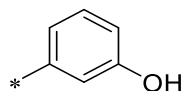
			<p>8.29 - 8.45 (m, 3 H) 11.86 (br s, 1 H) 13.13 (br s, 1 H)</p> <p>UPLC-MS: t_R= 0.80 min, MS (ESI): m/z 418.1 [M+H]⁺</p> <p>UPLC Purity= 94%</p> <p>Yield 30%</p>
A₁₂B₁			<p>¹H-NMR (400 MHz, DMSO-d₆) δ ppm 1.58 - 1.72 (m, 2 H) 2.04 (br dd, J=12.93, 3.29 Hz, 2 H) 3.48 - 3.58 (m, 2 H) 3.83 - 3.95 (m, 2 H) 4.68 (tt, J=8.60, 4.00 Hz, 1 H) 6.84 (dd, J=8.00, 1.86 Hz, 1 H) 7.19 (d, J=8.99 Hz, 2 H) 7.25 (t, J=7.89 Hz, 1 H) 7.57 (d, J=8.99 Hz, 2 H) 7.77 (d, J=1.75 Hz, 1 H) 7.92 - 8.00 (m, 2H) 8.38 (s, 1 H) 9.48 (s, 1 H) 11.70 (s, 1H)</p> <p>UPLC-MS: t_R= 0.86 min, MS (ESI): m/z 448.1 [M+H]⁺</p> <p>UPLC Purity= 95%</p> <p>Yield 18%</p>
A₁₂B₂			<p>¹H-NMR (400 MHz, DMSO-d₆) δ ppm 1.59 - 1.73 (m, 2 H) 2.00 - 2.15 (m, 2 H) 3.48 - 3.61 (m, 2 H) 3.91 (dt, J=11.62, 4.28 Hz, 2 H) 4.66 - 4.79 (m, 1 H) 7.19 - 7.29 (m, 2 H) 7.40 - 7.51 (m, 1 H) 7.61 - 7.69 (m, 3 H) 7.96 - 8.07 (m, 1 H) 8.40 (s, 1 H) 8.45 (d, J=7.23 Hz, 1 H) 8.57 (s, 1 H) 11.76 (s, 1 H) 13.18 (s, 1 H)</p> <p>UPLC-MS: t_R= 0.81 min, MS (ESI): m/z 472.0 [M+H]⁺</p> <p>UPLC Purity= 99%</p> <p>Yield 33%</p>
A₁₃B₁			<p>¹H-NMR (400 MHz, DMSO-d₆) δ ppm 11.97 (br. s., 1 H) 9.38 (br. s., 1 H) 8.43 (s, 1 H) 8.34 (d, J=8.82 Hz, 1 H) 7.94 - 8.09 (m, 3 H) 7.81 (d, J=7.94 Hz, 1 H) 7.55 (s, 1 H) 7.18 (t, J=7.94 Hz, 1 H) 6.79 (dd, J=7.94, 2.21 Hz, 1 H)</p>

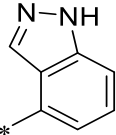
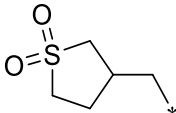
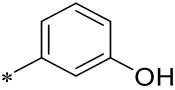
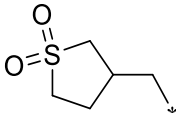
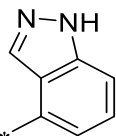
			<p>UPLC-MS: $t_R = 0.76$ min, MS (ESI): m/z 405.9 [M+H]⁺</p> <p>UPLC Purity= 90%</p> <p>Yield 13%</p>
A₁₃B₂			<p>¹H-NMR (400 MHz, DMSO-d₆) δ ppm 7.37 - 7.44 (m, 1 H) 7.60 (d, J=8.11 Hz, 1 H) 7.94 (s, 1 H) 8.00 - 8.15 (m, 3 H) 8.38 (dd, J=13.70, 8.00 Hz, 2 H) 8.45 (s, 1 H) 12.04 (br s, 1 H) 13.18 (br s, 1 H)</p> <p>UPLC-MS: $t_R = 0.75$ min, MS (ESI): m/z 430.1 [M+H]⁺</p> <p>UPLC Purity= 85%</p> <p>Yield 12%</p>
A₁₄B₁			<p>¹H-NMR (400 MHz, DMSO-d₆) δ ppm 11.75 (s, 1 H), 9.49 (s, 1 H), 8.38 (s, 1 H), 7.87 - 8.06 (m, 2 H), 7.73 - 7.80 (m, 1 H), 7.66 (d, J=8.4 Hz, 2 H), 7.49 (d, J=8.4 Hz, 2 H), 7.25 (t, J=7.7 Hz, 1 H), 6.84 (dd, J=7.9, 2.2 Hz, 1 H), 4.13 (q, J=7.1 Hz, 2 H), 3.80 (s, 2 H), 1.07 - 1.38 (m, 3 H)</p> <p>UPLC-MS: $t_R = 0.91$ min, MS (ESI): m/z 433.9 [M+H]⁺</p> <p>UPLC Purity= 94%</p> <p>Yield 38%</p>
A₁₄B₂			<p>¹H-NMR (400 MHz, DMSO-d₆) δ ppm 1.23 (t, J=7.02 Hz, 3 H) 3.83 (s, 2 H) 4.14 (q, J=7.02 Hz, 2 H) 7.42 - 7.50 (m, 1 H) 7.51 - 7.60 (m, 2 H) 7.65 (d, J=8.33 Hz, 1 H) 7.73 (d, J=8.33 Hz, 2 H) 8.02 (br s, 1 H) 8.35 - 8.49 (m, 2 H) 8.58 - 8.65 (m, 1 H) 11.81 (br s, 1 H) 13.18 (s, 1 H)</p> <p>UPLC-MS: $t_R = 0.87$ min, MS (ESI): m/z 458.1 [M+H]⁺</p> <p>UPLC Purity= 95%</p> <p>Yield 60%</p>

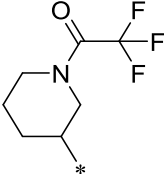
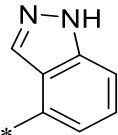
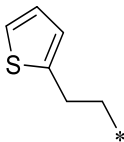
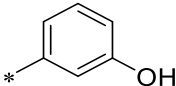
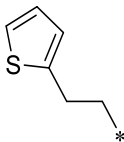
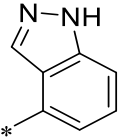
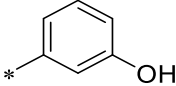
<p>A₁₅B₁</p>			<p>¹H-NMR (400 MHz, DMSO-d₆) δ ppm 7.19 (dd, J=5.37, 3.84 Hz, 1 H) 7.31 (t, J=7.89 Hz, 1 H) 7.49 - 7.54 (m, 1 H) 7.88 (dd, J=3.73, 1.32 Hz, 1 H) 7.94 (t, J=1.86 Hz, 1 H) 8.00 (s, 1 H) 8.05 (d, J=7.89 Hz, 1 H) 8.42 (s, 1 H) 9.56 (s, 1 H) 11.96 (s, 1 H)</p> <p>UPLC-MS: t_R= 0.86 min, MS (ESI): 354.0 [M+H]⁺</p> <p>UPLC Purity= 98%</p> <p>Yield 33%</p>
<p>A₁₅B₂</p>			<p>¹H NMR (400 MHz, DMSO-d₆) δ ppm 7.23 (dd, J=5.37, 3.84 Hz, 1 H) 7.50 (t, J=7.78 Hz, 1 H) 7.62 (dd, J=5.48, 1.10 Hz, 1 H) 7.69 (d, J=8.33 Hz, 1 H) 7.75 (dd, J=3.73, 1.10 Hz, 1 H) 8.06 (s, 1 H) 8.38 (s, 1 H) 8.47 (d, J=7.45 Hz, 1 H) 8.80 (s, 1 H) 11.99 (br s, 1 H) 13.25 (s, 1 H)</p> <p>UPLC-MS: t_R= 0.80 min, MS (ESI): m/z 377.9 [M+H]⁺</p> <p>UPLC Purity= 80%</p> <p>Yield= 51%</p>
<p>A₁₆B₁</p>			<p>¹H-NMR (400 MHz, DMSO-d₆) δ ppm 6.86 (br d, J=7.02 Hz, 1 H) 7.27 (br t, J=7.89 Hz, 1 H) 7.77 - 7.88 (m, 2 H) 7.95 - 8.01 (m, 2 H) 8.29 (br dd, J=8.44, 1.86 Hz, 1 H) 8.42 (br s, 1 H) 8.87 (br d, J=1.53 Hz, 1 H) 9.14 - 9.30 (m, 1 H) 9.38 - 9.67 (m, 1 H) 11.93 (br s, 1 H)</p> <p>UPLC-MS: t_R= 0.8 min, MS (ESI): m/z 383.2 [M+H]⁺</p> <p>UPLC Purity=87%</p> <p>Yield 59%</p>
			<p>¹H-NMR (400 MHz, DMSO-d₆) δ ppm 7.48 (t, J=7.78 Hz, 1 H) 7.68 (d, J=8.33 Hz, 1 H) 7.88 (d, J=8.55 Hz, 1 H) 8.06 (s, 1 H) 8.33 (dd, J=8.55, 2.63 Hz, 1H) 8.42 (br s, 1 H) 8.46 (d, J=7.23 Hz, 1 H) 8.58 (d, J=0.88 Hz, 1</p>

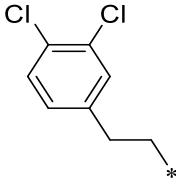
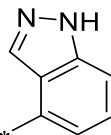
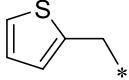
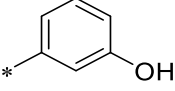
			<p>H) 8.92 (d, J=2.63 Hz, 1 H) 12.00 (s, 1 H) 13.28 (s, 1 H)</p> <p>UPLC-MS: t_R= 0.8 min, MS (ESI): m/z 383.2 [M+H]⁺</p> <p>UPLC Purity= 92%</p> <p>Yield 32%</p>
A₁₇B₁			<p>¹H-NMR (400 MHz, DMSO-d₆) δ ppm 3.28 (s, 1 H) 6.46 - 6.58 (m, 1 H) 6.78 - 6.85 (m, 1 H) 7.22 (t, J=7.89 Hz, 1 H) 7.34 - 7.44 (m, 3 H) 7.46 - 7.53 (m, 2H) 7.69 (s, 1 H) 7.86 (br d, J=7.67 Hz, 1 H) 7.99 (br s, 1 H) 8.42 (br s, 1 H) 9.46 (s, 1 H) 11.95 (br s, 1 H)</p> <p>UPLC-MS: t_R= 0.87 min, MS (ESI): m/z 429.0 [M+H]⁺</p> <p>UPLC Purity= 95%</p> <p>Yield 19%</p>
A₁₇B₂			<p>¹H-NMR (400 MHz, DMSO-d₆) δ ppm 13.19 (s, 1 H), 11.90 - 12.05 (s, 1 H), 8.23 - 8.62 (m, 3 H), 8.07 (s, 1 H), 7.59 - 7.67 (m, 1 H), 7.49 - 7.56 (m, 2 H), 7.36 - 7.46 (m, 4 H), 3.29 (s, 3 H)</p> <p>UPLC-MS: t_R= 0.82 min, MS (ESI): m/z 452.8 [M+H]⁺</p> <p>UPLC Purity= 96%</p> <p>Yield 12%</p>
A₁₈B₁			<p>¹H-NMR (400 MHz, DMSO-d₆) δ ppm 1.83 - 2.01 (m, 2 H) 2.91 - 3.06 (m, 5 H) 3.75 (br d, J=11.40 Hz, 2 H) 4.28 - 4.50 (m, 1 H) 6.81 - 6.99 (m, 1 H) 7.29 (t, J=7.89 Hz, 1 H) 7.82 - 8.06 (m, 3 H) 8.26 - 8.43 (m, 1 H) 9.48 - 9.60 (m, 1 H) 11.56 (br s, 1 H)</p> <p>UPLC-MS: t_R= 0.7 min, MS (ESI): m/z 433.0 [M+H]⁺</p> <p>UPLC Purity= 90%</p>

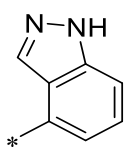
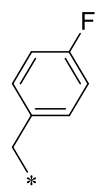
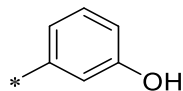
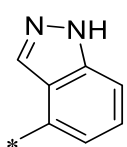
			Yield 10%
A₁₈B₂			<p>¹H-NMR (400 MHz, DMSO-d₆) δ ppm 1.92 (br d, J=11.40 Hz, 2 H) 2.55 - 2.67 (m, 2 H) 2.56 - 2.65 (m, 1 H) 2.92 - 3.02 (m, 5 H) 3.75 (br d, J=11.40 Hz, 2 H) 4.37 - 4.51 (m, 1 H) 6.85 - 6.93 (m, 1 H) 7.29 (t, J=7.89 Hz, 1 H) 7.85 - 8.00 (m, 3 H) 8.32 (br s, 1 H) 9.53 (s, 1 H) 11.56 (br s, 1 H)</p> <p>UPLC-MS: t_R= 0.67min, MS (ESI): m/z 457.0 [M+H]⁺</p> <p>UPLC Purity= 91%</p> <p>Yield 11%</p>
A₁₉B₁			<p>¹H-NMR (400 MHz, DMSO-d₆) δ ppm 1.61 - 1.75 (m, 2 H) 1.90 - 2.09 (m, 4 H) 2.15 - 2.30 (m, 2 H) 4.83 (quin, J=8.28 Hz, 1 H) 6.84 - 6.91 (m, 1 H) 7.28 (t, J=7.89 Hz, 1 H) 7.87 (s, 1 H) 7.91 (br s, 1 H) 7.96 - 8.05 (m, 1 H) 8.32 (br s, 1 H) 9.53 (s, 1 H) 11.49 (s, 1 H)</p> <p>UPLC-MS: t_R= 0.90 min, MS (ESI): m/z 340 [M-H]⁺</p> <p>UPLC Purity= 95%</p> <p>Yield 17%</p>
A₁₉B₂			<p>¹H-NMR (400 MHz, DMSO-d₆) δ ppm 1.66 - 1.78 (m, 2 H) 1.94 - 2.10 (m, 4 H) 2.26 2.39 (m, 2 H) 4.89 (quin, J=8.39 Hz, 1 H) 7.44 - 7.51 (m, 1 H) 7.67 (d, J=8.11 Hz, 1 H) 7.91 - 8.00 (m, 1 H) 8.26 (br s, 1 H) 8.38 (d, J=7.23 Hz, 1 H) 8.81 (s, 1 H) 11.55 (br s, 1 H) 13.23 (s, 1 H)</p> <p>UPLC-MS: t_R= 0.87 min, MS (ESI): m/z 364.1 [M+H]⁺</p> <p>UPLC Purity= 95%</p> <p>Yield 11%</p>
A₂₀B₁			<p>¹H-NMR (600 MHz, DMSO-d₆) δ ppm 11.43 - 11.63 (m, 1 H), 9.20 - 9.53 (m, 1 H), 8.24 - 8.40 (m, 1 H),</p>

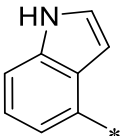
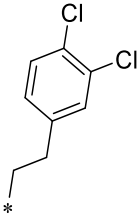
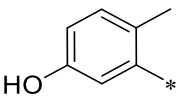
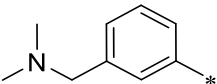
			<p>7.98 - 8.05 (m, 1 H), 7.82 - 7.95 (m, 2 H), 7.24 - 7.34 (m, 1 H), 6.68 - 6.90 (m, 1 H), 3.88 - 3.94 (m, 2 H), 3.78 - 3.85 (m, 1 H), 3.68 - 3.73 (m, 1 H), 3.58 - 3.66 (m, 2 H), 2.69 - 2.92 (m, 1 H), 1.89 - 2.02 (m, 1 H), 1.63 - 1.78 (m, 1 H)</p> <p>UPLC-MS: t_R = 2.06 min, MS (ESI): m/z 356.0 [M+H]⁺</p> <p>Method 2</p> <p>UPLC Purity= 93%</p> <p>Yield 68%</p>
A₂₀B₂			<p>¹H-NMR (400 MHz, DMSO-d₆) δ ppm 1.71 - 1.82 (m, 1 H) 1.94 - 2.05 (m, 1 H) 2.81 - 2.92 (m, 1 H) 3.59 - 3.75 (m, 3 H) 3.80 - 3.88 (m, 1 H) 3.95 - 4.03 (m, 2 H) 7.49 (t, J=7.78 Hz, 1 H) 7.68 (d, J=8.11 Hz, 1 H) 7.98 (br s, 1 H) 8.33 (br s, 1 H) 8.47 (d, J=7.45 Hz, 1 H) 8.89 (s, 1 H) 11.62 (br s, 1 H) 13.24 (s, 1 H)</p> <p>UPLC-MS: t_R = 0.66 min, MS (ESI): m/z 380.1 [M+H]⁺</p> <p>UPLC Purity= 90%</p> <p>Yield 30%</p>
A₂₁B₁			<p>¹H-NMR (400 MHz, DMSO-d₆) δ ppm 1.69 - 2.01 (m, 5 H) 3.57 - 3.69 (m, 1 H) 3.77 - 3.88 (m, 2 H) 3.92 - 4.04 (m, 1 H) 4.34 (quin, J=6.30 Hz, 1 H) 6.87 (dd, J=8.00, 2.08 Hz, 1 H) 7.28 (t, J=7.89 Hz, 1 H) 7.88 - 7.96 (m, 2 H) 8.01 (d, J=7.89 Hz, 1 H) 8.32 (br s, 1 H) 11.5 (br s, 1 H) 11.5 (br s, 1 H)</p> <p>UPLC-MS: t_R = 0.69 min, MS (ESI): m/z 356.0 [M+H]⁺</p> <p>UPLC Purity= 95%</p> <p>Yield 47%</p>

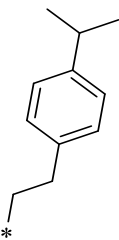
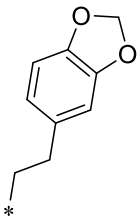
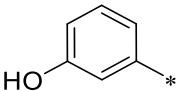
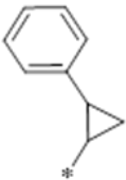
A ₂₁ B ₂			<p>¹H-NMR (400 MHz, DMSO-d₆) δ ppm 1.70 - 2.03 (m, 4 H) 3.55 - 3.65 (m, 1 H) 3.73 - 3.84 (m, 1 H) 3.88 - 3.97 (m, 1 H) 3.99 - 4.08 (m, 1 H) 4.34 (dt, J=12.44, 6.17 Hz, 1 H) 7.45 (t, J=7.78 Hz, 1 H) 7.65 (d, J=8.33 Hz, 1 H) 7.95 (br s, 1 H) 8.31 (br s, 1 H) 8.43 (d, J=7.23 Hz, 1 H) 8.89 (s, 1 H) 11.58 (br s, 1H) 13.19 (s, 1 H)</p> <p>UPLC-MS: t_R= 0.69 min, MS (ESI): m/z 380.1 [M+H]⁺</p> <p>UPLC Purity= 95%</p> <p>Yield 50%</p>
A ₂₂ B ₁			<p>¹H-NMR (400 MHz, DMSO-d₆) δ ppm 1.91 - 2.04 (m, 1 H) 2.21 - 2.35 (m, 1 H) 2.87 - 3.13 (m, 3 H) 3.15 - 3.27 (m, 1 H) 3.35 (br dd, J=12.61, 6.91 Hz, 1 H) 4.04 (d, J=6.36 Hz, 2 H) 6.88 (dd, J=8.00, 2.08 Hz, 1 H) 7.28 (t, J=7.89 Hz, 1 H) 7.91 (s, 2 H) 8.02 (d, J=7.89 Hz, 1 H) 8.32 (br s, 1 H) 9.51 (s, 1 H) 11.57 (brs, 1 H)</p> <p>UPLC-MS: t_R= 0.6 min, MS (ESI): m/z 404.2 [M+H]⁺</p> <p>UPLC Purity= 96%</p> <p>Yield 67%</p>
A ₂₂ B ₂			<p>¹H-NMR (400 MHz, DMSO-d₆) δ ppm 1.95 - 2.09 (m, 1 H) 2.23 - 2.37 (m, 1 H) 2.94 - 3.12 (m, 4 H) 3.18 - 3.26 (m, 1 H) 4.14 (br d, J=6.14 Hz, 2 H) 7.44 - 7.53 (m, 1 H) 7.68 (d, J=8.33 Hz, 1 H) 7.94 - 8.03 (m, 1 H) 8.28 - 8.35 (m, 1 H) 8.48 (d, J=7.45 Hz, 1 H) 8.92 (s, 1 H) 11.53 - 11.75 (m, 1 H) 13.24 (s, 1 H)</p> <p>UPLC-MS: t_R= 0.60 min, MS (ESI): m/z 428.1 [M+H]⁺</p> <p>UPLC Purity= 87%</p> <p>Yield 60%</p>

<p>A₂₃B₂</p>			<p>¹H NMR (400 MHz, DMSO-<i>d</i>₆) δ ppm 1.65 - 1.80 (m, 1 H) 1.95 - 2.13 (m, 1 H) 1.95 - 2.15 (m, 2 H) 2.63 - 2.83 (m, 2 H) 3.76 (br t, <i>J</i>=11.95 Hz, 1 H) 3.93 - 4.20 (m, 2 H) 4.39 - 4.63 (m, 3 H) 7.49 (t, <i>J</i>=7.78 Hz, 1 H) 7.69 (d, <i>J</i>=8.11 Hz, 1 H) 8.00 (br d, <i>J</i>=4.17 Hz, 1 H) 8.28 (br d, <i>J</i>=7.02 Hz, 1 H) 8.43 (t, <i>J</i>=6.36 Hz, 1 H) 8.83 (br d, <i>J</i>=4.60 Hz, 1 H) 11.67 (br d, <i>J</i>=7.67 Hz, 1 H) 13.27 (br s, 1 H)</p> <p>UPLC-MS: <i>t_R</i>= 0.84 min, MS (ESI): <i>m/z</i> 475.0 [M+H]⁺</p> <p>UPLC Purity= 96%</p> <p>Yield 39%</p>
<p>A₂₄B₁</p>			<p>¹H-NMR (400 MHz, DMSO-<i>d</i>₆) δ ppm 11.51 (s, 1 H), 9.49 (s, 1 H), 8.31 (br. s., 1 H), 7.99 (d, <i>J</i>=7.9 Hz, 1 H), 7.89 (d, <i>J</i>=1.8 Hz, 2 H), 7.21 - 7.32 (m, 2 H), 6.80 - 6.92 (m, 3 H), 4.16 (t, <i>J</i>=7.0 Hz, 2 H), 3.39 (t, <i>J</i>=7.0 Hz, 2 H)</p> <p>UPLC-MS: <i>t_R</i>= 0.87 min, MS (ESI): <i>m/z</i> 382.0 [M+H]⁺</p> <p>UPLC Purity= 94%</p> <p>Yield 28%</p>
<p>A₂₄B₂</p>			<p>¹H-NMR (400 MHz, DMSO-<i>d</i>₆) δ ppm 13.22 (m, 1 H), 11.60 (s, 1 H), 8.87 (s, 1 H), 8.43 - 8.48 (m, 1 H), 8.32 (bs, 1 H), 7.98 (bs, 1 H), 7.64 - 7.72 (m, 1 H), 7.44 - 7.51 (m, 1 H), 7.26 - 7.32 (m, 1 H), 6.85 - 6.96 (m, 2 H), 4.25 (t, <i>J</i>=7.2 Hz, 2 H), 3.43 (t, <i>J</i>=7.2 Hz, 2 H)</p> <p>UPLC-MS: <i>t_R</i>= 0.84 min, MS (ESI): <i>m/z</i> 406.3 [M+H]⁺</p> <p>UPLC Purity= 91%</p> <p>Yield 15%</p>
<p>A₂₅B₁</p>			<p>¹H-NMR (600 MHz, DMSO-<i>d</i>₆) δ ppm 11.49 (s, 1 H) 9.49 (s, 1 H) 8.31 (s, 1 H) 7.93 (d, <i>J</i>=8.82 Hz, 2 H) 7.92 (s, 1 H) 7.86 - 7.91 (m, 1 H) 7.53 (d,</p>

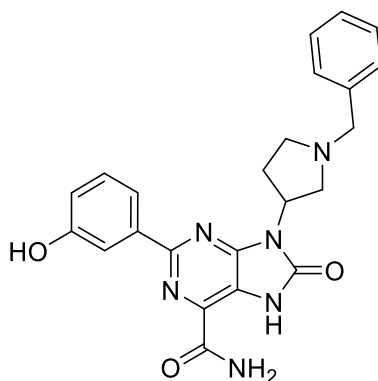
			<p>J=2.05 Hz, 1 H) 7.44 (d, J=8.21 Hz, 1 H) 7.27 (t, J=7.89 Hz, 1 H) 7.14 (dd, J=8.21, 2.05 Hz, 1 H) 6.88 (ddd, J=7.98, 2.53, 0.90 Hz, 1 H) 4.17 (t, J=6.73 Hz, 2 H) 3.14 (t, J=6.73 Hz, 2 H)</p> <p>¹³C NMR (151 MHz, DMSO-d₆) δ ppm 166.04 (s, 1 C) 157.95 (s, 1 C) 155.11 (s, 1 C) 154.03 (s, 1 C) 153.30 (s, 1 C) 140.05 (s, 1 C) 138.71 (s, 1 C) 132.80 (s, 1 C) 131.35 (s, 1 C) 131.28 (s, 1 C) 130.82 (s, 1 C) 129.74 (s, 1 C) 129.70 (s, 1 C) 129.55 (s, 1 C) 119.85 (s, 1 C) 119.18 (s, 1 C) 117.54 (s, 1 C) 114.92 (s, 1 C) 40.77 (s, 1 C) 32.85 (s, 1 C)</p> <p>UPLC-MS: t_R= 1.04 min, MS (ESI): m/z 445.9 [M+H]⁺</p> <p>UPLC Purity= 95%</p> <p>Yield 23%</p> <p>HRMS analysis: exp. 444.0623 [M+H]⁺, calc. 444.0625</p>
A₂₅B₂			<p>¹H-NMR (400 MHz, DMSO-d₆) δ ppm 3.18 (t, J=6.69 Hz, 2 H) 4.26 (t, J=6.80 Hz, 2 H) 7.15 (dd, J=8.22, 1.86 Hz, 1 H) 7.42 (d, J=8.33 Hz, 1 H) 7.48 (t, J=7.78 Hz, 1 H) 7.56 (d, J=1.75 Hz, 1 H) 7.68 (d, J=8.33 Hz, 1 H) 7.98 (br s, 1 H) 8.30 (br s, 1 H) 8.39 (d, J=7.45 Hz, 1 H) 8.85 (s, 1 H) 11.38 - 11.71 (m, 1H) 13.22 (s, 1 H)</p> <p>UPLC-MS: t_R= 0.99 min, MS (ESI): m/z 467.8 [M+H]⁺</p> <p>UPLC Purity= 96%</p> <p>Yield 60%</p>
A₂₆B₁			<p>¹H-NMR (400 MHz, DMSO-d₆) δ ppm 5.25 (s, 2 H) 6.89 (dd, J=7.89, 2.41 Hz, 1 H) 6.94 - 7.02 (m, 1 H) 7.22 (d, J=3.29 Hz, 1 H) 7.29 (t, J=8.00 Hz, 1 H) 7.45 (d, J=5.04 Hz, 1 H) 7.88 - 8.00 (m, 2 H) 8.05 (d, J=7.89 Hz, 1 H)</p>

			<p>8.33 (s, 1 H) 9.50 (br s, 1 H) 11.53 - 11.70 (m, 1 H)</p> <p>UPLC-MS: $t_R = 0.82$ min, MS (ESI): m/z 368.0 [M+H]⁺</p> <p>UPLC Purity= 85%</p> <p>Yield 45%</p>
A₂₆B₂		 <p>Chemical structure: Indazole ring with a substituent at the 5-position, indicated by an asterisk (*).</p>	<p>¹H-NMR (400 MHz, DMSO-d₆) δ ppm 5.36 (s, 2 H) 6.99 (dd, J=5.04, 3.51 Hz, 1 H) 7.22 (d, J=2.63 Hz, 1 H) 7.44 (dd, J=5.15, 1.21 Hz, 1 H) 7.49 (t, J=7.78 Hz, 1 H) 7.69 (d, J=8.33 Hz, 1 H) 7.99 (br s, 1 H) 8.35 (br s, 1 H) 8.50 (d, J=7.23 Hz, 1 H) 8.90 - 8.98 (m, 1 H) 8.93 (s, 1 H) 11.71 (br s, 1 H) 13.23 (s, 1 H)</p> <p>UPLC-MS: $t_R = 0.76$ min, MS (ESI): m/z 391.4 [M+H]⁺</p> <p>UPLC Purity= 96%</p> <p>Yield 10%</p>
A₂₇B₁	 <p>Chemical structure: Benzene ring with a fluorine atom at the para position and a methylene group at the other para position, both indicated by asterisks (*).</p>	 <p>Chemical structure: Benzene ring with a hydroxyl group (-OH) at the meta position and a substituent at the other meta position, indicated by an asterisk (*).</p>	<p>¹H NMR (400 MHz, DMSO-d₆) δ ppm 5.08 (s, 2 H) 6.80 - 6.94 (m, 2 H) 7.18 (br t, J=8.88 Hz, 2 H) 7.14 - 7.21 (m, 1 H) 7.28 (t, J=7.89 Hz, 1 H) 7.43 - 7.52 (m, 2 H) 7.91 (br d, J=8.11 Hz, 2 H) 7.97 - 8.04 (m, 1 H) 8.28 - 8.36 (m, 1 H) 9.50 (s, 1 H) 11.56 - 11.70 (m, 1 H)</p> <p>UPLC-MS: $t_R = 0.90$ min, MS (ESI): m/z 380.0 [M+H]⁺</p> <p>UPLC Purity= 85%</p> <p>Yield 34%</p>
A₂₇B₂		 <p>Chemical structure: Indazole ring with a substituent at the 5-position, indicated by an asterisk (*).</p>	<p>¹H-NMR (400 MHz, DMSO-d₆) δ ppm 13.20 (s, 1 H), 11.71 (s, 1 H), 8.74 (s, 1 H), 8.42 - 8.49 (m, 1 H), 8.33 (s, 1 H), 7.98 (s, 1 H), 7.61 - 7.72 (m, 1 H), 7.42 - 7.54 (m, 2 H), 7.10 - 7.20 (m, 3 H), 5.19 (s, 2 H)</p> <p>UPLC-MS: $t_R = 0.87$ min, MS (ESI): m/z 404.2 [M+H]⁺</p>

			<p>UPLC Purity= 95% Yield 77%</p>
A₂₅B₁₀			<p>¹H-NMR (400 MHz, DMSO-d₆) δ ppm 11.48 (s, 1 H), 11.28 (s, 1 H), 8.21 - 8.30 (m, 1 H), 8.16 (bs, 1 H), 7.98 (bs, 1 H), 7.58 (d, J=2.2 Hz, 1 H), 7.51 - 7.56 (m, 1 H), 7.44 - 7.50 (m, 2 H), 7.31 - 7.38 (m, 1 H), 7.19 - 7.24 (m, 1 H), 7.11 - 7.19 (m, 1 H), 4.17 - 4.26 (m, 2 H), 3.18 (s, 2 H)</p> <p>UPLC-MS: t_R= 1.12 min, MS (ESI): m/z 466.6 [M+H]⁺</p> <p>UPLC Purity= 98% Yield 50%</p>
A₂₅B₁₁			<p>¹H-NMR (400 MHz, DMSO-d₆) δ ppm 11.51 (s, 1 H), 9.26 (s, 1 H), 8.00 and 7.91 (2 bs, 2 H, 1 H each), 7.41 - 7.56 (m, 2 H), 7.24 - 7.31 (m, 1 H), 7.00 - 7.17 (m, 2 H), 6.66 - 6.81 (m, 1 H), 3.94 - 4.28 (t, J=1.0 Hz, 2 H), 3.11 (t, 3.11 (t, J=1.0 Hz, 2 H), 2.37 (s, 3 H)</p> <p>UPLC-MS: t_R= 1.08 min, MS (ESI): m/z 457.5 [M+H]⁺</p> <p>UPLC Purity= 98% Yield 46%</p> <p>HRMS analysis: exp. 458.0782 [M+H]⁺, calc. 458.0781</p>
A₂₅B₁₂			<p>¹H-NMR (400 MHz, DMSO-d₆) δ ppm 11.34 - 11.59 (bs, 1 H), 8.27 - 8.49 (m, 3 H), 7.85 - 8.00 (m, 1 H), 7.50 - 7.59 (m, 1 H), 7.35 - 7.45 (m, 3 H), 7.07 - 7.22 (m, 1 H), 4.06 - 4.31 (m, 2 H), 3.45 - 3.66 (m, 2 H), 2.95 - 3.18 (m, 2 H), 2.21 (s, 6 H)</p> <p>UPLC-MS: t_R= 0.66, MS (ESI): m/z 484.7 [M+H]⁺</p> <p>UPLC Purity= 97% Yield 41%</p>

<p>A₅₄B₁</p>		<p>¹H-NMR (400 MHz, DMSO-d₆) δ ppm 11.44 (s, 1 H), 9.45 (s, 1 H), 8.26 (br s, 1 H), 7.93 (br d, J=7.89 Hz, 1 H), 7.71 - 7.89 (m, 2 H), 7.24 (t, J=7.89 Hz, 1 H), 7.01 - 7.16 (m, 4 H), 6.84 (dd, J=7.89, 1.97 Hz, 1 H), 4.09 (br t, J=7.23 Hz, 2 H), 3.04 (br t, J=7.23 Hz, 2 H), 2.67 - 2.78 (m, 1 H), 1.05 (d, J=6.80 Hz, 6 H)</p> <p>UPLC-MS: t_R= 1.1 min, MS (ESI): m/z 418.0 [M+H]⁺</p> <p>UPLC Purity= 95%</p> <p>Yield 27.5%</p>
<p>A₅₅B₁</p>		 <p>¹H-NMR (400 MHz, DMSO-d₆) δ ppm 3.04 (br t, J=7.02 Hz, 2 H) 4.10 (br t, J=6.91 Hz, 2 H) 5.85 - 5.89 (m, 2 H) 5.94 - 6.00 (m, 1 H) 6.56 (d, J=7.89 Hz, 1H) 6.71 (d, J=7.89 Hz, 1 H) 6.83 - 6.93 (m, 2 H) 7.20 - 7.34 (m, 1 H) 7.82 - 7.93 (m, 2 H) 7.97 (br d, J=7.89 Hz, 1 H) 8.26 - 8.38 (m, 1 H) 9.44 - 9.58 (m, 1 H) 11.47 (br s, 1 H)</p> <p>UPLC-MS: t_R= 0.87 min, MS (ESI): m/z 419.8 [M+H]⁺</p> <p>UPLC Purity= 90%</p> <p>Yield 21%</p>
<p>A₅₆B₁</p>		<p>¹H-NMR (400 MHz, DMSO-d₆) δ ppm 11.41 (s, 1 H) 9.44 (s, 1 H) 8.28 (s, 1 H) 7.96 (d, J=7.67 Hz, 1 H) 7.85 - 7.92 (m, 2 H) 7.28 - 7.38 (m, 4 H) 7.21 - 7.28 (m, 2 H) 6.85 (dd, J=8.00, 2.30 Hz, 1 H) 3.06 - 3.12 (m, 1 H) 2.62 (ddd, J=9.76, 6.69, 3.29 Hz, 1 H) 1.79 - 1.88 (m, 1 H) 1.63 (q, J=6.72 Hz, 1 H)</p> <p>UPLC-MS: t_R= 0.96 min, MS (ESI): m/z 387.8 [M+H]⁺</p> <p>UPLC Purity= 96%</p> <p>Yield 85%</p>

5.3.1 Synthesis of 9-(1-benzylpyrrolidin-3-yl)-2-(3-hydroxyphenyl)-8-oxo-8,9-dihydro-7H-purine-6-carboxamide (**A₅₂B₁**)



3-hydroxybenzaldehyde (30 mg, 0.246 mmol) was dissolved in MeOH (Volume: 5 ml) and then intermediate **A₅₂** (100mg, 0.322 mmol) and triethylamine (17 μ L, 0.120 mmol) were added and then the solution was stirred for 2 hr, UPLC analysis revealed the presence of the dihydropurine moiety as impurity so a little amount of I₂ was added. Solvent was evaporated under vacuum. Crude was purified by flash chromatography (Biotage Isolera System), SNAP C18, 60 gr, gradient elution from 100:0 to 40:60 A/B in 15 CV, A: water/acetonitrile 95:5 + 0.1% conc HCOOH, B: acetonitrile/water 95:5 + 0.1% conc HCOOH. Purification yielded in 12 mg of **A₅₂B₁** (23.26 % yield) as formate salt

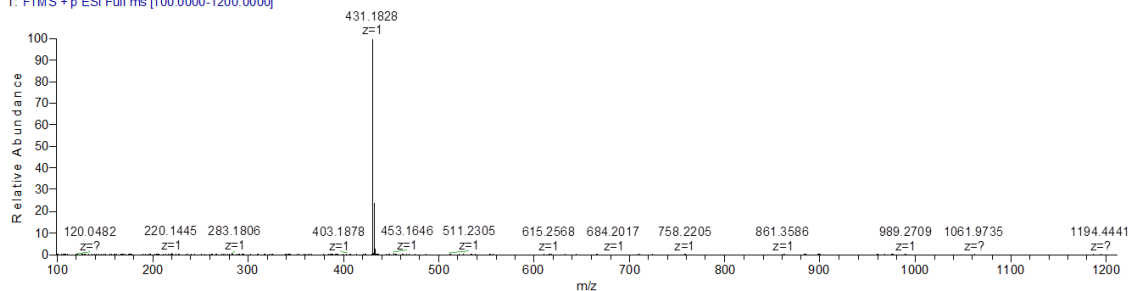
¹H-NMR= (400 MHz, DMSO-d₆) δ ppm 11.54 (br s, 1 H), 9.51 (s, 1 H), 8.31 (br s, 1 H), 7.99 (d, J=7.89 Hz, 1 H), 7.92 (br s, 2 H), 7.22 - 7.49 (m, 6 H), 6.90 (dd, J=7.78, 1.86 Hz, 1 H), 5.05 (br s, 1 H), 3.49 - 3.99 (m, 2 H), 2.10 - 3.11 (bs, 4 H)

UPLC-MS: t_R= 0.5 min, MS (ESI): m/z: 431.3 [M+H]⁺

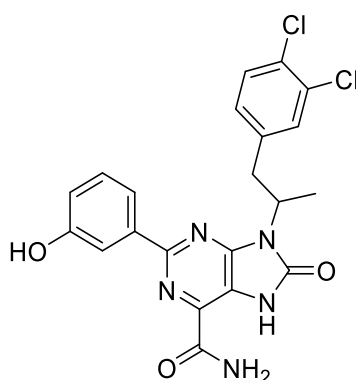
UPLC Purity: 93%

HRMS analysis: exp. 431.1828 [M+H]⁺, calc. 431.1826

200804_06 #41 RT: 0.16 AV: 1 SB: 24 0.07-0.13 , 0.24-0.52 NL: 6.16E8
T: FTMS + p ESI Full ms [100.0000-1200.0000]



5.3.2 Synthesis of 9-(1-(3,4-dichlorophenyl)propan-2-yl)-2-(3-hydroxyphenyl)-8-oxo-8,9-dihydro-7H-purine-6-carboxamide (**A₅₃B₁**)



Intermediate **A₅₃** (23 mg, 0.068 mmol) was dissolved in MeOH (Volume: 3 ml) then 3-hydroxybenzaldehyde (17.03 mg, 0.139 mmol) and triethylamine (9.45 μ l, 0.068 mmol) were added to the solution. After 24 hr, the solvent was evaporated under vacuum. Purification by flash chromatography, Biotage Isolera, SNAP (si) HP 10 g, eluting system DCM/MeOH. Compound eluted with 30% of MeOH. Appropriate fractions were combined and evaporated under vacuum to give 4.7 mg of **A₅₃B₁** (15% yield).

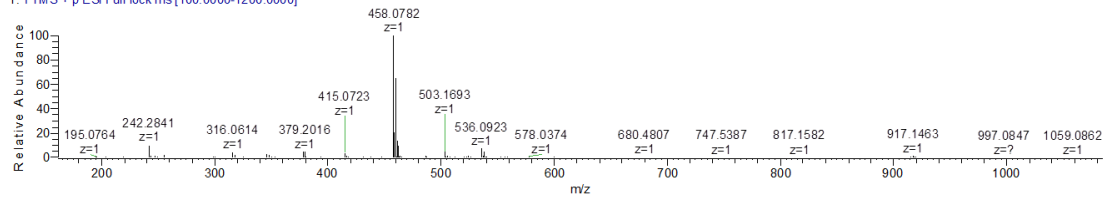
¹H NMR (400 MHz, DMSO-d₆) δ ppm 1.64 (d, J=6.80 Hz, 3 H) 3.21 (dd, J=13.81, 5.04 Hz, 1 H) 3.48 - 3.58 (m, 1 H) 4.76 - 4.86 (m, 1H) 6.88 (dd, J=7.89, 1.75 Hz, 1 H) 6.99 (dd, J=8.22, 1.86 Hz, 1 H) 7.30 (t, J=7.89 Hz, 1 H) 7.36 - 7.46 (m, 2 H) 7.89 (br s, 1 H) 7.92 (s, 1 H) 8.00 (br d, J=7.89 Hz, 1 H) 8.32 (br s, 1 H) 9.51 (s, 1 H) 11.42 (br s, 1 H)

UPLC-MS (Method 2): t_R = 1.10 min, m/z 458.0 [M+H]⁺

UPLC Purity = 99%

HRMS analysis: exp. 458.0782 [M+H]⁺, calc. 458.0781

200804_08#33 RT: 0.13 AV: 1 SB: 8 0.50-0.99 NL: 2.27E7
T: FTMS + p ESI Full lock ms [100.0000-1200.0000]



6. Biological Assays

6.1 PI3K δ , - γ , - β , - α ADP-Glo Assay

Human recombinant proteins PI3K α , PI3K β , PI3K γ and PI3K δ were purchased from Millipore Ltd (Billerica, MA). Compounds were dissolved at 0.5mM in DMSO and were tested at different concentrations for their activity against PBKs using the ADP-Glo™ Kinase Assay (Promega, Madison WI) according to the manufacturer's 15 instructions. Briefly, the kinase reactions were performed in 384-well white plates (Greiner Bio-One GmbH, Frickenhausen). Each well was loaded with 0.1 μ l of test compounds and 2.5 μ l of 2x reaction buffer (40 mM Tris pH7.5, 0.5 mM EGTA, 0.5 mM Na₃VO₄, 5 mM β -glycerophosphate, 0.1 mg/ml BSA, 1 mM DTT), containing 50 μ M PI and PS 20 substrates (L-a-phosphatidylinositol sodium salt and L-a-phosphatidyl-L-serine, Sigma-Aldrich, St. Louis MO) and the PBK recombinant proteins (PI3K γ 0.25 ng/ μ l, PI3K δ 1 ng/ μ l, PBK α 0.125 ng/ μ l, PI3K β 1 ng/ μ l). The reactions were started by adding 2.5 μ l of 2x ATP solution to each well (final concentrations: PK γ ATP 30 μ M; PI3K δ ATP 80 μ M; PBK α ATP 50 μ M; PBK β ATP 25 100 μ M) and incubated for 60 min at room temperature. Subsequently, each kinase reaction was incubated for 40 min with 5 μ l ADP-Glo™ Reagent, allowing depletion of unconsumed ATP. Then, the Kinase Detection Reagent (10 μ l) was added in each well to convert ADP to ATP and to allow the newly synthesized ATP to be measured using a luciferase/luciferin reaction. Following 60 min incubation, the luminescence signal was measured using a Wallac EnVision® multilabel reader (PerkinElmer, Waltham MA). Curve fitting and IC₅₀ calculation were carried out using a four-parameter logistic model in XLfit (IDBS, Guilford, UK) for Microsoft Excel (Microsoft, Redmont, WA).

6.2 THP-1 Cellular Assay

The inhibitory activity of compounds on PI3Kinase in living cells was determined by evaluating the inhibition of the PI3K δ -AKT pathway endogenously expressed on THP-1 cells. THP-1 cell suspension from T75 flask (0.4-1.0 x 10⁶/mL) was centrifuged and the cell pellet re-suspended in starvation medium at 1.5 x 10⁶ cells/mL. Cell plate was prepared by dispensing 3 x 10⁵ cells/well and incubated for 24 hours at 37°C before the assay. Test compounds were serially diluted 1:3 in DMSO and then further diluted 1:100 in compound medium. Starved THP-1 cells were pre-incubated at 37°C for 60 minutes with test compound solutions or vehicle. Cells are then stimulated for 10 minutes by Macrophage Colony-Stimulating Factor (M-CSF) 2.5 ng/mL or stimulus medium (control of basal

pAKT levels). Cells were then lysed and the amount of phosphorylated AKT measured by using a Cisbio p-Ser473 AKT HTRF assay kit. Stimulation was ended by the addition of supplemented lysis buffer. Cell plate was shaken for 30 minutes at room temperature to complete cell lysis, followed by the addition of HTRF conjugates and incubated for further 4 hours at room temperature. Conjugates react with pAKT causing an increase in HTRF signal that is measured with the Envision plate reader with a HTRF reading protocol. Ratio data were fitted using a logistical four-parameter equation to determine IC50. IPI-145 compound was used as pharmacological standard.

6.3 Solubility Measurements

The standard solution was prepared by dispensing 10 μ L from 10mM compound stock solution in DMSO in a well in duplicate. Then 190 μ L of DMSO were added in each well and mixed with shaking at room temperature for 10 minutes. Final concentration was 500 μ M.

The sample solution was prepared by dispensing 10 μ L of a 10 mM compound stock solution in a well in duplicate and adding 190 μ L of PBS buffer at pH=7.4 in each well. Wells were mixed with shaking at room temperature for 90 minutes, then solutions were filtered. 150 μ L of filtrate were transferred in a vial.

The measurement of concentration was achieved by comparison of UV absorbance of the sample solution and that of the known standard solution following an HPLC separation.

The solubility of each sample was expressed by the ratio of amount of compound in the sample test solution to the amount of compound in the standard solution as expressed in the equation below.

$$\text{Solubility of sample} = \frac{\text{Peak area of sample}}{\text{Peak area of standard}} \times \text{Conc. of Standard}$$

6.4 Caco-2 Cell Permeability Assay

Experimental setting

Passive cellular permeability (Papp) was determined by using Caco-2 cell line in a 96-well format.

Caco-2 cells are a human colon epithelial cancer cell line used as a model of human intestinal absorption of drugs and other compounds. Caco-2 cells express transporter proteins, efflux proteins, and Phase II conjugation enzymes to model a variety of transcellular pathways as well as metabolic transformation of test substances.

Test item transport is measured in two directions (apical-to-basolateral [A→B] and basolateral-to-apical [B→A]) in HBSS (Hank's Balanced Salt Solution) transport buffer at pH 7.4 (n= 3). This assay was also run in presence of a P-gp inhibitor to investigate any potential interaction of the testing compound with P-gp. Test items were investigated at a single concentration (i.e. 3 μM) at one timepoint (i.e. 60 minutes).

A P-gp substrate, a low - moderate permeable compound and a high permeable compound were included at a single concentration (3 μM) as reference compounds. All the reference compounds were tested in two directions, apical-to-basolateral [A→B]) and basolateral-to-apical [B→A]).

Samples were analyzed in an LC-MS/MS system to measure test items and reference compounds concentration levels, with compound concentration expressed as area ratio determined by dividing the analyte peak area to the internal standard peak area. To evaluate the integrity of the monolayers, the transepithelial electrical resistance (TEER) was measured before and after the experiment.

Cell culture were cultured for 21- 28 days at 37°C. During the Caco-2 cell assays, the compounds to be evaluated were either the apical [A→B] or the basolateral [B→A] side of each cell monolayer to simulate the influx or efflux of compounds across the epithelium.

At various time points (60, 90 or 120 min), the concentration of the test compounds in the receiving chambers were assayed and determined by LC/MS analysis.

Data Handling and Analysis

The apparent permeability (P_{app}) will be determined: in [A→B] and [B→A] directions.

In particular, the following parameters will be calculated.

1. P_{app} (apparent permeability)

P_{app} values were calculated for direction [A→B] and [B→A], according to the following equation:

$$P_{app} = \frac{dQ/dt}{C_0 \times A}$$

Where:

dQ/dt is the permeability rate (dQ/dt is amount of test/control items within the incubation period); amount of test/control items will be expressed as area ratio meaning analyte peak area divided by internal standard peak area ratio; C_0 is the initial concentration of test/control items (internal standard peak area ratios) in the donor compartment; A is the surface area of the filter, which corresponds to the surface area of the cell monolayer.

The Papp value has the dimension of a rate (nm/sec) and were reported as average Papp (nm/sec) \pm standard deviation from three monolayers for [A \rightarrow B] and for [B \rightarrow A] directions, where applicable. Permeability classification of compounds was made based on the comparison between its Papp values and those from reference permeability controls.

- 2. Monolayer efflux ratios (ER)** in Caco-2 cells was derived using mean Papp [A \rightarrow B] and [B \rightarrow A] direction according to the following equation:

$$Efflux\ Ratio = \left(\frac{P_{appBA}}{P_{appAB}} \right)$$

- 3. Mass balance (MB)** was calculated from this equation:

$$(MD + MR) / MO$$

Where

MD = amount of test/control items in donor chamber at time = 60, 90 or 120 min

MR = amount of test/control items in receiver chamber at time = 60, 90 or 120 min

MO = amount of test/control items in donor at time zero

Mass Balance will be reported as average MB \pm standard deviation from three monolayers.

To evaluate the cell integrity the percentage of LY rejection was calculated following the equation:

$$\% LY\ rejection = 100 \times [1 - RFU_{basolateral} / RFU_{apical}]$$

Where RFU values are subtracted by the background mean values. Wells are considered fully acceptable if the % LY rejection is >98%, acceptable with caution for values included between 98% and 95% and not acceptable for values <95%.

6.5 Determination of the hPI3K δ Crystal Structure.

The X ray structure was obtained at Proteros Biostructures GmbH.

The purified protein was used in crystallisation trials employing both, a standard screen with approximately 1200 different conditions, as well as crystallisation conditions identified using literature data. Conditions initially obtained have been optimised using standard strategies, systematically varying parameters critically influencing crystallisation, such as temperature, protein concentration, drop ratio, and others. These conditions were also refined by systematically varying pH or precipitant concentrations. Finally, crystallisation was obtained by Hanging Drop.

The X-ray diffraction data have been collected from complex crystals of human PI3K δ with the ligand **A₂₅B₁** at the SWISS LIGHT SOURCE (SLS, Villigen, Switzerland) using cryogenic conditions. Data were processed using programs XDS and XSCALE.

Part II: Exploring Macrocycles as New Rho-associated protein kinase (ROCK) Inhibitors

1. Introduction

1.1 Rho-Associated Protein Kinases (ROCK)

ROCKs are Serine-Threonine kinases belonging to the AGC (cAMP-dependent protein kinase/protein kinase G/ protein kinase C) family⁸⁶. They are most homologous to myotonic dystrophy kinase (DMPK), DMPK-related cell division control protein 42 (Cdc42)-binding kinases (MRCK) and citron kinase. ROCKs were first discovered as effectors of Rho, a small GTP binding protein implicated in several aspects of cell behavior, such as cell motility, cell proliferation and apoptosis⁸⁷.

Two different isoforms of ROCK were identified so far: ROCK I, also known as ROCK β or p160ROCK, and ROCK II which is also called ROCK α or Rho Kinase⁸⁸. ROCK isoforms are ubiquitously expressed in human tissues with a higher expression of ROCK II in the brain⁸⁶ compared to ROCK I.

ROCK I and ROCK II are protein kinases of ~160 kDa and they exhibit 65% overall identity in their amino-acid sequence and a 92% identity in their kinase domains^{87,88}.

The kinase domain in ROCK is located in the amino-terminus, followed by a potential coiled-coil forming region and by other functional motifs at the carboxyl terminus. These motifs include the Rho binding domain (RBD) and a pleckstrin homology (PH) domain that contains a cysteine-rich region/domain (CRD)⁸⁷. The sequence of the Rho-binding domain in ROCK I (residues 934-1015) is highly homologous in ROCK II (Figure 32).

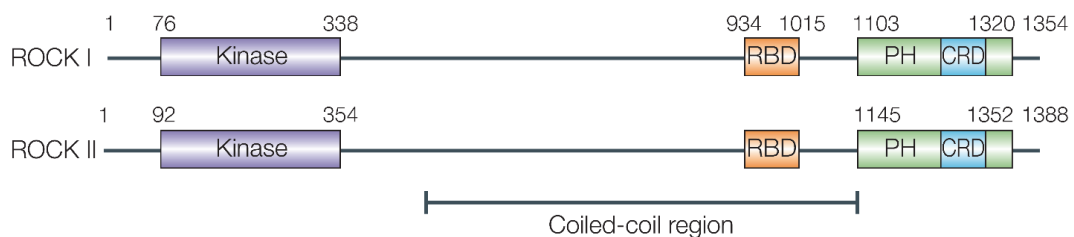


Figure 32: The Structure of ROCK I and ROCK II.⁸⁸

In the ROCK inactive form, the PH and the RBD domains can both bind to the amino-terminal kinase region creating an autoinhibitory loop that impairs the kinase activity. Rho in its activated form (GTP-bound Rho) interacting with the Rho binding domain is able to disrupt this negative regulatory interaction leading to an active, “open” kinase domain⁸⁹. The open conformation can also be obtained by the cleavage of the carboxyl-terminal domain in ROCK I by caspase-3 while in ROCK II

by granzyme B⁹⁰. ROCK activation can also be mediated by some lipids, particularly by arachidonic acid^{90,91}. The lipids seem to bind to the regulatory C-terminus of ROCK, disrupt the autoinhibitory interaction and thus lead to kinase activation⁹².

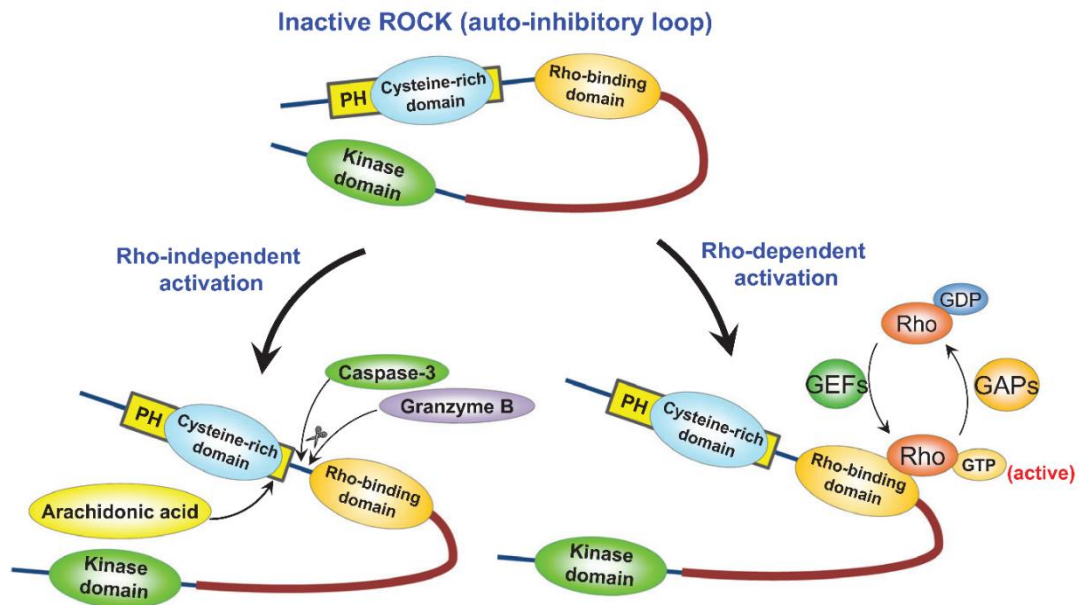


Figure 33: Different mechanisms of regulation of the ROCK function.⁹¹

1.2 ROCKs as Mediator of Vasoconstriction

Activation of Rho GTPases (RhoA, RhoB and RhoC) is mediated by guanidine exchange factors (GEFs) that catalyze exchange of GDP for GTP. GEFs are, in turn, activated in response to various environmental cues acting through G-protein coupled receptors (GPCR). Rho in its active form (GTP-bound) can stimulate ROCK I and ROCK II^{88,91,93}. ROCKs can in turn phosphorylate various substrates that are implicated in regulating actin-filament assembly and dynamics, organization of the cytoskeleton and cell contractility⁹² (**Figure 34**).

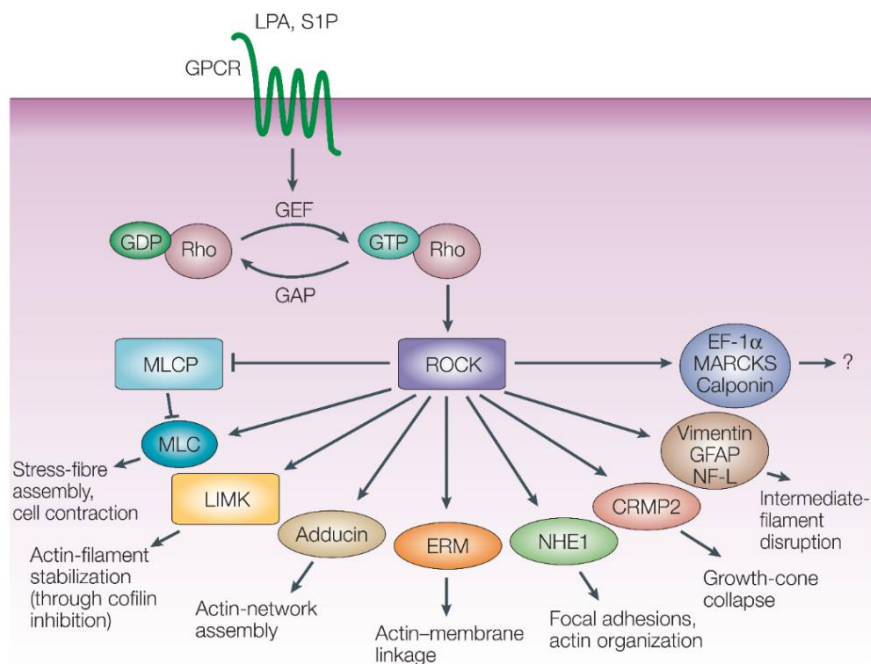


Figure 34: Downstream effectors of ROCKs.⁸⁸

RhoA/ROCK signalling plays an important part in the regulation of smooth muscle cells contraction. The smooth muscle cells state is mainly determined by the phosphorylation (contraction) and dephosphorylation of MLC (relaxation). The increase of cytosolic Ca^{2+} concentration which is caused by the activation of plasma membrane Ca^{2+} channels and/or Ca^{2+} release from sarcoplasmic reticulum (SR) results in the activation of MLCK. MLCK mediates the phosphorylation of MLC and thereby causes the contraction⁹⁴. This pathway is defined as Ca^{2+} -dependent. On the other hand, MLC can also be dephosphorylated Ca^{2+} independently by MLCP.^{88,92} (**Figure 35**). MLCP has a myosin binding unit that can be phosphorylated by ROCKs. The ROCKs-mediated phosphorylation of MLCP inhibits the enzyme allowing the light chain of myosin to remain phosphorylated, thereby promoting

contraction in a Ca^{2+} -independent way and promoting Ca^{2+} sensitization. Additionally, ROCK can directly phosphorylate MLC promoting in this fashion cell contraction.⁹⁵

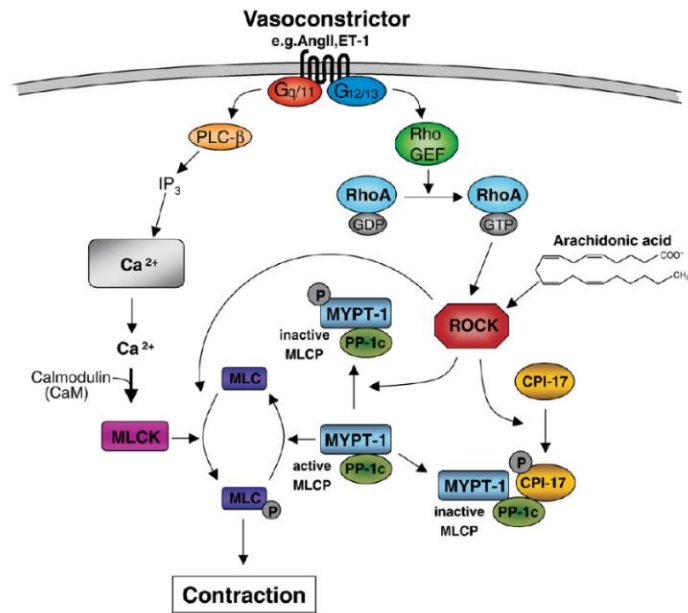


Figure 35: ROCKs in Smooth Muscles Cells (SMC) Contraction⁹².

Ca^{2+} sensitization has been determined in various smooth muscles cells including airway ones and vascular smooth muscles cells (VSMC)⁹⁵. Moreover, in endothelial cells (EC), Rho-Kinase pathway activation has been linked to the reduction of eNOS production, a key cellular factor in mediating vasodilatation⁹¹.

Some studies have also reported as ROCKs may play a role in the LPA and PDGF-induced SMC migration⁹⁶ and how SMC-induced matrix contraction is markedly blocked by inhibiting ROCK signalling⁹⁷.

1.3 ROCKs as Drug Target for Pulmonary Arterial Hypertension (PAH)

As explained in the previous paragraph Rho/ROCK pathway regulates the vascular tone making it a possible target for diseases in which a relaxation of smooth muscle cells is beneficial. Among those diseases, hypertension and in particular pulmonary arterial hypertension (PAH) is for sure one of the most relevant in terms of medical need.

PAH is a severe disease, with limited therapeutic approaches available and characterized by a 3-5 years survival from the diagnosis. PAH can be idiopathic, familial, associated with various diseases including connective tissue disorders, AIDS, and habitual drug use⁹⁸. It is defined hemodynamically by a mean pulmonary artery pressure (mPAP) increase of > 25 mmHg⁹⁹.

The increased pressure is determined by an increased pulmonary vascular resistance (PVR) due to progressive reduction and obliteration of small pulmonary arteries¹⁰⁰. High mPAP causes a hemodynamic load on right ventricle which progresses to ventricle remodeling and failure (**Figure 36**), leading to a premature death of the patient¹⁰¹.

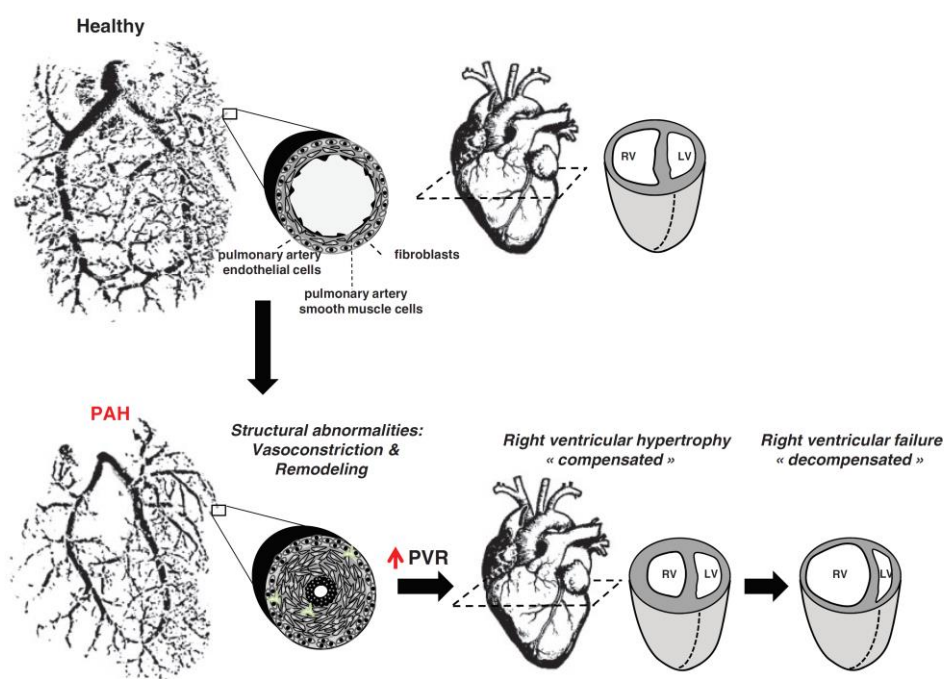


Figure 36: Schematic representation of remodelling of pulmonary arteries and Right Ventricle Failure (RVF)¹⁰².

At a cellular level, the restriction of distal pulmonary arteries is caused by sustained inflammation, endothelial cell dysfunction, smooth muscle cell proliferation, and resistance to apoptosis.

Inflammation is characterized by activation of monocytes and increased level of circulating inflammatory mediators such as interleukin-6, platelet-derived growth factor (PDGF), and endothelial growth factor⁹⁸. The sustained inflammation is associated with endothelial cell dysfunction which in turn leads to a persistent vasoconstriction. PAH patients show increased levels of endothelin-1 growth factor and decreased levels of vasodilators and antiproliferative agents, including prostacyclin and NO⁹⁸. Most importantly, blood vessels in PAH patients show an aberrant vascular remodeling which results in hypertrophy and hyperplasia leading to luminal obstruction¹⁰⁰.

In the last ten years, several drugs have been approved for the treatment of PAH: phosphodiesterase type 5 inhibitors such as sildenafil and tadalafil; prostacyclin analogues such as epoprostenol, treprostenil and iloprost; endothelin receptor antagonists such as bosentan, ambrisentan and macitentan; and soluble guanylyl cyclase agonists such as riociguat¹⁰³. Unfortunately, these treatments only relieve symptoms of the disease and only limited evidence for disease reversal have been observed so far¹⁰¹. Moreover, these agents suffer from several important shortcomings including short half-lives, invasive routes of administration, higher dose and frequency requirements, and several dose-related systemic side effects. There is an urgent medical need in identifying novel agents with ameliorate therapeutic efficacy and characterized by a non-invasive route of administration and less side-effects.

A growing number of evidences has highlighted as ROCKs signalling plays an important role in the pathogenesis of PAH¹⁰⁴. In lung homogenates from patients with idiopathic pulmonary hypertension (IPAH), ROCK pathway was found to be overactivated compared to healthy subjects¹⁰⁵.

Administration of inhaled or intravenous formulations of Fasudil, a clinically approved ROCK inhibitor, have shown favorable acute hemodynamic effects in both animals and humans^{106,107}. Moreover, Fasudil has been shown to lower pulmonary artery pressure, improve pulmonary vascular remodeling and RV hypertrophy in rats with PAH induced by Monocrotaline and hypoxia, as well as in mice with pulmonary fibrosis and PH induced by bleomycin¹⁰⁴.

Therefore, these studies reveal as ROCK inhibitors might have numerous beneficial effects such as potent vasodilating, anti-remodelling and anti-inflammatory effects and indirect 'collective' inhibition of other prohypertensive pathways¹⁰⁵, confirming it as promising drug target for the treatment of PAH.

1.4 Structural Biology of ROCK

Structural information about the Rho catalytic kinase domain have been obtained thanks to studies on its crystal structures in complex with many inhibitors^{108,109,110} (e.g. Fasudil, Hydroxyfasudil, Y-27632 and H-1152P).

These studies revealed as ROCK generally crystallizes as an N-terminal head-to head dimer (**Figure 37**)¹¹¹. ROCK kinases have a N-terminal and a C-terminal extensions to the kinase domain. These two extensions are common to other kinases belonging to the AGC family and are essential for their activity¹¹¹. In ROCK, the N-terminal extension is able to form an intermolecular helix-bundle fold, the capped helix-bundle (CHB) domain which brings to the formation of the homodimer, creating a dimerization domain.

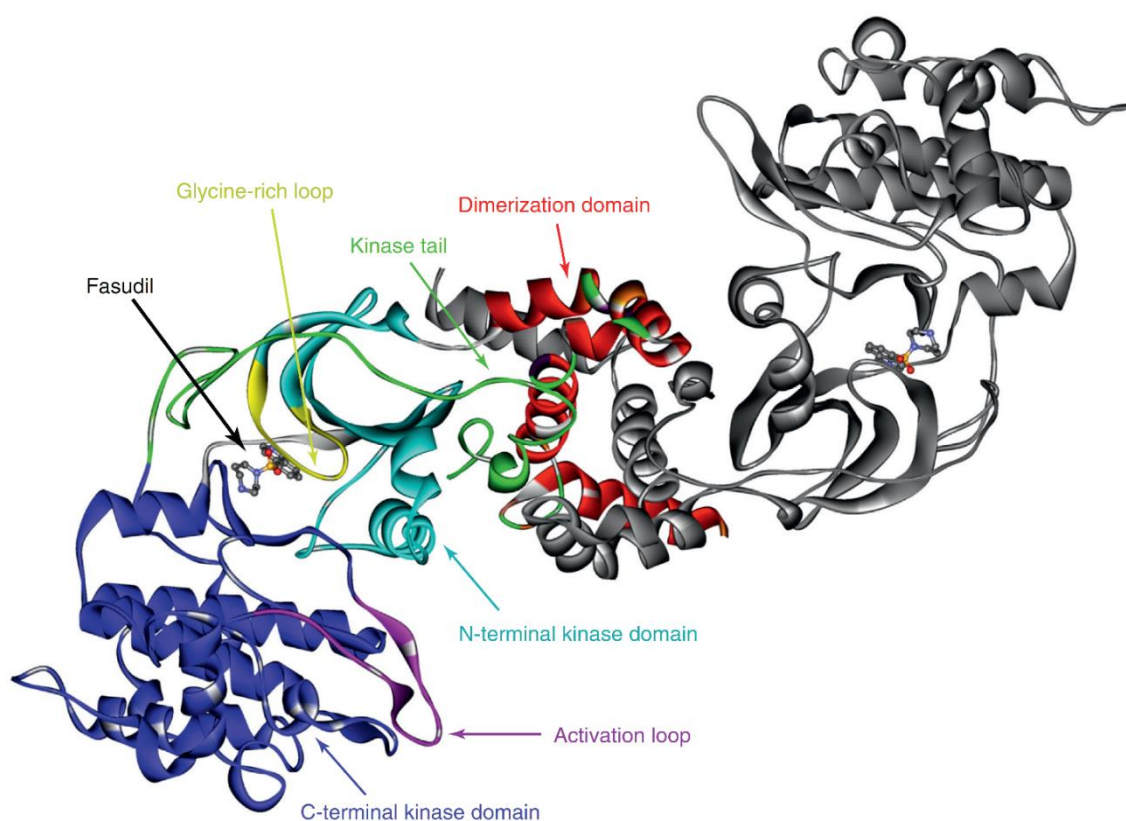


Figure 37: Dimeric Structure of Rho kinase in complex with Fasudil; The overall dimer structure is shown as a ribbon diagram. One monomer is coloured in grey. Dimerization domain is drawn in red. The C-terminal kinase domain is drawn in blue with the activation loop coloured in purple. The N-terminal kinase domain is shown in cyan with the glycine-rich loop in yellow (PDB ID 2F2U).¹¹²

The kinase domain presents a bilobed structure consisting of an N-terminal domain linked to a C-terminal domain by the hinge region. The smaller N-terminal lobe has twisted five stranded anti-parallel β -sheets and a single α -helix while the C-terminal lobe is mainly α -helical. The ATP binding site is formed by a cleft at the interface of these domains and it is surrounded by the hinge region, the P-loop and the activation loop¹⁰⁸. The ATP binding pocket has three regions: the adenine region, the furanose region and the distal region. Above the adenine region there is a spherical shaped region, the furanose region, which is also hydrophobic and the furanose ring of ATP can bind here. The last region is the distal region, which accommodates the pyrophosphoric acid group of ATP¹¹². Interestingly, these studies revealed that phosphorylation at the activation loop or C-terminal hydrophobic motif, which is necessary for the activation of most of other AGC kinases such as PKC and Akt, is absent from the Rho-kinase catalytic domain in its dimerized active conformation. Despite that, the unphosphorylated kinase is catalytically competent and this implies that the RhoA binding is sufficient to activate the protein⁸⁹.

1.4.1 Key Interactions of ROCK Inhibitors in the ATP Binding Site

The structural analysis of ROCK I and ROCK II in complex with their inhibitors highlights the key interactions in ATP binding pocket which are essential to achieve enzymatic inhibition.

Generally, a prototypical ROCK inhibitor shows a hinge binder motif that occupies the same space as the adenine six membered ring of ATP. The hinge binder mainly establishes hydrogen bonds with two conservative residues, Met156 and Glu154 in ROCK I¹⁰⁸, Met 170 and Glu170 in ROCK II respectively¹¹³(**Figure 38**). Hinge binder motif can be structural varied encompassing heterocycles (e.g. pyridine, F-pyridine, amino-pyridine, amino-pyrimidine, pyrazole), bicyclic heteroaromatic rings (e.g. indazole, azaindole, isoquinoline, isoquinolinone, aminoisoquinoline)⁸⁶, as well as benzoxaborole^{86,114} or variously substituted aromatic rings.

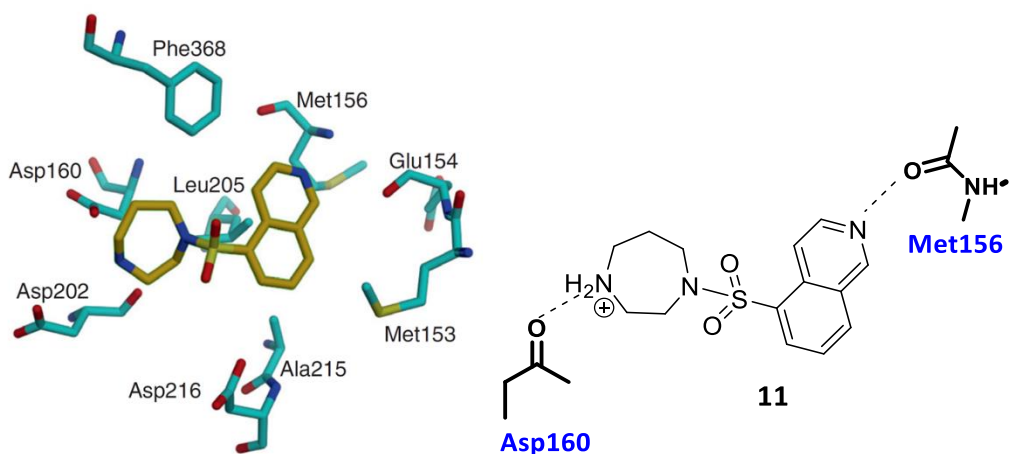


Figure 38: Schematic representation of Fasudil (**11**) in complex with ROCK I.

A ROCK inhibitor usually presents a linker (amides, urea or carbamates) which connects the Hinge binder to the terminal part of the molecule. From the hinge region, the inhibitor extends into the binding pocket establishing key interactions with two other conserved residues: the catalytic Lys105 (ROCK I) and Asp 216 (ROCK I) of the DFG segment. Moreover, ROCK inhibitors can establish additional hydrogen bonds with other Asp residues (Asp202, Asp160, Asp 117 in ROCK I). These additional interactions in most cases are obtained by inserting a basic moiety in the terminal portion of the molecule^{108,110}.

In ROCKs ATP-binding site, two hydrophobic regions have also been identified: one is in the proximity to the hinge region and the second one is located under the *P-loop*. Interactions with

residues of these two areas and with the of *P-loop* have been associated with improved potency^{113,115} and, in some cases, with the achievement of selectivity over other kinase such as PKA¹⁰⁸. Achieving selectivity over PKA is not so easy since the two kinases shows high structural homology in the kinase active site. However, as PKA is involved in so many cellular pathways, avoiding inhibition of PKA could be essential in a ROCK design for therapeutic use.

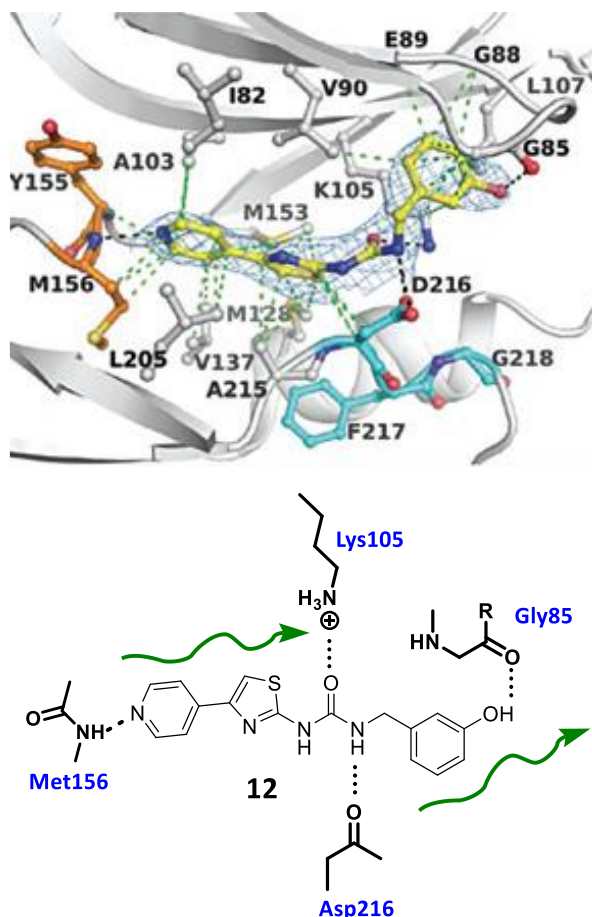


Figure 39: Schematic representation of a ROCK inhibitors (**12**) in complex with ROCK I. In green, the hydrophobic regions. Image adapted from Patel et al.¹¹⁶

Boland et al.¹¹³ discovered a series of soft ROCK inhibitors where the increased potency was due to the presence of a bi-phenyl structures that can sit under the *P-loop* and make extra π -stacking interactions with the side chain of Phe120 in ROCK I or Phe136 in ROCK II, demonstrating the importance of the interaction with the p-loop for the achievement of potency.

1.5 ROCK Inhibitors: State of Art

In literature, a high number of ROCK inhibitors has been reported. However, few ROCK inhibitors have reached clinical stages or even the market⁸⁶ so far.

Kinase inhibitors often failed to reach the market for countless reasons but one of the main problems is a not enough selectivity over other kinases leading to off target related side effects and hence tolerability and ROCK inhibitors are not exceptions in this regard. Despite many ROCK inhibitors with a good inhibitory profile have been reported, the majority showed off-targets activity, especially towards kinases belonging to AGC family. Moreover, ROCK inhibition has important systemic adverse effects (e.g. pronounced blood pressure reduction, increased in the heart rate) that makes the therapeutic window of a ROCK inhibitor very narrow.

At the moment, three ROCK inhibitors have been clinically approved and reached the market⁸⁶.

Fasudil (**11**) was the first ROCK inhibitor to enter the market for the treatment of cerebral vasospasm in 1995. It has been approved only in Japan and in China for acute treatment, but it has not been approved by the United States Food and Drug Administration (FDA) or by the European Medicines Agency (EMA). Fasudil has a moderate potency against ROCK with a K_i of 0.33 μM against ROCK II⁸⁶ and, more importantly, it has inhibitory activity against a number of other kinases belonging to the AGC family.

The second ROCK inhibitor being approved is Ripasudil (**13**) (trade name Glanatec). It is a close analogue of Fasudil and it has been the first ROCK inhibitor to be approved for the treatment of Glaucoma in Japan. Ripasudil is a potent inhibitor with IC_{50} of 51 nM and 19 nM for ROCK I and ROCK II.

Recently, a new ROCK inhibitor has entered the market for the treatment of glaucoma, Netarsudil (**15**). Netarsudil (trade name Rhopressa) has been developed by Aerie Pharmaceuticals and approved by the FDA in 2017. This molecule is commercialized as ROCK inhibitor and norepinephrine transport inhibitor. Like Fasudil, this compound shows some off-targets such as PKC θ and MRCK- α ⁸⁶. In the field of glaucoma treatment, AMA0076 (structure not disclosed), a potent and selective soft ROCK inhibitor¹¹³ developed by Amakem, has entered phase 2a. The soft drug approach could be a successful strategy in the design of new ROCK inhibitors aimed at optimizing pharmacokinetic properties by reducing systemic exposure¹¹⁷.

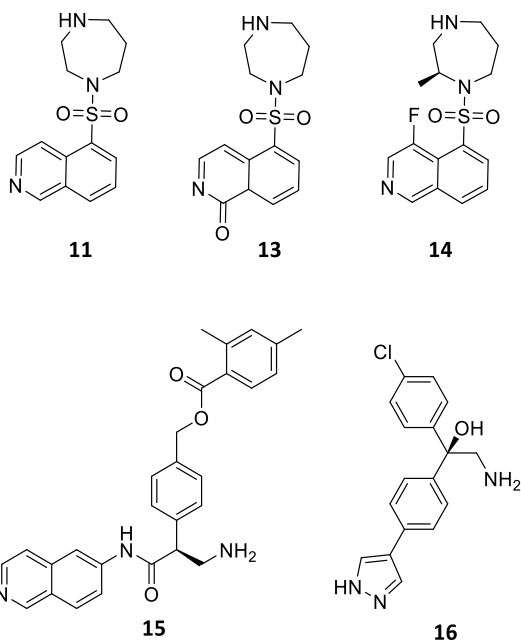


Figure 40: Structure of advanced ROCK inhibitors.

In oncology, the use of ROCK inhibitors has also been described. However, their potential systemic side effects have limited their application as therapeutics for cancer. At the moment, there is only one ROCK inhibitor, AT13148 (**16**) discovered by Astex, which has completed Phase I trial for patients with advanced cancer¹¹⁷. It is not a selective ROCK inhibitor because it shows inhibitory effects on many kinases of the AGC family⁸⁶.

As conclusions and future considerations, despite the high interest of pharmaceutical companies on developing new ROCK inhibitors, few compounds proved to have right profile to overcome clinical phases and enter the market. There is still a lot to do to achieve a good selectivity over AGC kinases and between the two isoforms. Moreover, only type-I inhibitors have been discovered so far. Developing type II and type III could be interesting since they are generally more selective than type I⁸⁶.

2. Aim of the Project

2.1 Design and Synthesis of New Macrocyclic Rho-associated protein kinase (ROCK) inhibitors

In literature, high number of ROCK inhibitors has been reported⁸⁶. However, as previously described, only three of these inhibitors have reached the market so far (Fasudil, Ripasudil and Netarsudil). One of the main challenges in the field of kinase inhibitors is obtaining a suitable selectivity across the kinome. Promiscuous kinase inhibitors may translate in a poor tolerability or in a narrow therapeutic window.

Nowadays, the design of macrocycles represents an emerging and promising approach in medicinal chemistry to obtain efficient molecules with enhanced selectivity and favourable Phys chem and ADME properties. Pacritinib and Lorlatinib are successful examples in this regard^{23,118}. Therefore, the use of macrocyclic scaffolds could represent an innovative strategy for the design of new ROCK inhibitors characterized by good efficacy and a favourable selectivity profile.

To our knowledge, no ROCK macrocyclic inhibitors have been reported in literature so far. Therefore, this pioneering research work will help to elucidate whether the design of macrocyclic ligands is a successful strategy to achieve ROCK inhibition.

Known ROCK inhibitors from literature were evaluated for opportunities of macrocyclization using knowledge-based approach supported by CADD (Computer Aided Drug Design). A synthetic strategy was identified and pursued to prepare these new derivatives and, ultimately, their inhibitor activity was evaluated in cell-free and cell-based ROCK I and ROCK II related assays.

3. Result and Discussion

3.1 Reference Compound Selection

Back in 2014, 35 macrocycles were reported in clinical trials while 68 macrocyclic drugs had already reached the market¹¹⁹. Most of them were macrolides or cyclic peptides. These natural products are very different from synthetic small molecules both in their structure and in their discovery paths. However, a small subset of “de Novo Designed” macrocycles has also been reported¹¹⁹. This group mainly contains peptide-inspired hepatitis C virus (HCV) protease and polymerase inhibitors and macrocyclic kinase inhibitors. All these new macrocyclic molecules are designed and developed through a Structure Based Approach.

The analysis of the structure of protein-ligand complexes represents the best starting point for the rational design of new macrocyclic drugs. Macrocyclic-like conformations (U-shaped, C-shaped etc.) are often recognized in non-macrocyclic small ligands bound to their protein targets. Therefore, the closing of their structures to form new macrocycles could represent the best way to obtain a molecule with optimal properties for the target of interest.

The design of new macrocyclic ROCK inhibitors was initiated by examining all human ROCK I and ROCK II crystal structures available in the Protein Data Bank (PDB): 26 ligands in complex with hROCK I and 7 ligands in complex with hROCK II were available at the time. The purpose of the evaluation was to find opportunities of macrocyclization in known ROCK inhibitors, or rather, to identify bound ligand conformations that appeared well suited for modification into macrocycles. Moreover, the *in vitro* biological profile of selected inhibitors was evaluated to understand whether macrocyclization would improve potency and selectivity with respect to parent compounds.

The selection of a specific ligand starting point among all the reported ROCK inhibitors was not straightforward.

As reported in paragraph 1.4.1, a prototypical ROCK inhibitor elongates in the ATP pocket in a very linear mode, with no hint to obvious macrocyclization opportunities. Nevertheless, an interesting X ray structure (PDB ID 3ndm) was identified in which the ligand shows a bound conformation that can be used as starting point to build cyclic derivatives. Ligand **17 (Figure 41)** belongs to a substituted

2H-isoquinolin-1-one series. The compound features an isoquinolinone as a Hinge binder, linked by an amidic spacer to a β -aryl substituted pyrrolidine¹²⁰.

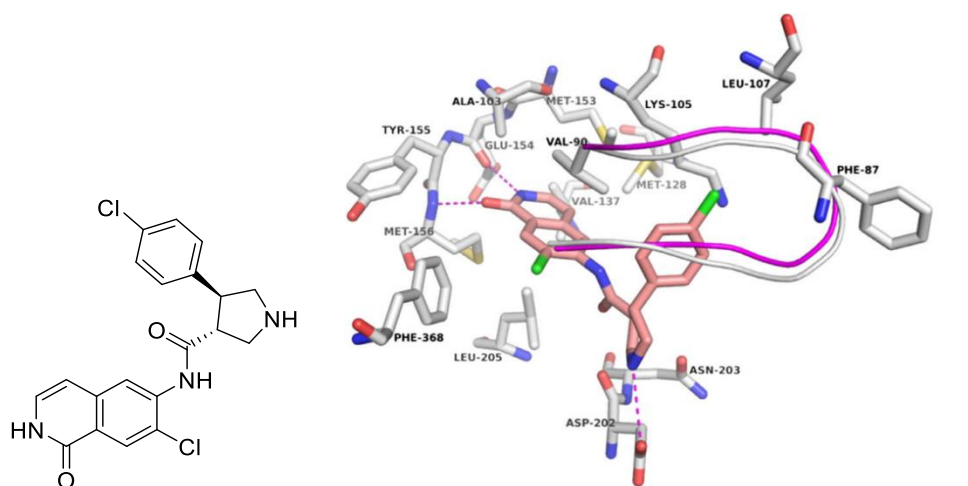


Figure 41: Structure of **17** bound to ROCKI, (PDB ID 3ndm).¹²⁰

The co-crystal structure of the ligand bound to ROCK I shows hydrogen bonding to backbone NH of Met156 and backbone carbonyl of Glu154 by the heteroatoms of the isoquinolone core. The pyrrolidine nitrogen forms a hydrogen bond with carboxylate of Asp202. The interesting feature of this binding mode is related to the position of the 4-chloro-phenyl group which lies beneath the *P-loop* establishing hydrophobic interactions with Leu107 and Lys105¹²⁰ (**Figure 41**). Moreover, the *P-loop* was shifted by ~ 1.8 Å if compared to the X ray structure (PDB ID 3ncz) of a similar compound lacking the chloro-phenyl group¹²¹. The nitrogen atom in the pyrrolidine ring in 3ndm is only 5.5 Å far from the Cl atom in the isoquinolone core. Therefore, an alkyl chain of appropriate length could represent a suitable linkage between the pyrrolidine and the central core, thus leading to a macrocyclic system that could pre-organize the phenyl ring in the same way of the pyrrolidine of compound **17**.

Compound **17** (configuration 3*R*,4*S*) inhibits ROCK II with an IC_{50} of 11 nM. The enantiomer of compound **17** (**Ent-17**, 3*S*,4*R*) displays a comparable IC_{50} of 4 nM. No crystal structure of Ent-17-ROCK complex has been published. However, based on their comparable potency a similar binding mode can be hypothesized. **Ent-17** is known to be promiscuous inhibitor (against AGC kinases family), inhibiting at least four kinases with sub micromolar potency (**Table 17**)¹²⁰.

Table 17: Off targets of **Ent-17**.

	Targets	IC₅₀
Ent-17	Protein kinase C epsilon type (PRKCE)	1000 nM
	Protein Kinase CGMP-Dependent 2 (PRKG2)	24 nM
	Cell division control protein 42 homolog (CDC42)	54 nM
	Serine/threonine-protein kinase N2 (PRKCL2)	14 nM

Compounds **17** and **Ent-17** were therefore considered good templates for the design and synthesis of novel macrocyclic ROCK inhibitors of improved selectivity.

The formation of the macrocycle was speculated to be beneficial in several aspects. Firstly, it could block the Cl-phenyl ring in its bioactive conformation, thus decreasing the entropic cost of the binding with a net potency gain. Reduction of allowed conformations could also positively impact selectivity towards other kinases. Secondly, the insertion of a linker would lead to the exploration of additional interactions in the binding site, possibly further boosting inhibitory potency.

3.2 The Rational Design of Macrocyclic Scaffolds

Based on the results of the structure-based analysis, new macrocyclic scaffolds were designed as potential ROCK-inhibiting molecules.

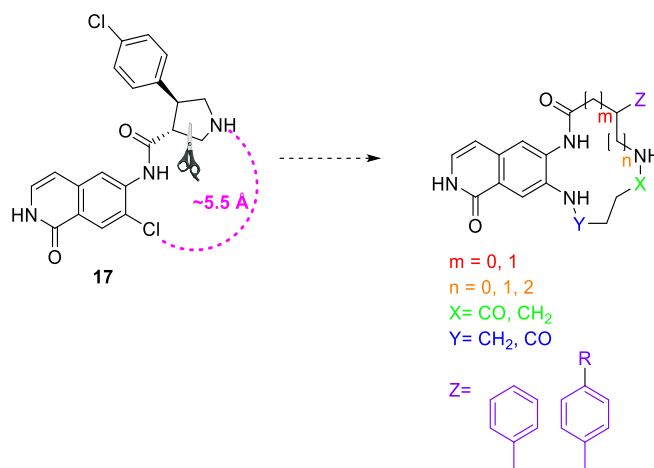


Figure 42: The design of new macrocyclic scaffolds.

As illustrated in **Figure 42**, the first design of macrocyclic scaffolds envisaged four key structural features:

- I. **The replacement of the pyrrolidine ring of compounds 17 and Ent-17 with a set of linear amino acids of different lengths bearing an aromatic decoration (Z).**

Two different lengths of the linear amino acids were considered, in order to access macrocycles of different size. This was done in the assumption that ring size would influence the overall shape and conformational equilibrium of the inhibitors and ultimately their binding affinity. Specific lengths of the amino acids were determined by independent variation of m and n . Therefore, phenyl glycine ($m, n = 0$; 11-membered macrocyclic ring), β -phenyl- β -alanine ($m=1, n=0$, 12-membered macrocyclic ring), β -phenyl-alanine ($m=0, n=1$, 12-membered macrocyclic ring), 4-amino-2-phenyl-butanoic acid ($m=0, n=2$, 13-membered macrocyclic ring) and 4-amino-3-phenyl-butanoic acid ($m=1, n=1$, 13-membered macrocyclic ring) were introduced in the design. The macrocycle itself could act as isostere of the pyrrolidine ring, with the purpose of pre-orienting the phenyl group under the *P-loop*. Moreover, the use of amino acids differently decorated at position 4 would allow us further exploration of this hydrophobic region.

- II. **Replacement of Cl atom on the isoquinolinone scaffold of parent compounds with a nitrogen atom, to be used as a handle for macrocycle formation.**
- III. **Insertion of a linker of 4 atoms between the nitrogen atom of linear amino acids and the nitrogen on scaffold.**

The length of the linker was chosen according to measured distance (5.5 Å) between pyrrolidine nitrogen and chlorine atom in parent compound. The nature of amino acid residues surrounding this region of binding pocket was also considered. An alkyl linker could perfectly fit this region and could establish favourable hydrophobic interactions with Phe368 residue. One unit of the linker was chosen to be a carbonyl for synthetic reasons. This carbonyl group was placed at either end of the linker by appropriately defining X and Y units in the general formula.

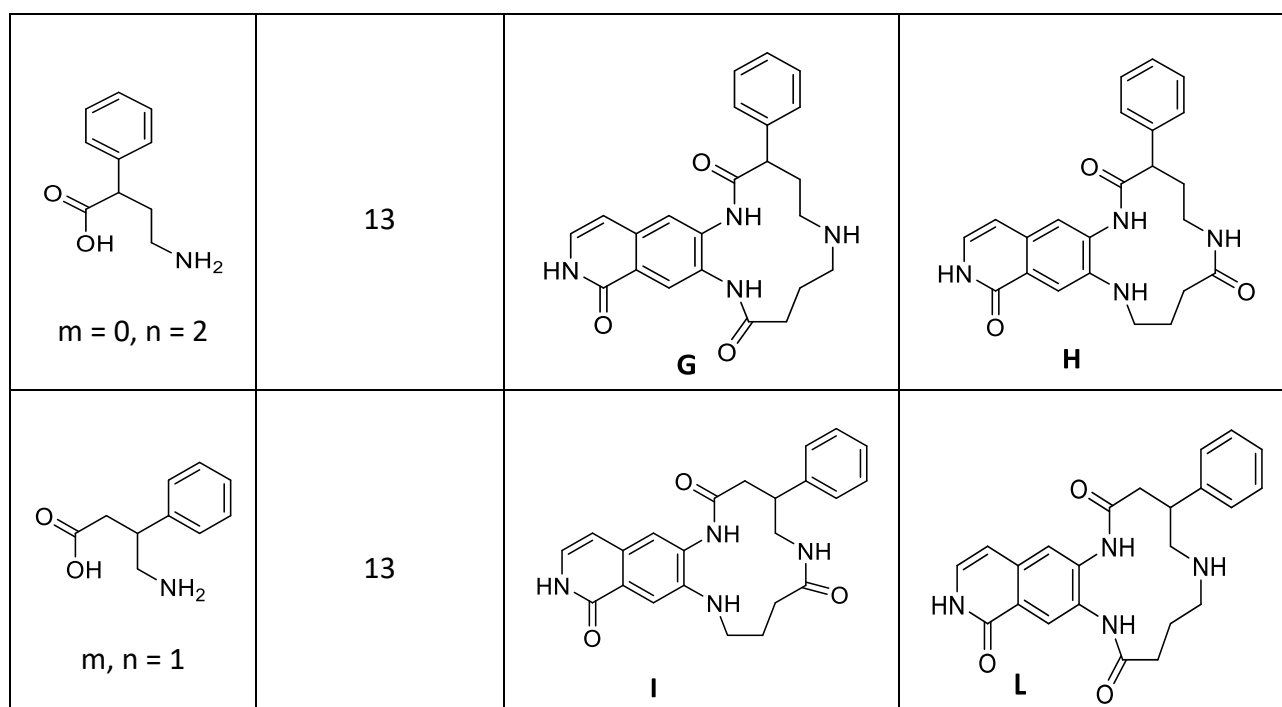
- IV. **The alternative introduction of an amide and of an amine groups at the extremities (X and Y) of the linker.**

The structure of 10 new designed macrocyclic compounds is reported in **Table 18**.

In the first column, the linear amino acid employed in the design is reported. The scaffolds were divided in **Anilide** and **Aniline** series, as determined by the specific position of the carbonyl group in the linker portion.

Table 18: Structures of 10 new macrocyclic scaffolds (A, B, C, D, E, F, G, H, I, L).

Employed Amino acids	Macrocycle size (atoms)	Anilide series X = CH ₂ Y = CO	Aniline series X = CO Y = CH ₂
 m, n = 0	11	 A	 B
 m = 1, n = 0	12	 C	 D
 m = 0, n = 1	12	 E	 F



Prime Macrocycle Conformational Sampling (Prime-MCS)²⁶ was employed to evaluate the new designed macrocycles. Prime-MCS is a computational tool (provided by Schrödinger®) which performs a conformational search for each newly designed macrocycle and provides an evaluation from both an energetic and geometric perspective.

The first aim of the tool is to explore the macrocycle conformational space to identify plausible minimum-energy conformations. This is carried out through the fragmentation of the main macrocycle ring and the conformational exploration of the resulting loose ends. Once the different macrocycles conformers are obtained, their deviation from the putative bioactive conformation of the original open derivative is analysed. The focus is to understand if a ring closure can preserve the geometry (RMSD) and whether the best fitting conformer is also the most energetically favoured one.

The tool calculates a weight w_i for each conformer which is proportional to dE_i , where dE_i is the difference between the energy value of the conformation with the energy of the global minimum conformation ($dE_i = E_i - E_0$). Therefore, each conformer receives a w which is equal to:
$$w = \frac{e^{-dE_i/KT}}{\sum_{i=0}^N e^{-dE_i/KT}}$$
 where N being the total number of conformers obtained from the conformational search.

At the end, for each macrocycle, the Schrodinger module provides two measures:

- “Boltzmann-aware probability below threshold” = $\sum_{RMSD < Threshold} W$

This is the sum of the Boltzmann weights for all those conformations showing an RMSD less than a user-defined threshold (2 Å) with respect to the open ligand (**the higher, the better [0,1]**).

- “stability metric expval” = $\sum_{i=0}^N w_i * RMSD_i$

The second measure is the sum of the products of weights and RMSD values for all conformers obtained from the conformational search (**the lower, the better**).

It would be expected that most energetically favoured conformer has also the lowest RMSD value in an ideal scenario.

In this study, for each scaffold, both enantiomers (*R* and *S*) were considered. In the first step of the analysis, templates with *m* = 0 (A, B, E, F, G and H) were discarded because they differed too much from the topology of the open ligand, **17**.

Therefore, as a result of this Prime-MCS evaluation, template **C1**, **D1**, **I1** and **L1** (where 1 stands for *S* configuration, **Table 18**) were identified as the best promising templates for the design of new macrocyclic ROCK inhibitors showing the lowest Boltzmann-weighted RMSD values and the highest values of Boltzmann-aware probability below threshold. (**Figure 43**).

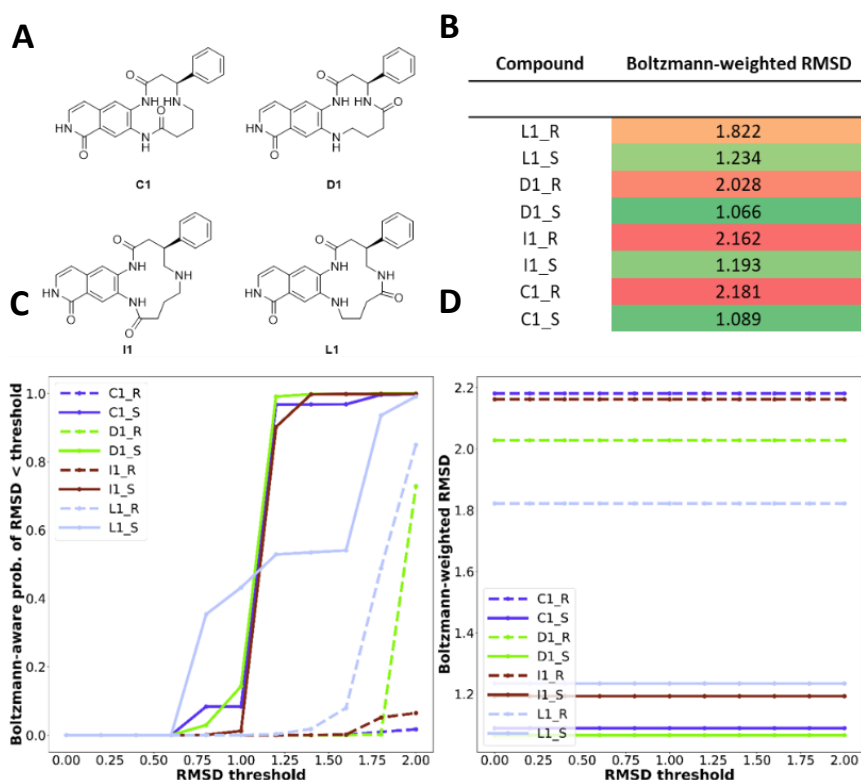


Figure 43: Structure of the four macrocyclic templates selected through Prime-MCS, where 1 stands for (*S*)-configuration (**A**); Boltzmann-weighted RMSD values (**B** and **D**); Boltzmann-aware probability of RMSD < 2 Å (**C**).

3.2.1 Synthetic Approach I

Considering the prime macrocycles evaluation scores and due to synthetic consideration, it was decided to prioritize the synthesis of template C1. The first attempted synthetic approach was based on an intramolecular reductive amination as a macrocyclization step (**Figure 44**).

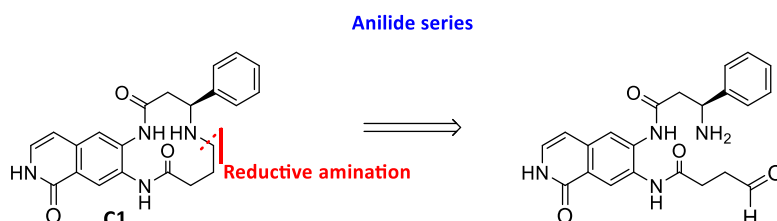
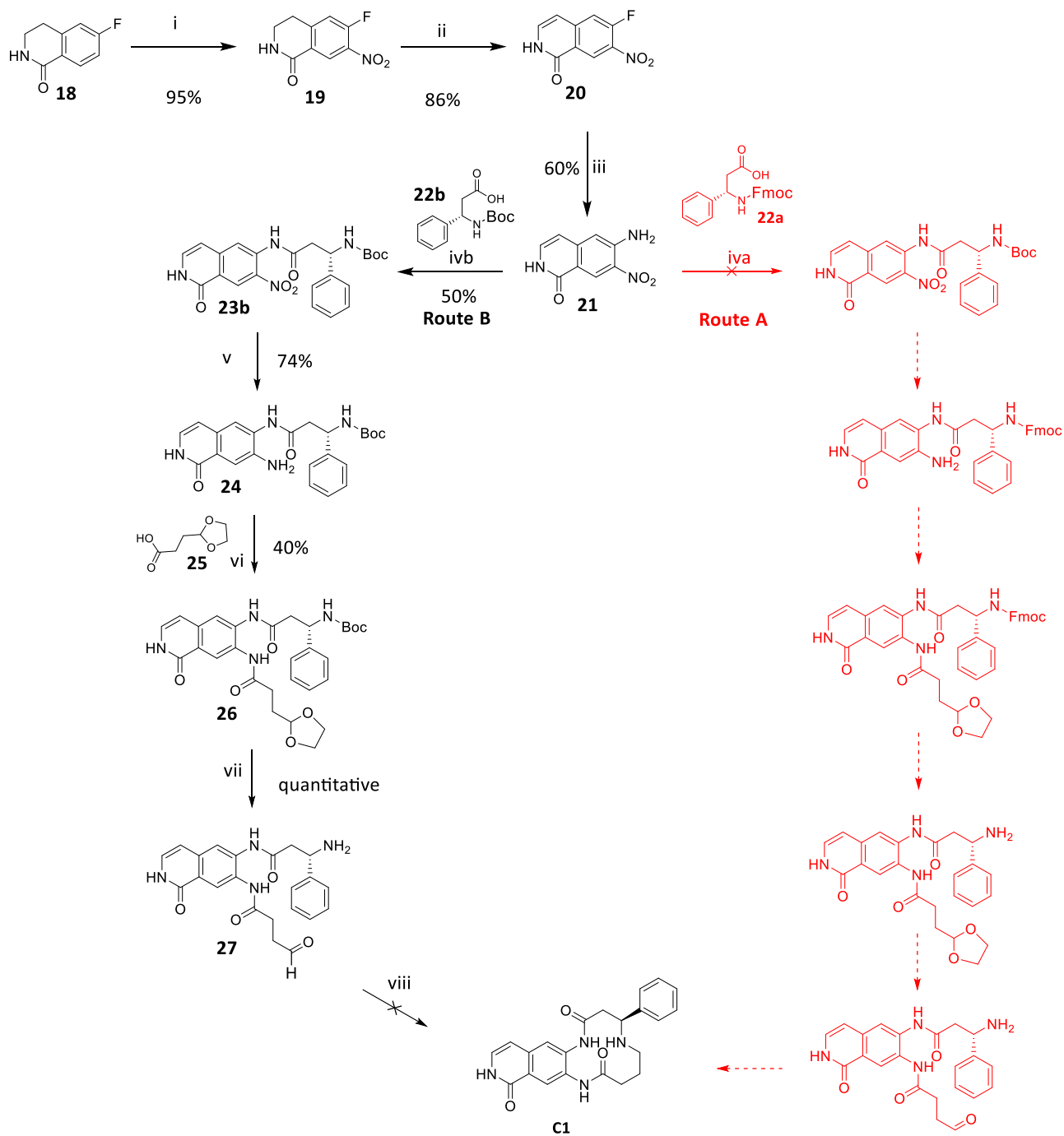


Figure 44: Retrosynthetic analysis.

The choice of reductive amination was driven by synthetic considerations. Reductive amination is considered the most remarkable way to obtain synthetically complex amines. As a matter of fact, a quarter of C-N bonds formed in pharma projects results from reductive amination reactions¹²². Moreover, formation of macrocycles through reductive amination are well reported in literature¹²³⁻¹²⁵.

The synthetic route attempted is reported in the following scheme (**Scheme 6**).



Scheme 6: Reagents and Conditions: i) H_2SO_4 , HNO_3 , 0°C , 30 min; ii) MnO_2 , Cl-Benzene, 150°C μW ; 1 hr iii) 7 N NH_3 in MeOH, Dioxane, 80°C , 24 hr; iv_b) **22**, POCl_3 , Pyridine, 0°C ; 1 hr; v) Fe, NH_4Cl , $\text{H}_2\text{O}/i\text{-PrOH}$, 80°C , 4 hr; vi) **25**, HATU, DIPEA, DMF, rt, 1 hr; vii) 0.3 M HCl in ACN.

Preparation of 6-amino-7-nitroisoquinolin-1(2H)-one (**21**)

The preparation of intermediate **21** emerged as a key, common requirement for the synthesis of designed macrocycles (**Figure 45**).

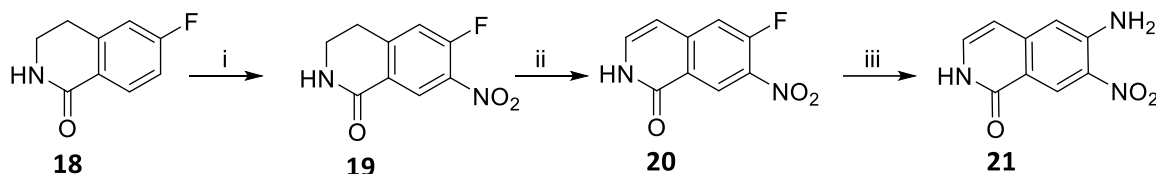
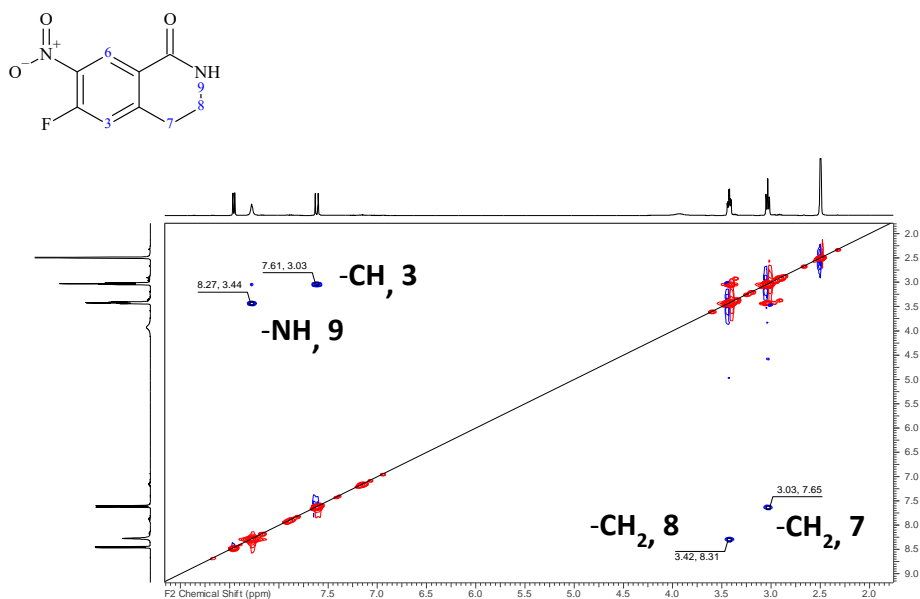


Figure 45: Zoom on Step i, ii and iii. Reagents and conditions: i) H_2SO_4 , KNO_3 (0°C), 30 min; ii) MnO_2 , Cl-Benzene, 150°C , 1hr-4hr; iii) 7N NH_3 , MeOH/Dioxane 1:1, 80°C , 12 hr.

Following the procedure reported by Fales *et al.*¹²⁶, synthesis started from commercially available 6-fluoro-3,4-dihydroisoquinolin-1(2H)-one (**18**). The selective nitration at *ortho*-position, using KNO_3 and H_2SO_4 at 0°C , at the *ortho*-position afforded the synthesis of the 7-nitro intermediate (**19**) in a quantitative yield.

The intermediate obtained was characterized by 2D NMR analysis to verify regioselectivity of the nitration. The ROESY spectra confirmed that nitration occurred at position 1 on Intermediate **18**. The reported ROESY spectra shows coupling between methylene at position 10 of the scaffold (multiplet at 3.03 ppm) and aromatic proton at position 5 (doublet at 7.62 ppm) (**Figure 46**).



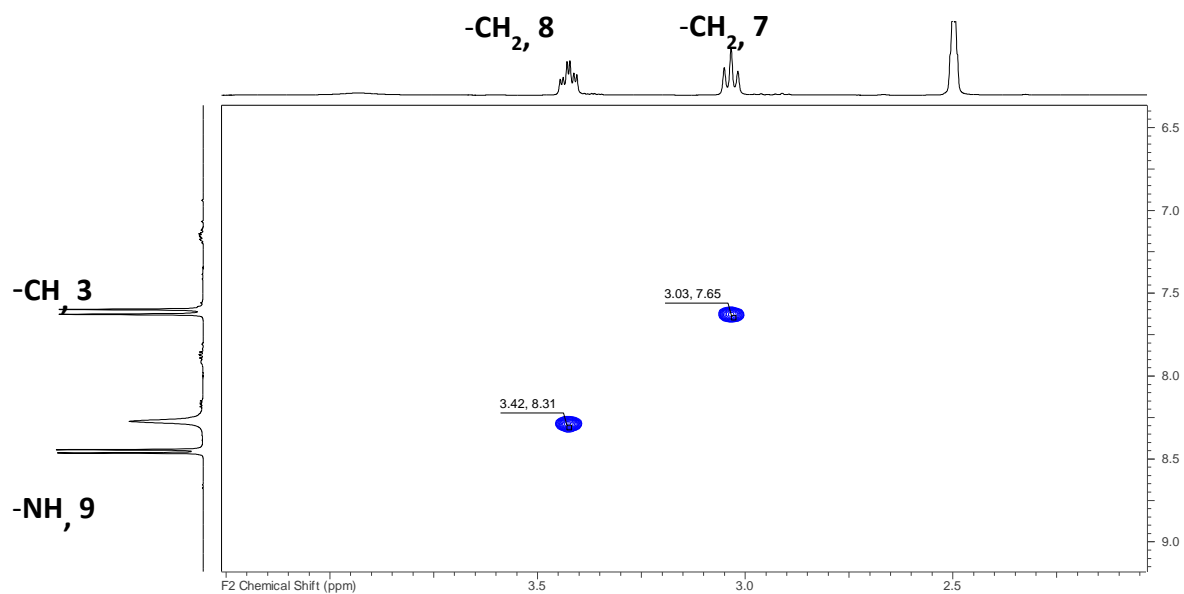


Figure 46: ROESY analysis of Intermediate **19**.

The oxidation of the 6-fluoro-3,4-dihydroisoquinolin-1(2H)-one to isoquinolone (**20**) was initially performed using 15 equivalents of MnO_2 in *i*-PrOH by heating at 80 °C. However, conversion of the starting material was slow (less than 90% after 24 hr) and the resulting yield was moderate, between 31% and 49%. This was probably due to the low solubility of the starting material. To improve dissolution, 1,4-dioxane was added as a co-solvent and the same reaction conditions were applied to a solution of starting material in a mixture 1:1 of *i*-PrOH/Dioxane. This resulted in an improved yield (87%) but reaction still proceeded slowly. Therefore, the mixture *i*-PrOH/Dioxane was replaced with Cl-benzene, a solvent with a higher boiling point, and reaction was performed at 150 °C. These new reaction conditions yield up to 86% in 1 hr under microwave irradiation and in 4 hr under thermal heating in a small reactor.

$\text{S}_{\text{N}}\text{Ar}$ of fluoride at position 6 was performed in methanolic ammonia¹²⁷ and afforded 6-amino-7-nitroisoquinolin-1(2H)-one (**21**) with an average yield of 60%.

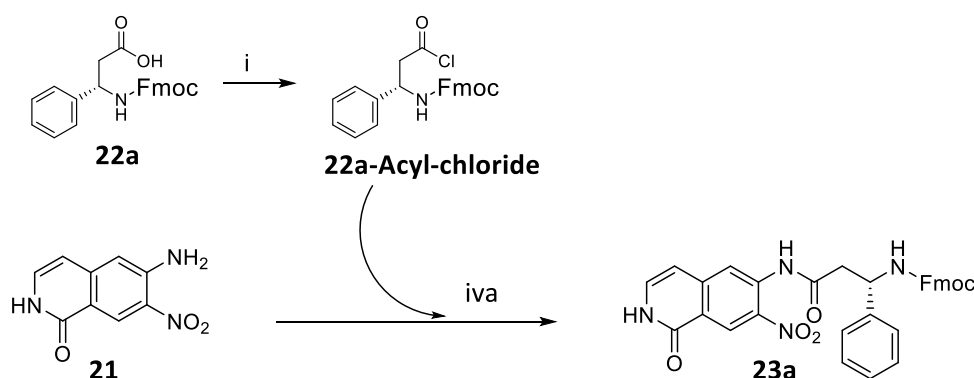
Reactions were initially tested in a mg scale and then repeated with the optimized conditions in gram scale.

Optimization of amide coupling

Route A

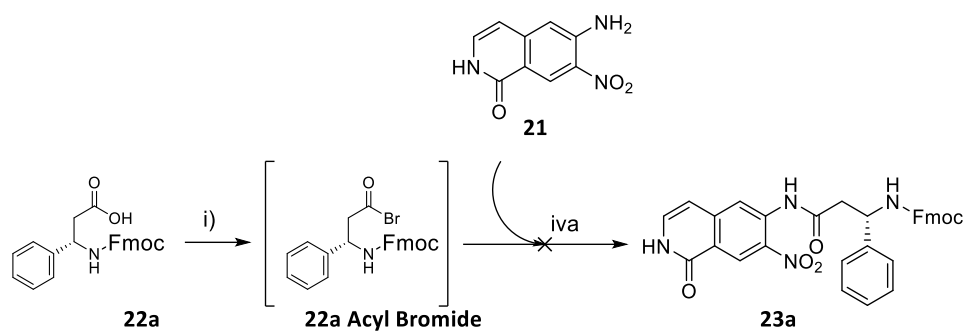
Once the preparation of the building block (**21**) was optimized, the initial idea was to introduce the first moiety, the Fmoc-protected (*S*)- β -Phenylalanine, via amide coupling (**Scheme 6**). Fmoc was selected as protecting group because of its orthogonality to the protected aldehyde as acetal. Fmoc removal in basic conditions (for example piperidine 20% in DMF) to yield amine would be followed by aldehyde deprotection and macrocyclization via reductive amination (**Scheme 6, Route A**).

Different amide coupling conditions were explored to introduce the Fmoc protected amino acid. First conditions envisaged the synthesis of the corresponding acyl chloride using oxalyl chloride in the presence of a catalytic amount of DMF. Synthesis of the acyl chloride was successful but the following reaction with Intermediate **21** led to the formation of the desired intermediate only in low yield (20%) (**Scheme 7**) due to the instability of acyl chlorides in the reaction media.



Scheme 7: Reagents and conditions: i) (COCl)₂, DMF, DCM, rt, quantitative ii) 22-Acyl-chloride DIPEA, DMA, 80 °C (20%).

Therefore, to avoid the degradation of the acyl chloride it was decided to move from a procedure involving isolation of intermediate acyl chloride to a one pot, two step procedure. Reaction was repeated using PyBrop as coupling reagent in presence of Intermediate **21**, with Pyridine in DMF heating up to 60 °C (**Scheme 8**). Nevertheless, even in these conditions, the conversion was slow and not complete. Moreover, Fmoc group cleavage was observed.



Scheme 8: Reagents and Conditions: i) PyBrop, Pyridine, DMF; rt ii) **21**, 60 °C.

Route B

Coupling efficiency was also hampered by the poor nucleophilic nature of the amino group of Intermediate **21**. Based on these considerations, both coupling conditions and amino acid protection were modified. It was decided to replace Fmoc protection with a Boc protecting group (**22b**) for its enhanced stability to basic conditions. On this reagent, conditions described by Ginn *et al*¹²⁸ were applied. Coupling was then performed utilizing a phosphorous oxychloride (POCl₃) in Pyridine, at 0°C, step iv_a (**Figure 47**). These conditions allowed for rapid formation of the desired amide. However, recovery of amide intermediate **23b** was always lower than 50% and of limited reproducibility, ranging from 11 to 48%. This was probably due to the low solubility of the reaction product, which made reaction work up and product isolation quite problematic.

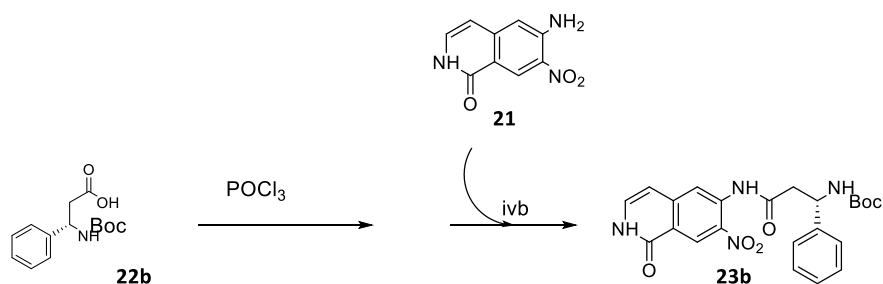


Figure 47: Zoom on step iv. Reagents and Conditions: iv) **22b**, POCl₃, Pyridine, 0 °C, 1 hr, 11-48%.

Reduction of nitro group and second amide coupling

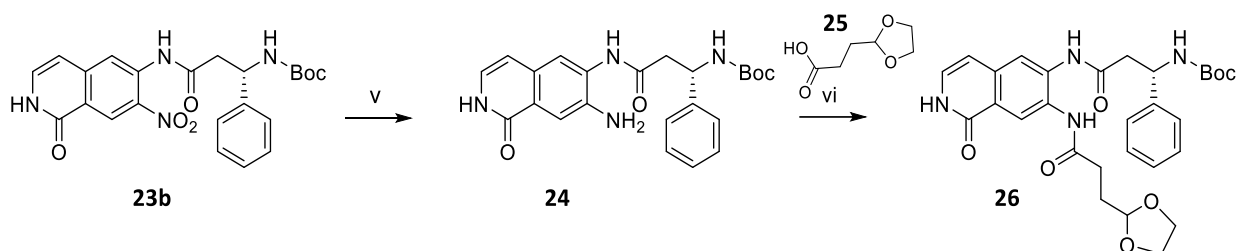


Figure 48: Zoom on steps v and vi. Reagents and conditions: v) Fe, NH₄Cl, H₂O/*i*-PrOH, 80 °C, 4 hr; vi) **25**, HATU, DIPEA, DMF, rt, 1 hr.

Intermediate **24** was obtained by reduction of the nitro group using Fe, in the presence of excess of NH₄Cl. Reaction was performed in a 1:1 *i*-PrOH/H₂O mixture, heating for 4 hr at 80 °C and yielded the desired intermediate in good yields (74% as average of 4 reactions), see **Figure 48**.

The following step involved the amide coupling between 3-(1,3-dioxolan-2-yl) propanoic acid (**25**) and Intermediate **24**. HATU was selected as coupling reagent and reaction was performed in DMF in presence of DIPEA. Purification by reverse phase flash chromatography gave desired intermediate **26** in a 40% yield.

Synthetic route completion: protecting groups removal and macrocyclization

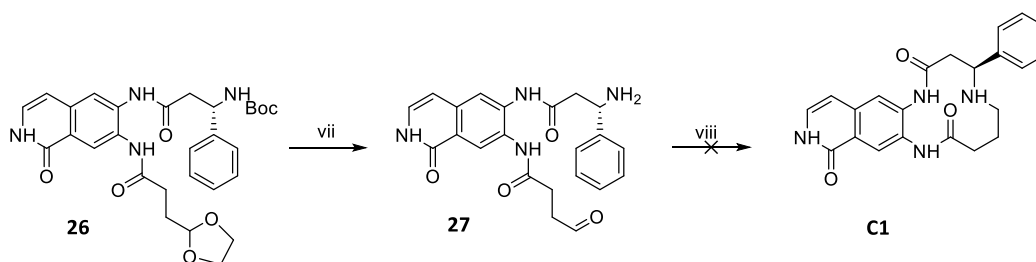


Figure 49: Zoom on steps vii and viii. Reagents and Conditions: vii) 0.3 M HCl in ACN.

Amine and aldehyde deprotection of Intermediate **26** in acidic conditions (step vii, **Figure 49**) proved less straightforward than expected. Conc HCl was added to a solution of Intermediate **26** in acetonitrile, until final concentration of HCl was 0.3 M. Isolation of the intermediate and consequent characterization was hard because intermediate was extremely polar and hydrophilic. Several attempts to isolate the product were carried out, such as THF extraction from basic aqueous solution

as well as purification by SCX, but all attempts were unsuccessful. Therefore, a simple evaporation under vacuum was carried out to obtain Intermediate **27** which was used in the following step as chloride salt without further purification.

Classical conditions for reductive amination were employed in the last step (step viii, **Figure 49**). Since Intermediate **27** was very polar, it was decided to dissolve it in MeOH and to use NaBH₃CN as reductive agent. Reaction was performed in high dilution to avoid oligomerization intermolecular oligomerization and favour intramolecular macrocycle formation. In the first attempt, (**Table 19**, entry 1) reaction was performed with NaBH₃CN in MeOH in presence of DIPEA to free the chloride salt. UPLC-MS analysis showed the formation of a product with a mass equivalent to the desired product. Purification by preparative HPLC coupled to mass detector yielded 2.3 mg of product. Even if UPLC-MS analysis showed a UV peak with a m/z corresponding to the desired product, it was not possible to confirm the structure by ¹H-NMR analysis due to the presence of impurities in the aliphatic region of the spectrum.

The reaction was repeated in the same conditions on slightly higher scale, but disappointingly reaction failed. UPLC-analysis revealed the formation of a main side product characterized by m/z 422 [M+H]⁺. It was hypothesised that this side product was generated by addition of MeOH to intermediate imine **28** to give the corresponding cyclic hemiaminal ether, as highlighted in the proposed mechanism (**Figure 50**). Any attempts to hydrolyse the acetal in acidic conditions failed.

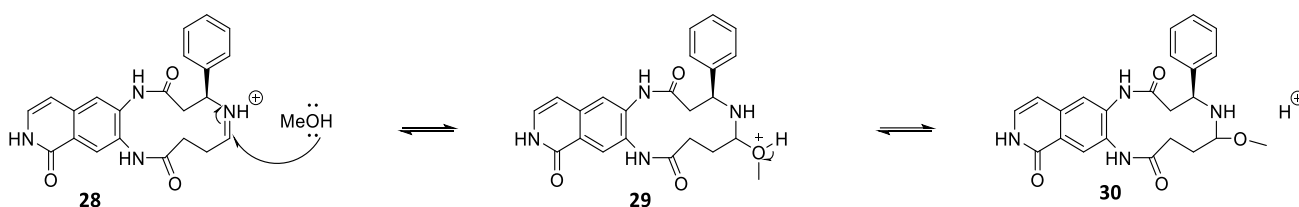


Figure 50: Proposed mechanism of the side product formation in macrocyclization step.

To avoid the formation of side product **35**, next attempts of macrocyclization were performed using THF as solvent (see **Table 19**, entry 3 and 4). Starting material proved not to be completely soluble in THF so *i*-PrOH was added as cosolvent and reaction was performed in the resulting THF/*i*-PrOH 5:1 mixture. Intermediate (**27**) was dissolved in *i*-PrOH/THF 1:5 in presence of MgSO₄ and 4 Å molecular sieves and the mixture was heated overnight at 50 °C for imine pre-formation. NaBH₃CN and CH₃COOH were then added and the resulting mixture was stirred at rt. Volatiles were

evaporated under vacuum and crude material was purified by SCX (see **Table 19**, entry 3) or by HPLC (see **Table 19**, entry 4). Unfortunately, in both cases, it was not possible to confirm the structure by ¹H-NMR analysis.

Table 19: Summary of conditions used for the macrocyclization step (step viii).

Entry	Scale	Reagents and conditions	Yield
1	10 mg	NaBH ₃ CN, MeOH, DIPEA, 50°C°→rt	26% Structure not confirmed
2	60 mg	NaBH ₃ CN, MeOH, DIPEA, 50°C°→rt	Reaction failed
3	50 mg	Step a) MgSO ₄ , Molecular Sieves 4 Å, THF/ <i>i</i> -PrOH 5:1 Step b) NaBH ₃ CN, CH ₃ COOH	Yield 19% Structure not confirmed
4	40 mg	Step a) MgSO ₄ , Molecular Sieves 4 Å, THF/ <i>i</i> -PrOH 5:1 Step b) NaBH ₃ CN, CH ₃ COOH	Yield 2.8% Structure not confirmed

Overall, this synthetic route showed many issues. First, the two amide couplings were extremely low yielding and represented limiting steps for the synthesis of the macrocycle C1. Secondly, the acidic cleavage of the cyclic acetal and the Boc group in one step did not allow to isolate and characterize properly intermediate **27**, consequently affecting the final step. Lastly, reductive amination proved to be low yielding and not reproducible.

For the above reasons, it was decided to abandon this synthetic route and to opt for another synthetic approach.

3.2.2 Synthetic Approach II

The new synthetic approach envisaged an intramolecular amide coupling as macrocyclization step.

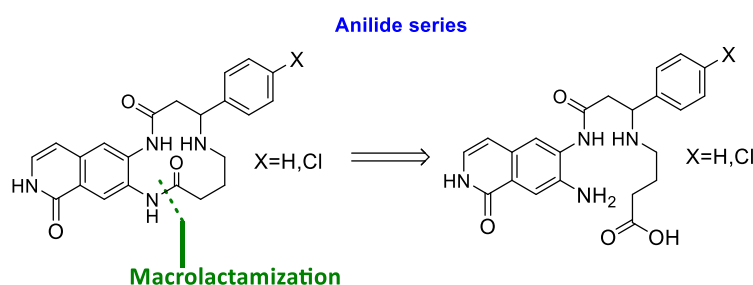
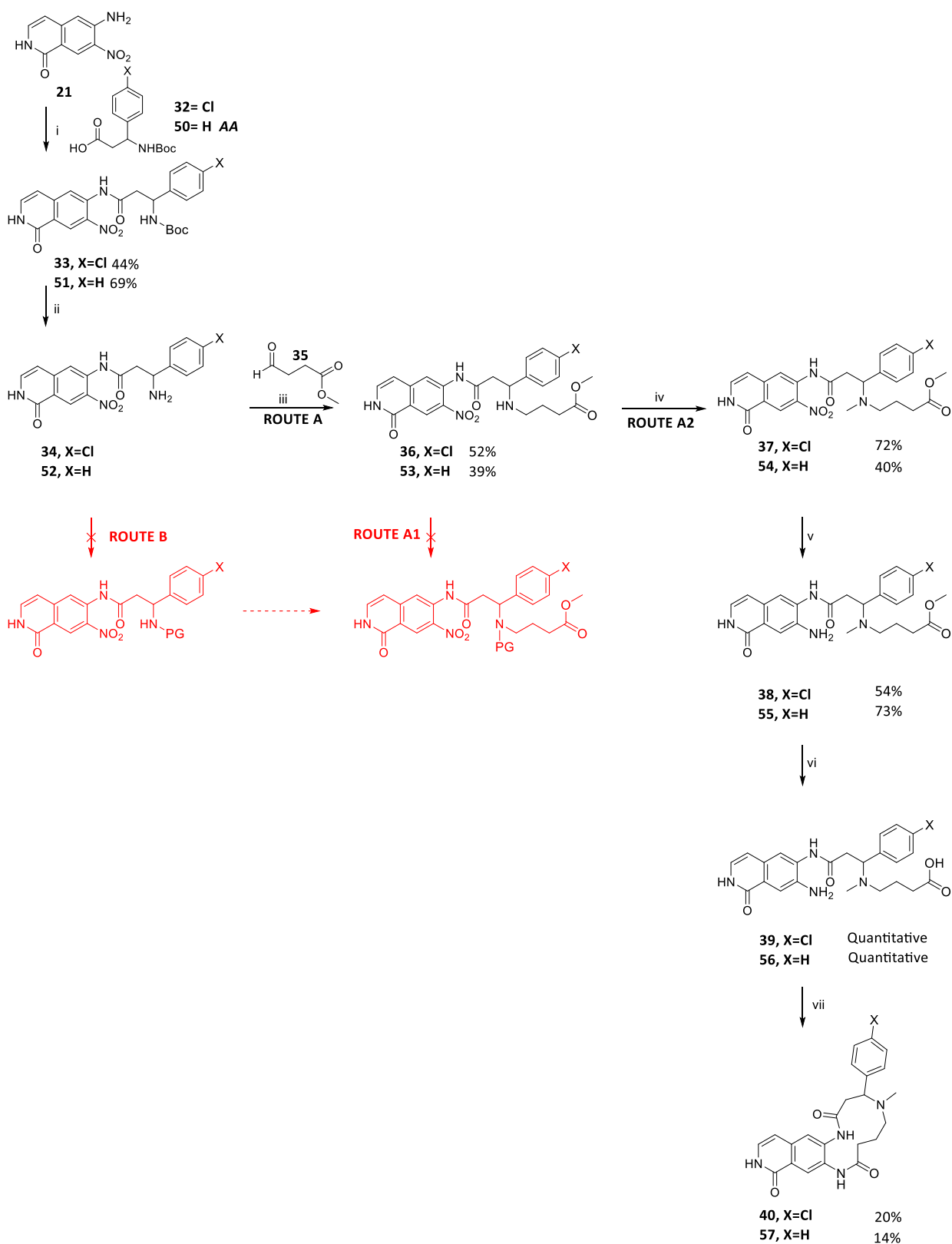


Figure 51: Retrosynthetic Analysis.

To obtain macrocyclic derivatives three different pathways (Route A1, Route A2 and Route B) were designed and attempted as described in **Scheme 9**.

The synthesis started from the Intermediate **33** which was synthesised following the same procedure used for Intermediate **23b**, using POCl_3 and 3-((tert-butoxycarbonyl)amino)-3-(4-chlorophenyl)propanoic acid. In this case, the synthesis of the Cl-derivative was prioritized over the synthesis of the phenyl derivative: the synthesis of the Cl-derivative was prioritized due to SAR considerations: the presence of Cl was considered key to achieve ROCK affinity¹²⁰. Additionally, because of many issues faced in the first synthetic approach, synthesis of macrocycles as racemic mixture was preferred over the synthesis of single enantiomers **5**. The following step was represented by Boc cleavage which was carried out at 60 °C in acidic condition (4M HCl in Dioxane). Using these conditions complete deprotection was achieved in 30 minutes obtaining the desired compound **34** in quantitative yield as chloride salt.



Scheme 9: Reagents and Conditions: i) POCl₃, Pyridine ii) 4M HCl in Dioxane, 60 °C; iii) **35**, NaBH₃CN, CH₃COOH, MgSO₄, 4 Å Molecular Sieves, MeOH/THF, rt; iv) HCOH, NaBH₃CN, CH₃COOH, MgSO₄, 4 Å Molecular Sieves, MeOH/THF, rt; v) SnCl₂, EtOH, rt; vi) LiOH, THF/H₂O 3:1; Pyridine/HCl, rt; vii) HATU, DIPEA, DMF, 0.02M, rt.

Route A

Next step took advantage of the use of commercially available methyl 4-oxobutanoate (**35**) which was used as new synthon for the aliphatic linker. Conditions reported by Clementson *et al.*¹²⁹ were followed for the reductive amination. Reductive amination yielded intermediate **36** with an average yield of 52%. Unfortunately, from UPLC-MS analysis was evident the formation of 33% of a side product which corresponds to the tertiary amine (**Figure 52**) that contributes to lower yield of intermediate **36**.

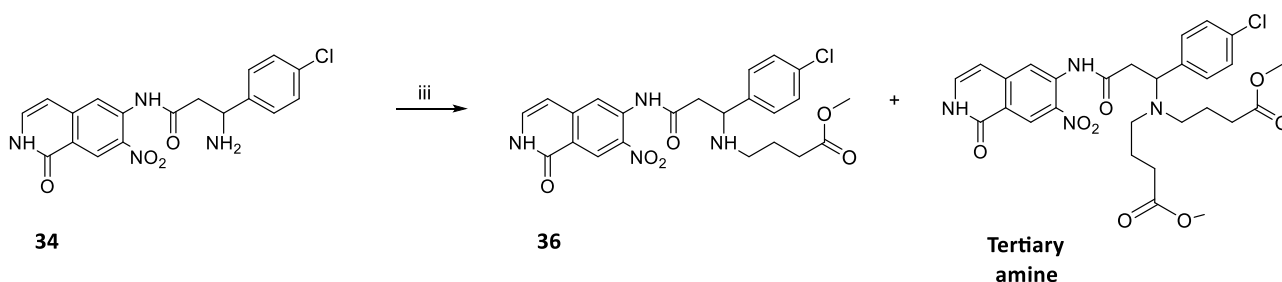


Figure 52: Zoom on step iii. Reagents and Conditions: iii) **35**, NaBH₃CN, CH₃COOH, MgSO₄, 4 Å Molecular Sieves, MeOH/THF, rt.

Route A1

Route A1 would involve the protection of the amino group of the intermediate **36**, (**Scheme 9**). The insertion of a protecting group orthogonal to the methyl ester was necessary to prevent the side reaction of the aliphatic amino group with the carboxylic acid in the macrolactamization step. The aliphatic nitrogen, being more nucleophilic compared with the anilinic nitrogen, would have reacted faster to give a five-ring side product (**Figure 53**).

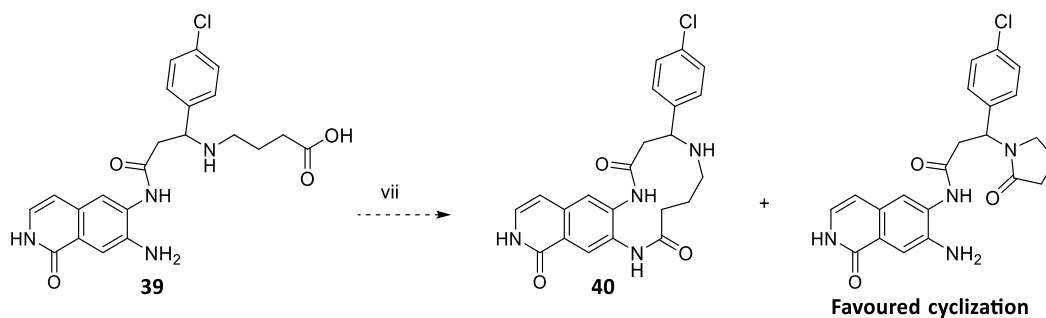


Figure 53: Formation of the five-ring side product.

Initially, it was decided to reintroduce Boc as protecting group. However, all the attempts to introduce it were unsuccessful. The main problem encountered was the high reactivity of the cyclic amide of isoquinolin-1(2H)-one scaffold as well as that of the amide at position 6. Both reacted with the Boc-anhydride leading to a mixture of bis or even tris protected products that were impossible to separate in attempted column chromatographies (**Figure 54**).

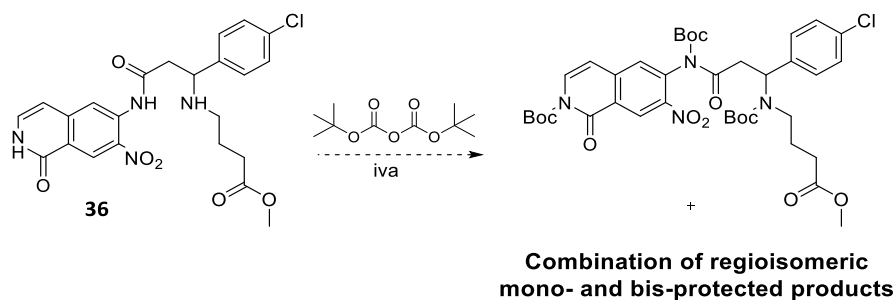


Figure 54: Route A1, Protection of the amino group with Boc anhydride.

Route B

Therefore, it was decided to replace Boc with the p-methoxybenzyl protecting group (PMB), to be installed before the aliphatic chain (**Figure 55**).

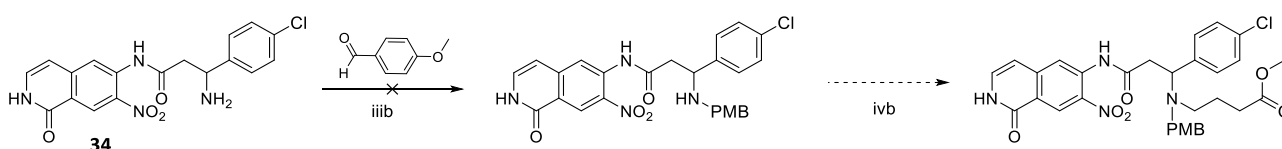


Figure 55: Route B, Protection of the amino group with para-methoxy-benzaldehyde.

PMB can be inserted via reductive amination using 4-methoxybenzaldehyde avoiding in this fashion the side reaction with the two amide groups. Moreover, PMB can be removed in mild acidic condition. The main problem of this synthetic strategy is that 4-methoxybenzaldehyde is a poor electrophile, thus, it does not react easily with the amino group to generate the resulting imine. Different conditions were used to perform the reductive amination but disappointingly it was not possible to obtain the desired intermediate. Conditions successfully used for the synthesis of Intermediate **36** did not work. Reaction proceed very slowly and monitoring by UPLC-MS showed formation of side products and reduction of the nitro group as well. Therefore, conditions reported by Neidigh et al¹³⁰ were attempted. Authors reported a highly efficient and mild procedure for

reductive aminations, employing the titanium(IV) isopropoxide chloride as a Lewis acid enhancing the formation of the imine. Intermediate **34** and 4-methoxybenzaldehyde were dissolved in MeOH/THF and titanium (IV) isopropoxide chloride, MgSO₄ and 4Å Molecular Sieves were added to this solution. The resulting reaction mixture was stirred at rt for 1 hr, then NaCNBH₃ was added. Disappointingly, only 5% conversion of the starting material was observed. Other conditions which involved the preformation of the imine were attempted. Starting materials were dissolved in Toluene with MgSO₄ and 4Å Molecular Sieves and stirred for 5 days at 90 °C. ¹H-NMR analysis of the crude showed only 20% formation of the imine. Therefore, Route B was discharged due to the difficulty to insert the protecting group.

Route A2

Since the identification of the right protecting group seemed challenging, an alternative synthetic pathway was attempted. It was decided to install a methyl group instead of a protecting group, thus obtaining the corresponding tertiary amine, see **Figure 56**.

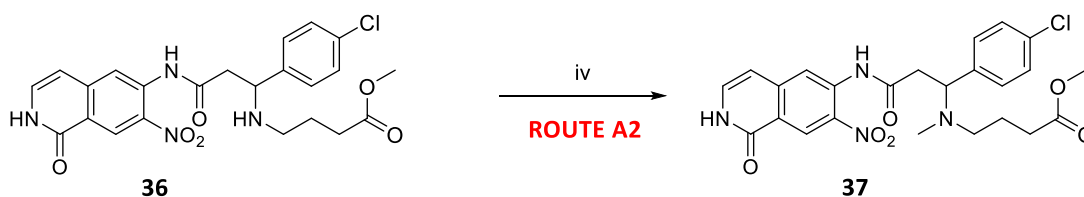


Figure 56: Zoom on Step iv. Reagent and Conditions: iv) HCOH, NaBH₃CN, MgSO₄, 4Å Molecular Sieves, CH₃COOH, MeOH/THF.

The methyl group was introduced by reductive amination. Reaction was performed following same conditions reported for the synthesis of Intermediate **36**. Intermediate **37** was obtained in a 72% yield.

A preliminary docking analysis of the methylated derivative (**40**) was carried out in order to understand whether this modification could affect the binding mode in the ATP binding site. As illustrated in **Figure 57**, compound **40** accommodated well within the main ATP-binding site of ROCK I, interacting with the hinge region *via* its isoquinolone ring and placing the chloro-phenyl moiety underneath the p-loop, similarly to the co-crystallized compound (PDB ID 3ndm). Not surprisingly, only *S* enantiomers of both ionization states allowed a proper accommodation of the pendant

phenyl group under the p-loop segment. Interestingly, strong polar intra-molecular interactions were observed in both poses. Based on these results, it was decided to proceed with the synthesis of compound **40** and its analogue, compound **57**. Even if the docking analysis showed *S* as favourite configuration, the synthesis of the racemate was prioritized to have as soon as possible a confirmation of activity as ROCK inhibitor of either two of the enantiomers.

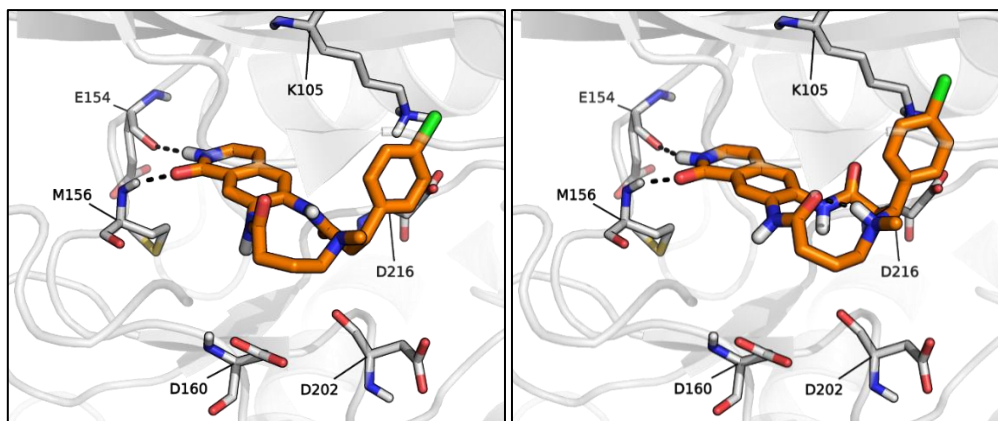


Figure 57: Best-ranked poses of the neutral (left) and protonated (right) form of compound **40** (orange sticks) within ROCK I (white, transparent cartoons). Key ligand-protein interactions are shown as dashed black lines.

Completion of the Synthesis

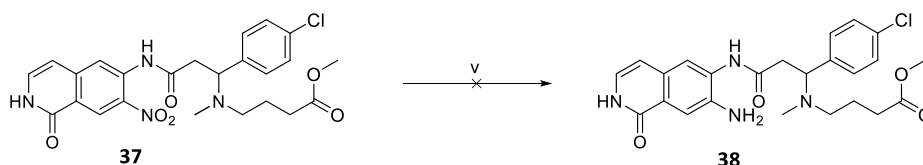


Figure 58: First attempted conditions for step v. Reagents and Conditions: v) Fe, NH₄Cl, *i*-PrOH/THF 1:1, 80 °C, 4 hr.

Reduction of the Nitro group (**Figure 58**) to obtain Intermediate **38** was initially carried out using Fe and NH₄Cl in a mixture 1:1 of *i*-PrOH and THF at 80 °C. These conditions were successful for the synthesis of Intermediate **18**, (**Scheme 6**). Disappointingly, in this case, UPLC reaction monitoring showed no conversion of the starting material into the desired product. Therefore, pH was lowered to 5 in order to promote the reduction of the nitro group. Lowering the pH led to the reduction of the nitro group but, at the same time, to the formation of two main side products. As reported

below (**Figure 59**), low pH and high temperature favoured the elimination of the amino derivative (**43**) leading to the formation of carbocation **42** which evolved in the corresponding alkene **43**, identified by UPLC-MS analysis. It was hypothesized that elimination occurred through a E1 mechanism since the carbocation **44** is stabilized by the presence of the Cl substituted aromatic ring which can delocalize the positive charge easily and furthermore by polar solvents, such as *i*-PrOH and H₂O, that stabilize the intermediate carbocation by solvation.

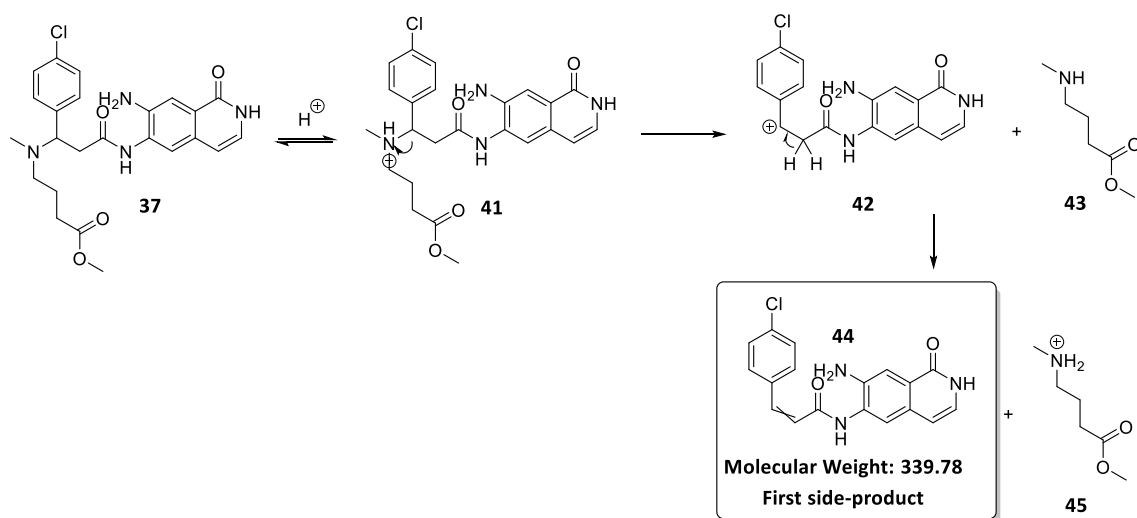


Figure 59: Proposed mechanism for the formation of side product **44**.

Additionally, in acidic conditions the protonated carbonyl group (**48**) underwent nucleophilic attack by the aromatic amino group which led to the formation of a five membered ring (**48**). After that, the loss of a molecule of water gave the side product **49**, (**Figure 60**).

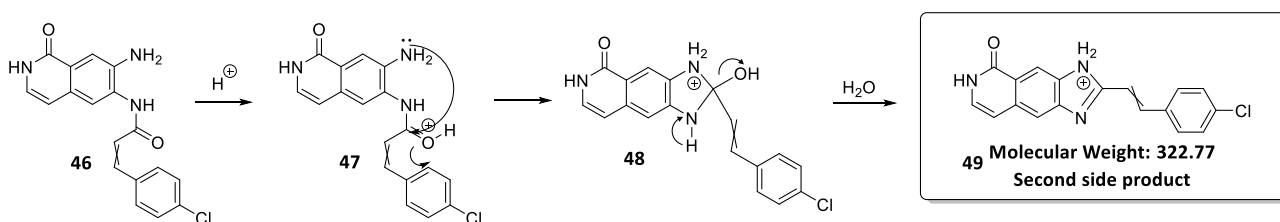


Figure 60: Proposed mechanism for the formation of the side product **49**.

To avoid the formation of these side products, alternative conditions for the nitro reduction were found. Conditions reported by Carreira *et al.*¹³¹ were applied. Reduction was performed with SnCl₂·2H₂O in EtOH at rt. These new conditions yielded **38** in a 54% yield (**Figure 61**). Subsequently, intermediate **39** was obtained by basic hydrolysis of the methyl ester. Hydrolysis was carried out

with a small excess of LiOH in a mixture of THF/H₂O 4:1 at rt. When conversion of the starting material was complete, Pyridinium chloride was added to quench the excess of LiOH and solvent was evaporated under vacuum.

The final macrolactamization step was carried out in classical conditions for the amide synthesis. Intermediate **39** was dissolved in DMF and solution was added of DIPEA and HATU. The reaction was performed in high dilution at 0.02 M concentration to avoid the oligomerization of the starting material. Eventually, the final product **40** was obtained in 20% yield after purification by reverse phase flash chromatography.

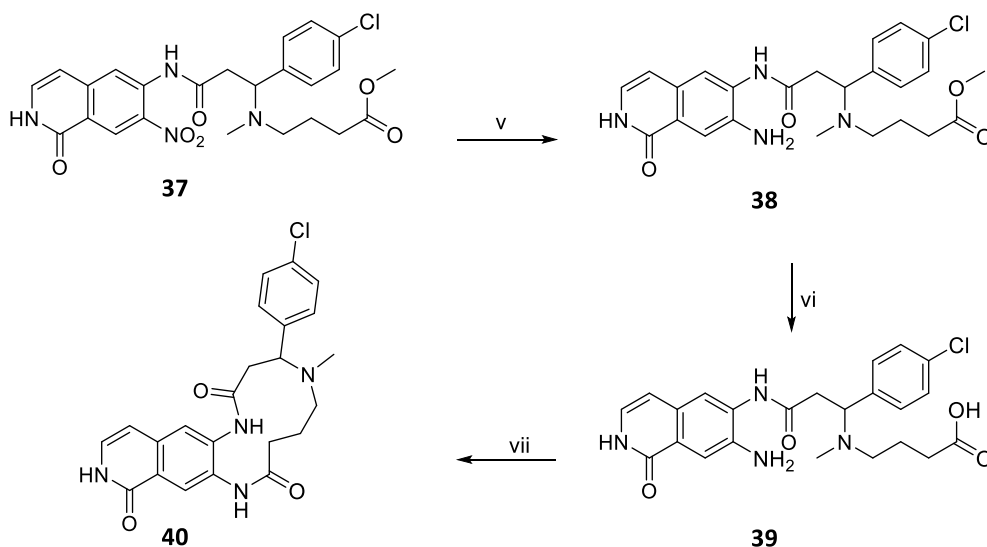


Figure 61: Steps v, vi and vii. Reagents and Conditions: v) SnCl₂·2H₂O, EtOH, rt; vi) LiOH, PyridiniumCl, THF/H₂O 4:1, rt; vii) HATU, DIPEA, 0.02M, rt.

This synthetic route was successfully repeated for the synthesis of the second macrocycle (**57**). For the details of this synthesis, see experimental procedure in Material and Methods chapter.

3.2.3 Macrocycles Characterization

Macrocycle **40** was fully characterized by $^1\text{H-NMR}$ and 2D-NMR and by single crystal X-ray crystallography.

$^1\text{H-NMR}$ and 2D-NMR analysis

$^1\text{H-NMR}$ spectrum of **40** was compared with that of the acyclic precursor **38** (Figure 62).

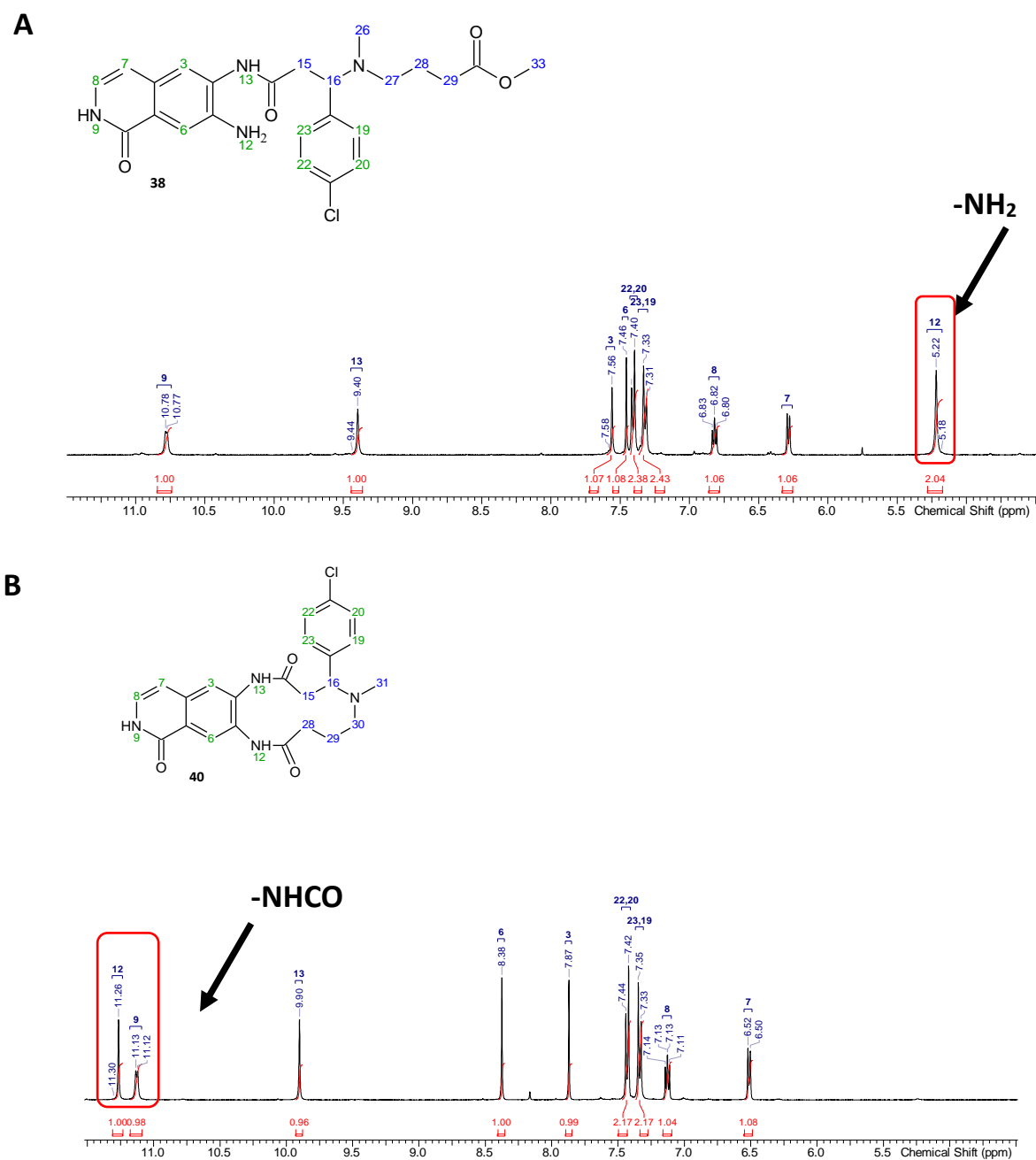
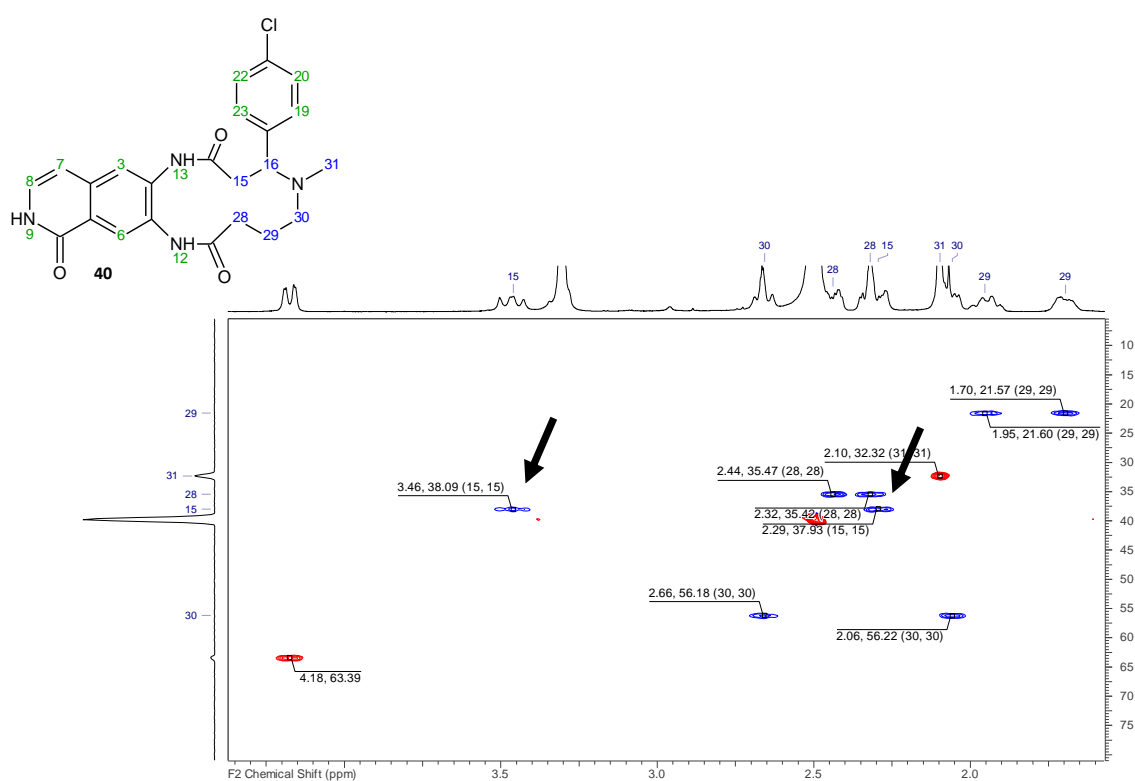


Figure 62: $^1\text{H-NMR}$ spectra of the acyclic compound **38** (A) and of the macrocycle **40** (B).

As reported and highlighted in **Figure 62**, the formation of the macrocycle is clearly demonstrated by the disappearance in spectrum **B** of the singlet at 5.22 p.p.m belonging to the amino group (-NH₂, spectrum **A**) and by the presence in spectrum **B** of a new singlet at 11.26 p.p.m, certainly belonging to the proton of the amide (-NHCO, spectrum **B**). Moreover, the two signals belonging to the aromatic protons -CH (**6**) and -CH (**3**) are shifted downfield in spectrum **B**. This is due to the presence of the amide group that has an electron-withdrawing effect on the two protons of the aromatic ring.

Additionally, comparing the two HSQC spectra, it is clear how the formation of the cycle changes the chemical environment of aliphatic protons. Chemical shifts of diastereotopic protons (-CH₂ **15**, 3.46 and 2.29 ppm) in macrocycle **40** are shifted from one each other, while same protons in the acyclic precursor **38** show more similar chemical shift (3.03 and 2.75 ppm) meaning that probably one of them might be affected by the proximity of the phenyl group or by the amide group at position 12 in the macrocyclic structure.



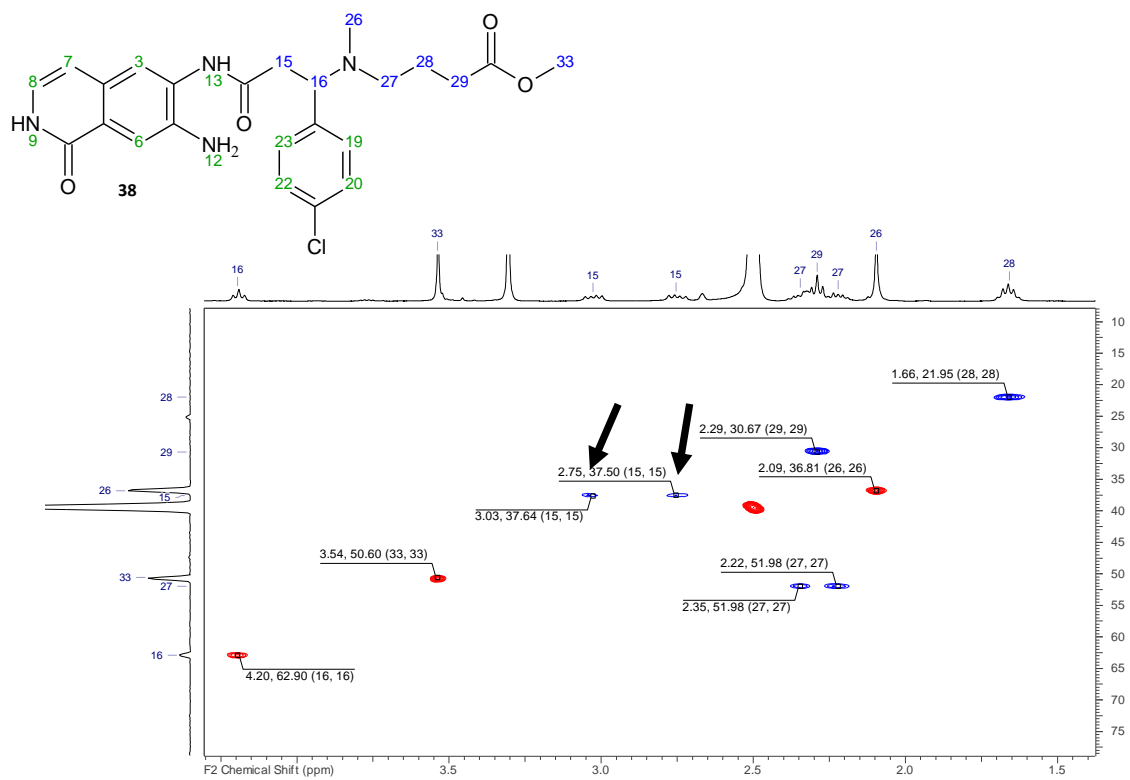


Figure 63: Comparison of HSQC spectra.

Molecular Structure

Additionally, an X-ray crystallographic analysis was conducted to confirm the structure of the compound **40**. The analysis reveals how compound **40** crystallizes in the triclinic P-1 space group, with an overall stoichiometry 2API·MeOH.

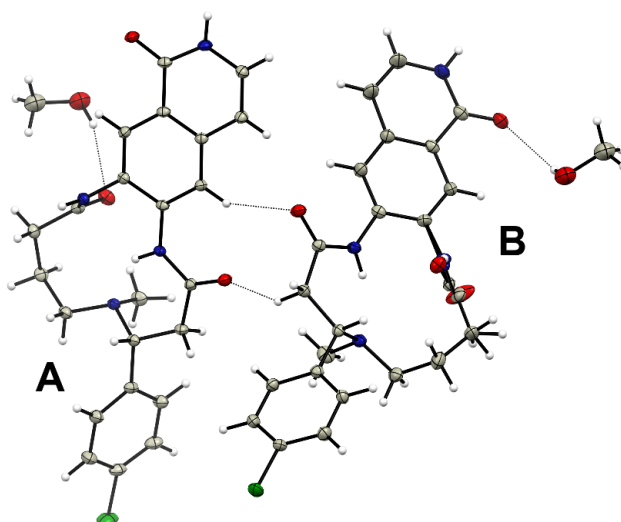


Figure 64: Molecular and weak interactions for compound **40**, thermal ellipsoids are drawn at the 30% probability level. The asymmetric unit comprises two API molecules (A, B) and one MeOH solvent of crystallization (disordered over two sites, refined with 0.75 and 0.25 site occupancy factors respectively). Color codes, C, gray; N, blue; O, red; H, white; Cl, green.

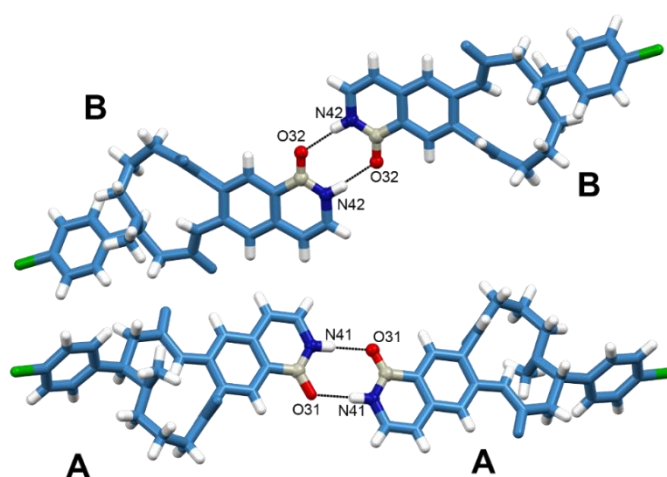


Figure 65: View of API dimers A---A and B---B, and relative hydrogen bonds interactions.

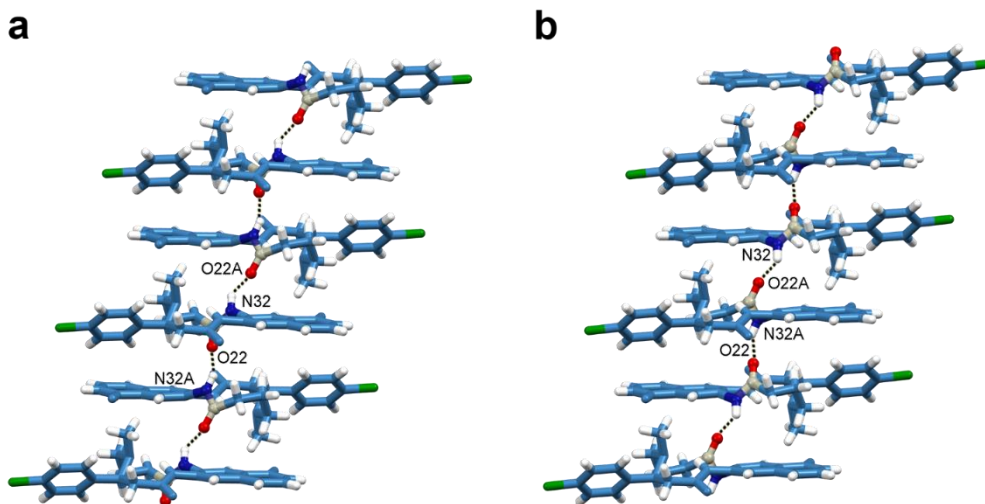


Figure 66: View of intermolecular hydrogen bond interactions involving API molecule B. The disordered amide moiety lead to two alternative orientations (a,b) of hydrogen bonds between neighboring molecules.

3.3 Acyclic Derivatives Series

Simultaneously, a structure-based approach for the design of new ROCK macrocyclic inhibitors was carried out.

In this case, all ROCK inhibitors reported in literature were evaluated by visual inspection and chemical series with structural similarities to our reference compound (3nd) were analysed. Among all the chemical series, the amino-isoquinoline series developed by Aerie Pharmaceuticals stood out as the most interesting and similar to compound **17**^{86,132}. As reported in **Figure 67**, this series was characterized by an isoquinoline or an isoquinolinone core, functioning as a hinge-binding moiety and an aniline nitrogen at position 6 decorated with a set of diverse substituted amino acids. Compounds in this series are ROCK inhibitors characterized by potencies in the low nanomolar range.

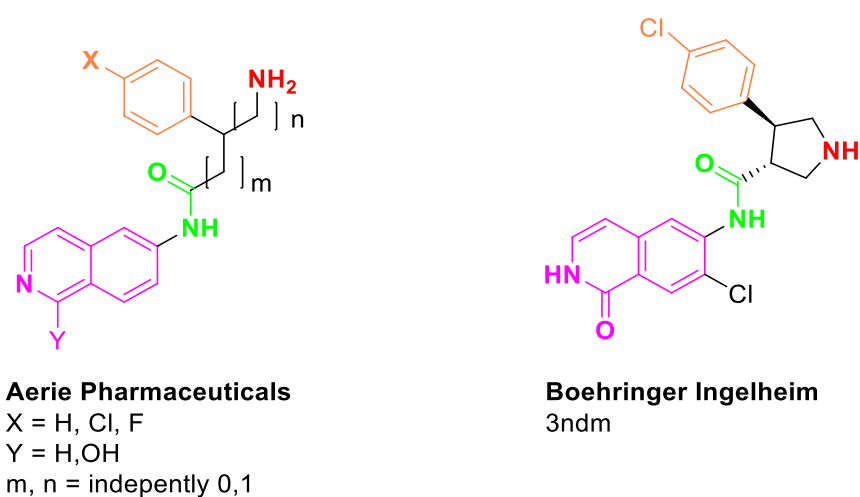


Figure 67: Structural similarities between Aeries Pharmaceuticals and Boehringer Ingelheim series.

Therefore, the aim of this work was to design new analogues of this series by introducing new chemical features to make new compounds more prone and compatible with macrocyclization. These new analogues were defined as new “acyclic derivatives”.

Accordingly, the design of the new series envisaged (**Figure 68**):

- I. The introduction of an indazole, as new hinge binder, in addition to isoquinoline.
- II. The exploration of the region under the P-loop by using different amino acids (Phenyl-β-alanine, Phenyl-alanine and phenyl-glycine).

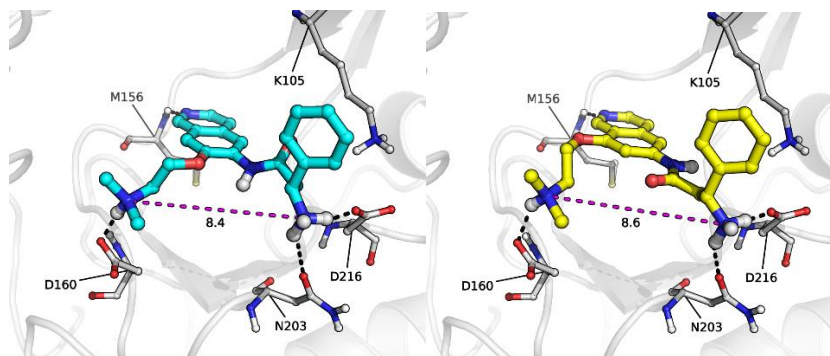


Figure 70: The putative binding mode of the two top-ranked “open derivatives”, compound **58** and **59**.

As shown in **Figure 70**, the two selected acyclic derivatives were able to form the same pattern of interactions observed for typical ROCK inhibitors, engaging key residues within the ATP-binding site cavity: Met156 in the hinge region, the acid residue (Asp216) of the DFG motif and the ceiling of the p-loop. Moreover, as highlighted in the figure, the two amino groups exhibited proximity in space to each other and a favourable orientation for a further cyclization.

3.3.1 Synthesis of Acyclic Derivatives

Acyclic derivatives **58** and **59** (Figure 71) were selected as target compounds to investigate their activity as ROCK I/ROCK II dual inhibitors and to evaluate the impact of the introduction of a *second arm* (basic tail) on ROCK activity. Once their activity as ROCK inhibitors is established, macrocycles analogues would be designed, evaluated by Prime MCS and tested to compare their activity with the non-macrocyclic parents.

It was decided to first set the synthetic route for the preparation of *ortho*-derivatives and then to move to the synthesis of *meta*-derivatives, where *ortho* and *meta* refer to the relative position on the scaffold of putative macrocycle anchor points.

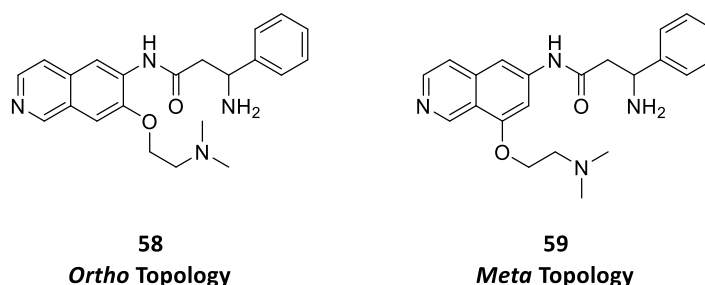


Figure 71: Structure of Compounds **58** and **59**.

Compounds **58** and **59** show the highest structural similarity to Aerie Pharmaceuticals compounds (**Ref-1** and **Ref-2**) reported in **Figure 72**. However, target compounds display a set of differences from comparator compounds and two additional reference compounds (**60** and **61**) were prepared in order to better understand the influence of each step of modification from inhibitors of known activity and to compare their activity with compounds belonging to Aerie's series (**Ref-1** and **Ref-2**).

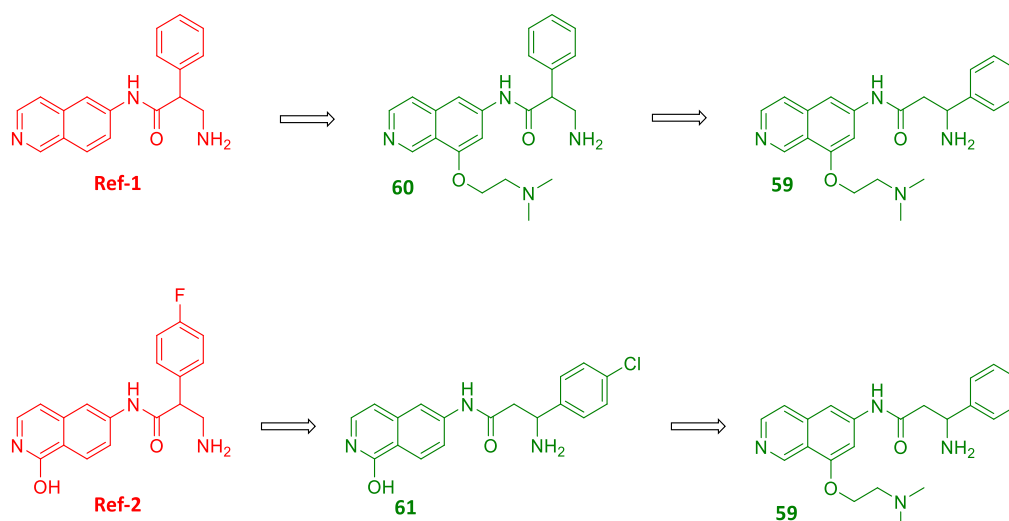
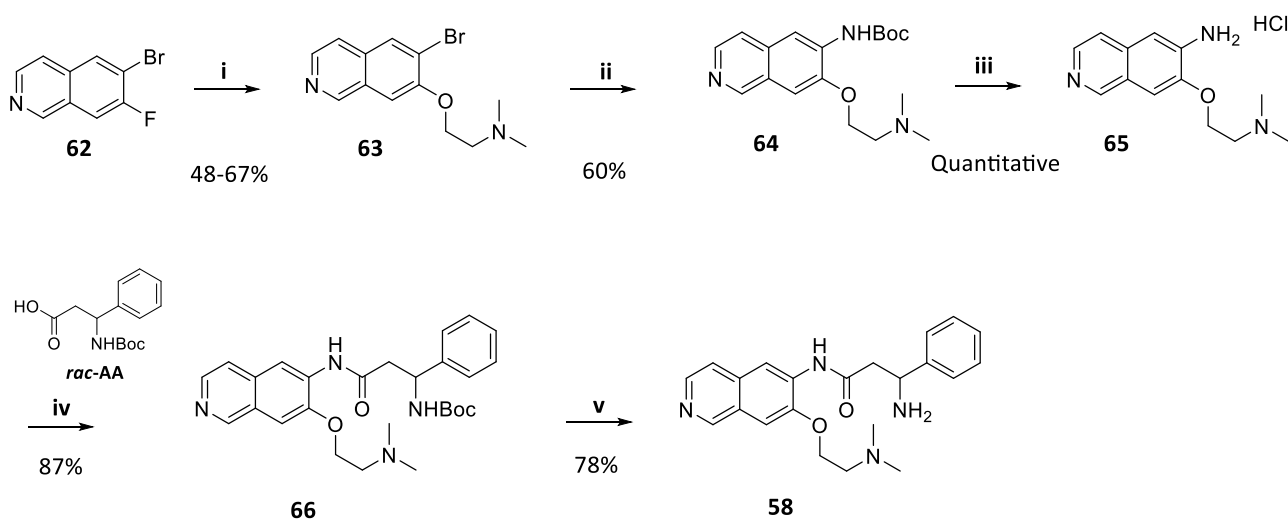


Figure 72: Structures of reference compounds (**Ref-1**, **Ref-2**, **60** and **61**).

The synthetic pathway for the synthesis of *ortho*-derivatives took advantage again of the high reactivity of fluoro-compounds in S_NAr reaction (**Scheme 10**). Reaction between 6-bromo-7-fluoroisquinoline and the *N,N*-Dimethylethanolamine allowed the synthesis of intermediate **63** with yields ranging from 48% to 67%. Reaction was performed in DMF using NaH as base which was added to the solution at 0 °C. Mixture then was heated up to 100 °C.



Scheme 10: Reagents and conditions: i) *N,N*-dimethylethanolamine, NaH, DMF, (0 °C→100 °C), ii) Tert-Butyl Carbamate, Xantphos, Pd(OAc)₂, Cs₂CO₃, Dioxane,(100 °C) mw; iii) 5M HCl, ACN;(rt); iv) HATU, DIPEA, DMF, (rt); 5M HCl, ACN, (rt).

Intermediate **64** was synthesised by palladium-catalysed Buchwald-Hartwig coupling reaction following conditions reported by Audisio et al.¹³³ for the synthesis of 3-(*N*-substituted)-aminocoumarins. These conditions involved the use of Pd(OAc)₂ as palladium source, Xantphos as a

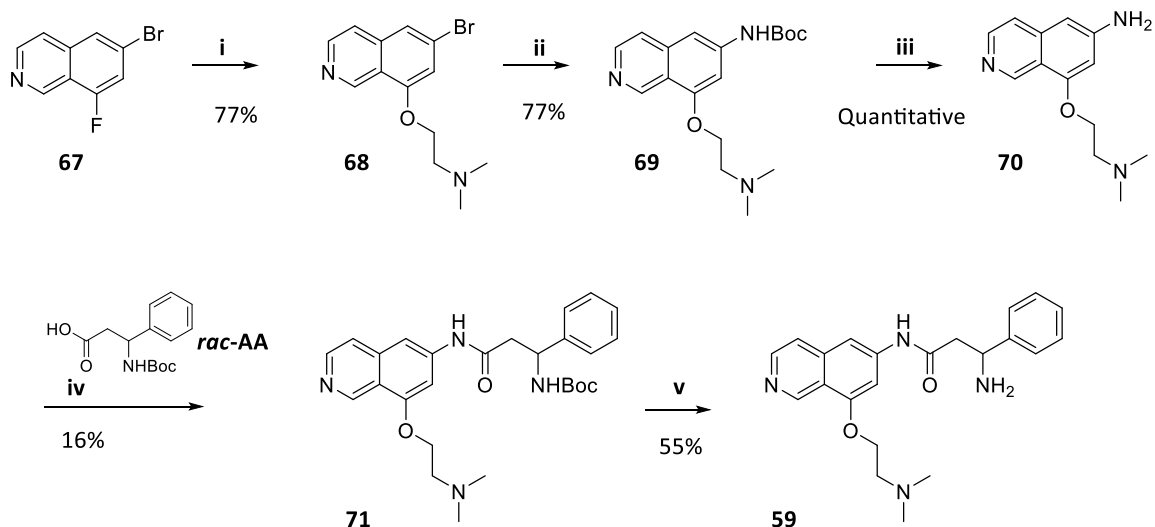
bidentate ligand phosphine and the base, Cs₂CO₃ in Dioxane. The reaction was performed under microwave irradiation and yielded the intermediate in an average yield of 60%.

The following Boc removal in acidic conditions with 5M aqueous HCl, afforded intermediate **65** which was not subjected to further purifications and was used as hydrochloride salt in next step.

The synthesis proceeded with the amide-coupling between the intermediate **65** and the racemate 3-((tert-butoxycarbonyl)amino)-3-phenylpropanoic acid (*rac-AA*).

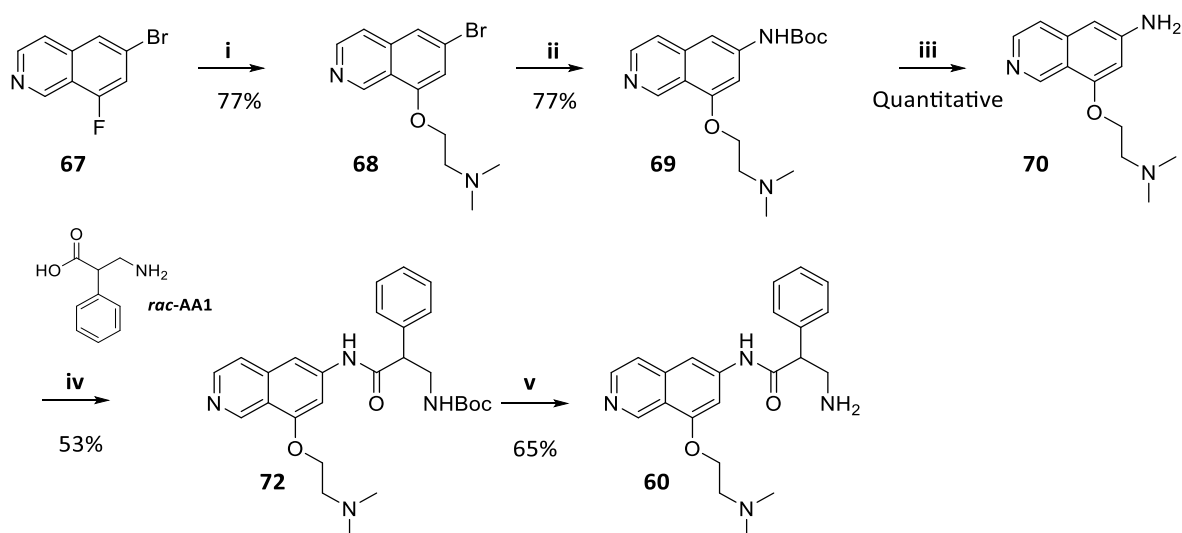
Docking studies indicated *R* as the favourite enantiomer, but it was decided to prioritize the synthesis of the racemic mixture in order to measure as quickly as possible a hint of activity as ROCK inhibitor of either two of the enantiomers.

The amide coupling was performed following classical conditions using HATU with DIPEA in DMF at rt. Amide coupling proceeded very slowly at rt and solution was stirred for 96 hr to obtain complete conversion of starting material. Furthermore, the presence of a decoration in the *ortho* position might impair the nucleophilic attack by the amino group to the activated acid. Despite the low rate of conversion, the desired intermediate was obtained in an 87% yield. Following deprotection with aqueous 5M HCl yielded the final product (**58**). This synthetic pathway was applied for the synthesis of *meta*-derivatives (**Scheme 11**). The synthesis started from the commercially available 6-bromo-8-fluoroisoquinoline (**66**). Minor changes were applied to the amide coupling between intermediate **69** and *rac-AA* in order to accelerate the conversion. In this case, DMAP was added in catalytic amount and the solution was heated at 80 °C for 12 hr. However, the conversion was still slow and the resulting yield lower than for *ortho* derivatives, probably as a consequence of degradation of the starting material.



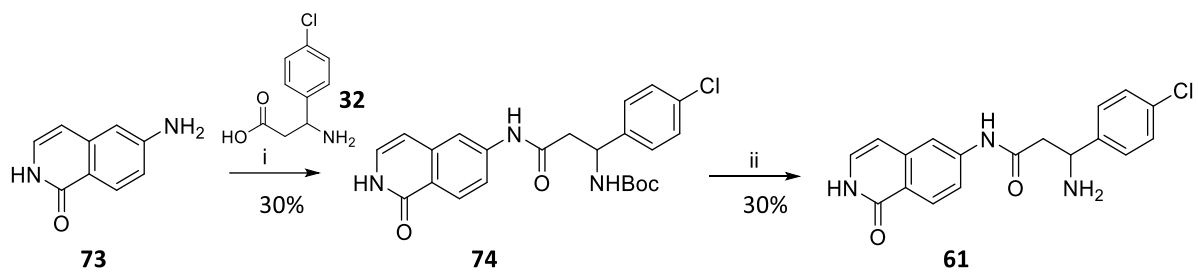
Scheme 11: Reagents and Conditions: i) N,N-dimethylethanolamine, NaH, DMF, (0 °C→100 °C), ii) Tert-Butyl Carbamate, Xantphos, Pd(OAc)₂, Cs₂CO₃, Dioxane,(100 °C) MW; iii) 5M HCl, ACN;(rt); iv) HATU, DIPEA, DMF, (rt); 5M HCl, ACN, (rt).

The first reference compound (**60**) was obtained from the amide coupling between intermediate **69** and amino acid *rac-AA1* as reported in **Scheme 12**.



Scheme 12: Reagents and Conditions: i) N,N-dimethylethanolamine, NaH, DMF, (0 °C→100 °C), ii) Tert-Butyl Carbamate, Xantphos, Pd(OAc)₂, Cs₂CO₃, Dioxane,(100 °C) ; iii) 5M HCl, ACN;(rt); iv) HATU, DIPEA, DMF, (rt); 5M HCl, ACN, (rt).

For the second reference compound (**61**), the synthesis was straightforward. It started with the amide coupling between two commercially available intermediates, **74** and **75**, which led to the formation of Intermediate **74**. Boc- cleavage in acidic conditions yielded **61** (**Scheme 13**).



Scheme 13: Reagents and Conditions: i) POCl₃, Pyridine, (0 °C), 1 hr; ii) 5M HCl in ACN, rt, 1 hr.

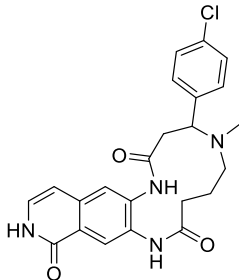
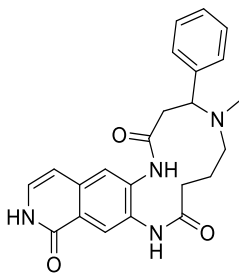
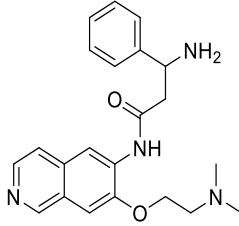
4. Biological Evaluation and SAR Considerations

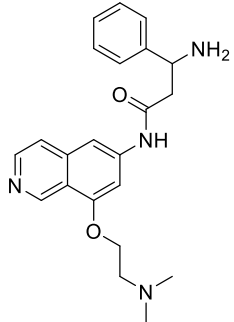
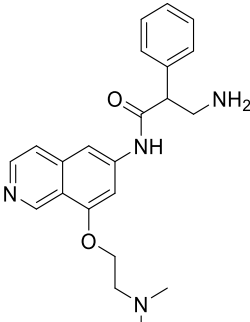
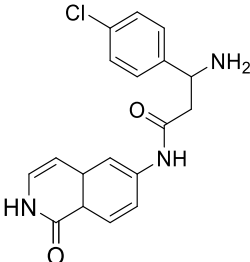
All six synthesized derivatives were evaluated for their biological activity as ROCK inhibitors. Each compound was submitted to cell free assay and cell-based assay.

Inhibition of ROCK I and ROCK II enzymatic activity was determined in Glutathione S-transferase (GST)-tagged 1–535 human ROCK I and GST-tagged 1–552 human ROCK II by means of a flash-type luminescence assay, named ADP-Glo. The experiment was carried out at 200 μ M ATP.

Cellular inhibition was determined in Pulmonary Artery Smooth Cells (PASMCs) model. In this assay, levels of phosphorylated Myosin Light Chain 2 (pMLC2) were measured after incubation with test compounds. For further details, see the experimental part in Material and Methods section.

Table 20: Enzymatic pK_i for ROCK I and ROCK II and pIC₅₀.

Compound	Structure	pK _i ROCK I	pK _i ROCK II	PASMCs Model pIC ₅₀ (pMLC)
40		< 5	< 5	< 5
57		< 5	7.0	< 5
58		< 5	< 5	< 5

59		< 5	< 5	< 5
60		< 5	< 5	< 5
61		8.1	8.4	7.4

Disappointingly, as reported in **Table 20**, compounds **40**, **58**, **59** and **60** did not show inhibition on ROCK I or ROCK II kinases up to the maximum inhibitor concentration tested (10 μ M). On the other hand, **61** shows good enzymatic and cellular potency and compound **57** showed good enzymatic activity on ROCK II.

SAR considerations on acyclic derivatives:

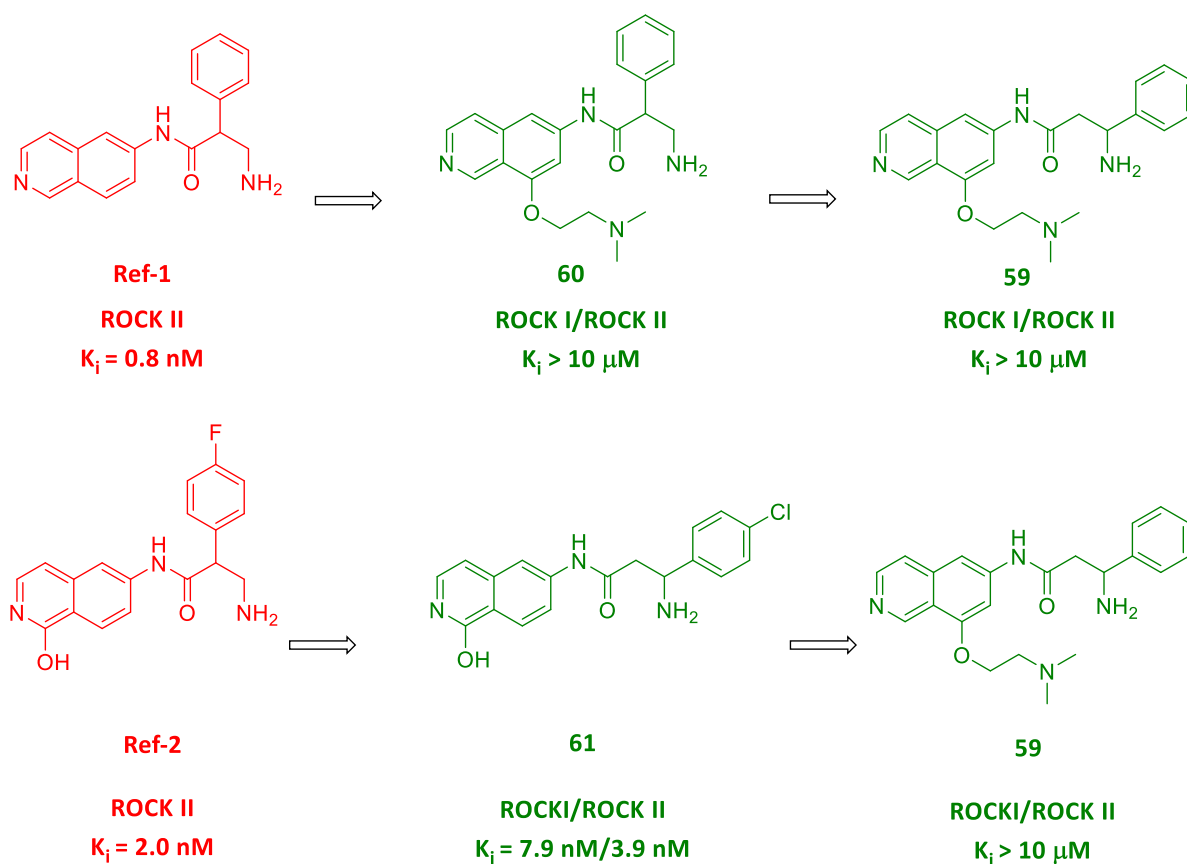


Figure 73: SAR analysis of acyclic compounds.

Biological data of **Ref-1** and **Ref-2** (**Figure 73**) show that different hinge binders and diverse decorations at *para* position of the phenyl ring do not affect ROCK inhibition, since **Ref-1** and **Ref-2** can be considered equipotent. Additionally, moving the phenyl ring from alpha to beta position of the amide does not impact activity on ROCK, as demonstrated by biological data of **Ref-2** and **61**, both low nanomolar ROCK inhibitors. Therefore, the combination of these data strongly highlights that the presence of the dimethyl amino ethoxy linker is the true responsible for the complete loss of activity for compound **59** and, most probably, also for compound **58**. Moreover, inactivity of **60**, close analogue of **Ref-1**, represents the best proof of concept of the above-mentioned statement. To better understand the reason of the inactivity of the acyclic derivatives (**58** and **59**) a further docking analysis was carried out. Compounds were docked in ROCK I (PDB ID 3ndm) and up to 50 ligand conformations were docked within the ATP-binding site of 3ndm. The first result from docking analysis was that (*R*)-enantiomers are energetically favoured with respect to (*S*)-enantiomers.

This was also partially the case for compound **59**, as the ionic interaction between the protonated amine in aminoacidic chain and Asp216 (D216) was observed in only 60% of frames. Additionally, ionic interaction between protonated amine of dimethyl amino ethoxy linker and Asp160 (D160) was not conserved during the MD simulation at all (**Figure 76**). This observation seems to be a possible explanation of inactivity of compounds **58** and **59**.

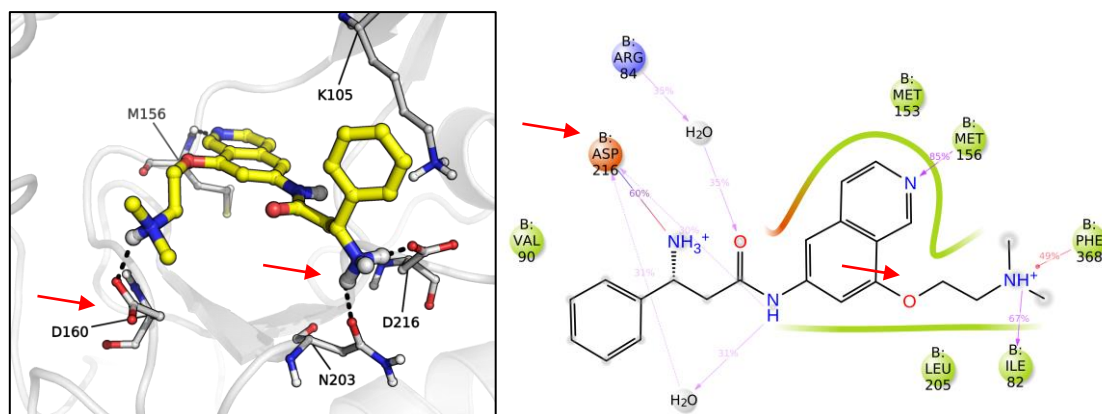


Figure 76: Results from Molecular Dynamics Simulation of **59**.

SAR considerations on Macrocyclic derivatives:

Regarding the newly designed macrocycles, compound **57** showed ROCK II pKi equal to 7 while it did not show ROCK I inhibition up to the maximum inhibitor concentration tested (10 μ M). Unexpectedly, compound **40** displayed no inhibition on neither ROCK I nor ROCK II. More analogues need to be synthesized in order to draw a SAR evaluation and to understand which modifications can be inserted to boost potency over ROCK I and ROCK II. Further investigation on the binding mode of compound **57** will be also carried out to understand why it inhibits ROCK II but not ROCK I.

Additionally, it is important to highlight that these compounds were tested at high concentration of ATP and not at the Km of the enzyme, a condition that is not ideal to determine activity for compound with low affinity for the enzyme.

However, even though these preliminary results are not optimal, the inhibition of ROCK II indicated that the macrocycle is tolerated in ROCK II ATP binding site demonstrating that macrocyclization could represent a valid option for the design of new ROCK inhibitors.

5. Conclusion and Perspectives

This project was dedicated to the identification of new potential ROCKs inhibitors starting from the rational design of macrocyclic scaffolds.

Through a knowledge-based approach, newly designed macrocycles were identified and then selected using Prime MS²⁶, an innovative computational tool for the evaluation of macrocycles. Subsequently, different synthetic strategies were planned and attempted in order to prepare the selected macrocyclic template. These efforts allowed the synthesis of two new macrocyclic structures (**40** and **57**). Compound **57** displayed enzymatic activity in the low micro molar range against ROCK II. Even though only two derivatives have been synthesized so far, this first encouraging result validates the innovative approach applied for the design of new ROCKs inhibitors and established the initial proof of concept for the development of this new series.

At the same time, a series from literature was selected and two acyclic analogues were designed through a Structure Based approach. Modifications were introduced to make them more prone and compatible with macrocyclization. Docking studies, carried out on these new analogues, revealed that the pattern of interactions observed for prototypical ROCK inhibitors was maintained. The new acyclic analogues were synthesized and tested to determine their activity on ROCK I and ROCK II. Disappointingly, compounds did not show any activity on the targets of interest. Even though preliminary docking studies had highlighted favourable interactions in ROCK binding site, a more advanced molecular dynamic computational study helped to rationalize the apparent mismatch. Comparing these biological data with data from reference compounds, showed how inserted modifications, specifically the amino linker, had a detrimental effect on activity. Based on these considerations, macrocyclic analogues of these compounds are expected inactive on ROCK and their synthesis has not been pursued.

6. Material and Methods

6.1 General Chemistry Methods

Chemicals:

Reagents and solvents were used as supplied from different providers without any further purification. All deuterated and dry solvents were purchased from Merk-Sigma-Aldrich. Anhydrous sodium sulphate (Na_2SO_4) was used as the drying agent for organic phases.

Microwave assisted synthesis:

Reactions were carried out under microwave irradiation in sealed vessels using a Biotage Initiator Sixty with robotic sample bed. Reactions were irradiated at 2.45 GHz and were able to reach temperatures up to 250°C at a rate of 2-5°C/sec and pressure up to 20 bars.

Freeze drying:

Freeze drying was performed using a freeze dryer Alpha 1-2 LDplus, Martin Christ Gefriertrocknungsanlagen GmbH.

Chromatography:

When needed, purifications were performed on flash chromatography, with a Biotage Isolera instrument or Puriflash 125 Interchim, using Biotage Columns (SNAP Cartridges, Silica, Silica NH and C18) or Sepachrom columns (C18) and Sylicycle columns (C18). In one case purification was performed on a FractionLynk Instrument with a preparative C18 column.

In some cases, final products or intermediates were purified using a pre-packed polypropylene column containing a non-end-capped propylsulphonic acid functionalised silica strong cation exchange sorbent (Isolute SCX cartridge).

Thin layer chromatography was performed on Glass TLC plates (5X10 cm), silica gel coated with fluorescent indicator F254 or on Biotage TLC plates (5X10 cm) KP-NH.

Analytical Techniques:

- **Ultra-Pressure Liquid Chromatography**

Analytical UPLC and Electron Spray Ionization (ESI) condition were performed on a Waters ACQUITY UPLC equipped with a Photo Diode Array (PDA) detector and a Single Quadrupole Mass Detector (QDA) or equipped with a Triple Quadrupole (Waters Xevo -TQS).

UPLC-MS Methods:

- ❖ **Method 1:** Acquity UPLC CSH C18 column (50mm x 2.1mm i.d. 1.7 μ m particle size). Column Temperature ($^{\circ}$ C) 40.0. Mobile phases: 0.1% v/v solution of HCOOH in water (A); 0.1% v/v solution of HCOOH in Acetonitrile (B). Flow (ml/min) 1. Stop Time (mins) 2.0.
- ❖ **Method 2:** Acquity UPLC CSH C18 column (50mm x 2.1mm i.d. 1.7 μ m particle size). Column Temperature ($^{\circ}$ C) 50.0. Mobile phases: HCOONH₄, 0.025M, pH=3 (A); 0.1% v/v solution of HCOOH in Acetonitrile (B). Flow (ml/min) 0.35 Stop Time (mins) 10.0.
- ❖ **Method 3:** Acquity UPLC BEH C18 column (50mm x 2.1mm i.d. 1.7 μ m particle size). Column Temperature ($^{\circ}$ C) 40.0. Mobile phases: 0.1% v/v solution of HCOOH in water (A); 0.1% v/v solution of HCOOH in Acetonitrile (B). Flow (ml/min) 1. Stop Time (mins) 2.0.

Data were processed using Masslynk software.

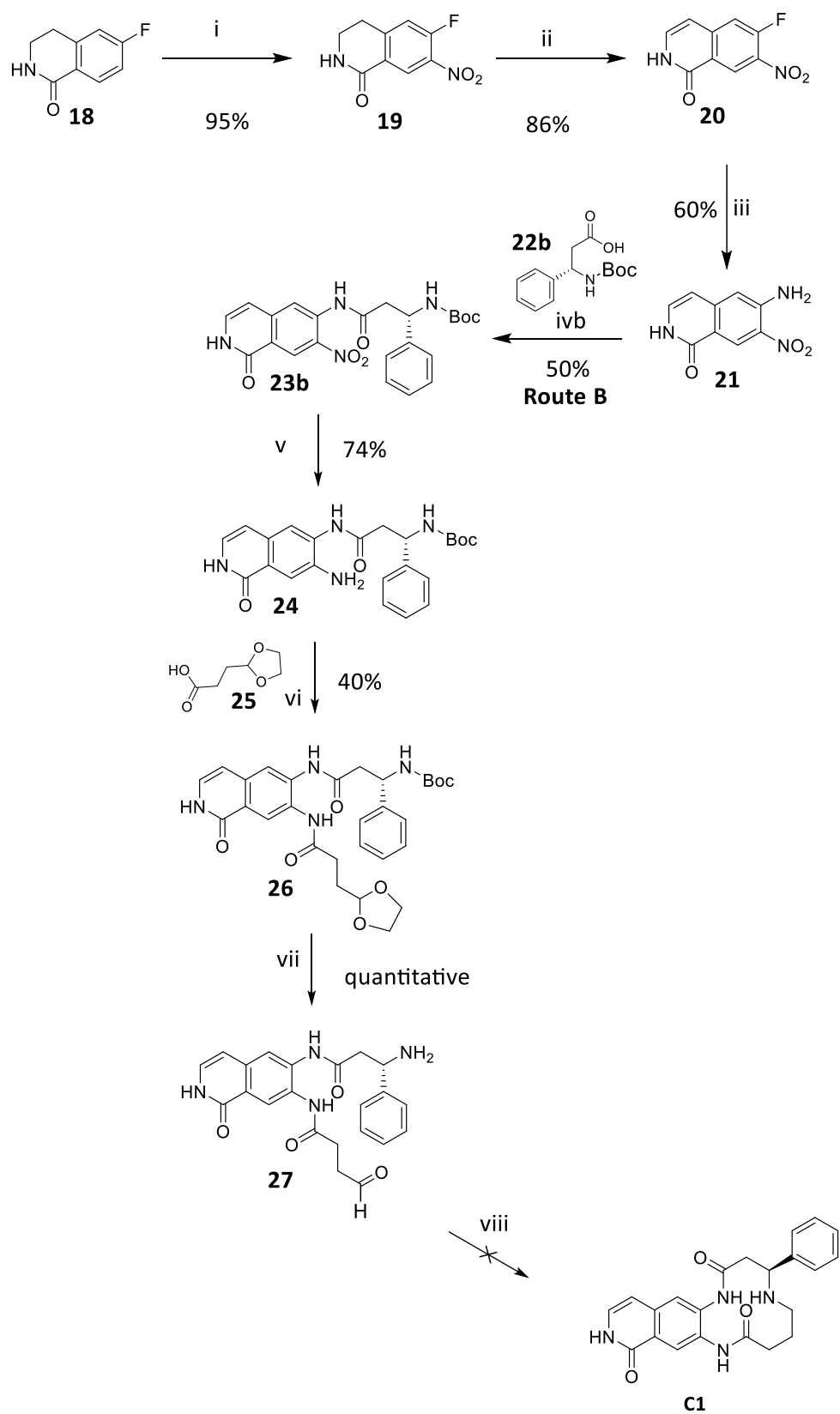
- **NMR Spectroscopy**

¹H-NMR, ROESY and HSQC spectra were recorded at room temperature on a Varian spectrometer operating at 400 MHz or on a Bruker Avance 600 spectrometer. Chemical shifts are reported as δ values in ppm relative to trimethyl silane (TMS) as an internal standard. Coupling constants (J values) are given in hertz (Hz) and multiplicities are reported using the following abbreviations (s= singlet, d=doublet, t=triplet, q=quartet, m=multiplet, br=broad, nd=not determined).

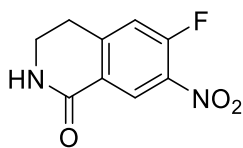
- **High Resolution Mass Spectrometry**

HRMS analysis for compounds (**43**, **53**, **59**, **60**, **61** and **62**) was performed with a Q Exactive Hybrid Quadrupole-Orbitrap Mass Spectrometer.

6.2 Scheme 6-Route B



6-fluoro-7-nitro-3,4-dihydroisoquinolin-1(2H)-one (**19**)



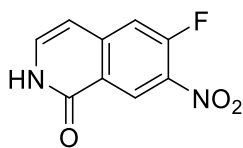
A solution of 6-fluoro-3,4-dihydroisoquinolin-1(2H)-one (3.5 g, 21.19 mmol) in sulfuric acid (28.2 ml, 530 mmol) was cooled to 0 °C, and KNO₃ (2.357 g, 23.31 mmol) was added portion wise. The resulting mixture was stirred in the ice bath for 20 min. The mixture was poured into ice -water and the resulting precipitate filtered. Filtration yielded Intermediate **19** (4.39 g, 20.89 mmol, 99 % yield).

¹H NMR: (400 MHz, DMSO-d₆) δ ppm 3.03 (t, J=6.58 Hz, 1 H) 3.02 - 3.04 (m, 1 H) 3.42 (td, J=6.58, 2.85 Hz, 2 H) 7.62 (d, J=11.62 Hz, 1 H) 8.28 (br s, 1 H) 8.46 (d, J=7.89 Hz, 1 H)

UPLC-MS (Method 1): t_R= 0.69 min; MS (ESI): m/z 210.9 [M + H]⁺

UPLC Purity: 97%

6-fluoro-7-nitroisoquinolin-1(2H)-one (**20**)



In a 100 mL Mettler-Toledo reactor, Intermediate **19** (4 g, 19.03 mmol) was dissolved in Cl-benzene(70 ml), added of MnO₂ (16.55 g, 190 mmol) and stirred at 140 °C for 5 hr. The solution was filtered, and the filter was washed with warm dioxane.

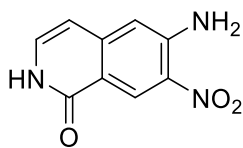
Organic phase was evaporated under vacuum to give Intermediate **20** (3.2 g, 15.37 mmol, 81 % yield) which was used in the next step without further purifications.

¹H NMR (400 MHz, DMSO-d₆) δ ppm 6.65 (d, J=7.23 Hz, 1 H) 7.48 (t, J=6.58 Hz, 1 H) 7.85 (d, J=12.50 Hz, 1 H) 8.82 (d, J=7.89 Hz, 1 H) 11.77 (br s, 1 H)

UPLC-MS (Method 1): t_R= 0.67 min; MS (ESI): m/z 208.9 [M + H]⁺

UPLC Purity: 96%

6-amino-7-nitroisoquinolin-1(2H)-one (**21**)



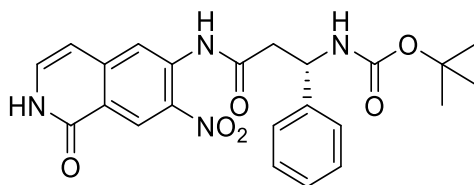
Intermediate **20** (3.2 g, 15.37 mmol) was dissolved in Dioxane (Volume: 35 ml) and added of ammonia (15 ml, 105 mmol) 7 N in MeOH. Solution was stirred at 80 °C for 24 hr. The formation of a brown precipitate was observed. The precipitate was filtered and washed with MeOH, water and Et₂O. Filtration yielded Intermediate **21** (2 g, 9.75 mmol, 63.4 % yield).

¹H NMR (400 MHz, DMSO-d₆) δ ppm 6.27 (d, J=7.23 Hz, 1 H) 6.94 (s, 1 H) 7.12 (br dd, J=6.69, 4.71 Hz, 1 H) 7.53 (s, 2 H) 10.95 (br s, 1 H)

UPLC-MS (Method 1): t_R= 0.53 min; MS (ESI): m/z 206.2 [M + H]⁺

UPLC Purity: 92%

Tert-butyl (S)-3-((7-nitro-1-oxo-1,2-dihydroisoquinolin-6-yl)amino)-3-oxo-1-phenylpropyl)carbamate (23b)



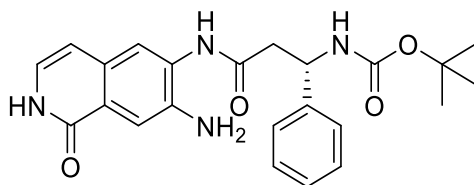
To a solution of Intermediate **21** (250 mg, 1.218 mmol) and (S)-3-((tert-butoxycarbonyl)amino)-3-phenylpropanoic acid (970 mg, 3.66 mmol) in anhydrous Pyridine (Volume: 10 ml) at 0 °C POCl₃ (0.057 ml, 0.609 mmol) was added in one portion. The proceeding of the reaction was monitored through UPLC-MS analysis. The solution was stirred for 1 hr. After 1 hr reaction did not get completion so (S)-3-((tert-butoxycarbonyl)amino)-3-phenylpropanoic acid (323 mg, 1.218 mmol) and POCl₃ (0.057 ml, 0.609 mmol) were added again at 0 °C, then solution was stirred for 1 hr at rt. Solution was diluted with water (20mL) and extracted twice with DCM (20mL). Organic phase was evaporated under vacuum and the red solid was triturated with MeOH and DCM to give Intermediate **23b** (268 mg, 0.592 mmol, 48.6 % yield).

¹H NMR (400 MHz, DMSO-d₆) δ ppm 1.33 (s, 8 H) 2.76 - 2.89 (m, 2 H) 4.96 - 5.08 (m, 1 H) 6.59 (d, J=7.02 Hz, 1 H) 7.20 - 7.27 (m, 1 H) 7.29 - 7.40 (m, 5H) 7.51 (br d, J=8.55 Hz, 1 H) 8.03 (s, 1 H) 8.66 (s, 1 H)

UPLC-MS (Method 1): t_R= 1.03 min; MS (ESI): m/z 451.0 [M - H]⁻

UPLC Purity: 98%

(S)-3-((7-amino-1-oxo-1,2-dihydroisoquinolin-6-yl)amino)-3-oxo-1-phenylpropylcarbamate (24)



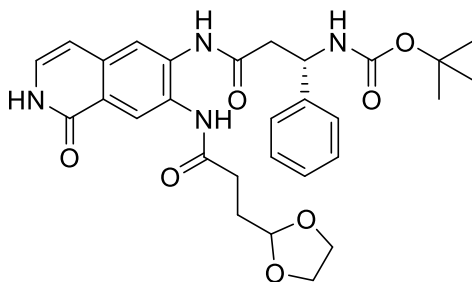
Intermediate **23b** (265 mg, 0.586 mmol) was dissolved Water (Volume: 2 ml, Ratio: 1.000) and 2-Propanol (Volume: 4.000 ml, Ratio: 2.000) then Fe (392 mg, 7.03 mmol) and NH₄Cl (1128 mg, 21.08 mmol) were added. The mixture was stirred at 80 °C for 4 hr. LC-MS analysis showed complete conversion and the mixture was filtered over celite with warm *i*-PrOH, diluted with DCM (50 mL) and washed with water (50mL). Organic phase was evaporated under vacuum to give Intermediate **24** (164 mg, 0.388 mmol, 66.3 % yield) as reddish solid.

¹H NMR (400 MHz, DMSO-d₆) δ ppm 1.35 (br s, 9 H) 2.73 - 2.85 (m, 2 H) 5.00 - 5.12 (m, 1 H) 5.24 (br s, 2 H) 6.29 (d, J=7.02 Hz, 1 H) 6.78 - 6.86 (m, 1 H) 7.20 - 7.27 (m, 1 H) 7.29 - 7.39 (m, 5 H) 7.46 (s, 1 H) 7.52 (br d, J=8.77 Hz, 1 H) 7.61 (br s, 1 H) 9.19 (br s, 1 H) 10.78 (br d, J=4.60 Hz, 1 H)

UPLC-MS (Method 1): t_R= 0.83 min; MS (ESI): m/z 423.0 [M + H]⁺

UPLC Purity: 84%

Tert-butyl (S)-3-((7-(3-(1,3-dioxolan-2-yl)propanamido)-1-oxo-1,2-dihydroisoquinolin-6-yl)amino)-3-oxo-1-phenylpropyl)carbamate (26)



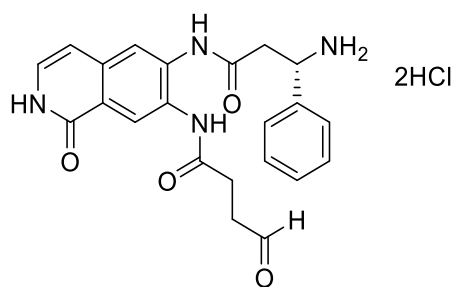
3-(1,3-dioxolan-2-yl)propanoic acid (**25**), (208 mg, 1.420 mmol) was dissolved in DMF (4 ml) with HATU (540 mg, 1.420 mmol) and N-ethyl-N-isopropylpropan-2-amine (0.248 ml, 1.420 mmol) and reacted for 10 minutes then Intermediate **24** (300 mg, 0.710 mmol) was added. Reaction was stirred at rt for 5 hr and then diluted with water (20 ml) and DCM (20 ml). Organic phase was evaporated under vacuum and crude material was purified by flash chromatography, Biotage Isolera, Ultra C18 60 gr, C-18 silica, gradient elution from 100% of A to 30% of B in 10 CV, A: water/acetonitrile 95:5 + 0.1% conc HCOOH, B: acetonitrile/water 95:5 + 0.1% HCOOH. Fractions were combined and freeze-dried affording Intermediate **26** (165 mg, 0.300 mmol, 42.2 % yield).

¹H NMR (400 MHz, DMSO-d₆) δ ppm 1.35 (s, 9 H) 1.85 - 2.04 (m, 2 H) 2.46 (br s, 1 H) 2.73 - 2.93 (m, 2 H) 3.73 - 3.96 (m, 4 H) 4.91 (t, J=4.38 Hz, 1 H) 5.02 - 5.20 (m, 1 H) 6.43 (d, J=7.23 Hz, 1 H) 7.05 - 7.12 (m, 1 H) 7.20 - 7.26 (m, 1 H) 7.29 - 7.41 (m, 4 H) 7.55 (br d, J=8.77 Hz, 1 H) 7.86 (br s, 1 H) 8.32 (s, 1 H) 9.36 - 9.50 (m, 2 H) 11.11 (br d, J=5.70 Hz, 1 H)

UPLC-MS (Method 1): t_R= 0.91min; MS (ESI): m/z 450.6 [M -100]⁺

UPLC Purity: 100%

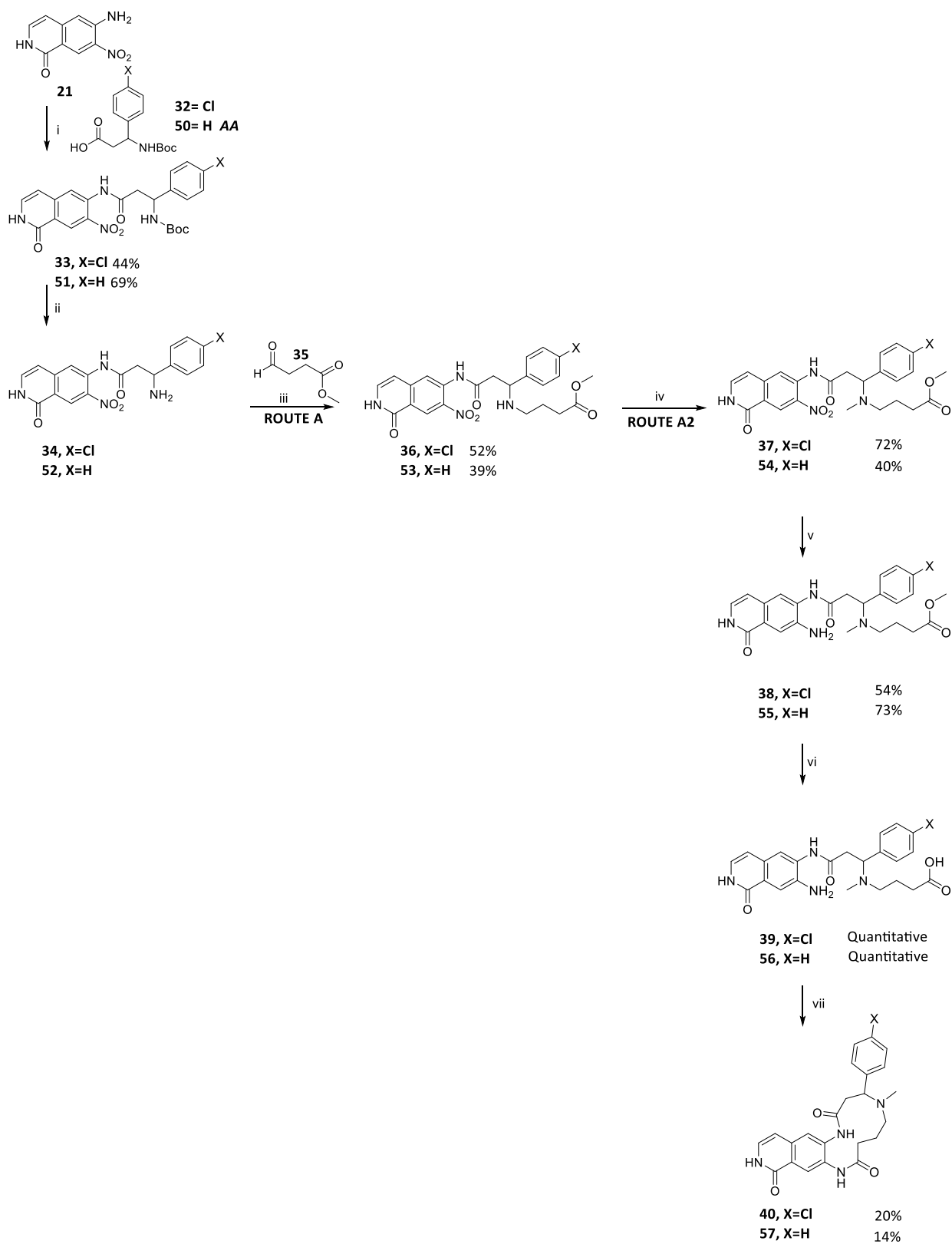
(S)-N-(6-(3-amino-3-phenylpropanamido)-1-oxo-1,2-dihydroisoquinolin-7-yl)-4-oxobutanamide (27)



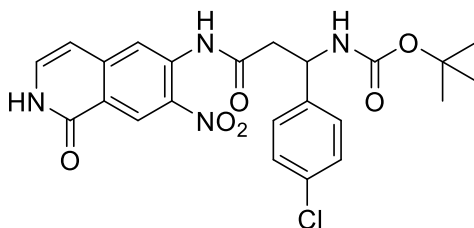
Intermediate **26** (14 mg, 0.025 mmol) was dissolved in THF (1 ml) and Water (1000 μ l) then added of 37% HCl solution (hydrogen chloride (60 μ l, 0.720 mmol). The solution was stirred at 50 deg for 8 hr and then left at rt on. Solvent was evaporated to give Intermediate **27** (10 mg, 0.021 mmol, 82 % yield) as chloride salt. Intermediate **27** was used in the next step without further purifications.

UPLC-MS (Method 1): t_R = 0.3 min; MS (ESI): m/z 407.0 [M +H]⁺

6.3 Scheme 9-Route A/A2



Tert-butyl (1-(4-chlorophenyl)-3-((7-nitro-1-oxo-1,2-dihydroisoquinolin-6-yl)amino)-3-oxopropyl)carbamate (33)



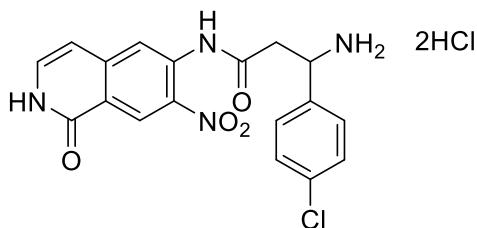
Intermediate **21** (1. g, 4.87 mmol) was dissolved in Pyridine (20 ml) and then **32** (1.753 g, 5.85 mmol) and phosphoryl trichloride (0.545 ml, 5.85 mmol) were added and stirred at 0 °C. Solution was quenched with water (50mL) and extracted with DCM (50mL). Formation of a yellow precipitate was observed. Trituration with DCM and filtration yielded the desired compound **33** (1058 mg, 2.173 mmol, 44.6 % yield).

¹H NMR (400 MHz, DMSO-d₆) δ ppm 1.26 - 1.43 (m, 9 H) 2.73 - 2.90 (m, 2 H) 4.95 - 5.09 (m, 1 H) 6.60 (d, J=7.02 Hz, 1 H) 7.30 - 7.44 (m, 5 H) 7.49 - 7.61(m, 1 H) 8.00 (s, 1 H) 8.66 (s, 1 H) 10.41 (s, 1 H) 11.56 (br d, J=5.26 Hz, 1 H)

UPLC-MS (Method 1): t_R= 1.1 min; MS (ESI): m/z 485.2 [M - H]⁻

UPLC Purity: 95%

3-amino-3-(4-chlorophenyl)-N-(7-nitro-1-oxo-1,2-dihydroisoquinolin-6-yl)propanamide (34)



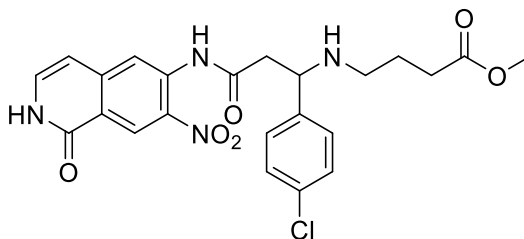
Intermediate **33** (250 mg, 0.513 mmol) was dissolved in 3 mL of 4M HCl in Dioxane and stirred at rt for 8 hr. Then mixture was added of Et₂O and solvent was evaporated under vacuum to give **34** (247 mg, 0.537 mmol). The desired product was obtained in quantitative yield and was used in the next step without further purifications.

¹H NMR (400 MHz, DMSO-d₆) δ ppm 3.18 (br d, J=7.23 Hz, 2 H) 3.57 (s, 1 H) 4.73 (br d, J=5.48 Hz, 1 H) 6.60 (d, J=7.23 Hz, 1 H) 7.34 - 7.42 (m, 1 H) 7.49- 7.61 (m, 4 H) 7.78 - 7.88 (m, 1 H) 8.51 (br d, J=3.51 Hz, 3 H) 8.62 (s, 1 H) 10.75 (s, 1 H) 11.61 (br d, J=5.26 Hz, 1 H)

UPLC-MS (Method 1): t_R= 0.47 min; MS (ESI): m/z 387.1 [M + H]⁺

UPLC Purity: 94%

Methyl 4-((1-(4-chlorophenyl)-3-((7-nitro-1-oxo-1,2-dihydroisoquinolin-6-yl)amino)-3-oxopropyl)amino)butanoate (36)



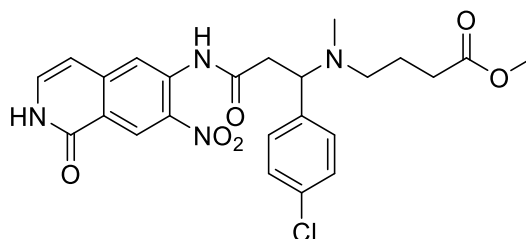
Compound **34** (850 mg, 1.849 mmol) was dissolved in THF (4 ml) and MeOH (10 ml) then added of methyl 4-oxobutanoate (**35**), (429 mg, 3.70 mmol). The resulting mixture was stirred for 10 minutes, and NaBH₃CN (349 mg, 5.55 mmol) was added slowly. After 3 hr, monitoring of the reaction by UPLC-MS showed 65% of conversion, 1.5 eq of NaBH₃CN were added and reaction was stirred at room temperature on. Following day, 0.5 eq of aldehyde and 1.5 eq of NaBH₃CN were added again. Reaction got 74% of conversion. Reaction was quenched with NaHCO₃ sat solution and extracted with DCM twice. Organic phases were combined, washed again with NaHCO₃ sat solution and evaporated under vacuum to give 1.1 g of crude material. The resulting crude was purified by Flash chromatography, SNAP 60 gr, C18-silica by eluting with 0-30% B in A (A: water/acetonitrile 95/5 + 0.1% HCOOH, B: acetonitrile/water 95/5 + 0.1% HCOOH). Appropriate fractions were combined and evaporated under vacuum to give Intermediate **36**, (514 mg, 0.964 mmol, 52.2 % yield) as formate salt.

¹H NMR (400 MHz, DMSO-d₆) δ ppm 1.56 - 1.72 (m, 2 H) 2.24 - 2.41 (m, 4 H) 2.57 (br dd, J=15.02, 5.15 Hz, 2 H) 2.80 (dd, J=14.91, 8.77 Hz, 1 H) 3.52 (s, 3 H) 4.04 (dd, J=8.66, 5.15 Hz, 1 H) 6.60 (d, J=7.23 Hz, 1 H) 7.34 - 7.44 (m, 5 H) 8.11 (s, 1 H) 8.69 (s, 1 H) 10.81 - 11.10 (m, 1 H) 11.56 (br s, 1 H)

UPLC-MS (Method 1): t_R= 0.59 min, m/z: 487.3 [M+H]⁺

UPLC Purity: 95%

Methyl 4-((1-(4-chlorophenyl)-3-((7-nitro-1-oxo-1,2-dihydroisoquinolin-6-yl)amino)-3-oxopropyl)(methylamino)butanoate (37)



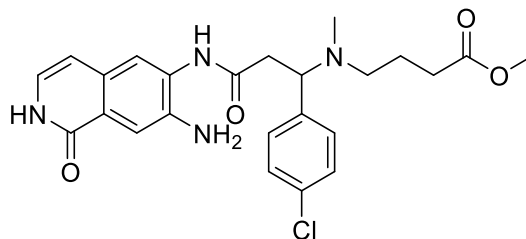
Intermediate **36** (459 mg, 0.943 mmol) was dissolved in THF (3 ml) and MeOH (6 ml), added of MgSO_4 and then added of formaldehyde (0.164 ml, 2.83 mmol). Solution was stirred for 10 minutes and then added of acetic acid (0.054 ml, 0.943 mmol) and NaBH_3CN (207 mg, 3.30 mmol). Solution was stirred for 2 hr at rt. The proceeding of the reaction was monitored by UPLC-MS. After 12 hr, UPLC-MS analysis still showed presence of 30% of the imine so NaBH_3CN (207 mg, 3.30 mmol) was added again. After 24 hr, reaction was quenched with NaHCO_3 sat solution and extracted with DCM (20mL). Aqueous phase was washed twice and combined organic phases were evaporated under vacuum. Purification by flash chromatography on silica NH, Biotage Isolera Instrument, SNAP column 55 gr, gradient elution from 100% of DCM to 15% of Acetone in 10 CV yielded the desired product **37** (340 mg, 0.679 mmol, 72.0 % yield).

$^1\text{H NMR}$ (400 MHz, DMSO-d_6) δ ppm 1.57 - 1.74 (m, 2 H) 2.15 - 2.22 (m, 1 H) 2.26 (t, $J=7.23$ Hz, 2 H) 2.30 - 2.42 (m, 1 H) 2.75 (dd, $J=15.24, 6.91$ Hz, 1 H) 3.15 (dd, $J=15.13, 8.11$ Hz, 1 H) 3.50 (s, 3 H) 4.18 (t, $J=7.34$ Hz, 1 H) 6.59 (d, $J=7.02$ Hz, 1 H) 7.29 - 7.44 (m, 5 H) 8.13 (s, 1 H) 8.69 (s, 1 H) 10.75 (s, 1 H) 11.55 (br d, $J=5.04$ Hz, 1 H)

UPLC-MS (Method 1): $t_R=$ 0.61 min, m/z : 501.2 $[\text{M}+\text{H}]^+$

UPLC purity: 98%

Methyl 4-((3-((7-amino-1-oxo-1,2-dihydroisoquinolin-6-yl)amino)-1-(4-chlorophenyl)-3-oxopropyl)(methyl)amino)butanoate (38)



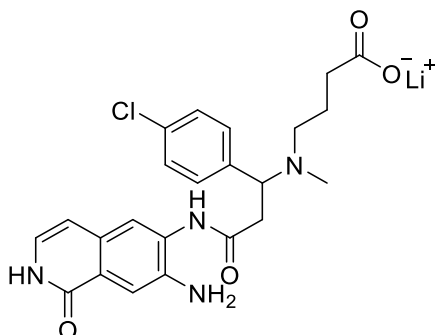
Intermediate **37** (250 mg, 0.499 mmol) was dissolved in EtOH (8 ml) and mixture was added of Tin Chloride (473 mg, 2.495 mmol). Mixture was stirred for 4 hr at rt. Then reaction was quenched slowly with NaHCO₃ sat solution (6mL) and extracted 3 times with DCM. Crude was purified by flash chromatography on NH silica, SNAP column 28 gr from 100% of DCM to 5% of *i*-PrOH in 12 CV. UPLC analysis showed that product was still contaminated so purification was repeated on NH silica 28 gr from 100% of DCM to 5% of MeOH. Pure fractions were combined and evaporated under vacuum to give 60 mg of the desired compound. Fraction still contaminated were combined, solvent was evaporated under vacuum and the resulting red solid was triturated with ACN and Et₂O affording 52 mg of pure compound **38**. Total yield 54%.

¹H NMR (400 MHz, DMSO-d₆) δ ppm 1.04 (d, J=5.92 Hz, 1 H) 1.66 (quin, J=6.91 Hz, 2 H) 2.10 (s, 3 H) 2.18 - 2.40 (m, 5 H) 2.75 (br dd, J=14.58, 7.56 Hz, 1H) 3.03 (br dd, J=14.47, 7.45 Hz, 1 H) 3.50 - 3.58 (m, 3 H) 4.19 (br t, J=7.45 Hz, 1 H) 5.15 - 5.30 (m, 2 H) 6.29 (d, J=7.02 Hz, 1 H) 6.82 (t, J=6.36 Hz, 1 H) 7.30 - 7.35 (m, 2 H) 7.38 - 7.43 (m, 2 H) 7.46 (s, 1 H) 7.56 (s, 1 H) 9.40 (s, 1 H) 10.78 (br d, J=4.38 Hz, 1 H)

UPLC-MS (Method 1): t_R= 0.50 min, m/z: 471.3 [M+H]⁺

UPLC Purity: 90%

4-((3-((7-amino-1-oxo-1,2-dihydroisoquinolin-6-yl)amino)-1-(4-chlorophenyl)-3-oxopropyl)(methyl)amino)butanoic acid, Lithium (39)

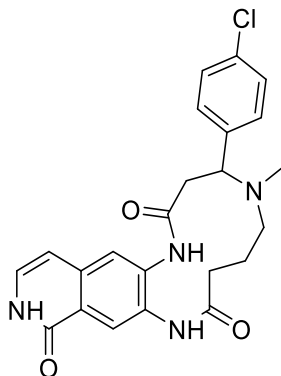


Intermediate **38** (103 mg, 0.219 mmol) was dissolved in THF (2 ml) and Water (0.5 ml). Lithium hydroxide (10.47 mg, 0.437 mmol) was added to the reaction. Mixture was stirred for 1 hr at rt. Once the hydrolysis was completed, pyridine hydrochloride (25.3 mg, 0.219 mmol) was added to quench the lithium hydroxide (10.47 mg, 0.437 mmol) in excess and the resulting mixture was evaporated under vacuum to give Intermediate **39** in quantitative yield. Intermediate **39** was not purified further and used it as it was in the last step.

UPLC-MS (Method 1): $t_R = 0.44$ min, m/z : 457.3 [M+H]⁺

UPLC Purity: 70%

4-(4-chlorophenyl)-5-methyl-3,4,5,6,7,8,10,13-octahydro-[1,4,8]triazacyclododecino[3,2-g]isoquinoline-2,9,12(1H)-trione (40)



Intermediate **39** (107 mg, 0.231 mmol) was dissolved in DMF (12 ml) and added of DIPEA (0.161 ml, 0.923 mmol) and HATU (88 mg, 0.231 mmol) and stirred for 5 hr at rt. Reaction was diluted with DMC (30mL) and organic phase was washed with NaHCO₃ sat solution (20mL) twice. Organic phase was evaporated under vacuum to give a red solid (175 mg). The resulting crude was purified by flash chromatography, Sylicycle 25 gr column, C18-silica by eluting with 0-10% B in A (A: water/acetonitrile 95/5 + 0.1% HCOOH, B: acetonitrile/water 95/5 + 0.1% HCOOH) in 12 CV. Purification yielded compound **40** in a 20% yield.

¹H NMR (400 MHz, DMSO-d₆) δ ppm 11.23 (s, 1 H), 11.10 (s, 1 H), 9.87 (s, 1 H), 8.34 (s, 1 H), 7.84 (s, 1 H), 7.40 (m, J=8.33 Hz, 2 H), 7.30 (m, J=8.33 Hz, 2 H), 7.09 (dd, J=6.91, 6.03 Hz, 1 H), 6.48 (d, J=7.02 Hz, 1 H), 4.14 (br dd, J=12.17, 2.30 Hz, 1 H), 3.43 (br dd, J=17.10, 13.59 Hz, 1 H), 2.55 - 2.65 (m, 1 H), 2.38 - 2.43 (m, 1 H), 2.24 - 2.31 (m, 2 H), 2.07 (s, 3 H), 2.00 - 2.06 (m, 1 H), 1.86 - 1.95 (m, 1 H), 1.67 (br d, J=10.52 Hz, 1 H)

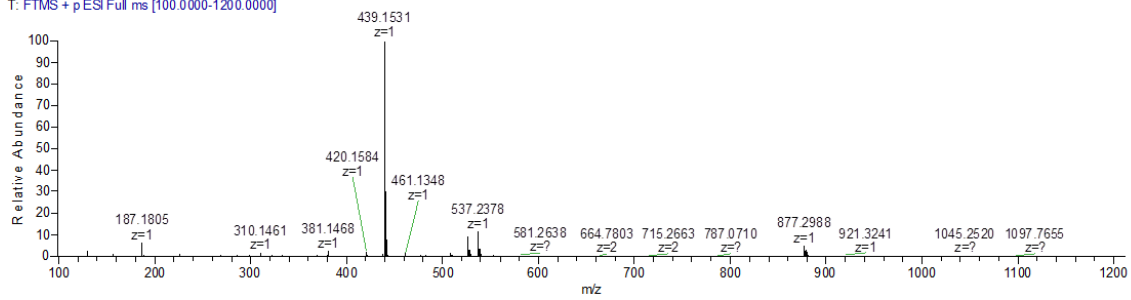
¹³C NMR (151 MHz, METHANOL-d₄) δ ppm 176.2, 172.5, 164.3, 141.2, 140.2, 135.1, 131.7, 129.8, 129.5, 128.2, 126.8, 123.1, 118.7, 107.8, 65.7, 49.3, 49.0, 39.5, 37.1, 23.5, 5.68, 58.13, 49.00, 39.48, 37.07, 23.48"

UPLC-MS (Method 2): t_R= 4.44 min, m/z: 439.2 [M+H]⁺

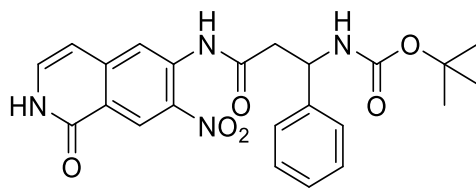
UPLC Purity: 95%

HRMS: exp. 439.1531, calc. 439.1531

200804_16_#41 RT: 0.16 AV: 1 SB: 29 0.00-0.14 , 0.20-0.49 NL: 1.65E8
T: FTMS + pESI Full ms [100.0000-1200.0000]



Tert-butyl(3-((7-nitro-1-oxo-1,2-dihydroisoquinolin-6-yl)amino)-3-oxo-1-phenylpropyl)carbamate (51)



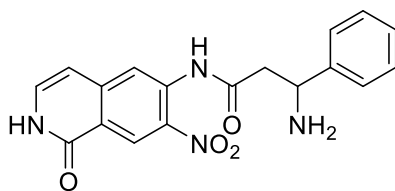
Intermediate **21** (1 g, 4.87 mmol) and **50** (1.681 g, 6.34 mmol) were dissolved in Pyridine (20 ml) then POCl₃ (0.545 ml, 5.85 mmol) was added slowly at 0 °C. Mixture was stirred at 0°C for 1.5 hr. Then mixture was quenched with NaHCO₃ sat solution (20 mL) and extracted with EtOAc (20mL). Organic phase was washed once with H₂O (20 mL) then evaporated under vacuum to give a yellow solid. Precipitation by DMSO/H₂O yielded the desired compound **51** (1537 mg, 3.40 mmol, 69.7 % yield).

¹H NMR (400 MHz, DMSO-d₆) δ ppm 1.33 (br s, 9 H) 2.77 - 2.89 (m, 2 H) 4.95 - 5.09 (m, 1 H) 6.60 (d, J=7.23 Hz, 1 H) 7.20 - 7.27 (m, 1 H) 7.29 - 7.38 (m, 5 H) 8.03 (s, 1 H) 8.62 - 8.72 (m, 1 H) 10.33 - 10.47 (m, 1 H) 11.56 (br d, J=5.26 Hz, 1 H)

UPLC-MS (Method-1): t_R= 1.02 min, m/z: 353.4 [M-100]⁺

UPLC Purity= 80%

3-amino-N-(7-nitro-1-oxo-1,2-dihydroisoquinolin-6-yl)-3-phenylpropanamide, 2HCl (52)



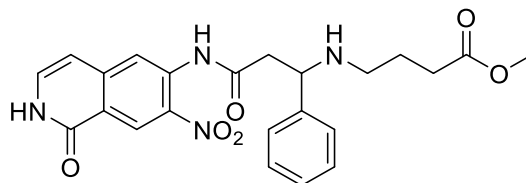
Compound **51** was dissolved in 12 mL of 4M HCl in Dioxane. The solution was stirred at 60 °C for 2 hr. Then solvent was evaporated under vacuum affording **52**, as bis chloride salt, in a quantitative yield. Solid was used in the next step without further purification.

¹H NMR (400 MHz, DMSO-d₆) δ ppm 3.19 (br d, J=5.26 Hz, 2 H) 4.70 (br s, 1 H) 6.60 (d, J=7.23 Hz, 1 H) 7.34 - 7.48 (m, 4 H) 7.54 (br d, J=7.23 Hz, 2 H) 7.81 - 7.87 (m, 1 H) 8.42 - 8.58 (m, 2 H) 8.62 (s, 1 H) 11.61 (br d, J=4.60 Hz, 1 H)

UPLC-MS (Method-1): t_R= 0.40 min, m/z: 353.3 [M+H]⁺

UPLC Purity: 89%

Methyl-4-((3-((7-nitro-1-oxo-1,2-dihydroisoquinolin-6-yl)amino)-3-oxo-1-phenylpropyl)amino)butanoate (53)



Compound **52** (718 mg, 1.688 mmol) was dissolved in THF (2 ml) and MeOH (10 ml) with 4A Molecular Sieves and MgSO₄ then added of methyl 4-oxobutanoate (**35**), (235 mg, 2.026 mmol). The resulting mixture was stirred for 10 minutes, then acetic acid (0.193 ml, 3.38 mmol) and NaBH₃CN (212 mg, 3.38 mmol) was added slowly. After 5 hr, monitoring of the reaction by UPLC-MS showed 50% of conversion, 1.5 eq of NaBH₃CN was added and reaction was stirred at room temperature on. Following day, 0.5 eq of aldehyde and 1.0 eq of NaBH₃CN were added again. Reaction was quenched with NaHCO₃ sat solution and extracted with DCM twice. Organic phases were combined, washed again with NaHCO₃ sat solution and evaporated under vacuum. The resulting crude was purified by Flash chromatography, SNAP 60 gr, C18-silica by eluting with 0-30% B in A (A: water/acetonitrile 95/5 + 0.1% HCOOH, B: acetonitrile/water 95/5 + 0.1% HCOOH) in 12 CV. Appropriate fractions were combined and evaporated under vacuum to give Intermediate **53** (330 mg, 0.662 mmol, 39.2 % yield), as formate salt.

¹H NMR (400 MHz, DMSO-d₆) δ ppm 1.57 - 1.74 (m, 2 H) 2.22 - 2.42 (m, 5 H) 2.57 (br dd, J=15.24, 4.71 Hz, 2 H) 2.81 (dd, J=15.13, 9.21 Hz, 1 H) 3.51 (s, 3 H) 4.03 (dd, J=9.10, 4.71 Hz, 1 H) 6.60 (d, J=7.23 Hz, 1 H) 7.21 - 7.27 (m, 1 H) 7.29 - 7.42 (m, 5 H) 8.13 - 8.17 (m, 1 H) 8.70 (s, 1 H) 11.55 (br d, J=3.51)

UPLC-MS (Method-1): t_R= 0.49 min, m/z: 453.4 [M+H]⁺

UPLC Purity: 98%

Methyl 4-(methyl(3-((7-nitro-1-oxo-1,2-dihydroisoquinolin-6-yl)amino)-3-oxo-1-phenylpropyl)amino)butanoate (54)



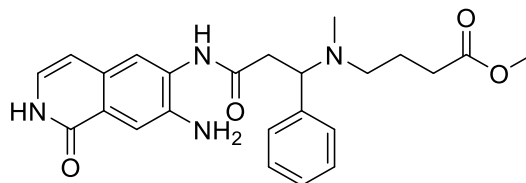
Intermediate **53** (330 mg, 0.694 mmol) was dissolved in THF (2 ml) and MeOH (5 ml), 4Å Molecular Sieves added of MgSO₄ and then added of formaldehyde (0.121 ml, 2.082 mmol). Solution was stirred for 10 minutes and then added of acetic acid (0.040 ml, 0.694 mmol) and NaBH₃CN (131 mg, 2.082 mmol). Solution was stirred for 2 hr, presence of 30% of imine was detected by UPLC-analysis, formaldehyde (0.121 ml, 2.082 mmol) and NaBH₃CN (131 mg, 2.082 mmol) were added again. After 12 hr, still presence of the imine so NaBH₃CN (131 mg, 2.082 mmol) was added again. After 24 hr, reaction was quenched with NaHCO₃ sat solution and extracted with DCM (20mL). Aqueous phase was washed twice and combined organic phases were evaporated under vacuum. Purification by flash chromatography, Biotage Isolera, on silica NH, SNAP column 55 gr, gradient elution from 100% of DCM to 15% of Acetone in 10 CV yielded the desired product **55** (130 mg, 0.279 mmol, 40.2 % yield).

¹H NMR (400 MHz, DMSO-d₆) δ ppm 1.58 - 1.73 (m, 2 H) 2.10 (s, 3 H) 2.16 - 2.28 (m, 1 H) 2.16 - 2.23 (m, 1 H) 2.18 - 2.22 (m, 1 H) 2.26 (t, J=7.34 Hz, 1H) 2.35 - 2.43 (m, 1 H) 2.72 (dd, J=15.24, 6.25 Hz, 1 H) 3.18 (dd, J=15.24, 8.66 Hz, 1 H) 3.49 (s, 3 H) 4.18 (dd, J=8.33, 6.58 Hz, 1 H) 6.59 (d, J=7.02 Hz, 1H) 7.26 - 7.39 (m, 6 H) 8.17 (s, 1 H) 8.69 (s, 1 H) 10.66 - 11.05 (m, 1 H) 11.35 - 11.69 (m, 1 H)

UPLC-MS (Method 1): t_R= 0.50 min, m/z: 467.3 [M+H]⁺

UPLC Purity: 92%

Methyl-4-((3-((7-amino-1-oxo-1,2-dihydroisoquinolin-6-yl)amino)-3-oxo-1-phenylpropyl)(methyl)amino)butanoate (55)



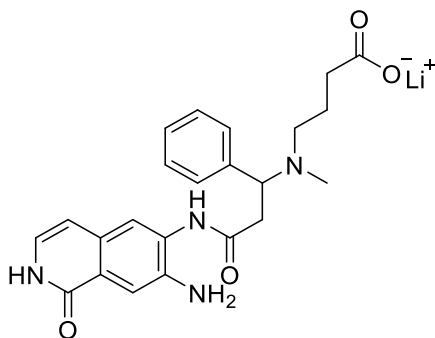
Intermediate **54** (130 mg, 0.279 mmol) was dissolved in EtOH (5 ml) and mixture was added of Tin Chloride(0.301 ml, 1.393 mmol). Mixture was stirred for 4 hr at rt. Then reaction was quenched slowly with NaHCO₃ sat solution (6mL) and extracted three times with DCM. The formation of a precipitate was observed. Organic phase was evaporated under vacuum and crude was triturated with Et₂O to give Intermediate **55** (89 mg, 0.204 mmol, 73.2 % yield) as reddish solid.

¹H NMR (400 MHz, DMSO-d₆) δ ppm 1.61 - 1.73 (m, 2 H) 2.10 (s, 3 H) 2.23 (dt, J=12.55, 6.55 Hz, 1 H) 2.30 (t, J=7.56 Hz, 2 H) 2.34 - 2.41 (m, 1 H) 2.74(br dd, J=14.36, 7.34 Hz, 1 H) 3.05 (br dd, J=14.47, 7.89 Hz, 1 H) 3.54 (s, 3 H) 4.20 (t, J=7.56 Hz, 1 H) 5.20 (s, 2 H) 6.28 (d, J=7.02 Hz, 1 H) 6.79 - 6.84 (m, 1 H) 7.26 - 7.31 (m, 3 H) 7.32 - 7.38 (m, 2 H) 7.43 - 7.48 (m, 1 H) 7.58 (s, 1 H) 9.42 (s, 1 H) 10.73 - 10.81 (m, 1 H)

UPLC-MS (Method 1): t_R= 0.40 min, m/z: 437.3 [M+H]⁺

UPLC Purity: 80%

Lithium 4-((3-((7-amino-1-oxo-1,2-dihydroisoquinolin-6-yl)amino)-3-oxo-1-phenylpropyl)(methyl)amino)butanoate (56)

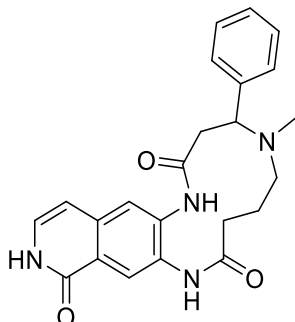


Intermediate **55** (69 mg, 0.204 mmol) was dissolved in THF (2 ml) and Water (0.5 ml). Lithium hydroxide (9.46 mg, 0.395mmol) was added then to the reaction. Mixture was stirred for 1 hr at rt. Once the hydrolysis was completed, 0.237 mL of a solution 1M of pyridine hydrochloride was added to quench the lithium hydroxide in excess and then solution was evaporated under vacuum to give Intermediate **56** in quantitative yield. Intermediate **56** was not purified further and used it as it was in the last step.

UPLC-MS (Method -1): $t_R = 0.43$ min, m/z : 457.3 [M+H]⁺

UPLC Purity: 74%

5-methyl-4-phenyl-3,4,5,6,7,8,10,13-octahydro-[1,4,8]triazacyclododecino[3,2-g]isoquinoline-2,9,12(1H)-trione (57)



Intermediate **56** (100 mg, 0.233 mmol) was dissolved in DMF (12 ml) and added of DIPEA (0.163 ml, 0.931 mmol) and HATU (177 mg, 0.466 mmol) and stirred for 5 hr at rt. Reaction was diluted with EtOAc (30mL) and organic phase was washed with NaHCO₃ sat solution (20mL) twice. Organic phase was evaporated under vacuum to give a red oil (215 mg). The resulting crude was purified by Flash chromatography, SNAP 30 gr, C18-silica by eluting with 0-20% B in A (A: water/acetonitrile 95/5 + 0.1% HCOOH, B: acetonitrile/water 95/5 + 0.1% HCOOH) in 10 CV. Purification yielded the final compound in a 14% yield.

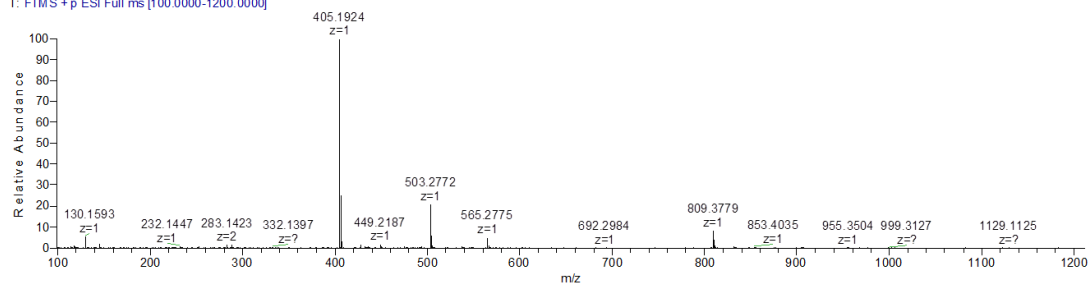
¹H NMR (400 MHz, DMSO-d₆) δ ppm 11.33 (s, 1 H), 11.10 (br d, J=5.48 Hz, 1 H), 9.88 (s, 1 H), 8.36 (s, 1 H), 7.85 (s, 1 H), 7.22 - 7.38 (m, 5 H), 7.10 (t, J=6.36 Hz, 1 H), 6.48 (d, J=7.02 Hz, 1 H), 4.12 (br dd, J=12.17, 2.52 Hz, 1 H), 3.45 (br dd, J=16.22, 12.72 Hz, 1 H), 2.54 - 2.71 (m, 1 H), 2.38 - 2.44 (m, 1 H), 2.25 - 2.35 (m, 2 H), 2.09 (s, 3 H), 2.03 - 2.06 (m, 1 H), 1.86 - 1.96 (m, 1 H), 1.68 (br d, J=10.30 Hz, 1 H)

UPLC-MS (Method-2): t_R= 3.6 min, m/z: 405.3 [M+H]⁺

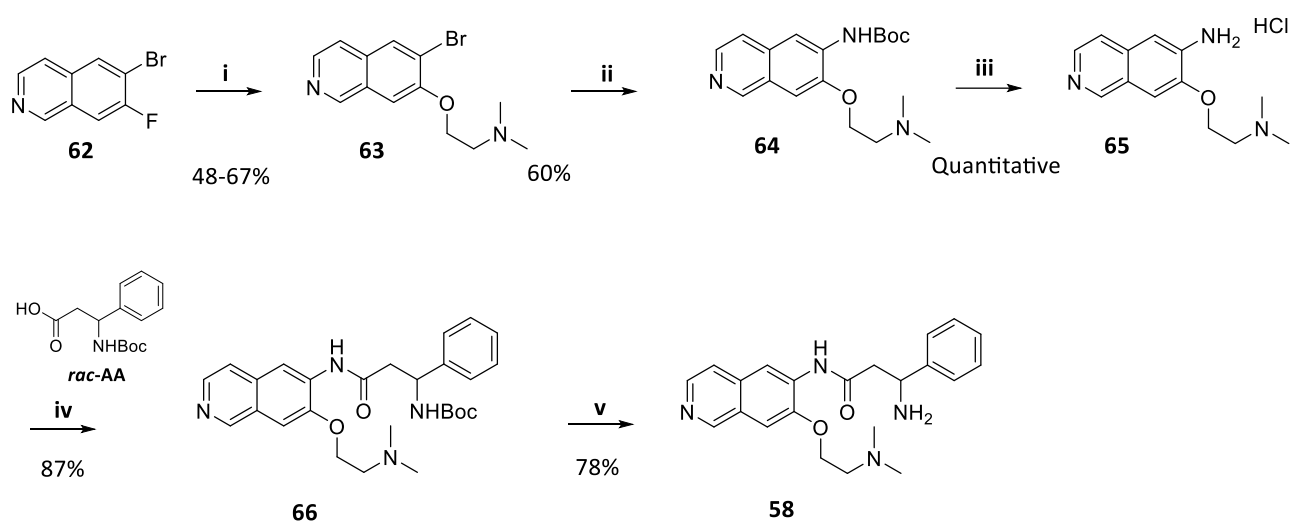
UPLC Purity: 91%

HRMS analysis: exp. 405.1924 (M+1), calc. 405.1921

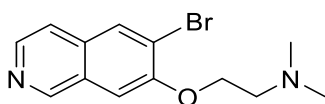
200804_20 #45 RT: 0.18 AV: 1 SB: 29 0.00-0.15 , 0.20-0.49 NL: 2.02E8
T: FTMS +p ESI Full ms [100.0000-1200.0000]



6.4 Scheme 10



2-((6-bromoisoquinolin-7-yl)oxy)-*N,N*-dimethylethan-1-amine (63)



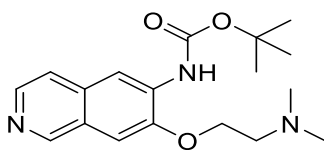
In a 100 ml round-bottom flask, *N,N*-dimethylethanolamine (0.900 ml, 8.85 mmol) was dissolved in DMF (5 ml) then sodium hydride (0.212 g, 8.85 mmol) was added in one portion and the reaction was stirred at 0 °C for 10 minutes. 6-bromo-7-fluoroisoquinoline (**62**) (1 g, 4.42 mmol) was added to the mixture and stirred at 80 °C. After 4 hr, UPLC-analysis still showed presence of starting material. Therefore, sodium hydride (0.212 g, 8.85 mmol) and *N,N* dimethylethanolamine (0.900 ml, 8.85 mmol) were added again and stirring was maintained 12 hr to get complete conversion. Mixture was quenched with water (20 ml) and extracted with EtOAc (20 ml). Organic phase was dried with Na₂SO₄ and evaporated under vacuum and purified by flash chromatography on NH silica (Biotage, SNAP 55 gr column) by eluting with a mixture of Heptane/EtOAc 50:50.

Fractions were combined and evaporated under vacuum to give intermediate **63** (0.875 g, 2.96 mmol, 67.0 % yield).

¹H NMR: (400 MHz, DMSO-*d*₆) δ ppm 2.28 (s, 6 H) 2.77 (t, *J*=5.59 Hz, 2 H) 4.26 - 4.33 (m, 2 H) 7.69 (s, 1 H) 7.68 - 7.70 (m, 1 H) 7.73 (d, *J*=5.70 Hz, 1 H) 8.34 (s, 1 H) 8.41 (d, *J*=5.70 Hz, 1 H) 9.22 (s, 1 H)

UPLC-MS (Method-1): *t*_R= 0.19 min; MS (ESI): *m/z* 295.1/297.1 [M + H]⁺

Tert-butyl (7-(2-(dimethylamino)ethoxy)isoquinolin-6-yl)carbamate (**64**)



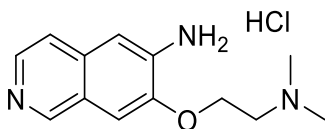
A MW vial (20 mL) was loaded with Cs₂CO₃ (1932 mg, 5.93 mmol) Xantphos (343 mg, 0.593 mmol) Tert-Butyl Carbamate (0.475 ml, 3.56 mmol), Pd(OAc)₂ (66.6 mg, 0.296 mmol), **63** and 1,4-Dioxane (15 ml). The mixture was purged with Ar and then irradiated at 100 °C for 2 hr. Dioxane was evaporated under vacuum. Solid was dissolved in EtOAc (30 mL) and washed with NaHCO₃ (30mL) twice. Organic phase was evaporated under vacuum and purified by flash chromatography, puriflash 125 instrument, NH silica (Biotage SNAP 110 gr), by eluting with a mixture of Heptane/EtOAc 50:50. Fractions were combined and evaporated under vacuum to give **64** (577 mg, 1.741 mmol, 58.7 % yield).

¹H NMR (400 MHz, DMSO-d₆) δ ppm 1.51 (s, 9 H) 2.27 (s, 6 H) 2.66 - 2.69 (m, 2 H) 4.24 (t, J=5.70 Hz, 2 H) 7.67 (s, 1 H) 8.31 (d, J=5.48 Hz, 1 H) 8.38 (s, 1H) 9.03 - 9.07 (m, 2 H)

UPLC-MS (Method 1): t_R= 0.31 min; MS (ESI): m/z 332.4 [M + H]⁺

UPLC Purity=95%

7-(2-(dimethylamino)ethoxy)isoquinolin-6-amine hydrochloride (65)

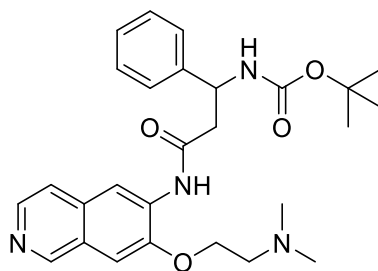


In a 100 ml round bottom flask Intermediate **64** (577 mg, 1.741 mmol) was dissolved in Acetonitrile (3 ml) and EtOH (2.00 ml) and added of aqueous hydrogen chloride 37% (5 ml, 60.0 mmol). Solution was stirred for 1 hr at rt. Then solvents were evaporated under vacuum to give **65**. Intermediate **65** was used as chloride salt in next steps and used as it was without further purifications.

¹H NMR (400 MHz, DMSO-d₆) δ ppm 2.30 (s, 6 H) 2.81 (br t, J=5.59 Hz, 2 H) 4.22 (t, J=5.81 Hz, 2 H) 5.72 (br s, 2 H) 6.82 (s, 1 H) 7.29 - 7.35 (m, 2 H) 8.10 (d, J=5.70 Hz, 1 H) 8.81 (s, 1 H)

UPLC-MS (Method 1): t_R= 0.10 min; MS (ESI): m/z 232.3 [M + H]⁺

Tert-butyl(3-((7-(2-(dimethylamino)ethoxy)isoquinolin-6-yl)amino)-3-oxo-1-phenylpropyl)carbamate (66)



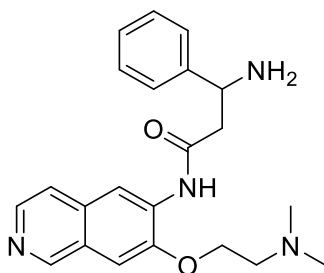
3-((tert-Butoxycarbonyl)amino)-3-phenylpropanoic acid (**Rac-AA**) (368 mg, 1.385 mmol), HATU (527 mg, 1.385 mmol) and DIPEA (0.484 ml, 2.77 mmol) were dissolved in DMF (5 ml) and reacted for 10 minutes, then solution was added of **65** (236 mg, 0.693 mmol) dissolved in DMF (2mL) and then solution was stirred on. Following day, UPLC-MS analysis showed still presence of SM, so 1 eq of acid and HATU were added to the solution and stirring was maintained at rt for 96 hr. Reaction was diluted with EtOAc (20mL) and then washed with NaHCO₃ sat solution (20mL). Organic phase was dried with Na₂SO₄, evaporated under vacuum and purified by flash chromatography on silica NH by eluting with 0% - 10% Acetone in DCM. Appropriate fractions were combined and evaporated under vacuum to give Intermediate **66** (290 mg, 0.606 mmol, 87 % yield) as white solid.

¹H NMR (400 MHz, DMSO-d₆) δ ppm 1.33 (br s, 9 H) 2.27 (s, 6 H) 2.76 (br t, J=5.59 Hz, 2 H) 4.24 - 4.35 (m, 2 H) 7.19 - 7.28 (m, 1 H) 7.28 - 7.40 (m, 5 H) 7.46 - 7.56 (m, 1 H) 7.63 - 7.73 (m, 2 H) 8.32 (d, J=5.70 Hz, 1 H) 8.63 (s, 1 H) 9.07 (s, 1 H) 9.34 (s, 1 H)

UPLC-MS (Method 1): t_R= 0.45 min; MS (ESI): m/z 479.3 [M + H]⁺

UPLC Purity:95%

3-amino-N-(7-(2-(dimethylamino)ethoxy)isoquinolin-6-yl)-3-phenylpropanamide (58)

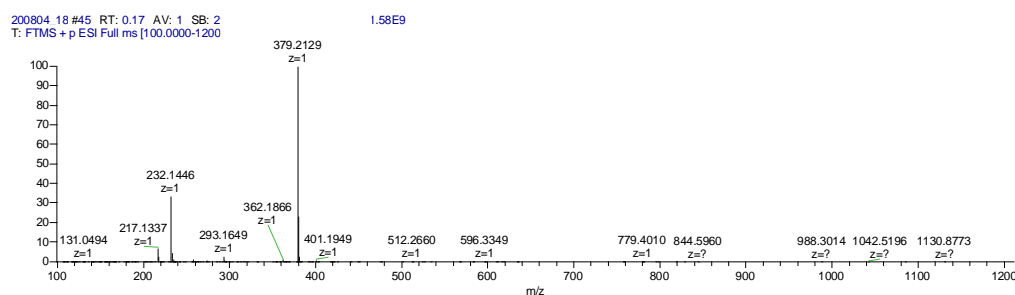


Intermediate **66** (130 mg, 0.272 mmol) was dissolved in ACN (1.000 ml) and then added of aqueous hydrogen chloride 37% (2 ml, 24.00 mmol). Solution was stirred for 1 hr at rt then solvent was evaporated under vacuum. Crude was purified on a SCX cartridge elution with 7 N NH₃ in MeOH yielded in **58** (80 mg, 0.211 mmol, 78 % yield).

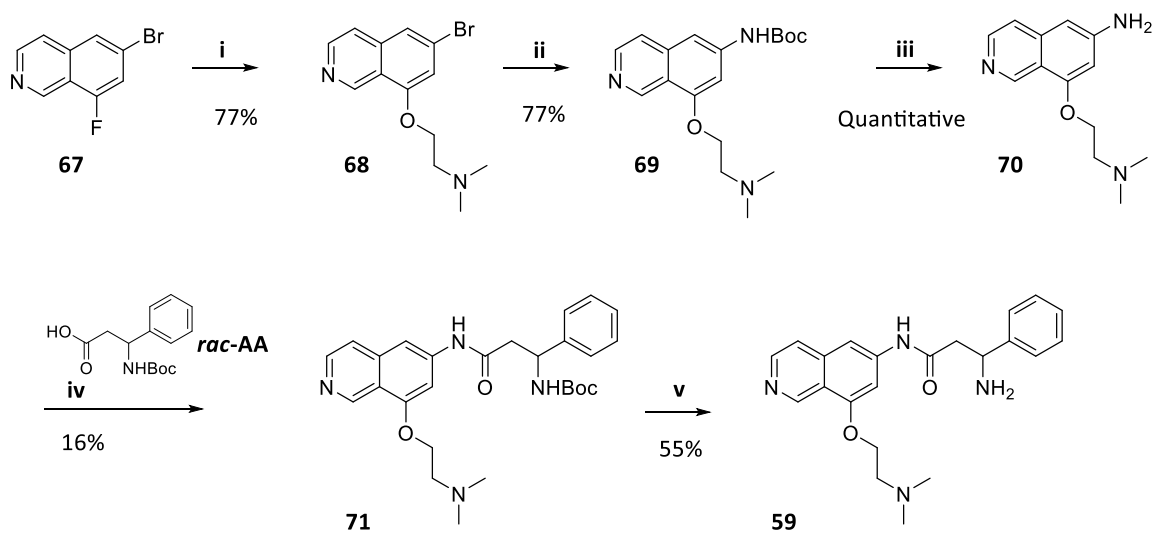
¹H NMR (400 MHz, DMSO-d₆) δ ppm 11.36 (bs, 1 H), 9.03 (s, 1 H), 8.68 (s, 1 H), 8.27 (d, J=5.70 Hz, 1 H), 7.61 (d, J=5.70 Hz, 1 H), 7.58 (s, 1 H), 7.43 (d, J=7.45 Hz, 2 H), 7.18 - 7.35 (m, 3 H), 4.16 - 4.34 (m, 3 H), 2.73 - 2.85 (m, 3 H), 2.59 - 2.69 (m, 1 H), 2.24 (s, 6 H)

¹H-NMR purity: 85%

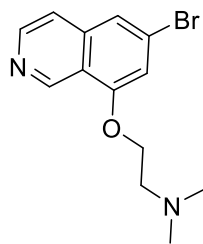
HRMS analysis: exp. 379.2129 (M+1), calc. 379.2129



6.5 Scheme 11



2-((6-bromoisoquinolin-8-yl)oxy)-*N,N*-dimethylethan-1-amine (68)

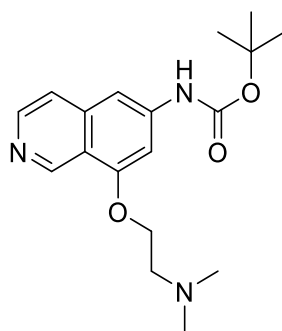


In a 100 ml round-bottom flask, *N,N*-dimethylethanolamine (0.900 ml, 8.85 mmol) was dissolved in DMF (5 ml) then sodium hydride (0.212 g, 8.85 mmol) was added in one portion and the reaction was stirred at 0 °C for 10 minutes. 6-bromo-8-fluoroisoquinoline (**67**) (1 g, 4.42 mmol) was added to the mixture and solution was stirred at 80 °C. Mixture was quenched with NaHCO₃ sat. solution (20 ml) and extracted with EtOAc (20 ml). Organic phase was evaporated under vacuum and purified by flash chromatography, Biotage Isolera Instrument on NH silica (Biotage SNAP 110 gr), by eluting with a mixture of Heptane/EtOAc 50:50. Appropriate fractions were combined to give intermediate **68** (1 g, 3.39 mmol, 77 % yield) as a colorless oil.

¹H NMR (400 MHz, DMSO-d₆) δ ppm 2.27 (s, 6 H) 2.79 (t, J=5.48 Hz, 2 H) 4.31 (t, J=5.59 Hz, 2 H) 7.26 - 7.30 (m, 1 H) 7.73 (d, J=5.70 Hz, 1 H) 7.78 (s, 1H) 8.55 (d, J=5.92 Hz, 1 H) 9.42 (s, 1 H).

UPLC-MS (Method 1): t_R= 0.24 min; MS (ESI): m/z 294.8/296.8 [M + H]⁺

Tert-butyl-(8-(2-(dimethylamino)ethoxy)isoquinolin-6-yl)carbamate (69)



A MW vial (20 mL) was loaded with Cs_2CO_3 (2.208 g, 6.78 mmol), Xantphos (0.392 g, 0.678 mmol) Tert-Butyl Carbamate (0.543 ml, 4.07 mmol), $\text{Pd}(\text{OAc})_2$ (0.076 g, 0.339 mmol) (66.6 mg, 0.296 mmol), Intermediate **68** (1 g, 3.39 mmol) and 1,4-Dioxane (15 ml). The mixture was purged with Ar and then irradiated at 100 °C for 2 hr. Dioxane was evaporated under vacuum. Solid was dissolved in EtOAc (30 mL) and washed with NaHCO_3 (30mL) twice. Organic phase was washed with NaCl sat solution and dried with Na_2SO_4 , evaporated under vacuum and purified by flash chromatography, Biotage Isolera Instrument, on NH silica (Biotage SNAP 110 gr), by eluting with a mixture of Heptane/EtOAc 50:50.

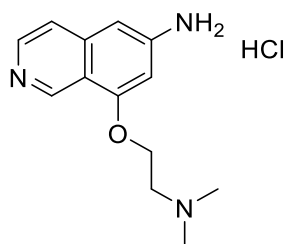
Purification yielded intermediate **69** (862 mg, 2.60 mmol, 77 % yield)

$^1\text{H NMR}$ (400 MHz, DMSO-d_6) δ ppm 1.51 (s, 9 H) 2.29 (s, 6 H) 2.81 (t, $J=5.59$ Hz, 2 H) 4.20 (t, $J=5.59$ Hz, 2 H) 7.18 (d, $J=1.53$ Hz, 1 H) 7.59 (d, $J=5.70$ Hz, 1 H) 7.65 (s, 1 H) 8.36 (d, $J=5.70$ Hz, 1 H) 9.26 (s, 1 H) 9.72 (s, 1 H)

UPLC-MS (Method 1): $t_R = 0.38$ min; MS (ESI): m/z 332.3 $[\text{M} + \text{H}]^+$

UPLC Purity: 98%

8-(2-(dimethylamino)ethoxy)isoquinolin-6-amine hydrochloride (70)



In a 100 ml round-bottom flask, intermediate **69** (862 mg, 2.60 mmol) was dissolved in H₂O (1 ml) and THF (3 ml), then solution was added of 3 mL of aqueous HCl 37%. Solution was stirred at rt for 24 hr. Then solvents were removed under vacuum to give intermediate **70** as chloride salt in a quantitative yield.

¹H NMR (400 MHz, DMSO-d₆) δ ppm 2.86 (d, J=4.60 Hz, 6 H) 3.64 (br d, J=4.17 Hz, 2 H) 4.47 - 4.54 (m, 2 H) 6.55 (s, 1 H) 6.69 (s, 1 H) 7.34 - 7.51 (m, 2H) 7.66 (d, J=6.80 Hz, 1 H) 8.04 (s, 1 H) 9.67 (s, 1 H)

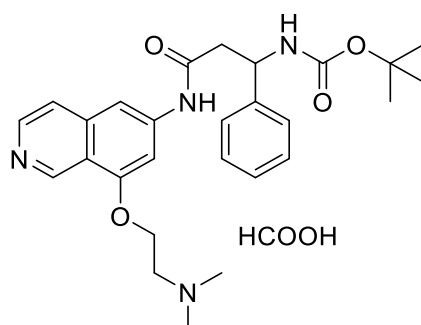
50 mg were sampled and purified by SCX. The resulting material was submitted to ¹H NMR analysis to have the spectra of the free base:

¹H NMR (400 MHz, DMSO-d₆) δ ppm 2.30 (s, 6 H) 2.81 (t, J=5.48 Hz, 2 H) 4.17 (t, J=5.59 Hz, 2 H) 5.93 (s, 2 H) 6.29 (s, 1 H) 6.46 (d, J=1.32 Hz, 1 H) 7.24 (d, J=5.70 Hz, 1 H) 8.11 (d, J=5.70 Hz, 1 H) 9.02 (s, 1 H)

UPLC-MS (Method 1): t_R= 0.11 min; MS (ESI): m/z 232.3 [M + H]⁺

UPLC-MS Purity: 95%

Tert-butyl (3-((8-(2-(dimethylamino)ethoxy)isoquinolin-6-yl)amino)-3-oxo-1-phenylpropyl)carbamate formate (71)



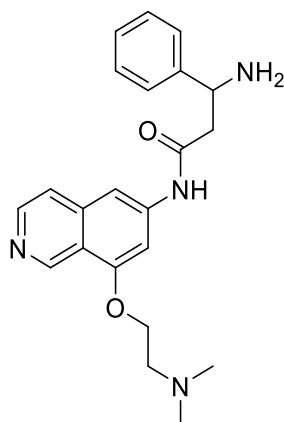
In a 20 mL vial, 3-((tert-butoxycarbonyl)amino)-3-phenylpropanoic acid (**Rac-AA**) (312 mg, 1.174 mmol), HATU (446 mg, 1.174 mmol) and DIPEA 200uL were dissolved in 2 mL of DMF and reacted for 10 minutes. In another 20mL vial, intermediate **70** (200 mg, 0.587 mmol) and DIPEA 200uL were dissolved in DMSO (2 mL). The resulting solution was added to the previous one. DMAP (35.9 mg, 0.294 mmol) was added to the resulting solution. Solution was stirred for 5 hr at 80 deg. After 5 hr, UPLC-MS analysis still showed presence of starting material. Acid (312 mg, 1.174 mmol), HATU (446 mg, 1.174 mmol) and DIPEA 200uL were added again and solution was stirred at 80 deg for 12 hr. The solution was diluted with EtOAc (20mL) and washed twice with NaHCO₃ sat solution (20mL). Organic phase was evaporated under vacuum and crude was purified by flash chromatography on C18-silica by eluting with 0-30% B in A (A: water/acetonitrile 95/5 + 0.1% HCOOH, B: acetonitrile/water 95/5 + 0.1% HCOOH). Purification yielded Intermediate **71** (50 mg, 0.095 mmol, 16.23 % yield).

¹H NMR (400 MHz, DMSO-d₆) δ ppm 1.35 (br s, 9 H) 2.88 (br d, J=7.23 Hz, 2 H) 2.95 (br s, 7 H) 3.70 (br s, 2 H) 4.51 (br s, 2 H) 5.01 - 5.14 (m, 1 H) 7.18 -7.25 (m, 1 H) 7.27 - 7.40 (m, 1 H) 7.27 - 7.48 (m, 1 H) 7.41 (br s, 1 H) 7.50 - 7.60 (m, 1 H) 7.96 (br s, 1 H) 8.11 - 8.16 (m, 1 H) 8.49 (br d, J=6.36 Hz, 1 H) 9.63 (s, 1 H) 10.56 (br s, 1 H)

UPLC-MS (Method 3): t_R= 0.45 min; MS (ESI): m/z 479.3 [M + H]⁺

UPLC Purity: 98%

**3-amino-N-(8-(2-(dimethylamino)ethoxy)isoquinolin-6-yl)-3-phenylpropanamide
(59)**



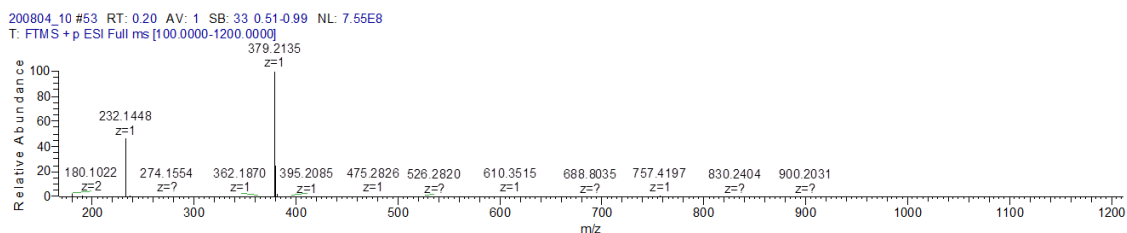
Intermediate **71** (50 mg, 0.095 mmol) was dissolved in Acetonitrile (1 ml) and Water (1 ml) and then added of 1 ml of aqueous 37% HCl. Solution was stirred for 1 hr at rt and then solvent was evaporated under vacuum. Crude was dissolved in MeOH, pH was adjusted to 5 with NaHCO₃ sat solution and then purified by SCX, eluting with 7N of NH₃ in MeOH to give compound **59** (20 mg, 0.053 mmol, 55.4 % yield)

¹H NMR (400 MHz, DMSO-d₆) δ ppm 10.42 (bs, 1 H), 9.26 (s, 1 H), 8.36 (d, J=5.70 Hz, 1 H), 7.81 (s, 1 H), 7.60 (d, J=5.70 Hz, 1 H), 7.10 - 7.40 (m, 7 H), 4.33 (br t, J=6.69 Hz, 1 H), 4.20 (t, J=5.59 Hz, 2 H), 2.78 (t, J=5.48 Hz, 2 H), 2.50 - 2.69 (m, 2 H), 2.26 (s, 6 H)

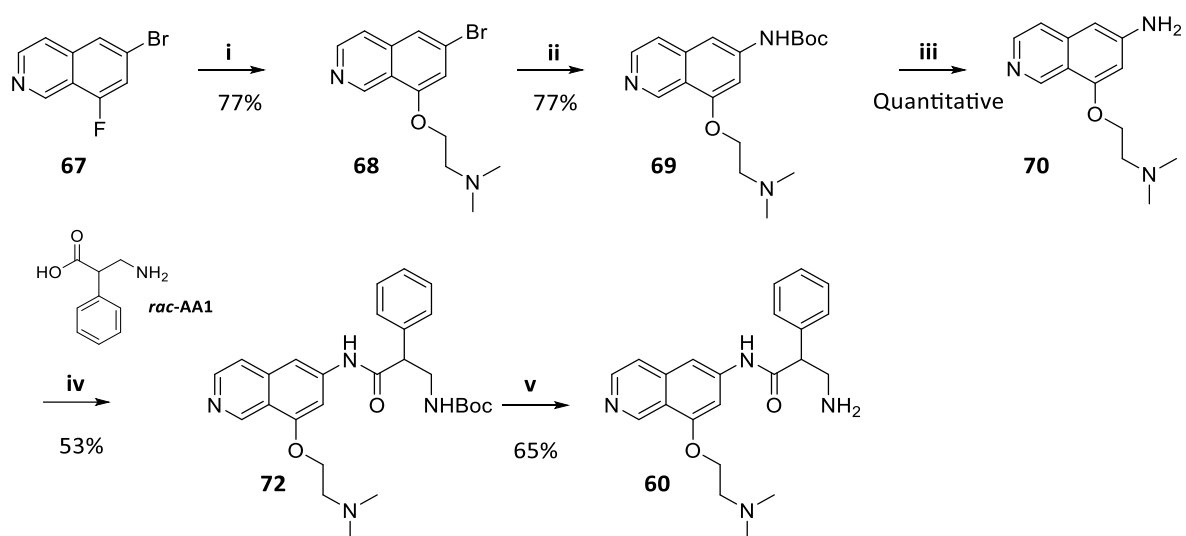
UPLC-MS Method B: t_R= 2.35 min; MS (ESI): m/z 379.2 [M + H]⁺

UPLC Purity=96%

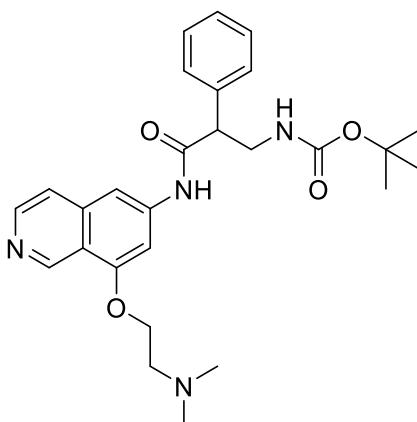
HRMS analysis: exp. 379.2135 (M+1), calc. 379.2129



6.6 Scheme 12



Tert-butyl (3-((8-(2-(dimethylamino)ethoxy)isoquinolin-6-yl)amino)-3-oxo-2-phenylpropyl)carbamate (72)



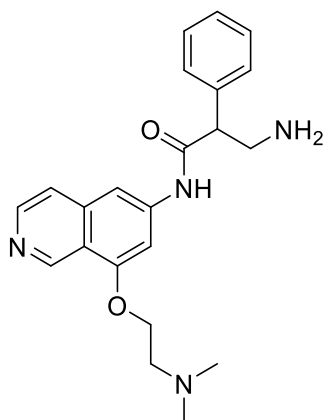
Rac-AA1, 3-[[[(tert-butoxy)carbonyl]amino]-2-phenylpropanoic acid (312 mg, 1.174 mmol) was dissolved in DMF (4mL) and added of DIPEA (0.410 ml, 2.348 mmol), a catalytic amount of DMAP and HATU (446 mg, 1.174 mmol). The resulting solution was stirred for 10 minutes, then Intermediate **70** was added and the solution was stirred for 48 hr at rt. Then solution was diluted with EtOAc (20mL) and washed twice with NaHCO₃ sat solution (20mL). Purification by flash chromatography on C18-silica by eluting with 0-30% B in A (A: water/acetonitrile 95/5 + 0.1% HCOOH, B: acetonitrile/water 95/5 + 0.1% HCOOH) yielded intermediate **72** in a 53% yield.

¹H NMR (400 MHz, DMSO-d₆) δ ppm 1.35 (s, 10 H) 2.76 (br s, 6 H) 3.33 - 3.36 (m, 1 H) 3.45 (br s, 2 H) 3.54 (ddd, J=13.32, 7.84, 5.37 Hz, 1 H) 4.07 (br t, J=7.23 Hz, 1 H) 4.40 (br s, 2 H) 7.00 (br t, J=5.26 Hz, 1 H) 7.22 - 7.32 (m, 2 H) 7.24 - 7.31 (m, 1 H) 7.31 - 7.43 (m, 4 H) 7.65 (d, J=5.70 Hz, 1 H) 7.89 (s, 1H) 8.13 (s, 1 H) 8.39 - 8.47 (m, 1 H) 9.48 (s, 1 H) 10.54 (s, 1 H)

UPLC-MS Method A: t_R= 0.48 min; MS (ESI): m/z 479.4 [M + H]⁺

UPLC Purity: 95%

3-amino-N-(8-(2-(dimethylamino)ethoxy)isoquinolin-6-yl)-2-phenylpropanamide (60)



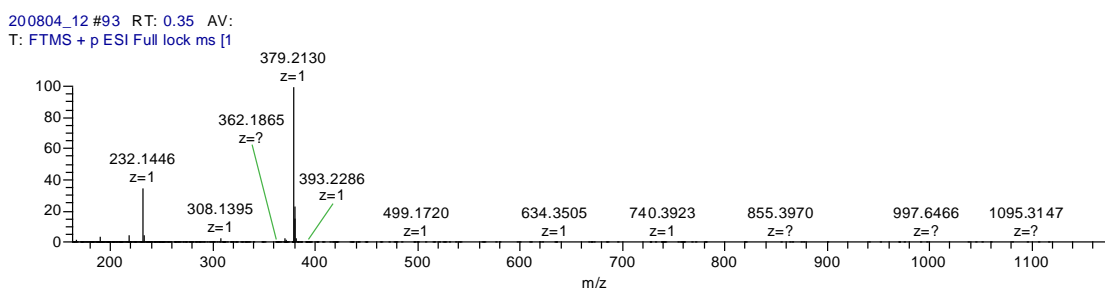
Intermediate **72** (150 mg, 0.313 mmol) was dissolved in Acetonitrile (1 ml) and Water (1 ml) and then added of 1 ml of aqueous 37% HCl. Solution was stirred for 1 hr and then solvent was evaporated under vacuum. Crude was dissolved in MeOH, pH was adjusted to 5 with NaHCO₃ sat solution and then purified by SCX, eluting with 7N of NH₃ in MeOH to give **60** in a 65% yield.

¹H NMR (400 MHz, DMSO-d₆) δ ppm 9.25 (s, 1 H), 8.36 (d, J=5.70 Hz, 1 H), 7.89 (s, 1 H), 7.59 (d, J=5.92 Hz, 1 H), 7.15 - 7.38 (m, 6 H), 4.20 (t, J=5.59 Hz, 2 H), 3.78 (br dd, J=8.99, 5.26 Hz, 1 H), 3.19 - 3.30 (m, 3 H), 2.25 (s, 6 H)

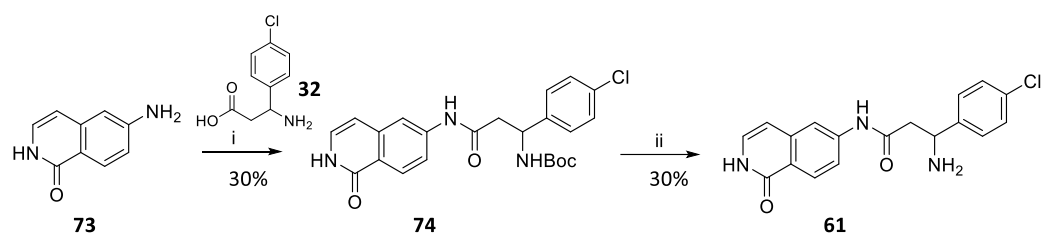
UPLC-MS Method 2: t_R= 4.14 min; MS (ESI): m/z 379.3 [M + H]⁺

UPLC Purity: 94%

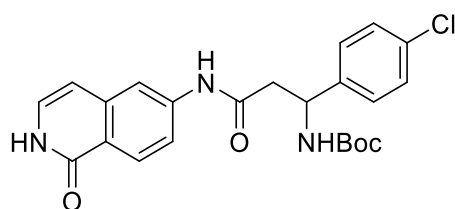
HRMS analysis: exp. 379.2130 (M+1), calc. 379.2129



6.7 Scheme 13



Tert-butyl (1-(4-chlorophenyl)-3-oxo-3-((1-oxo-1,2-dihydroisoquinolin-6-yl)amino)propyl)carbamate (74)



Intermediate **73** (500 mg, 3.12 mmol) was dissolved in Pyridine (10 ml) then **32** (1123 mg, 3.75 mmol) and POCl₃(0.545 ml, 5.85 mmol) were added and stirred at 0 °C.

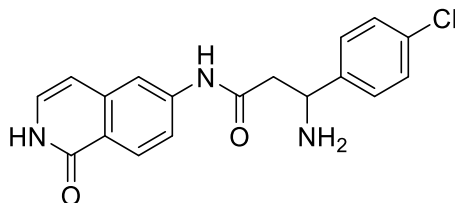
Then mixture was quenched with NaHCO₃ sat solution (20 mL) and extracted with EtOAc (20mL). Organic phase was washed once with H₂O (20mL) then evaporated under vacuum to give a yellow solid. Purification by flash chromatography on C-18 silica column, Biotage Isolera, SNAP 120 gr, by eluting with 0-100% B in A (A: water/acetonitrile 95/5 + 0.1% HCOOH, B: acetonitrile/water 95/5 + 0.1% HCOOH) yielded intermediate **74** in a 30% yield.

¹H NMR (400 MHz, DMSO-d₆) δ ppm 1.34 (br s, 10 H) 2.74 (br s, 1 H) 2.79 (br d, J=7.45 Hz, 1 H) 4.81 - 4.92 (m, 1 H) 4.98 - 5.08 (m, 1 H) 5.19 - 5.19 (m, 1H) 6.43 (d, J=7.02 Hz, 1 H) 7.05 - 7.16 (m, 1 H) 7.30 - 7.42 (m, 5 H) 7.43 - 7.51 (m, 1 H) 7.53 - 7.64 (m, 1 H) 7.94 (d, J=1.32 Hz, 1 H) 8.07 (d, J=8.55 Hz, 1H) 10.21 (s, 1 H) 11.05 (br d, J=5.26 Hz, 1 H)

UPLC-MS Method 1: t_R= 1.0 min; MS (ESI): m/z 342.3[M -100]⁺

UPLC-Purity: 94%

3-amino-3-(4-chlorophenyl)-N-(1-oxo-1,2-dihydroisoquinolin-6-yl)propenamide (61)



Intermediate **73** (140 mg, 0.317 mmol) was dissolved in 4M HCl Dioxane (4mL) and stirred at rt. After 1 hr, LC-MS showed reaction was complete. Solvent was evaporated under vacuum and crude was purified by flash on C-18 silica Sepachrom 12 gr column, Biotage Isolera, by eluting with 0-30% B in A (A: water/acetonitrile 95/5 + 0.1% HCOOH, B: acetonitrile/water 95/5 + 0.1% HCOOH). Purification yielded compound **61** in a 30% yield.

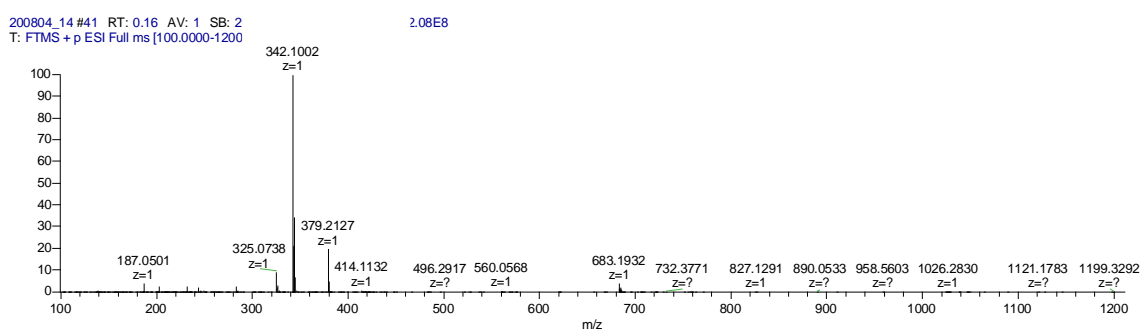
Fractions were combined and added of 25uL of HCL 37% mol to obtain the chloride salt.

$^1\text{H NMR}$ (400 MHz, DMSO- d_6) δ ppm 3.06 - 3.19 (m, 2 H) 4.76 (br s, 1 H) 6.43 (d, $J=7.02$ Hz, 1 H) 7.08 - 7.16 (m, 1 H) 7.47 - 7.62 (m, 5 H) 7.87 - 7.94 (m, 1 H) 8.05 - 8.12 (m, 1 H) 8.51 (br s, 2 H) 10.56 (s, 1 H) 11.10 (br d, $J=5.04$ Hz, 1 H)

UPLC-MS Method 2: $t_R= 3.4$ min; MS (ESI): m/z 342.2 $[\text{M} + \text{H}]^+$

UPLC-Purity: 99%

HRMS analysis: exp. 342.1002 ($\text{M}+1$), calc. 342.1004



7. Biological Assays

7.1 In vitro Inhibitory Activity Assay

The effectiveness of compounds to inhibit Rho kinase activity can be determined in a 10 μ l assay containing 40mM Tris pH7.5, 20mM MgCl₂ 0.1mg/ml BSA, 50 μ M DTT and 2.5 μ M peptide substrate (Myelin Basic Protein) using an ADP-Glo kit (Promega). Compounds were dissolved in DMSO such that the final concentration of DMSO was 1% in the assay. All reactions/incubations are performed at 25°C. Compound (2 μ l) and either Rho kinase 1 or 2 (4 μ l) were mixed and incubated for 30 mins. Reactions were initiated by addition of ATP (4 μ l) such that the final concentration of ATP in the assay was 200 μ M. After a 1 hour incubation 10 μ l of ADP-Glo Reagent was added and after a further 45 minute incubation 20 μ l of Kinase Detection Buffer was added and the mixture incubated for a further 30 minutes. The luminescent signal was measured on a luminometer. Controls consisted of assay wells that did not contain compound with background determined using assay wells with no enzyme added. Compounds were tested in dose-response format and the inhibition of kinase activity was calculated at each concentration of compound. To determine the IC₅₀ (concentration of compound required to inhibit 50% of the enzyme activity) data were fit to a plot of % inhibition vs Log₁₀ compound concentration using a sigmoidal fit with a variable slope and fixing the maximum to 100% and the minimum to 0%. To determine the K_i values the Cheng-Prusoff equation was utilized ($K_i = IC_{50} / (1 + [S] / K_m)$).

7.2 Cell-based Assay

This is an ELISA-based assay carried out using the MesoScale Discovery system. Pulmonary Artery Smooth Muscle Cells (PASMC) cells are incubated with test compound for 1 hour, lysed and then levels of phosphorylated MLC2 are assessed using MSD plate technology. MSD plates are supplied pre-coated with anti-rabbit Ig. After blocking, plates are coated with anti-phospho MLC2 (rabbit) capture antibody, and then washed before the addition of cell lysate, which is incubated overnight at 4°C. Plates are washed; an anti-MLC2 detection antibody (mouse) is added followed by an anti-mouse-Ig-Sulpho-tag secondary antibody. The resulting signal is read on the Mesoscale Sector S 600 machine and is proportional to the levels of pMLC2 present in the cell lysate.

% of Inhibition is equal to $100 - ((100 * (\text{sample} - \text{LC}) / (\text{HC} - \text{LC}))$ where LC is the mean of the blank low control values (PASMC cells treated with a known ROCK inhibitor) and HC is the mean of the high control values (PASMC cells treated with 0.3% DMSO). To determine the EC₅₀ a curve is fitted to the plot of % Inhibition vs Log₁₀ compound concentration using a sigmoidal fit with a variable slope. The top and the bottom of the curve are unconstrained.

8. Computational Methodologies

8.1 Prime Macrocycle Conformational Sampling (Prime-MCS)

For the evaluation of newly designed macrocycles through Prime-MCS see the experimental procedure reported in this paper: “Sindhikara, D.; Spronk, S. A.; Day, T.; Borrelli, K.; Cheney, D. L.; Posy, S. L. Improving Accuracy, Diversity, and Speed with Prime Macrocycle Conformational Sampling. *J. Chem. Inf. Model.* 2017, 57 (8), 1881–1894. <https://doi.org/10.1021/acs.jcim.7b00052>.

8.2 General Procedure for Docking Simulations

Docking simulations were performed using the crystal structure of human ROCK I in complex with ligand 17 (PDB ID: 3NDM). The X-ray structure was initially prepared with the Protein Preparation Wizard tool and then used as starting point for docking calculations with Glide, applying default settings. Ligand 3D structures were prepared with the LigPrep utility, generating all possible tautomeric and ionization states at physiological pH. To avoid potential biases related to the initial ligand geometry, up to 50 conformers were generated for each ligand state with ConfGenx and then docked within Glide grids. Only the best-ranked pose of each compound was selected for further analyses.

9. Crystal Structure Determination

Prismatic orangish crystals suitable for X-ray data collection were obtained from a THF/heptane solvent mixture. Crystal data and structure refinement for compound 40 are reported in the following table.

Crystal data and structure refinement for compound 40

Empirical formula	C ₄₇ H ₅₀ Cl ₂ N ₈ O ₇
Formula weight	909.85
Temperature/K	220.0
Crystal system	triclinic
Space group	P-1
a/Å	9.84414(11)
b/Å	13.32904(16)
c/Å	16.7462(2)
α/°	91.0137(10)
β/°	99.8500(10)
γ/°	98.6931(9)
Volume/Å ³	2137.91(4)
Z	2
ρ _{calc} /cm ³	1.413
μ/mm ⁻¹	0.216
F(000)	956.0
Crystal size/mm ³	0.22 × 0.07 × 0.05
Radiation	MoKα (λ = 0.71073)

2 θ range for data collection/° 3.872 to 51.352

Index ranges -11 \leq h \leq 11, -16 \leq k \leq 16, -18 \leq l \leq 20

Reflections collected 36576

Independent reflections 8070 [R_{int} = 0.0282, R_{sigma} = 0.0234]

Data/restraints/parameters 8070/14/610

Goodness-of-fit on F² 1.071

Final R indexes [$I \geq 2\sigma(I)$] R₁ = 0.0699, wR₂ = 0.2097

Final R indexes [all data] R₁ = 0.0719, wR₂ = 0.2112

Largest diff. peak/hole / e Å⁻³ 0.35/-0.60

Acknowledgements

First of all, I would like to sincerely thank Dr. Maurizio Delcanale for giving me the opportunity to carry out this Industrial PhD in the CRDD department.

Then, very special thanks to my Supervisor, Prof. Marinella Roberti, and my Co-supervisor, Dr. Fabio Rancati. They entirely guided and supported me in this exciting and enriching professional experience.

I would like also to thank all my friends and colleagues from CRDD department; especially Dr. Alessandro Accetta, Dr. Daniele Pala and Dr. Matteo Biagetti for their precious help and valuable advises.

I need also to thank people from other R&D departments whose contribution was essential for the realization of this research work: thanks to Dr. Tania Bellomi, Dr. Anna Maria Capelli, Dr. Irene Bassanetti, Dr. Elisa Moretti, Dr. Silvia Capacchi and to my friend, bandmate and colleague Dr. Fabrizio Facchinetti.

Particular thanks go to Dr. Greta Bagnolini who, with her helpfulness, always answered to my countless questions on UNIBO world.

A special thank also to the Barcelona “Amyloid Teams”, in particular to Natàlia, Montserrat and Silvia since they taught me to never give up and always fight for the things I care.

I am sincerely grateful to my friends and my family for their love and endless support.

Finally, my most heartfelt thanks go to Paolo who always stands with me and believes in me.

References

- (1) de la Torre, B. G.; Albericio, F. The Pharmaceutical Industry in 2019. An Analysis of FDA Drug Approvals from the Perspective of Molecules. *Molecules* **2020**, *25* (3). <https://doi.org/10.3390/molecules25030745>.
- (2) EZEKIEL J. EMANUEL. The Solution to Drug Prices. *New York Times* **2015**.
- (3) Brown, D. G. Where Do Recent Small Molecule Clinical Development Candidates Come From? **2018**. <https://doi.org/10.1021/acs.jmedchem.8b00675>.
- (4) Stocks, M.; Alcaraz, L.; Griffen, E. *On Medicinal Chemistry*; Sigma Aldrich, A., Ed.; 2007.
- (5) Perola, E. An Analysis of the Binding Efficiencies of Drugs and Their Leads in Successful Drug Discovery Programs. *J. Med. Chem.* **2010**, *53* (7), 2986–2997. <https://doi.org/10.1021/jm100118x>.
- (6) Goodnow, R. A. Hit and Lead Identification: Integrated Technology-Based Approaches. *Drug Discov. Today Technol.* **2006**, *3* (4), 367–375. <https://doi.org/10.1016/j.ddtec.2006.12.009>.
- (7) Favalli, N.; Bassi, G.; Scheuermann, J.; Neri, D. DNA-Encoded Chemical Libraries – Achievements and Remaining Challenges. *FEBS Lett.* **2018**, *592* (12), 2168–2180. <https://doi.org/10.1002/1873-3468.13068>.
- (8) Mannocci, L.; Leimbacher, M.; Wichert, M.; Scheuermann, J.; Neri, D. 20 Years of DNA-Encoded Chemical Libraries. *Chem. Commun.* **2011**, *47* (48), 12747–12753. <https://doi.org/10.1039/c1cc15634a>.
- (9) Bilous, I. A. B. A Market Review Of DNA-Encoded Libraries Technology In Drug Discovery. *BiopharmaTrend.com* **2019**.
- (10) Harris, P. A.; Berger, S. B.; Jeong, J. U.; Nagilla, R.; Bandyopadhyay, D.; Campobasso, N.; Capriotti, C. A.; Cox, J. A.; Dare, L.; Dong, X.; Eidam, P. M.; Finger, J. N.; Hoffman, S. J.; Kang, J.; Kasparcova, V.; King, B. W.; Lehr, R.; Lan, Y.; Leister, L. K.; Lich, J. D.; MacDonald, T. T.; Miller, N. A.; Ouellette, M. T.; Pao, C. S.; Rahman, A.; Reilly, M. A.; Rendina, A. R.; Rivera, E. J.; Schaeffer, M. C.; Sehon, C. A.; Singhaus, R. R.; Sun, H. H.; Swift, B. A.; Totoritis, R. D.; Vossenkämper, A.; Ward, P.; Wisnoski, D. D.; Zhang, D.; Marquis, R. W.; Gough, P. J.; Bertin, J. Discovery of a First-in-Class Receptor Interacting Protein 1 (RIP1) Kinase Specific Clinical Candidate (GSK2982772) for the Treatment of Inflammatory Diseases. *J. Med. Chem.* **2017**, *60* (4), 1247–1261. <https://doi.org/10.1021/acs.jmedchem.6b01751>.
- (11) Jörg, D. W. W. M. F. R. M. B. F. S. M. A. Z. Y. N. D. S. Automated Screening for Small Organic Ligands Using DNA-Encoded Chemical Libraries. *Nat. Protoc.* **2016**, *11* (4), 764–780. <https://doi.org/10.1038/nprot.2016.039>.
- (12) Scott, D. E.; Coyne, A. G.; Hudson, S. A.; Abell, C. Fragment-Based Approaches in Drug Discovery and Chemical Biology. *Biochemistry* **2012**, *51* (25), 4990–5003. <https://doi.org/10.1021/bi3005126>.

- (13) Erlanson, D. A.; de Esch, I. J. P.; Jahnke, W.; Johnson, C. N.; Mortenson, P. N. Fragment-to-Lead Medicinal Chemistry Publications in 2018. *J. Med. Chem.* **2020**, *63* (9), 4430–4444. <https://doi.org/10.1021/acs.jmedchem.9b01581>.
- (14) Kalyaanamoorthy, S.; Chen, Y. P. P. Structure-Based Drug Design to Augment Hit Discovery. *Drug Discov. Today* **2011**, *16* (17–18), 831–839. <https://doi.org/10.1016/j.drudis.2011.07.006>.
- (15) Batool, M.; Ahmad, B.; Choi, S. A Structure-Based Drug Discovery Paradigm. *Int. J. Mol. Sci.* **2019**, *20* (11). <https://doi.org/10.3390/ijms20112783>.
- (16) Mallinson, J.; Collins, I. Macrocycles in New Drug Discovery. *Future Med. Chem.* **2012**, *4* (11), 1409–1438. <https://doi.org/10.4155/fmc.12.93>.
- (17) Cummings, M. D.; Sekharan, S. Structure-Based Macrocyclic Design in Small-Molecule Drug Discovery and Simple Metrics to Identify Opportunities for Macrocyclization of Small-Molecule Ligands. *J. Med. Chem.* **2019**, *62* (15), 6843–6853. <https://doi.org/10.1021/acs.jmedchem.8b01985>.
- (18) Driggers, E. M.; Hale, S. P.; Lee, J.; Terrett, N. K. The Exploration of Macrocycles for Drug Discovery - An Underexploited Structural Class. *Nat. Rev. Drug Discov.* **2008**, *7* (7), 608–624. <https://doi.org/10.1038/nrd2590>.
- (19) Rezai, T.; Yu, B.; Millhauser, G. L.; Jacobson, M. P.; Lokey, R. S. Testing the Conformational Hypothesis of Passive Membrane Permeability Using Synthetic Cyclic Peptide Diastereomers. *J. Am. Chem. Soc.* **2006**, *128* (8), 2510–2511. <https://doi.org/10.1021/ja0563455>.
- (20) Tao, Z. F.; Wang, L.; Stewart, K. D.; Chen, Z.; Gu, W.; Bui, M. H.; Merta, P.; Zhang, H.; Kovar, P.; Johnson, E.; Park, C.; Judge, R.; Rosenberg, S.; Sowin, T.; Lin, N. H. Structure-Based Design, Synthesis, and Biological Evaluation of Potent and Selective Macrocyclic Checkpoint Kinase 1 Inhibitors. *J. Med. Chem.* **2007**, *50* (7), 1514–1527. <https://doi.org/10.1021/jm061247v>.
- (21) Corte, J. R.; Pinto, D. J. P.; Fang, T.; Osuna, H.; Yang, W.; Wang, Y.; Lai, A.; Clark, C. G.; Sun, J. H.; Rampulla, R.; Mathur, A.; Kaspady, M.; Neithnadka, P. R.; Li, Y. X. C.; Rossi, K. A.; Myers, J. E.; Sheriff, S.; Lou, Z.; Harper, T. W.; Huang, C.; Zheng, J. J.; Bozarth, J. M.; Wu, Y.; Wong, P. C.; Crain, E. J.; Seiffert, D. A.; Luetzgen, J. M.; Lam, P. Y. S.; Wexler, R. R.; Ewing, W. R. Potent, Orally Bioavailable, and Efficacious Macrocyclic Inhibitors of Factor XIa. Discovery of Pyridine-Based Macrocycles Possessing Phenylazole Carboxamide P1 Groups. *J. Med. Chem.* **2020**, *63* (2), 784–803. <https://doi.org/10.1021/acs.jmedchem.9b01768>.
- (22) Breslin, H. J.; Lane, B. M.; Ott, G. R.; Ghose, A. K.; Angeles, T. S.; Albom, M. S.; Cheng, M.; Wan, W.; Haltiwanger, R. C.; Wells-Knecht, K. J.; Dorsey, B. D. Design, Synthesis, and Anaplastic Lymphoma Kinase (ALK) Inhibitory Activity for a Novel Series of 2,4,8,22-Tetraazatetracyclo[14.3.1.1 3,7.1 9,13]Docosa-1(20),3(22),4,6,9(21),10,12,16,18-Nonaene Macrocycles. *J. Med. Chem.* **2012**, *55* (1), 449–464. <https://doi.org/10.1021/jm201333e>.
- (23) Johnson, T. W.; Richardson, P. F.; Bailey, S.; Brooun, A.; Burke, B. J.; Collins, M. R.; Cui, J. J.; Deal, J. G.; Deng, Y. L.; Dinh, D.; Engstrom, L. D.; He, M.; Hoffman, J.; Hoffman, R. L.; Huang,

- Q.; Kania, R. S.; Kath, J. C.; Lam, H.; Lam, J. L.; Le, P. T.; Lingardo, L.; Liu, W.; McTigue, M.; Palmer, C. L.; Sach, N. W.; Smeal, T.; Smith, G. L.; Stewart, A. E.; Timofeevski, S.; Zhu, H.; Zhu, J.; Zou, H. Y.; Edwards, M. P. Discovery of (10 R)-7-Amino-12-Fluoro-2,10,16-Trimethyl-15-Oxo-10,15,16,17-Tetrahydro-2H-8,4-(Metheno)Pyrazolo[4,3-h][2,5,11]-Benzoxadiazacyclotetradecine-3-Carbonitrile (PF-06463922), a Macrocyclic Inhibitor of Anaplastic Lymphoma Kinase (ALK) And . *J. Med. Chem.* **2014**, *57* (11), 4720–4744. <https://doi.org/10.1021/jm500261q>.
- (24) Engelhardt, H.; Bo, D.; Petronczki, M.; Scharn, D.; Bader, G.; Baum, A.; Bergner, A.; Chong, E.; Do, S.; Egger, G.; Engelhardt, C.; Etmayer, P.; Fuchs, J. E.; Gerstberger, T.; Gonnella, N.; Grimm, A.; Grondal, E.; Haddad, N.; Hopfgartner, B.; Kousek, R.; Krawiec, M.; Kriz, M.; Lamarre, L.; Leung, J.; Mayer, M.; Patel, N. D.; Simov, B. P.; Reeves, J. T.; Schnitzer, R.; Schrenk, A.; Sharps, B.; Solca, F.; Stadtmu, H.; Tan, Z.; Wunberg, T.; Zoephel, A.; Mcconnell, D. B. Start Selective and Rigidify: The Discovery Path toward a Next Generation of EGFR Tyrosine Kinase Inhibitors. **2019**. <https://doi.org/10.1021/acs.jmedchem.9b01169>.
- (25) Qian, Z.; Dougherty, P. G.; Pei, D. Chemical Approaches to Macrocyclic Libraries. *Pract. Med. Chem. with Macrocycles* **2017**, 133–154. <https://doi.org/10.1002/9781119092599.ch6>.
- (26) Sindhikara, D.; Spronk, S. A.; Day, T.; Borrelli, K.; Cheney, D. L.; Posy, S. L. Improving Accuracy, Diversity, and Speed with Prime Macrocyclic Conformational Sampling. *J. Chem. Inf. Model.* **2017**, *57* (8), 1881–1894. <https://doi.org/10.1021/acs.jcim.7b00052>.
- (27) Rosenquist, Å.; Samuelsson, B.; Johansson, P. O.; Cummings, M. D.; Lenz, O.; Raboisson, P.; Simmen, K.; Vendeville, S.; De Kock, H.; Nilsson, M.; Horvath, A.; Kalmeijer, R.; De La Rosa, G.; Beumont-Mauviel, M. Discovery and Development of Simeprevir (TMC435), a HCV NS3/4A Protease Inhibitor. *J. Med. Chem.* **2014**, *57* (5), 1673–1693. <https://doi.org/10.1021/jm401507s>.
- (28) World Health Organization (WHO). Chronic respiratory diseases https://www.who.int/health-topics/chronic-respiratory-diseases#tab=tab_1.
- (29) Cukic, V.; Lovre, V.; Dragisic, D.; Ustamujic, A. Asthma and Chronic Obstructive Pulmonary Disease (COPD) and #8211; Differences and Similarities. *Mater. Socio Medica* **2012**, *24* (2), 100. <https://doi.org/10.5455/msm.2012.24.100-105>.
- (30) Barnes, P. J. Kinases as Novel Therapeutic Targets in Asthma and Chronic Obstructive Pulmonary Disease. *Pharmacol. Rev.* **2016**, *68* (3), 788–815. <https://doi.org/10.1124/pr.116.012518>.
- (31) Chung, K. F.; Wenzel, S. E.; Brozek, J. L.; Bush, A.; Castro, M.; Sterk, P. J.; Adcock, I. M.; Bateman, E. D.; Bel, E. H.; Bleecker, E. R.; Boulet, L. P.; Brightling, C.; Chanez, P.; Dahlen, S. E.; Djukanovic, R.; Frey, U.; Gaga, M.; Gibson, P.; Hamid, Q.; Jajour, N. N.; Mauad, T.; Sorkness, R. L.; Teague, W. G. International ERS/ATS Guidelines on Definition, Evaluation and Treatment of Severe Asthma. *Eur. Respir. J.* **2014**, *43* (2), 343–373. <https://doi.org/10.1183/09031936.00202013>.
- (32) Piuvezam, M. R.; Ferreira, L. K. D. P.; Monteiro, T. M.; Vieira, G. C.; Bezerra-Santos, C. R. Severe

Asthma: Updated Therapy Approach Based on Phenotype and Biomarker. *Asthma Diagnosis Manag. - Approach Based Phenotype Endotype* **2018**.
<https://doi.org/10.5772/intechopen.74775>.

- (33) Busse, W. W. Biological Treatments for Severe Asthma: A Major Advance in Asthma Care. *Allergol. Int.* **2019**, *68* (2), 158–166. <https://doi.org/10.1016/j.alit.2019.01.004>.
- (34) Stokes, J. R.; Casale, T. B. Characterization of Asthma Endotypes: Implications for Therapy. *Ann. Allergy, Asthma Immunol.* **2016**, *117* (2), 121–125. <https://doi.org/10.1016/j.anai.2016.05.016>.
- (35) Barnes, P. J.; Shapiro, S. D.; Pauwels, R. A. Chronic Obstructive Pulmonary Disease: Molecular and Cellular Mechanisms. *Eur. Respir. J.* **2003**, *22* (4), 672–688. <https://doi.org/10.1183/09031936.03.00040703>.
- (36) Barnes, P. J. Inflammatory Endotypes in COPD. *Allergy Eur. J. Allergy Clin. Immunol.* **2019**, *74* (7), 1249–1256. <https://doi.org/10.1111/all.13760>.
- (37) Montuschi, P. Pharmacological Treatment of Chronic Obstructive Pulmonary Disease. **2006**, *1* (4), 409–423.
- (38) Marwick, J. A.; Caramori, G.; Casolari, P.; Mazzoni, F.; Kirkham, P. A.; Adcock, I. M.; Chung, K. F.; Papi, A. A Role for Phosphoinositol 3-Kinase δ in the Impairment of Glucocorticoid Responsiveness in Patients with Chronic Obstructive Pulmonary Disease. *J. Allergy Clin. Immunol.* **2010**, *125* (5), 1146–1153. <https://doi.org/10.1016/j.jaci.2010.02.003>.
- (39) Ito, K.; Caramori, G.; Adcock, I. M. Therapeutic Potential of Phosphatidylinositol 3-Kinase Inhibitors in Inflammatory Respiratory Disease. *J. Pharmacol. Exp. Ther.* **2007**, *321* (1), 1–8. <https://doi.org/10.1124/jpet.106.111674>.
- (40) Okkenhaug, K.; Bilancio, A.; Farjot, G.; Priddle, H.; Sancho, S.; Peskett, E.; Pearce, W.; Meek, S. E.; Salpekar, A.; Waterfield, M. D.; Smith, A. J. H.; Vanhaesebroeck, B. Impaired B and T Cell Antigen Receptor Signaling in P110 δ PI 3-Kinase Mutant Mice. *Science (80-.)*. **2002**, *297* (5583), 1031–1034. <https://doi.org/10.1126/science.1073560>.
- (41) Ali, K. Essential Role for the P110 Delta Phosphoinositide 3-Kinase. *Nature* **2004**, *752* (2000), 1007–1011.
- (42) Lee, K. S.; Lee, H. K.; Hayflick, J. S.; Lee, Y. C.; Puri, K. D. Inhibition of Phosphoinositide 3-kinase δ Attenuates Allergic Airway Inflammation and Hyperresponsiveness in Murine Asthma Model. *FASEB J.* **2006**, *20* (3), 455–465. <https://doi.org/10.1096/fj.05-5045com>.
- (43) Puri, K. D.; Doggett, T. A.; Douangpanya, J.; Hou, Y.; Tino, W. T.; Wilson, T.; Graf, T.; Clayton, E.; Turner, M.; Hayflick, J. S.; Diacovo, T. G. Mechanisms and Implications of Phosphoinositide 3-Kinase δ in Promoting Neutrophil Trafficking into Inflamed Tissue. *Blood* **2004**, *103* (9), 3448–3456. <https://doi.org/10.1182/blood-2003-05-1667>.
- (44) Barnes, P. J. Mechanisms and Resistance in Glucocorticoid Control of Inflammation. *J. Steroid*

Biochem. Mol. Biol. **2010**, *120* (2–3), 76–85. <https://doi.org/10.1016/j.jsbmb.2010.02.018>.

- (45) Koziol-White, C. J.; Yoo, E. J.; Cao, G.; Zhang, J.; Papanikolaou, E.; Pushkarsky, I.; Andrews, A.; Himes, B. E.; Damoiseaux, R. D.; Liggett, S. B.; Di Carlo, D.; Kurten, R. C.; Panettieri, R. A. Inhibition of PI3K Promotes Dilatation of Human Small Airways in a Rho Kinase-Dependent Manner. *Br. J. Pharmacol.* **2016**, 2726–2738. <https://doi.org/10.1111/bph.13542>.
- (46) Vanhaesebroeck, B.; Leever, S. J.; Timms, J.; Katso, R.; Driscoll, P. C.; Woscholski, R.; Parker, P. J.; Michael, D. 3- Phosphorylated Inositol Lipids. *In Vivo (Brooklyn)*. **2001**, 535–602.
- (47) Lorenzen, A.; Schwabe, U. P1 Receptors. *Purinergic Pyrimidinergetic Signal. I* **2001**, 19–45. https://doi.org/10.1007/978-3-662-09604-8_2.
- (48) Foster, F. M.; Traer, C. J.; Abraham, S. M.; Fry, M. J. The Phosphoinositide (PI) 3-Kinase Family. *J. Cell Sci.* **2003**, *116* (15), 3037–3040. <https://doi.org/10.1242/jcs.00609>.
- (49) Vanhaesebroeck, B.; Guillermet-Guibert, J.; Graupera, M.; Bilanges, B. The Emerging Mechanisms of Isoform-Specific PI3K Signalling. *Nat. Rev. Mol. Cell Biol.* **2010**, *11* (5), 329–341. <https://doi.org/10.1038/nrm2882>.
- (50) Steven T. Staben. Isoform Selective PI3K Inhibitors for Treating Cancer. *Top Med Chem* **2018**, *28* (July), 333–370. <https://doi.org/10.1007/7355>.
- (51) Vanhaesebroeck, B.; Leever, S. J.; Panayotou, G.; Waterfield, M. D.; Waterfield, M. D. Phosphoinositide 3-Kinases: A Conserved Family of Signal Transducers. *Trends Biochem. Sci.* **1997**, *22* (7), 267–272. [https://doi.org/10.1016/S0968-0004\(97\)01061-X](https://doi.org/10.1016/S0968-0004(97)01061-X).
- (52) Sword, A. D.; Shintani, T.; Klionsky, D. J. REVIEW Autophagy in Health and Disease : **2004**, *306* (November), 990–996.
- (53) Vanhaesebroeck, B.; Welham, M. J.; Kotani, K.; Stein, R.; Warne, P. H.; Zvelebil, M. J.; Higashi, K.; Volinia, S.; Downward, J.; Waterfield, M. D. P110 δ , A Novel Phosphoinositide 3-Kinase in Leukocytes. *Proc. Natl. Acad. Sci. U. S. A.* **1997**, *94* (9), 4330–4335. <https://doi.org/10.1073/pnas.94.9.4330>.
- (54) Kriplani, N.; Hermida, M. A.; Brown, E. R.; Leslie, N. R. Class I PI 3-Kinases: Function and Evolution. *Adv. Biol. Regul.* **2015**, *59*, 53–64. <https://doi.org/10.1016/j.jbior.2015.05.002>.
- (55) Marwick, J. A.; Chung, K. F.; Adcock, I. M. Phosphatidylinositol 3-Kinase Isoforms as Targets in Respiratory Disease. *Ther. Adv. Respir. Dis.* **2010**, *4* (1), 19–34. <https://doi.org/10.1177/1753465809352792>.
- (56) Knight, Z. A.; Gonzalez, B.; Feldman, M. E.; Zunder, E. R.; David, D.; Williams, O.; Loewith, R.; Stokoe, D.; Balla, A.; Balla, T.; Weiss, W. A.; Williams, R. L.; Shokat, K. M. A Pharmacological Map of the PI3-K Family Defines a Role for P110 α in Insulin Signaling. *Cell.* **2010**, *125* (4), 733–747. <https://doi.org/10.1016/j.cell.2006.03.035.A>.
- (57) Jackson, S. P.; Schoenwaelder, S. M.; Goncalves, I.; Nesbitt, W. S.; Yap, C. L.; Wright, C. E.;

- Kenche, V.; Anderson, K. E.; Dopheide, S. M.; Yuan, Y.; Sturgeon, S. A.; Prabakaran, H.; Thompson, P. E.; Smith, G. D.; Shepherd, P. R.; Daniele, N.; Kulkarni, S.; Abbott, B.; Saylik, D.; Jones, C.; Lu, L.; Giuliano, S.; Hughan, S. C.; Angus, J. A.; Robertson, A. D.; Salem, H. H. PI 3-Kinase P110 β : A New Target for Antithrombotic Therapy. *Nat. Med.* **2005**, *11* (5), 507–514. <https://doi.org/10.1038/nm1232>.
- (58) Kok, K.; Geering, B.; Vanhaesebroeck, B. Regulation of Phosphoinositide 3-Kinase Expression in Health and Disease. *Trends Biochem. Sci.* **2009**, *34* (3), 115–127. <https://doi.org/10.1016/j.tibs.2009.01.003>.
- (59) Edward H. Walker*, Olga Perisic*, Christian Ried*, L. S. & R. L. W. Structural Insights into Phosphoinositide 3-Kinase Catalysis and Signalling. **1999**, *944* (1995), 313–320.
- (60) Huang, C. H.; Mandelker, D.; Schmidt-Kittler, O.; Samuels, Y.; Velculescu, V. E.; Kinzler, K. W.; Vogelstein, B.; Gabelli, S. B.; Amzel, L. M. The Structure of a Human P110 α /P85 α Complex Elucidates the Effects of Oncogenic PI3K α Mutations. *Science* (80-.). **2007**, *318* (5857), 1744–1748. <https://doi.org/10.1126/science.1150799>.
- (61) Zanto, T. P.; Hennigan, K.; Östberg, M.; Clapp, W. C.; Gazzaley, A. Structural Comparisons of Class I Phosphoinositide 3-Kinases. *Nat Rev Cancer* **2008**, *46* (4), 665–669. <https://doi.org/10.1016/j.cortex.2009.08.003>. Predictive.
- (62) Walker, E. H.; Pacold, M. E.; Perisic, O.; Stephens, L.; Hawkins, P. T.; Wymann, M. P.; Williams, R. L. Structural Determinants of Phosphoinositide 3-Kinase Inhibition by Wortmannin, LY294002, Quercetin, Myricetin, and Staurosporine. *Mol. Cell* **2000**, *6* (4), 909–919. [https://doi.org/10.1016/S1097-2765\(05\)00089-4](https://doi.org/10.1016/S1097-2765(05)00089-4).
- (63) Berndt, A.; Miller, S.; Williams, O.; Le, D. D.; Houseman, B. T.; Pacold, J. I.; Gorrec, F.; Hon, W. C.; Liu, Y.; Rommel, C.; Gaillard, P.; Rückle, T.; Schwarz, M. K.; Shokat, K. M.; Shaw, J. P.; Williams, R. L. The P110 δ Structure: Mechanisms for Selectivity and Potency of New PI(3)K Inhibitors. *Nat. Chem. Biol.* **2010**, *6* (2), 117–124. <https://doi.org/10.1038/nchembio.293>.
- (64) Williams, R.; Berndt, A.; Miller, S.; Hon, W. C.; Zhang, X. Form and Flexibility in Phosphoinositide 3-Kinases. *Biochem. Soc. Trans.* **2009**, *37* (4), 615–626. <https://doi.org/10.1042/BST0370615>.
- (65) Miller, M. S.; Thompson, P. E.; Gabelli, S. B. Structural Determinants of Isoform Selectivity in PI3k Inhibitors. *Biomolecules* **2019**, *9* (3), 1–34. <https://doi.org/10.3390/biom9030082>.
- (66) Somoza, J. R.; Koditek, D.; Villaseñor, A. G.; Novikov, N.; Wong, M. H.; Licican, A.; Xing, W.; Lagpacan, L.; Wang, R.; Schultz, B. E.; Papalia, G. A.; Samuel, D.; Lad, L.; McGrath, M. E. Structural, Biochemical, and Biophysical Characterization of Idelalisib Binding to Phosphoinositide 3-Kinase δ . *J. Biol. Chem.* **2015**, *290* (13), 8439–8446. <https://doi.org/10.1074/jbc.M114.634683>.
- (67) Zheng, Z.; Miller, M. S.; Jennings, I. G.; Thompson, P. E. Mechanisms of PI3K β -Selective Inhibition Revealed by Reciprocal Mutagenesis. *ACS Chem. Biol.* **2013**, *8* (4), 679–683. <https://doi.org/10.1021/cb300666s>.

- (68) Garces, A. E.; Stocks, M. J. Class 1 PI3K Clinical Candidates and Recent Inhibitor Design Strategies: A Medicinal Chemistry Perspective. *J. Med. Chem.* **2019**, *62* (10), 4815–4850. <https://doi.org/10.1021/acs.jmedchem.8b01492>.
- (69) Cushing, T. D.; Metz, D. P.; Whittington, D. A.; McGee, L. R. PI3K δ and PI3K γ as Targets for Autoimmune and Inflammatory Diseases. *J. Med. Chem.* **2012**, *55* (20), 8559–8581. <https://doi.org/10.1021/jm300847w>.
- (70) Perry, M. W. D.; Abdulai, R.; Mogemark, M.; Petersen, J.; Thomas, M. J.; Valastro, B.; Westin Eriksson, A. Evolution of PI3K γ and Δ inhibitors for Inflammatory and Autoimmune Diseases. *J. Med. Chem.* **2019**, *62* (10), 4783–4814. <https://doi.org/10.1021/acs.jmedchem.8b01298>.
- (71) Erra, M.; Taltavull, J.; Bernal, F. J.; Caturla, J. F.; Carrascal, M.; Pagès, L.; Mir, M.; Espinosa, S.; Gràcia, J.; Domínguez, M.; Sabaté, M.; Paris, S.; Maldonado, M.; Hernández, B.; Bravo, M.; Calama, E.; Miralpeix, M.; Lehner, M. D.; Calbet, M. Discovery of a Novel Inhaled PI3K δ Inhibitor for the Treatment of Respiratory Diseases. *J. Med. Chem.* **2018**, *61* (21), 9551–9567. <https://doi.org/10.1021/acs.jmedchem.8b00873>.
- (72) Sutherlin, D. P.; Baker, S.; Bisconte, A.; Blaney, P. M.; Brown, A.; Chan, B. K.; Chantry, D.; Castanedo, G.; Depledge, P.; Goldsmith, P.; Goldstein, D. M.; Hancox, T.; Kaur, J.; Knowles, D.; Kondru, R.; Lesnick, J.; Lucas, M. C.; Lewis, C.; Murray, J.; Nadin, A. J.; Nonomiya, J.; Pang, J.; Pegg, N.; Price, S.; Reif, K.; Safina, B. S.; Salphati, L.; Staben, S.; Seward, E. M.; Shuttleworth, S.; Sohal, S.; Sweeney, Z. K.; Ultsch, M.; Waszkowycz, B.; Wei, B. Potent and Selective Inhibitors of PI3K δ : Obtaining Isoform Selectivity from the Affinity Pocket and Tryptophan Shelf. *Bioorganic Med. Chem. Lett.* **2012**, *22* (13), 4296–4302. <https://doi.org/10.1016/j.bmcl.2012.05.027>.
- (73) Hoegenauer, K.; Soldermann, N.; Zécéri, F.; Strang, R. S.; Graveleau, N.; Wolf, R. M.; Cooke, N. G.; Smith, A. B.; Hollingworth, G. J.; Blanz, J.; Gutmann, S.; Rummel, G.; Littlewood-Evans, A.; Burkhart, C. Discovery of CDZ173 (Leniolisib), Representing a Structurally Novel Class of PI3K Delta-Selective Inhibitors. *ACS Med. Chem. Lett.* **2017**, *8* (9), 975–980. <https://doi.org/10.1021/acsmedchemlett.7b00293>.
- (74) Down, K.; Amour, A.; Baldwin, I. R.; Cooper, A. W. J.; Deakin, A. M.; Felton, L. M.; Guntrip, S. B.; Hardy, C.; Harrison, Z. A.; Jones, K. L.; Jones, P.; Keeling, S. E.; Le, J.; Livia, S.; Lucas, F.; Lunniss, C. J.; Parr, N. J.; Robinson, E.; Rowland, P.; Smith, S.; Thomas, D. A.; Vitulli, G.; Washio, Y.; Hamblin, J. N. Optimization of Novel Indazoles as Highly Potent and Selective Inhibitors of Phosphoinositide 3-Kinase δ for the Treatment of Respiratory Disease. *J. Med. Chem.* **2015**, *58* (18), 7381–7399. <https://doi.org/10.1021/acs.jmedchem.5b00767>.
- (75) Marandi, Y.; Farahi, N.; Hashjin, G. S. Asthma: Beyond Corticosteroid Treatment. *Arch. Med. Sci.* **2013**, *9* (3), 521–526. <https://doi.org/10.5114/aoms.2013.33179>.
- (76) Chung, C. R.; Han, H. J.; Puri, K. D.; Lee, Y. C. In a Murine Asthma Model. **2010**, *36* (6), 1448–1459. <https://doi.org/10.1183/09031936.00106609>.
- (77) Nagarajan, S.; Skoufias, D. A.; Kozielski, F.; Pae, A. N. Receptor-Ligand Interaction-Based Virtual Screening for Novel Eg5/Kinesin Spindle Protein Inhibitors. *J. Med. Chem.* **2012**, *55* (6),

2561–2573. <https://doi.org/10.1021/jm201290v>.

- (78) Kr, K. R.; Regents, O. F. Wo 2008/030744 A2. **2008**, No. 12.
- (79) MORTENSEN, Deborah, Sue;MEDEROS, Maria Mercedes, Delgado;SAPIENZA, John, Joseph;ALBERS, Ronald, J.;LEE, Branden, G.;HUANG, Dehua;SCHWARZ, Kimberly, Lyn;PARNES, Jason, Simon;RIGGS, Jennifer, R.;PAPA, Patrick, W. HETEROARYL COMPOUNDS, COMPOSITIONS THEREOF, AND USE THEREOF AS PROTEIN KINASE INHIBITORS, 2008.
- (80) Folkes, A. J.; Ahmadi, K.; Alderton, W. K.; Alix, S.; Baker, S. J.; Box, G.; Chuckowree, I. S.; Clarke, P. A.; Depledge, P.; Eccles, S. A.; Friedman, L. S.; Hayes, A.; Hancox, T. C.; Kugendradas, A.; Lensun, L.; Moore, P.; Olivero, A. G.; Pang, J.; Patel, S.; Pergl-Wilson, G. H.; Raynaud, F. I.; Robson, A.; Saghir, N.; Salphati, L.; Sohal, S.; Ultsch, M. H.; Valenti, M.; Wallweber, H. J. A.; Nan, C. W.; Wiesmann, C.; Workman, P.; Zhyvoloup, A.; Zvelebil, M. J.; Shuttleworth, S. J. The Identification of 2-(1H-Indazol-4-Yl)-6-(4-Methanesulfonyl-Piperazin-1- Ylmethyl)-4-Morpholin-4-Yl-Thieno[3,2-d]Pyrimidine (GDC-0941) as a Potent, Selective, Orally Bioavailable Inhibitor of Class I PI3 Kinase for the Treatment of Cancer. *J. Med. Chem.* **2008**, *51* (18), 5522–5532. <https://doi.org/10.1021/jm800295d>.
- (81) Booth, B. L.; Dias, A. M.; Proença, M. F.; Zaki, M. E. A. The Reactions of Diaminomaleonitrile with Isocyanates and Either Aldehydes or Ketones Revisited. *J. Org. Chem.* **2001**, *66* (25), 8436–8441. <https://doi.org/10.1021/jo010595w>.
- (82) Yung-Chi, C.; Prusoff, W. H. Relationship between the Inhibition Constant (KI) and the Concentration of Inhibitor Which Causes 50 per Cent Inhibition (I50) of an Enzymatic Reaction. *Biochem. Pharmacol.* **1973**, *22* (23), 3099–3108. [https://doi.org/10.1016/0006-2952\(73\)90196-2](https://doi.org/10.1016/0006-2952(73)90196-2).
- (83) Lovering, F.; Bikker, J.; Humblet, C. Escape from Flatland: Increasing Saturation as an Approach to Improving Clinical Success. *J. Med. Chem.* **2009**, *52* (21), 6752–6756. <https://doi.org/10.1021/jm901241e>.
- (84) Barreiro, E. J.; Kümmerle, A. E.; Fraga, C. A. M. The Methylation Effect in Medicinal Chemistry. *Chem. Rev.* **2011**, *111* (9), 5215–5246. <https://doi.org/10.1021/cr200060g>.
- (85) Ishikawa, M.; Hashimoto, Y. Improvement in Aqueous Solubility in Small Molecule Drug Discovery Programs by Disruption of Molecular Planarity and Symmetry. *J. Med. Chem.* **2011**, *54* (6), 1539–1554. <https://doi.org/10.1021/jm101356p>.
- (86) Feng, Y.; Lograsso, P. V.; Defert, O.; Li, R. Rho Kinase (ROCK) Inhibitors and Their Therapeutic Potential. *J. Med. Chem.* **2016**, *59* (6), 2269–2300. <https://doi.org/10.1021/acs.jmedchem.5b00683>.
- (87) Nakagawa, O.; Fujisawa, K.; Ishizaki, T.; Saito, Y.; Nakao, K.; Narumiya, S. ROCK-I and ROCK-II, Two Isoforms of Rho-Associated Coiled-Coil Forming Protein Serine/Threonine Kinase in Mice. *FEBS Lett.* **1996**, *392* (2), 189–193. [https://doi.org/10.1016/0014-5793\(96\)00811-3](https://doi.org/10.1016/0014-5793(96)00811-3).
- (88) Riento, K.; Ridley, A. J. Rocks: Multifunctional Kinases in Cell Behaviour. *Nat. Rev. Mol. Cell*

Biol. **2003**, 4 (6), 446–456. <https://doi.org/10.1038/nrm1128>.

- (89) Matsui, T.; Amano, M.; Yamamoto, T.; Chihara, K.; Nakafuku, M.; Ito, M.; Nakano, T.; Okawa, K.; Iwamatsu, A.; Kaibuchi, K. Rho-Associated Kinase, a Novel Serine/Threonine Kinase, as a Putative Target for Small GTP Binding Protein Rho. *EMBO J.* **1996**, 15 (9), 2208–2216. <https://doi.org/10.1002/j.1460-2075.1996.tb00574.x>.
- (90) Fukumoto, Y.; Shimokawa, H. Rho-Kinase Inhibitors. *Handb. Exp. Pharmacol.* **2013**, 218 (1), 351–363. <https://doi.org/10.1007/978-3-642-38664-0-14>.
- (91) Shimokawa, H.; Sunamura, S.; Satoh, K. RhoA/Rho-Kinase in the Cardiovascular System. *Circ. Res.* **2016**, 118 (2), 352–366. <https://doi.org/10.1161/CIRCRESAHA.115.306532>.
- (92) Wirth, A. Rho Kinase and Hypertension. *Biochim. Biophys. Acta - Mol. Basis Dis.* **2010**, 1802 (12), 1276–1284. <https://doi.org/10.1016/j.bbadis.2010.05.002>.
- (93) Fernandes, L. B.; Henry, P. J.; Goldie, R. G. Review: Rho Kinase as a Therapeutic Target in the Treatment of Asthma and Chronic Obstructive Pulmonary Disease. *Ther. Adv. Respir. Dis.* **2007**, 1 (1), 25–33. <https://doi.org/10.1177/1753465807080740>.
- (94) Chiba, Y.; Matsusue, K.; Misawa, M. RhoA, a Possible Target for Treatment of Airway Hyperresponsiveness in Bronchial Asthma. *J. Pharmacol. Sci.* **2010**, 114 (3), 239–247. <https://doi.org/10.1254/jphs.10R03CR>.
- (95) Sanderson, M. J.; Delmotte, P.; Bai, Y.; Perez-Zogbhi, J. F. Regulation of Airway Smooth Muscle Cell Contractility by Ca²⁺ Signaling and Sensitivity. *Proc. Am. Thorac. Soc.* **2008**, 5 (1), 23–31. <https://doi.org/10.1513/pats.200704-050VS>.
- (96) Ai, S.; Kuzuya, M.; Koike, T.; Asai, T.; Kanda, S.; Maeda, K.; Shibata, T.; Iguchi, A. Rho-Rho Kinase Is Involved in Smooth Muscle Cell Migration through Myosin Light Chain Phosphorylation-Dependent and Independent Pathways. *Atherosclerosis* **2001**, 155 (2), 321–327. [https://doi.org/10.1016/S0021-9150\(00\)00585-2](https://doi.org/10.1016/S0021-9150(00)00585-2).
- (97) Tang, L.; Dai, F.; Liu, Y.; Yu, X.; Huang, C.; Wang, Y.; Yao, W. RhoA/ROCK Signaling Regulates Smooth Muscle Phenotypic Modulation and Vascular Remodeling via the JNK Pathway and Vimentin Cytoskeleton. *Pharmacol. Res.* **2018**, 133 (January), 201–212. <https://doi.org/10.1016/j.phrs.2018.05.011>.
- (98) Vaidya, B.; Pangallo, M.; Ruffenach, G.; Cunningham, C. M.; Perron, J. C.; Kolluru, S.; Eghbali, M.; Gupta, V. Advances in Treatment of Pulmonary Arterial Hypertension: Patent Review. *Expert Opin. Ther. Pat.* **2017**, 27 (8), 907–918. <https://doi.org/10.1080/13543776.2017.1313232>.
- (99) Galiè, N.; Humbert, M.; Vachiery, J. L.; Gibbs, S.; Lang, I.; Torbicki, A.; Simonneau, G.; Peacock, A.; Vonk Noordegraaf, A.; Beghetti, M.; Ghofrani, A.; Gomez Sanchez, M. A.; Hansmann, G.; Klepetko, W.; Lancellotti, P.; Matucci, M.; McDonagh, T.; Pierard, L. A.; Trindade, P. T.; Zompatori, M.; Hoeper, M.; Aboyans, V.; Vaz Carneiro, A.; Achenbach, S.; Agewall, S.; Allanore, Y.; Asteggiano, R.; Paolo Badano, L.; Albert Barberà, J.; Bouvaist, H.; Bueno, H.;

Byrne, R. A.; Carerj, S.; Castro, G.; Erol, Ç.; Falk, V.; Funck-Brentano, C.; Gorenflo, M.; Granton, J.; lung, B.; Kiely, D. G.; Kirchhof, P.; Kjellstrom, B.; Landmesser, U.; Lekakis, J.; Lionis, C.; Lip, G. Y. H.; Orfanos, S. E.; Park, M. H.; Piepoli, M. F.; Ponikowski, P.; Revel, M. P.; Rigau, D.; Rosenkranz, S.; Völler, H.; Luis Zamorano, J.; Myftiu, S.; Bonderman, D.; Firdovsi, I.; Lazareva, I.; De Pauw, M.; Sokolović, Š.; Velchev, V.; Čikeš, M.; Moutiris, J. A.; Jansa, P.; Nielsen-Kudsk, J. E.; Anton, L.; Jääskeläinen, P.; Bauer, F.; Chukhruidze, A.; Opitz, C.; Giannakoulas, G.; Karlócai, K.; Oddsson, H.; Gaine, S.; Menachemi, D.; Emdin, M.; Sooronbaev, T.; Rudzītis, A.; Gumbiene, L.; Lebrun, F.; Micallef, J.; Botnaru, V.; Oukerraj, L.; Andreassen, A. K.; Kurzyna, M.; Leite Baptista, M. J. R.; Coman, I. M.; Moiseeva, O.; Stefanović, B. S.; Šimková, I.; Wikström, G.; Schwerzmann, M.; Srbinovska-Kostovska, E.; van Dijk, A. P. J.; Mahdhaoui, A.; Kaymaz, C.; Coghlan, G.; Sirenko, Y. 2015 ESC/ERS Guidelines for the Diagnosis and Treatment of Pulmonary Hypertension. *Eur. Heart J.* **2016**, *37* (1), 67–119. <https://doi.org/10.1093/eurheartj/ehv317>.

- (100) Ranchoux, B.; Harvey, L. D.; Ayon, R. J.; Babicheva, A.; Bonnet, S.; Chan, S. Y.; Yuan, J. X. J.; Perez, V. de J. Endothelial Dysfunction in Pulmonary Arterial Hypertension: An Evolving Landscape (2017 Grover Conference Series). *Pulm. Circ.* **2018**, *8* (1). <https://doi.org/10.1177/2045893217752912>.
- (101) Hu, J.; Xu, Q.; McTiernan, C.; Lai, Y. C.; Osei-Hwedieh, D.; Gladwin, M. Novel Targets of Drug Treatment for Pulmonary Hypertension. *Am. J. Cardiovasc. Drugs* **2015**, *15* (4), 225–234. <https://doi.org/10.1007/s40256-015-0125-4>.
- (102) Boucherat, O.; Vitry, G.; Trinh, I.; Paulin, R.; Provencher, S.; Bonnet, S. The Cancer Theory of Pulmonary Arterial Hypertension. *Pulm. Circ.* **2017**, *7* (2), 285–299. <https://doi.org/10.1177/2045893217701438>.
- (103) Summary, A. P. Drugs in Clinical Development for Pulmonary Hypertension: Summary and Table. *Pharmaceut. Med.* **2015**, *29* (3), 179–182. <https://doi.org/10.1007/s40290-015-0100-z>.
- (104) Oka, M.; Fagan, K. A.; Jones, P. L.; McMurtry, I. F. Therapeutic Potential of RhoA/Rho Kinase Inhibitors in Pulmonary Hypertension. *Br. J. Pharmacol.* **2008**, *155* (4), 444–454. <https://doi.org/10.1038/bjp.2008.239>.
- (105) Antoniu, S. A. Targeting RhoA/ROCK Pathway in Pulmonary Arterial Hypertension. *Expert Opin. Ther. Targets* **2012**, *16* (4), 355–363. <https://doi.org/10.1517/14728222.2012.671811>.
- (106) O’Callaghan, D. S.; Savale, L.; Montani, D.; Jaïs, X.; Sitbon, O.; Simonneau, G.; Humbert, M. Treatment of Pulmonary Arterial Hypertension with Targeted Therapies. *Nat. Rev. Cardiol.* **2011**, *8* (9), 526–538. <https://doi.org/10.1038/nrcardio.2011.104>.
- (107) Hensley, M. K.; Levine, A.; Gladwin, M. T.; Lai, Y. C. Emerging Therapeutics in Pulmonary Hypertension. *Am. J. Physiol. Lung Cell. Mol. Physiol.* **2018**, *314* (5), L769–L781. <https://doi.org/10.1152/ajplung.00259.2017>.
- (108) Jacobs, M.; Hayakawa, K.; Swenson, L.; Bellon, S.; Fleming, M.; Taslimi, P.; Doran, J. The Structure of Dimeric ROCK I Reveals the Mechanism for Ligand Selectivity. *J. Biol. Chem.* **2006**,

281 (1), 260–268. <https://doi.org/10.1074/jbc.M508847200>.

- (109) Yamaguchi, H.; Miwa, Y.; Kasa, M.; Kitano, K.; Amano, M.; Kaibuchi, K.; Hakoshima, T. Structural Basis for Induced-Fit Binding of Rho-Kinase to the Inhibitor Y-27632. *J. Biochem.* **2006**, *140* (3), 305–311. <https://doi.org/10.1093/jb/mvj172>.
- (110) Gao, H.; Marhefka, C.; Jacobs, M. D.; Cao, J.; Bandarage, U. K.; Green, J. ROCK Inhibitors 2. Improving Potency, Selectivity and Solubility through the Application of Rationally Designed Solubilizing Groups. *Bioorganic Med. Chem. Lett.* **2018**, *28* (15), 2616–2621. <https://doi.org/10.1016/j.bmcl.2018.06.043>.
- (111) Yamaguchi, H.; Kasa, M.; Amano, M.; Kaibuchi, K.; Hakoshima, T. Molecular Mechanism for the Regulation of Rho-Kinase by Dimerization and Its Inhibition by Fasudil. *Structure* **2006**, *14* (3), 589–600. <https://doi.org/10.1016/j.str.2005.11.024>.
- (112) Pan, P.; Shen, M.; Yu, H.; Li, Y.; Li, D.; Hou, T. Advances in the Development of Rho-Associated Protein Kinase (ROCK) Inhibitors. *Drug Discov. Today* **2013**, *18* (23–24), 1323–1333. <https://doi.org/10.1016/j.drudis.2013.09.010>.
- (113) Boland, S.; Bourin, A.; Alen, J.; Geraets, J.; Schroeders, P.; Castermans, K.; Kindt, N.; Boumans, N.; Panitti, L.; Fransen, S.; Vanormelingen, J.; Stassen, J. M.; Leysen, D.; Defert, O. Design, Synthesis, and Biological Evaluation of Novel, Highly Active Soft Rock Inhibitors. *J. Med. Chem* **2015**, *58* (10), 4309–4324. <https://doi.org/10.1021/acs.jmedchem.5b00308>.
- (114) Akama, T.; Dong, C.; Virtucio, C.; Sullivan, D.; Zhou, Y.; Zhang, Y. K.; Rock, F.; Freund, Y.; Liu, L.; Bu, W.; Wu, A.; Fan, X. Q.; Jarnagin, K. Linking Phenotype to Kinase: Identification of a Novel Benzoxaborole Hinge-Binding Motif for Kinase Inhibition and Development of High-Potency Rho Kinase Inhibitors. *J. Pharmacol. Exp. Ther.* **2013**, *347* (3), 615–625. <https://doi.org/10.1124/jpet.113.207662>.
- (115) Pireddu, R.; Forinash, K. D.; Sun, N. N.; Martin, M. P.; Sung, S. S.; Alexander, B.; Zhu, J. Y.; Guida, W. C.; Schönbrunn, E.; Sebti, S. M.; Lawrence, N. J. Pyridylthiazole-Based Ureas as Inhibitors of Rho Associated Protein Kinases (ROCK1 and 2). *Medchemcomm* **2012**, *3* (6), 699–709. <https://doi.org/10.1039/c2md00320a>.
- (116) Patel, R. A.; Forinash, K. D.; Pireddu, R.; Sun, Y.; Sun, N.; Martin, M. P.; Schönbrunn, E.; Lawrence, N. J.; Sebti, S. M. RKI-1447 Is a Potent Inhibitor of the Rho-Associated ROCK Kinases with Anti-Invasive and Antitumor Activities in Breast Cancer. *Cancer Res.* **2012**, *72* (19), 5025–5034. <https://doi.org/10.1158/0008-5472.CAN-12-0954>.
- (117) Defert, O.; Boland, S. Rho Kinase Inhibitors: A Patent Review (2014–2016). *Expert Opin. Ther. Pat.* **2017**, *27* (4), 507–515. <https://doi.org/10.1080/13543776.2017.1272579>.
- (118) William, A. D.; Lee, A. C. H.; Blanchard, S.; Poulsen, A.; Teo, E. L.; Nagaraj, H.; Tan, E.; Chen, D.; Williams, M.; Sun, E. T.; Goh, K. C.; Ong, W. C.; Goh, S. K.; Hart, S.; Jayaraman, R.; Pasha, M. K.; Ethirajulu, K.; Wood, J. M.; Dymock, B. W. Discovery of the Macrocyclic 11-(2-Pyrrolidin-1-yl-ethoxy)-14,19-dioxo-5,7,26-triaza-tetracyclo[19.3.1.1(2,6).1(8,12)]heptacosan-1(25),2(26),3,5,8,10,12(27),16,21,23-decaene (SB1518), a Potent Janus Kinase 2/Fms-like

- Tyrosine Kinase-3 (JAK2/FLT3) Inhibitor. *J. Med. Chem.* **2011**, *54* (13), 4638–4658. <https://doi.org/10.1021/jm200326p>.
- (119) Giordanetto, F.; Kihlberg, J. Macrocyclic Drugs and Clinical Candidates: What Can Medicinal Chemists Learn from Their Properties? *J. Med. Chem.* **2014**, *57* (2), 278–295. <https://doi.org/10.1021/jm400887j>.
- (120) Bosanac, T.; Hickey, E. R.; Ginn, J.; Kashem, M.; Kerr, S.; Kugler, S.; Li, X.; Olague, A.; Schlyer, S.; Young, E. R. R. Substituted 2H-Isoquinolin-1-Ones as Potent Rho-Kinase Inhibitors: Part 3, Aryl Substituted Pyrrolidines. *Bioorganic Med. Chem. Lett.* **2010**, *20* (12), 3746–3749. <https://doi.org/10.1016/j.bmcl.2010.04.069>.
- (121) Wu, F.; Büttner, F. H.; Chen, R.; Hickey, E.; Jakes, S.; Kaplita, P.; Kashem, M. A.; Kerr, S.; Kugler, S.; Paw, Z.; Prokopowicz, A.; Shih, C. K.; Snow, R.; Young, E.; Cywin, C. L. Substituted 2H-Isoquinolin-1-One as Potent Rho-Kinase Inhibitors. Part 1: Hit-to-Lead Account. *Bioorganic Med. Chem. Lett.* **2010**, *20* (11), 3235–3239. <https://doi.org/10.1016/j.bmcl.2010.04.070>.
- (122) Afanasyev, O. I.; Kuchuk, E.; Usanov, D. L.; Chusov, D. Reductive Amination in the Synthesis of Pharmaceuticals. *Chem. Rev.* **2019**, *119* (23), 11857–11911. <https://doi.org/10.1021/acs.chemrev.9b00383>.
- (123) Nie, Z.; Perretta, C.; Erickson, P.; Margosiak, S.; Lu, J.; Averill, A.; Almassy, R.; Chu, S. Structure-Based Design and Synthesis of Novel Macrocyclic Pyrazolo[1,5-a] [1,3,5]Triazine Compounds as Potent Inhibitors of Protein Kinase CK2 and Their Anticancer Activities. *Bioorganic Med. Chem. Lett.* **2008**, *18* (2), 619–623. <https://doi.org/10.1016/j.bmcl.2007.11.074>.
- (124) Zhou, J.; Reidy, M.; Oreilly, C.; Jarikote, D. V.; Negi, A.; Samali, A.; Szegezdi, E.; Murphy, P. V. Decorated Macrocycles via Ring-Closing Double-Reductive Amination. Identification of an Apoptosis Inducer of Leukemic Cells That at Least Partially Antagonizes a 5-HT₂ Receptor. *Org. Lett.* **2015**, *17* (7), 1672–1675. <https://doi.org/10.1021/acs.orglett.5b00404>.
- (125) Adebomi, V.; Cohen, R. D.; Wills, R.; Chavers, H. A. H.; Martin, G. E.; Raj, M. CyClick Chemistry for the Synthesis of Cyclic Peptides. *Angew. Chemie - Int. Ed.* **2019**, *58* (52), 19073–19080. <https://doi.org/10.1002/anie.201911900>.
- (126) Fales, K. R.; Njoroge, F. G.; Brooks, H. B.; Thibodeaux, S.; Torrado, A.; Si, C.; Toth, J. L.; Mc Cowan, J. R.; Roth, K. D.; Thrasher, K. J.; Frimpong, K.; Lee, M. R.; Dally, R. D.; Shepherd, T. A.; Durham, T. B.; Margolis, B. J.; Wu, Z.; Wang, Y.; Atwell, S.; Wang, J.; Hui, Y. H.; Meier, T. I.; Konicek, S. A.; Geeganage, S. Discovery of N-(6-Fluoro-1-Oxo-1,2-Dihydroisoquinolin-7-yl)-5-[(3R)-3-Hydroxypyrrolidin-1-yl]Thiophene-2-Sulfonamide (LSN 3213128), a Potent and Selective Nonclassical Antifolate Aminoimidazole-4-Carboxamide Ribonucleotide Formyltransferase (AICARFT) Inhi. *J. Med. Chem.* **2017**, *60* (23), 9599–9616. <https://doi.org/10.1021/acs.jmedchem.7b01046>.
- (127) Charifson, P. S.; Grillot, A. L.; Grossman, T. H.; Parsons, J. D.; Badia, M.; Bellon, S.; Deininger, D. D.; Drumm, J. E.; Gross, C. H.; LeTiran, A.; Liao, Y.; Mani, N.; Nicolau, D. P.; Perola, E.; Ronkin, S.; Shannon, D.; Swenson, L. L.; Tang, Q.; Tessier, P. R.; Tian, S. K.; Trudeau, M.; Wang, T.; Wei, Y.; Zhang, H.; Stamos, D. Novel Dual-Targeting Benzimidazole Urea Inhibitors of DNA Gyrase

and Topoisomerase IV Possessing Potent Antibacterial Activity: Intelligent Design and Evolution through the Judicious Use of Structure-Guided Design and Structure-Activity Relationships. *J. Med. Chem.* **2008**, *51* (17), 5243–5263. <https://doi.org/10.1021/jm800318d>.

- (128) Ginn, J. D.; Bosanac, T.; Chen, R.; Cywin, C.; Hickey, E.; Kashem, M.; Kerr, S.; Kugler, S.; Li, X.; Prokopowicz, A.; Schlyer, S.; Smith, J. D.; Turner, M. R.; Wu, F.; Young, E. R. R. Substituted 2H-Isoquinolin-1-Ones as Potent Rho-Kinase Inhibitors: Part 2, Optimization for Blood Pressure Reduction in Spontaneously Hypertensive Rats. *Bioorganic Med. Chem. Lett.* **2010**, *20* (17), 5153–5156. <https://doi.org/10.1016/j.bmcl.2010.07.014>.
- (129) Clementson, S.; Jessing, M.; Pedersen, H.; Vital, P.; Kristensen, J. L. Enantioselective Total Synthesis of (+)-Dihydro- β -Erythroidine. *J. Am. Chem. Soc.* **2019**, *141* (22), 8783–8786. <https://doi.org/10.1021/jacs.9b04626>.
- (130) Neidigh, K. A.; Avery, M. A.; Williamson, J. S.; Bhattacharyya, S. Facile Preparation of N-Methyl Secondary Amines by Titanium(IV) Isopropoxide-Mediated Reductive Animation of Carbonyl Compounds. *J. Chem. Soc. - Perkin Trans. 1* **1998**, No. 16, 2527–2531. <https://doi.org/10.1039/a803703e>.
- (131) Breder, A.; Chinigo, G. M.; Waltman, A. W.; Carreira, E. M. Towards the Synthesis of Massadine: A Unified Strategy for the Stereoselective Synthesis of the Carbocyclic C,D-Ring Subunit. *Chem. - A Eur. J.* **2011**, *17* (44), 12405–12416. <https://doi.org/10.1002/chem.201101862>.
- (132) Sturdivant, J. M.; Royalty, S. M.; Lin, C. W.; Moore, L. A.; Yingling, J. D.; Laethem, C. L.; Sherman, B.; Heintzelman, G. R.; Kopczynski, C. C.; Delong, M. A. Discovery of the ROCK Inhibitor Netarsudil for the Treatment of Open-Angle Glaucoma. *Bioorganic Med. Chem. Lett.* **2016**, *26* (10), 2475–2480. <https://doi.org/10.1016/j.bmcl.2016.03.104>.
- (133) Audisio, D.; Messaoudi, S.; Peyrat, J. F.; Brion, J. D.; Alami, M. A Convenient and Expedient Synthesis of 3-(N-Substituted) Aminocoumarins via Palladium-Catalyzed Buchwald-Hartwig Coupling Reaction. *Tetrahedron Lett.* **2007**, *48* (39), 6928–6932. <https://doi.org/10.1016/j.tetlet.2007.07.166>.